



University of HUDDERSFIELD

University of Huddersfield Repository

Khizer, Zara

Novel Technological and Material Insights for Personalised Drug Delivery

Original Citation

Khizer, Zara (2022) Novel Technological and Material Insights for Personalised Drug Delivery. Doctoral thesis, University of Huddersfield.

This version is available at <http://eprints.hud.ac.uk/id/eprint/35746/>

The University Repository is a digital collection of the research output of the University, available on Open Access. Copyright and Moral Rights for the items on this site are retained by the individual author and/or other copyright owners. Users may access full items free of charge; copies of full text items generally can be reproduced, displayed or performed and given to third parties in any format or medium for personal research or study, educational or not-for-profit purposes without prior permission or charge, provided:

- The authors, title and full bibliographic details is credited in any copy;
- A hyperlink and/or URL is included for the original metadata page; and
- The content is not changed in any way.

For more information, including our policy and submission procedure, please contact the Repository Team at: E.mailbox@hud.ac.uk.

<http://eprints.hud.ac.uk/>

Novel Technological and Material Insights for Personalised Drug Delivery

ZARA KHIZER (PharmD, MSc)

A thesis submitted in partial fulfilment of the requirements for the
degree of Doctor of Philosophy (PhD)

University of
HUDDERSFIELD
Inspiring global professionals

**The University of Huddersfield
2022**

Copyright Declaration

1. The author of this thesis (including any appendices and/or schedules to this thesis) owns any copyright in it (the “Copyright”) and he has given The University of Huddersfield the right to use such Copyright for any administrative, promotional, educational and/or teaching purposes.
2. Copies of this thesis, either in full or in extracts, may be made only in accordance with the regulations of the University Library. Details of these regulations may be obtained from the Librarian. This page must form part of any such copies made.
3. The ownership of any patents, designs, trademarks, and all other intellectual property rights except for the Copyright (the “Intellectual Property Rights”) and any reproductions of copyright works, for example graphs and tables (“Reproductions”), which may be described in this thesis, may not be owned by the author and may be owned by third parties. Such Intellectual Property Rights and Reproductions cannot and must not be made available for use without the prior written permission of the owner(s) of the relevant Intellectual Property Rights and/or Reproductions.

Declaration Statement

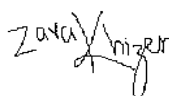
I, Zara Khizer, declare that the work presented in this thesis entitled "*Novel Technological and Material Insights for Personalised Drug Delivery*", is mainly my own.

Moreover, I confirm that:

- 1- All the experimental work was carried out during my PhD candidature at the School of Applied Sciences, University of Huddersfield, UK.
- 2- In case I have consulted published work of others, it is clearly credited and stated.
- 3- In case of any collaborative work the role has been clearly stated.
- 4- I have acknowledged all the facilitators and sources of help.

With exception to above, this thesis is entirely my own work.

Name: Zara Khizer



Signed: _____

Dated: 25-04-2022

Publication Declaration

This is to declare that this thesis has been published in the form of following research manuscripts where Zara Khizer has done data generation, data analyse and writing as a first author.

1. Khizer, Z., Akram, M. R., Sarfraz, R. M., Nirwan, J. S., Farhaj, S., Yousaf, M., ... & Ghori, M. U. (2019). Plasticiser-free 3D printed hydrophilic matrices: Quantitative 3D surface texture, mechanical, swelling, erosion, drug release and pharmacokinetic studies. *Polymers*, 11(7), 1095.
2. Khizer, Z., Sadia, A., Sharma, R., Farhaj, S., Nirwan, J. S., Kakadia, P. G., ... & Ghori, M. U. (2021). Drug Delivery Approaches for Managing Overactive Bladder (OAB): A Systematic Review. *Pharmaceuticals*, 14(5), 409.
3. Khizer, Z., Lou, S., Khan, N., Timmins, P., Conway, B.R., & Ghori, M. U. (2022). 3D Printed Patient Centric Medicines: A Systematic Review. *RSC Advances* (Submitted)
4. Khizer, Z., Akram, M. R., Conway, B.R., & Ghori, M. U. (2022). Personalised 3D printed Mucoadhesive Gastroretentive Hydrophilic Matrices for Managing Overactive Bladder (OAB). *Bio-design and Manufacturing* (Submitted)

Abstract

The thesis illustrates the clinical importance of personalised drug delivery devices and compare its effectiveness with the existing dosage forms of predefined strengths. The conventional system of manufacturing has its advantages and disadvantages. These methods are difficult to use in developing personalised drug delivery devices, but the recent emergence of 3D printing technologies has brought the development of personalised drug delivery devices near to reality. Among all the 3D printing technologies, fused deposition modelling (FDM) is the most commonly and widely used technique. However, the technology has limitation due to non-availability of pharmaceutical polymers approved by food and drug administration (FDA). Researchers have investigated already established pharmaceutical materials in FDM printing. Moreover, drug-loaded filaments feasible for FDM printing are not available commercially. Therefore, this thesis is aimed at firstly, to systematically review the role of 3D printing technology in developing personalised dosage forms. Secondly, feasibility of different polymers for hot-melt extrusion (HME) and for FDM printing was investigated by developing plasticiser-free HPMC polymers-based filaments using HME intended for FDM printing. Thirdly, a systematic review on the drug delivery routes available for the treatment of overactive bladder (OAB) was conducted. Lastly, plasticiser free filaments of PEO were extruded to develop gastroretentive floating drug delivery system for gabapentin to manage OAB.

A systematic review was conducted following preferred reporting items for systematic reviews and meta-analyses (PRISMA) guidelines to identify the research studies contributing to the practicability of 3D printing technologies in developing novel personalised drug delivery devices. A total of 241 studies were included and were further categorised according to the types of 3D printing technologies. The review has comprehensively outlined the role of these technologies which will be helpful for researchers in the future.

Plasticiser free filaments were successfully extruded using three different grades of HPMC. Filaments were produced successfully and used to produce matrix tablets. The viscosity of HPMC had a discernible impact on the swelling, erosion, HPMC dissolution, drug release and pharmacokinetic findings. The highest viscosity grade (K100M) results in higher degree of swelling, decreased HPMC dissolution, low matrix erosion, decreased drug release and extended drug absorption profile.

Another systematic review was conducted to evaluate the various drug delivery strategies used in practice to manage OAB. A total of 24 studies reporting the development of novel formulations for the management of OAB were considered eligible and were further categorised according to the route of drug administration. The review found that various drug delivery routes (transdermal, intravesicular, oral, vaginal, and intramuscular) are used for the administration of drugs for managing OAB, however, the outcomes illustrated the marked potential of transdermal drug delivery route and limitations of using oral antimuscarinic drugs-based formulations due to their adverse effects.

Gastroretentive floating drug delivery system was developed to overcome the absorption related issues of gabapentin, an effective drug in the treatment of OAB. Plasticiser free PEO filaments were extruded. Tablets were printed with varying shell number and infill density to investigate the floating capacity. Among seven different tablet formulations F2 (2 shells, 0% infill) showed highest floating time i.e., more than 10 hours. Drug release studies showed the extended release of the drug in a 12-hour study. It was observed that the drug release was decreased with increase in infill density and shell number. However, among all the formulations, F2 was the optimum formulation with longer floating time and sustained release of the drug and was chosen for *in vivo* studies. The extended-release effect of PEO was also seen during the pharmacokinetic studies that made the drug to be absorbed into bloodstream over longer period. It was concluded that the *in vitro*, and *in vivo* studies showed successful fabrication of the tablets.

Overall, the results obtained can be a helpful resource in the future contributing to the further development, optimisation, and clinical translation of personalised drug delivery systems.

Dedication

I would like to dedicate this thesis to my husband, parents, and siblings, without their love, prayers, and support, I would not have been able to do this.

Acknowledgements

I would like to thank my extremely supportive supervisor Dr Muhammad Usman Ghori; working under your supervision was not only inspiring but it was an honour for me. The skills and knowledge I have gained throughout these years of PhD, I perceive it as a very valuable component in my future career development. Thank you for being my mentor. There were times where you have acted as a father figure, understood the problems, and helped me in every possible way. The support and guidance you have provided is second to none. I cannot thank you enough for all that you have done.

I would also like thank Prof Barbara Conway (Head of Pharmacy, University of Huddersfield) for her support throughout my PhD.

My thanks is due to the University of Huddersfield for providing me a 100% fee-waiver scholarship to pursue my PhD at the Department of Pharmacy, University of Huddersfield.

Sincere thanks to Dr Muhammad Rauf Akram, Dr Rai Sarfaraz and University of Sargodha, Sargodha, Pakistan for providing support and facilities for pharmacokinetic testing.

I express my thanks to Ibrahim George, James Rooney, Hayley Markham, Richard Hughes, and Jack Edwards who taught me how to operate the instruments. And an especial thanks to Hayley Markham whose help had always made my things easier. I would also like to say thank you to Julie Walker and Urfan Sabir for their administrative support.

I also want to say thanks to my colleagues, Samia Farhaj and Jorabar Nirwan. A huge thanks to Samia Farhaj for her friendship and support during this journey. Her presence has really made this journey memorable and full of joy.

Last but not the least; I am here because of the blessings and support of my husband, parents, and siblings. I truly appreciate their constant encouragement. Thank you so much for being with me.

Finally, I thank all the people who have supported me directly or indirectly in this endeavour.

Table of Content

Contents

Copyright Declaration.....	ii
Declaration Statement	iii
Publication Declaration	iv
Abstract	v
Dedication.....	vi
Acknowledgements	vii
Table of Content.....	viii
List of Figures	xii
List of Tables	xvii
List of Abbreviations.....	xix
CHAPTER 1	xix
Graphical abstract	2
Notes for readers	3
1. Introduction	4
1.1. Personalised drug delivery	4
1.2. Aim and objectives	15
1.3. Thesis structure	18
References	20
CHAPTER 2	24
Graphical abstract	25
Notes for readers	26
2. 3D printed patient centric medicines: a systematic review	27
2.1. Introduction	27
2.2. Methodology.....	28
2.2.1. Search plot, information sources and screening process	28
2.2.2. Study selection	28
2.2.3. Data extraction and collection	29
2.2.4. Risk of bias assessment.....	29
2.3. Results and discussion	51
2.3.1. Key findings of the current systematic review	56
2.4. Advantages and limitations of 3D printing technologies	219

2.5.	Regulatory challenges	225
2.6.	Future prospects and outlook	226
2.7.	Conclusions	227
	References	229
	CHAPTER 3	242
	Graphical abstract	243
	Notes for readers	244
3.1.	Introduction	245
3.2.	Material and methods	246
3.2.1.	Materials	246
3.2.2.	Preparation of filaments	247
3.2.3.	Physicochemical characterisation of filaments	247
3.2.4.	Fabrication of 3D printed glipizide matrix tablets	248
3.2.5.	Characterisation of 3D printed matrices	249
3.2.6.	Pharmacokinetic studies	251
3.3.	Results and discussion	252
3.3.1.	Development and characterisation of filaments	252
3.3.2.	Development and characterisation of 3D printed matrix tablets	257
3.3.3.	Swelling and HPMC dissolution studies	260
3.3.4.	Drug release studies	262
3.3.5.	Erosion studies	263
3.3.6.	Pharmacokinetic studies of HPMC/glipizide hydrophilic matrices	265
3.4.	Conclusions	267
	References	268
	CHAPTER 4	270
	Graphical abstract	271
	Notes for readers	272
4.1.	Introduction	273
4.2.	Methodology	276
4.2.1.	Search plot, information sources and screening process	276
4.2.2.	Study selection	277
4.2.3.	Data extraction and collection	278
4.2.4.	Risk of bias assessment	278

4.3.	Results and discussion	278
4.3.1.	Transdermal route	289
4.3.2.	Intravesical route.....	293
4.3.3.	Vaginal route	294
4.3.4.	Intramuscular route	295
4.3.5.	Oral route.....	296
4.4.	Conclusions	300
	References	301
	CHAPTER 5	304
	Graphical abstract	305
	Notes for readers	306
5.1.	Introduction	307
5.2.	Materials and methods.....	310
5.2.1.	Materials	310
5.2.2.	Preparation of filaments	310
5.2.3.	Physicochemical characterisation of filaments	311
5.2.4.	Fabrication of 3D printed tablets.....	312
5.2.5.	Characterisation of 3D Printed Matrices.....	312
5.2.6.	<i>In vitro</i> dissolution testing.....	315
5.2.7.	Floating test.....	315
5.2.8.	Pharmacokinetic studies	316
5.3.	Results and discussion	317
5.3.1.	Development and characterisation of filaments	317
5.3.2.	Development and characterisation of 3D printed tablets.....	320
5.3.3.	Mucoadhesion analysis.....	324
5.3.4.	<i>In vitro</i> floating and drug release.....	326
5.3.5.	Pharmacokinetic parameters	328
5.4.	Conclusions	331
	References	332
	CHAPTER 6	334
6.1.	Conclusions	335
	CHAPTER 7	338
7.1.	Future work.....	339

Appendix I..... 340

List of Figures

Chapter 1

Figure 1.1: Types of 3D printing techniques and their brief description.....	7
Figure 1.2: Schematic illustration of FDM printer.	9
Figure 1.3: Schematic presentation of HME process for filament production.....	10
Figure 1.4: Schematic illustrating the aim and objectives of the thesis.	17

Chapter 2

Figure 2.1: Illustration depicting the selection process of eligible studies.	52
Figure 2.2: Distribution of studies based on the used 3D printing technology.	53
Figure 2.3: Assessment of risk of bias for (a) overall distribution of bias among each study included in the systematic review (b) extrusion-based studies (c) vat polymerisation studies (d) powder bed fusion studies (e) jetting technique studies.....	54
Figure 2.4: Overall trend of research studies across the years.	55
Figure 2.5: Distribution of frequently used model drugs.	55
Figure 2.6: Distribution of included studies based on extrusion-based printing techniques.....	56
Figure 2.7: Schematic illustration depicted the working principle of FDM, reproduced with permission from ¹⁶	57
Figure 2.8: Dosage from design (A) infill patterns, base, caps and shell of the designed tablets (B) Chrono-controlled release tablets (C) Pulsatile-release tablets, reproduced with permission from ²⁹	61
Figure 2.9: (A) STL model of three-compartment tablet with hollow cylinder (B) Demonstrating dimensions of tablets (C) FDM printed formulation (D) Half-printed formulation with inner binding PLA ring, reproduced with permission from ³⁰	62
Figure 2.10: Schematic illustration of STL model of tablet with 25% infill density. Reproduced with permission from ³⁶	64
Figure 2.11: Images of 3D printed tablets fabricated at constant (A) surface area (B) surface area/mass ratio (C) mass with different geometries, reproduced with permission from ⁴²	66
Figure 2.12: 3D design of printed formulations (A) halved multilayer device (B) halved DuoCaplet, reproduced with permission from ⁴⁶	68
Figure 2.13: Digital design representing perforating square sectioned channels in capsule design (a) parallel to long axis (b) at right angle with long axis with frontal, side and top view of channelled tablet designs. Reproduced with permission from ⁴⁷	68
Figure 2.14: Digital schematic showing comparison of multi-block unit with non-block design (A) Solid-block tablet (B) Tablet with 9 block units joined together by 3 bridges (C) three sets of tablets with different block size (0.5, 1 and 1.5 mm), reproduced with permission from ⁴⁹	69
Figure 2.15: Digital design of the 3D printed tablet with enteric shell. Reproduced with permission from ⁵³	71
Figure 2.16: FDM printed middle and hollow parts of dual compartment device, reproduced with permission from ⁷¹	75
Figure 2.17: Cross-section and isometric views of dual compartment devices with (A) same or (B) different thickness, reproduced with permission from ⁷⁵	77
Figure 2.18: 3D printed scaffolds with various dimensions and shapes, reproduced with permission from ⁹²	82

Figure 2.19: Images of the CBS (chlobetasol propionate)-loaded and VA (vanillic acid)-loaded mouth guards before and after the in vitro dissolution study, reproduced with permission from ¹⁰⁷	86
Figure 2.20: STL model of vaginal rings (A) O-shaped (B) Y-shaped (C) M-shaped, reproduced with permission from ¹¹³	89
Figure 2.21: Distribution of pharmaceutical dosage forms developed using FDM technique.....	91
Figure 2.22: Schematic diagram illustrating working principle of pneumatic extrusion, reproduced with permission from ¹¹⁹	92
Figure 2.23: Schematic illustration of tablets with solid, ring and mesh geometries along with their top view and side view, reproduced with permission from ¹¹⁹	97
Figure 2.24: 3D printed multiplexed capsule arrays (A) cylindrical and (B) square hydrogel matrices, reproduced with permission from ¹³⁶	99
Figure 2.25: Picture of 3D printed grid structures, from left placebo grid 0.5, 0.5%. 1% and 1.5% drug containing grids, reproduced with permission from ¹³⁸	100
Figure 2.26: Distribution of pharmaceutical dosage forms developed using pneumatic extrusion. .	101
Figure 2.27: Schematic diagram illustrating working principle of paste extrusion, reproduced with permission from ¹⁴⁰	103
Figure 2.28: Distribution of pharmaceutical dosage forms developed using paste extrusion technique.....	112
Figure 2.29: Distribution of included studies based on vat polymerisation-based techniques.....	155
Figure 2.30: Schematic diagram illustrating working principle of stereolithography, reproduced with permission from ¹⁸⁵	156
Figure 2.31: Images of 3D printed tablets loaded with (A) paracetamol (B) 4-ASA with different percentages of PEG/PEGDA, reproduced with permission from ¹⁸⁹	158
Figure 2.32: Schematic diagram illustrating working principle of CLIP, reproduced with permission from ¹⁹⁸	161
Figure 2.33: Schematic diagram illustrating working principle of 2PP, reproduced with permission from ²⁰³	162
Figure 2.34: Schematic diagram illustrating working principle of DLP, reproduced with permission from ²¹⁴	164
Figure 2.35: Distribution of pharmaceutical dosage forms developed using Vat polymerisation techniques.....	165
Figure 2.36: Distribution of included studies based on powder bed fusion techniques.....	172
Figure 2.37: Schematic diagram illustrating working principle of SLS, reproduced with permission from ²²²	173
Figure 2.38: Images of HPMC and Kollidon printlets (scale is in cm), reproduced with permission from ²²⁸	175
Figure 2.39: Schematic diagram illustrating working principle of powder bed printing. Reproduced with permission from ²²¹	177
Figure 2.40: Schematic of tablet representing material gradients (a) barrier layer (b) region containing drug (c) retarded release material, reproduced with permission from ²³⁶	179
Figure 2.41: Schematic diagram of fast disintegrating tablet, reproduced with permission from ²³⁷	180
Figure 2.42: Isoniazid-PLLA implant ideograph. CST: columnar shaped tablet, DST: doughnut-shaped tablet, MDST: multilayer doughnut shaped tablet, reproduced with permission from ²⁴²	181
Figure 2.43: Schematic diagram illustrating working principle of selective laser melting. Reproduced with permission from ²⁴⁷	183

Figure 2.44: Bar chart representing the distribution of pharmaceutical dosage forms developed using powder bed fusion techniques. (others include resorbable devices, gyroid lattices, cylindrical disc matrices, and shell core structure).....	184
Figure 2.45: Distribution of included studies based on jetting techniques.....	192
Figure 2.46: Schematic diagram illustrating working principle of inkjet printing, reproduced with permission from ²⁵¹	193
Figure 2.47: SPM topographical images of inkjet-printed substances (a) caffeine printed on coated paper, (b) theophylline printed on Mica, and (c) paracetamol printed on PET, reproduced with permission from ²⁶³	198
Figure 2.48: Schematic diagram illustrating working principle of drop on demand printing. Reproduced with permission from ²⁶⁹	200
Figure 2.49: Schematic diagram illustrating working principle of material jetting, reproduced with permission from ²²¹	203
Figure 2.50: Schematic diagram illustrating working principle of binder jetting. Reproduced with permission from ²⁷⁹	204
Figure 2.51: Deposition and quantification of four nasal sprays in the nose, reproduced with permission from ²⁸⁴	206
Figure 2.52: Schematic diagram illustrating working principle of E-jet printing technique. Reproduced with permission from ²⁸⁶	207
Figure 2.53: Bar chart representing the distribution of pharmaceutical dosage forms developed using Jetting techniques.....	209

Chapter 3

Figure 3.1: (a) Hot melt extruded filaments and (b) 3D printed hydrophilic matrices.....	253
Figure 3.2: DSC profiles of (a) glipizide, (b) HPMC (K4M, K15M and K100M) and (c) K4M/GLP, K15M/GLP and K100M/GLP filaments.....	254
Figure 3.3: TGA profiles of (a) glipizide, (b) HPMC (K4M, K15M and K100M) and (c) K4M/GLP, K15M/GLP and K100M/GLP filaments.....	254
Figure 3.4: XRD profiles of (a) glipizide, (b) HPMC (K4M, K15M and K100M) and (c) K4M/GLP, K15M/GLP and K100M/GLP filaments.....	254
Figure 3.5: SEM micrographs of (a-d) K4M based filament and matrix tablet (a= filament, b= whole matrix tablet, c= side view of matrix tablet and d, surface view showing edges), (e-h) K15M based filament and matrix tablet (e= filament, f= whole matrix tablet, g= side view of matrix tablet and h, surface view showing edges) and (i-l) K100M based filament and matrix tablet (i= filament, j= whole matrix tablet, k= side view of matrix tablet and l, surface view showing edges).....	256
Figure 3.6: 3D surface texture images (a) K4M (b) K15M and (c) K100M based matrix tablet.....	259
Figure 3.7: Swelling vs time profile of 3D printed HPMC matrix tablets.....	261
Figure 3.8: HPMC dissolution vs time profile of 3D printed HPMC matrix tablets.....	262
Figure 3.9: Drug (glipizide) release vs time profile of 3D printed HPMC matrix tablets.	263
Figure 3.10: Overall matrix erosion vs time profile of 3D printed HPMC matrix tablets.	264
Figure 3.11: Drug (glipizide) absorption vs time profile of 3D printed HPMC matrix tablets.	265

Chapter 4

Figure 4.1: Cross-sectional view of urinary bladder showing different regions.....	274
Figure 4.2: Systematic search and study selection process.....	277

Figure 4.3: Distribution of eligible studies focused on different drug delivery routes.	279
Figure 4.4: Risk of bias assessment of eligible articles.	279
Figure 4.5: (a) Recovery of pilocarpine-induced salivation secretion in rats after transdermal administration of oxybutynin chloride (b) Appearance of commercial product in primary package, reproduced with permission from ^{38, 39}	291
Figure 4.6: Real-time morphological changes during film-forming process of transparent hydrogels, reproduced with permission from ⁴³	292
Figure 4.7: Blood oxybutynin concentration profiles of oral and vaginally administered formulations, CH3 (1% w/v glacial acetic acid and 3% w/v Chitosan H), H2 (2% w/v hypromellose K100M), reprinted with permission from ³¹	295
Figure 4.8: Illustration depicted the formulation principle of membrane-coated multiple units extended-release pellets, reproduced with permission from ⁵⁰	297
Figure 4.9: Plasma profiles of (a) gabapentin and (b) flurbiprofen after single dose administration in fed conditions of (●) TLT_HPMC Type I, (■) TLT_HPMC Type II and (◆) Immediate release dosage form (mean values ± SD; n =24), reproduced with permission from ⁶⁶	299

Chapter 5

Figure 5.1: Schematic illustration of electrically tunable lens (ETL)-based variable focus imaging system used for the surface texture analysis of the 3D printed tablets, (1) computer; (2) ETL driver; (3) camera; (4) ETL; (5) automatic motorized vertical translation stage ; and (6) stage controlling system ⁴⁹	313
Figure 5.2: Schematic illustration of mucoadhesive testing of 3D printed tablets using texture analyser with specialised mucoadhesive holder (a) probe attached with 3D printed tablet was moved downward, (b) 3D printed tablet was attached with gastrointestinal mucosa with specified force and time and (c) probe was moved upward at a specified rate.	314
Figure 5.3: A typical Force vs Distance profile for 3D printed tablet (F2, (2 shell with 0 % infill)) from the mucoadhesion test performed in 0.1N HCl (150 mL) at 37 °C using texture analyser. F _{max} is the highest force required to separate the probe from the gastric tissue which is determined from the maximum peak height of the profile. However, W _{ad} is the total force involved in the probe separation during withdrawal phase which is calculated from the area under the curve (AUC) of the force vs distance profile.	315
Figure 5.4: (a) hot-melt extruded filament of gabapentin/polyethylene oxide (PEO)/polyethylene glycol (PEG), (b) F1 (1 shell with 0 % infill), (c) F2 (2 shell with 0 % infill), (d) F3 (3 shell with 0 % infill), (e) F4 (4 shell with 0 % infill), (f) F5 (2 shell with 10 % infill), (g) F6 (2 shell with 20 % infill) and (h) F7 (2 shell with 30% infill).	318
Figure 5.5: DSC profiles of (a) gabapentin (b) polyethylene oxide (PEO) (c) GBP/PEO filament.	318
Figure 5.6: TGA profiles of (a) gabapentin (b) polyethylene oxide (PEO) (c) GBP/PEO filament.	319
Figure 5.7: XRD profiles of (a) gabapentin (b) polyethylene oxide (PEO) (c) GBP/PEO filament.	319
Figure 5.8: SEM micrographs of 3D printed tablet, F2 (2 shell with 0 % infill), (a) whole matrix tablet, (b) side view of matrix tablet and (c) side surface view.	322
Figure 5.9: 2D surface texture images of 3D printed tablet, (a) F1 (1 shell with 0 % infill) , (b) F2 (2 shell with 0 % infill), (c) F3 (3 shell with 0 % infill), (d) F4 (4 shell with 0 % infill), (e) F5 (2 shell with 10 % infill), (f) F6 (2 shell with 20 % infill) and (g) F7 (2 shell with 30% infill).	323
Figure 5.10: 3D surface texture images of 3D printed tablet, (a) F1 (1 shell with 0 % infill) , (b) F2 (2 shell with 0 % infill), (c) F3 (3 shell with 0 % infill), (d) F4 (4 shell with 0 % infill), (e) F5 (2 shell with 10 % infill), (f) F6 (2 shell with 20 % infill) and (g) F7 (2 shell with 30% infill).	323

Figure 5.11: Surface roughness properties of 3D printed tablets, showing the effect of (a) shell number and (b) infill percentage (n= 5). F1 (1 shell with 0 % infill), F2 (2 shell with 0 % infill), F3 (3 shell with 0 % infill), F4 (4 shell with 0 % infill), F5 (2 shell with 10 % infill), F6 (2 shell with 20 % infill) and F7 (2 shell with 30% infill).	324
Figure 5.12: (a and b) maximum mucoadhesion detachment force and (c and d) work of adhesion, against porcine stomach mucosa in 0.1N HCl solution at 37±0.5 °C (n= 3). F1 (1 shell with 0 % infill), F2 (2 shell with 0 % infill), F3 (3 shell with 0 % infill), F4 (4 shell with 0 % infill), F5 (2 shell with 10 % infill), F6 (2 shell with 20 % infill) and F7 (2 shell with 30% infill).	325
Figure 5.13: Images of 3D printed tablet, F2 (2 shell with 0 % infill) floating in dissolution medium (0.1N HCl solution) at 37 ± 0.5 °C (a) t = 2h, (b) t = 4h, (c) t = 6h, (d) t=8h, (e) t = 10h and (f) t = 12h.	326
Figure 5.14: Drug release profile 3D printed tablets (n=5), (a) effect of number of shells and (b) influence of percentage infill. F1 (1 shell with 0 % infill) , F2 (2 shell with 0 % infill), F3 (3 shell with 0 % infill), F4 (4 shell with 0 % infill), F5 (2 shell with 10 % infill), F6 (2 shell with 20 % infill) and F7 (2 shell with 30% infill).	328
Figure 5.15: Plasma drug (gabapentin) absorption vs time profile of oral solution and 3D printed tablet, F2 (2 shell with 0 % infill), n=6.....	329

List of Tables

Chapter 1

Table 1.1: Advantages and disadvantages of conventional manufacturing method.	5
Table 1.2: Advantages and challenges of 3D printing technology.	8
Table 1.3: Different variables that can affect the mechanical properties of the object to be printed.	10
Table 1.4: key physicommechanical properties of filaments intended for 3D printing applications.....	13

Chapter 2

Table 2.1: Form used for the data extraction from eligible studies.	29
Table 2.2: List of various quality assessment and risk of bias assessment tools considered.	31
Table 2.3: Detailed description of risk of bias assessment process.	32
Table 2.4: Summary of an approach for assessing the risk of bias within and across studies.	33
Table 2.5: Assessment of risk of bias for studies based on extrusion technique included in the systematic review	34
Table 2.6: Assessment of risk of bias for studies based on vat polymerisation included in the systematic review.	44
Table 2.7: Assessment of risk of bias for powder bed fusion studies included in the systematic review.....	46
Table 2.8: Assessment of risk of bias for studies based on jetting technique included in the systematic review.	48
Table 2.9: Summarised characteristics of eligible studies used extrusion printing techniques for developing medicines.	113
Table 2.10: Summarised characteristics of eligible studies used vat polymerisation printing techniques for developing medicines.	166
Table 2.11: Summarised characteristics of eligible studies used powder bed fusion printing techniques for developing medicines.	185
Table 2.12: Summarised characteristics of eligible studies used jetting printing techniques for developing medicines.	210
Table 2.13: Summary of advantages and disadvantages of 3D printing techniques.	221

Chapter 3

Table 3.1: Specifications of different HPMC grades used in this study.	247
Table 3.2: Parameters used for the 3D printing of HPMC/glipizide matrices.	249
Table 3.3: Drug loading and three-point bending results of filaments (*n=10, standard deviations are in parenthesis).	256
Table 3.4: Geometrical and morphological characteristics of 3D printed hydrophilic matrices (n=5, standard deviations are in parenthesis).	258
Table 3.5: 3D quantitative surface texture parameters of HPMC/glipizide hydrophilic matrices (n= 10, standard deviations are in parenthesis).	259
Table 3.6: Swelling and erosion kinetics parameters of HPMC/glipizide hydrophilic matrices (n=5).	261

Table 3.7: Pharmacokinetic parameters of hypromellose/glipizide hydrophilic matrices (n= 5, standard deviations are in parenthesis).	265
---	-----

Chapter 4

Table 4.1: Summarised characteristics of eligible studies.....	280
Table 4.2: List of commercial products of drugs used for managing OAB.	286

Chapter 5

Table 5.1: HME parameters for developing filaments.	311
Table 5.2: Drug loading and three-point bending results of filaments (*n=10, standard deviations are in parenthesis).	320
Table 5.3: Formulation composition, dimension, and printing parameters of tablets.	320
Table 5.4: Drug loading and mechanical properties of 3D printed tablets (n=5).	321
Table 5.5: Physical parameters and floating time of 3D printed tablets (n=5).	327
Table 5.6: Pharmacokinetic parameters of gabapentin solution and 3D printed tablet (F2, 2 shell with 0 % infill) after oral administration, n=6.	330

List of Abbreviations

3D = Three dimensional

ABS = acrylonitrile butadiene styrene

AUC = area under the curve

BBB = blood brain barrier

BJ = binder jetting

CaCl₂ = calcium chloride

CAP = cellulose acetate phthalate

CaSO₄ = calcium sulphate

CGRP = Calcitonin gene related peptide

CLIP = continuous liquid interface production

CMC = carboxy methyl cellulose

Cu₂O = copper oxide

CuSO₄ = copper sulphate

DLP = digital light processing

DoD = drop on demand

DSC = Differential scanning calorimetry

E = Erosion

EC = ethyl cellulose

EG = ethylene glycol

E-jetting= electrohydrodynamic

EVA = ethylene vinyl acetate

FDM = Fuse deposition modelling

GO = graphene oxide

HA = hydroxyapatite

HEC = hydroxyethyl cellulose

HECE = hydroxyethyl cellulose ethoxylate

HEMA = hydroxyethyl methacrylate

HLA = hyaluronic acid

HME = Hot-melt extrusion

HPC = hydroxypropyl cellulose

HPMC = hydroxypropyl methyl cellulose

HPMCAS (LG, MG, HG) = hydroxypropyl methyl cellulose acetate succinate (low grade, medium grade, high grade)

HPMCAS = hydroxypropyl methyl cellulose acetate succinate

IPA = isopropyl alcohol

MBG = mesoporous bioactive glass

MCC = microcrystalline cellulose

MJ = material jetting

MoO₃ = molybdenum trioxide

MPa = Megapascals

MSNs = mesoporous silica nanoparticles

N-DEO = N-desethoxybutynin

OAB = overactive bladder

PA = polyamide

PAA = polyacrylic acid

PBP = powder bed printing

PCL= polycaprolactone

PCL-tMa = polycaprolactone trimethacrylate

PDLLA = poly-DL-lactic acid

PDMS = poly dimethyl siloxane

PE = paste extrusion

PEG = polyethylene glycol

PEGDA = polyethylene glycol diacrylate

PEGDMA = polyethylene glycol dimethacrylate

PEGDME = polyethylene glycol dimethyl ether

PEGDT = polyethylene glycol dithiol

PEGMEMA = polyethylene glycol methyl ether methacrylate

PEG-PCL = polyethylene glycol-polycaprolactone
PEG-PLGA = Polyethylene glycol-poly(lactic-co-glycolic acid)
PEO = polyethylene oxide
PET = polyethylene terephthalate
PEU = polyester urea
PG = propylene glycol
PLA = poly lactic acid
PLGA = poly(lactic-co-glycolic acid)
PLLA = poly-L-lactic acid
PMA = propyl methacrylate
PMMA = poly methyl meth acrylate
PnE = pneumatic extrusion
PP = polypropylene
PPF = polypropylene fumarate
PRISMA = Preferred reporting items for systematic reviews and metaanalyses
PU = polyurethane
PVA = poly vinyl alcohol
PVAc = polyvinyl acetate
PVA-PAA = polyvinyl alcohol-polyacrylic acid
PVA-PEG = polyvinyl alcohol-polyethylene glycol
PVP = poly vinyl pyrrolidone
PVP-PVAc = polyvinyl pyrrolidone-polyvinyl acetate
rpm = revolution per minute
S = Degree of swelling
SEDDS = Self-emulsifying drug delivery system
SEM = Scanning electron microscope
SLA = stereolithography
SLM = selective laser melting
SLS = selective laser sintering

STL = stereolithography

TCP = tricalcium phosphate

TEC = Triethylcitrate

Tg = glass transition

TGA = Thermogravimetric analysis

TiO₂ = Titanium dioxide

TLT = Three layered tablet

TPO = trimethylbenzoyl diphenylphosphine oxide (diphenyl(2,4,6-trimethylbenzoyl)phosphine oxide)

TPP = two photon polymerisation

TPU = thermoplastic polyurethane

UTI = urinary tract infection

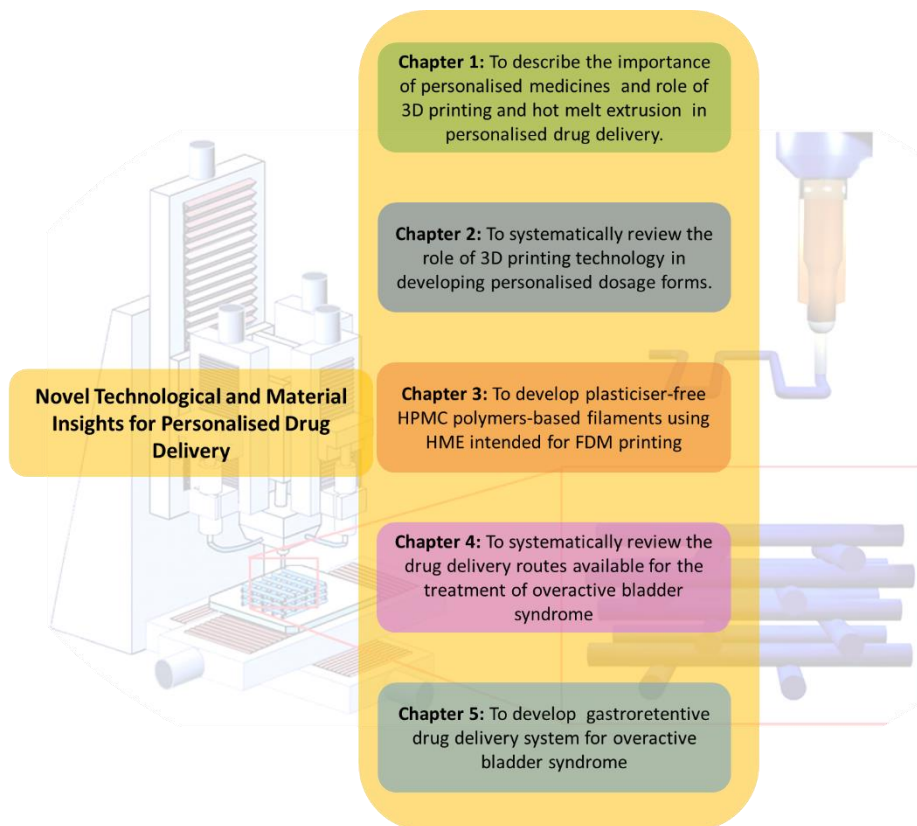
UV = ultraviolet

XRPD = X-ray powder diffraction

CHAPTER 1

INTRODUCTION

Graphical abstract



Notes for readers

- Personalised drug delivery devices are of great clinical importance as they provide treatment titrated to individual's requirements to achieve maximum therapeutic effectiveness. Whereas with the existing dosage forms of predefined strengths some of the patients get the desired therapeutic effect while others suffer from adverse reactions or achieve inadequate therapeutic effect or no therapeutic effect.
- 3D printing technologies provides a simple and effective way of developing personalised drug delivery devices in comparison to traditional manufacturing methods.
- Though there are many 3D printing technologies available, FDM is the most commonly and widely used technique. Nonetheless, the non-availability of FDA approved pharmaceutical polymers has caused limitations, in addition to this, drug loaded filaments are also not available commercially.
- Therefore, our aim was to investigate the feasibility of different polymers for hot-melt extrusion (HME) and for FDM printing. For this purpose, the feasibility of HPMC and PEO was investigated for extrusion and printing by developing plasticiser-free filaments using glipizide and gabapentin as model drugs. The filaments were then used to print hydrophilic matrices and gastroretentive floating drug delivery system. Moreover, systematic reviews were also conducted to identify the pharmaceutical applications of 3D printing technologies and the drug delivery routes available for the treatment of overactive bladder syndrome.

1. Introduction

1.1. Personalised drug delivery

Should there be a change in delivering the medicines in the 21st century? Should the established practice of producing dosage forms of predetermined dosage strengths and shape remain or is there any way to steer the course towards formulating the bespoke or personalised dosage forms where dose and other attributes can be titrated specifically to meet the individual's requirements for improved and better outcomes. The awareness about the limitations of mass-produced dosage forms is increasing and the development of smart and modern technologies offer an opportunity to develop personalised drug delivery devices.

The medicines and healthcare regulatory authority define personalised drug delivery as the individualisation of drug therapy in both choice and dose ¹. Personalised drug delivery systems are quite distinct from the mass-produced delivery systems ². Florence and Lee states that personalised medicine does not mean that it should include only matching of the genetic profile of the patient to the new drugs instead it should also include the improved methods of delivering drugs to the patients ³. Overall, the personalised drug delivery should cover all the aspects of individualising treatment including on-demand manufacturing, tailoring dose and shape and improved drug delivery systems.

The importance of the individualised treatment is evident by the advice of Hippocrates i.e., "to treat the person not the disease". Therefore, such treatment requires effective personalised drug delivery system which is consistent with the diversity of the human being and with the continuous needs of dosing rather than the mass-produced medicines of predetermined dosage strengths that are not truly consistent with the diverse population ⁴.

Although the current tablet manufacturing methods are well-established and are in use for centuries, however, there are certain drawbacks of these methods that limit its use ⁵. Some of the major advantages and disadvantages of conventional tablet manufacturing methods are given in the Table 1.1. It produces tablets of predetermined dosage strengths and shape at large scale to cover the large area of population, inevitable results have occurred due to the limited doses, some of the patients get the desired therapeutic effect while others suffer from adverse reactions or achieve inadequate therapeutic effect or no therapeutic effect ^{6,7}. These methods lack flexibility in tailoring the drug dose, importantly when various drug

combinations are involved. Therefore, these methods offer little room for personalisation and small-scale manufacturing of dosage forms as change in size, shape and dose of a tablet will require change in each manufacturing step and retooling of tableting machines ^{8,9}.

Table 1.1: Advantages and disadvantages of conventional manufacturing method.

Conventional manufacturing method	
Advantages	<ul style="list-style-type: none"> • Suitable for large scale production • Customisation is difficult to achieve • Suitable for known products
Disadvantages	<ul style="list-style-type: none"> • Provides no individualisation • Fixed doses and size of dosage forms • Often neglects orphan drugs

Several cases have been reported in the literature that highlight the limitations of the conventional system of manufacturing dosage forms. Splitting of tablets, polypharmacy and availability of predefined strengths of dosage forms only, are entirely not appropriate means of achieving personalised dosing of drugs ¹⁰. The diversity of population is another important factor which needs to be considered while approaching for personalised dosage forms ¹¹. For instance, a case associated with the inflexibility of dose in the dosage forms manufactured by conventional methods was seen in 1976, when 100 mg atenolol tablets for hypertension were introduced. The geriatric patients required the lower doses leading to the introduction of 50 mg tablets in 1980. Further lower dose of 25 mg was introduced in 1989 ¹². Another case highlighting the problem associated with the availability of only limited number of strengths of dosage forms was reported in 1995 ¹³. An insomniac patient was prescribed with 5 mg of zolpidem at first. The patient did not achieve therapeutic effects at this dose. The next available dose of zolpidem, 10 mg, was then prescribed which resulted in adverse effects. Finally, a personalised dose of 7.5 mg was then prescribed according to the patient's specific needs but unfortunately zolpidem tablet of this strength did not exist. Predetermined and limited dose strengths are available to such a diverse population and response of each individual to doses varies that's why these dosage forms are unable to provide patient specific therapeutic needs ¹⁰.

Clinically patients have considerable differences, for example, weight, age, disease severity, compromised organ functionality and multiple diseases. Due to these differences, the demand and importance of the personalised dosage forms has become evident. Personalised dosage forms aim to suit patient's individual therapeutic needs by modifying the dose according to the requirements and to provide patients with the treatments tailored to their pathophysiology¹⁴. There is a crucial demand of personalised dosage forms for geriatric and paediatric patients according to their weight, age, height and including other aspects required for the correct and accurate dosing. The metabolic and physiological functionality of each individual is different from each other which in turn requires dose adjustment accordingly i.e. paediatric patient exhibit fast changes in physiological and metabolic functions while gastrointestinal pathologies, renal clearance and body fat is different for geriatrics⁴. Another issue faced by geriatrics is polypharmacy, the use of five or more drugs, and in the UK it has been reported in more than 10% of people older than 65 years, which in turn also complicates personalisation³. The issues and challenges imposed by the predefined and limited dose strengths urge for the need of personalised dosage forms to control or modify the dose specifically according to the patient's requirements and thereby preventing adverse drug reactions and drug-drug interactions to provide safe and effective treatment.

On the other hand, the method to achieve personalised dosage form should be cheap, simple and accurate¹⁵. Three-dimensional (3D) printing was first demonstrated in 1996 as a promising candidate to replace conventional tableting techniques¹⁶. 3D printing technologies (powder bed printing, semi-solid extrusion, fused deposition modelling (FDM) etc.) are set to revolutionise the individualisation of dosage forms¹⁷. The digital control of these highly attractive technologies, via a computer software, produces 3D objects of any shape and promises to enable rapid fabrication of formulations with patient-specific dosages¹⁸.

3D printing was initially introduced during the 1980s by Charles Hull¹⁹. This methodology fabricates 3D objects by depositing printable materials in a controlled and layer-by-layer manner until the completion of the structure^{20,21}. It is due to the layer-by-layer deposition of material that 3D structure is achieved and is therefore this technique is also known as additive manufacturing. It utilises computer-aided design (CAD) file to design objects with varying size and geometry and perform digital slicing of the object and converts file into stereolithography format which is supported by the 3D printer²². It is an easy, efficient and quick method of

developing physical objects from digital design ²³. With regards to the feeding materials, the technology is versatile i.e., it uses powders, thermoplastic polymers, and resins. This technology is suitable for customised or bespoke manufacturing of the objects and is set to revolutionise the traditional tablet manufacturing methods by developing on-demand and customised pharmaceutical dosage forms that can be easily tailored to meet the specific requirements of the individuals and thus brings personalisation to the printed objects ²⁴.

In 2009, the American society for testing and materials international committee performed classification of different additive manufacturing processes which includes material extrusion, material jetting, binder jetting, sheet lamination, vat polymerisation, and powder bed fusion (Figure 1.1) ²⁵.

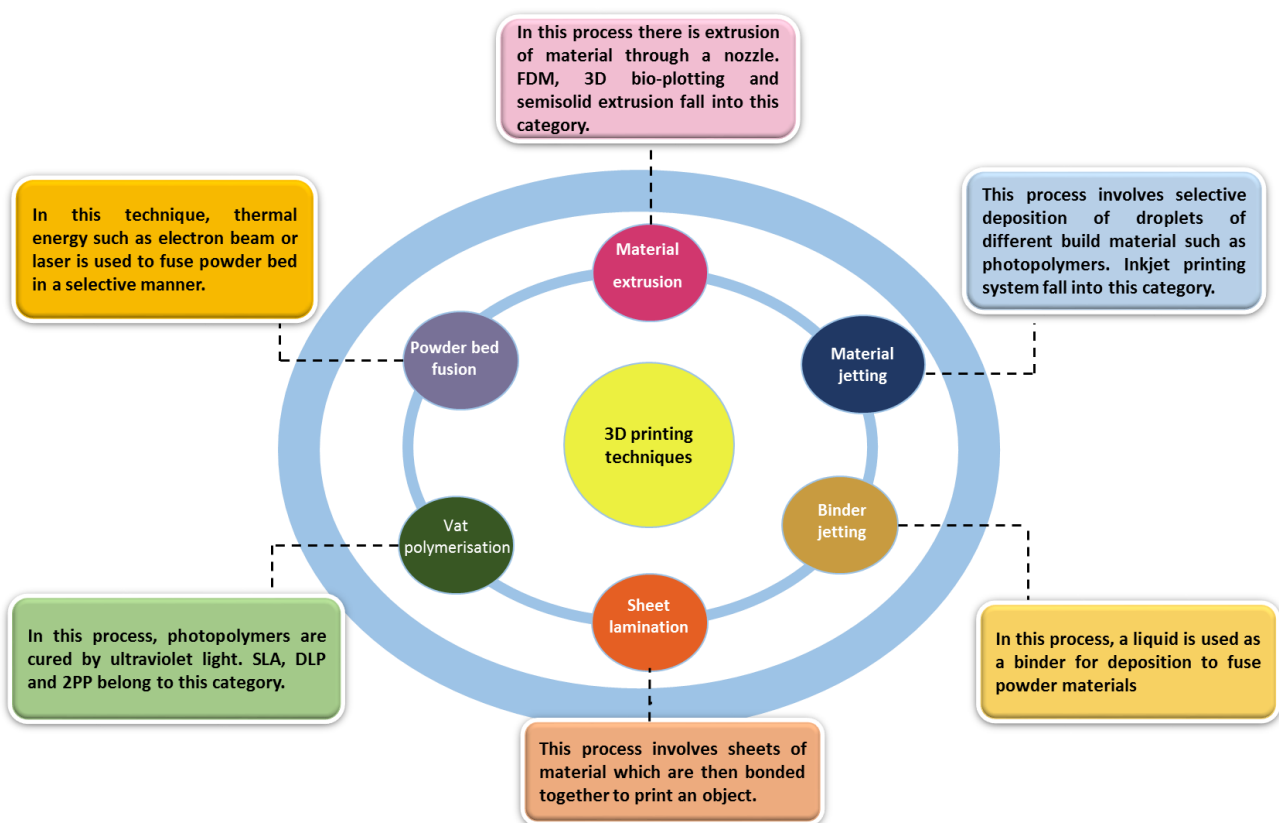


Figure 1.1: Types of 3D printing techniques and their brief description.

Although 3D printing is gaining huge importance and popularity by the researchers with the passage of time, it also has its challenges. The advantages along with the challenges of 3D printing technology are tabulated in the Table 1.2.

Table 1.2: Advantages and challenges of 3D printing technology.

Advantages	Challenges
<ul style="list-style-type: none"> • Small batches of customisable products are better than mass produced dosage forms. 	<ul style="list-style-type: none"> • Cost of the production.
<ul style="list-style-type: none"> • Does not require moulds and tools for switch over due to the 3D CAD models. 	<ul style="list-style-type: none"> • Need to change the way of using 3D printing.
<ul style="list-style-type: none"> • Provides digital files that are easy to share customise and modify. 	<ul style="list-style-type: none"> • Development of new standardise materials.
<ul style="list-style-type: none"> • Less wastage of material, waste material can be reused e.g., powder and resins. 	<ul style="list-style-type: none"> • Validate the thermal and mechanical properties of existing materials.
<ul style="list-style-type: none"> • Development of complex structures, geometrical shape is easy. 	<ul style="list-style-type: none"> • Improvement of manufacturing efficiency by automation of system.
<ul style="list-style-type: none"> • Produces final products of very low porosity. 	<ul style="list-style-type: none"> • Postprocessing procedure is required.
<ul style="list-style-type: none"> • Can provide direct interaction between the producer and the consumer. 	<ul style="list-style-type: none"> • Designer and engineers lack skills in 3D printing.

In this work, we have utilised fused deposition modelling (FDM) which is basically categorised as a material extrusion additive manufacturing technology. FDM was first invented and patented by Scott Crump in 1989 and after a while Stratasys company was founded marketing the first FDM 3D printers ^{26, 27}.

FDM printing requires filament as feeding material and is basically a three-step process which includes melting, extrusion, and solidification of the filament. Figure 1.2 shows schematic illustration of FDM. At first, filament is fed into the heated extruder by feeding gears, the filament get softens and then melts. The molten filament is then extruded through the nozzle which is then deposited onto the build plate in a layer-by-layer manner followed by the

solidification of the deposited material. To deposit the first layer, the nozzle moves in the X-Y plane ^{28, 29}, whereas the following layers are printed by moving the nozzle or the build plate in the Z-plane. The distance equivalent to the thickness of the layer is required by the nozzle or the build plate to move in Z-plane which is determined by the travelling speed, diameter and extruding speed of the nozzle ³⁰.

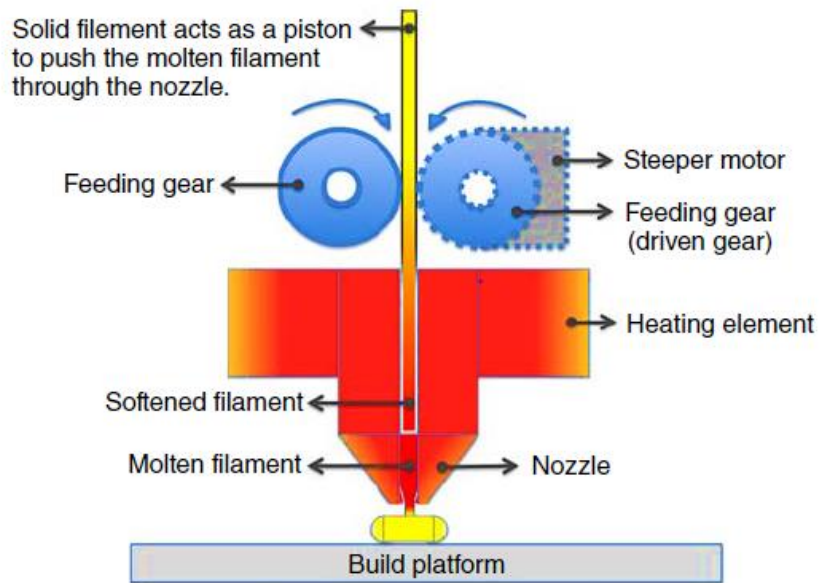


Figure 1.2: Schematic illustration of FDM printer.

The process of FDM printing is associated with different variables that affect the mechanical properties of the object to be printed. It is not only important but also essential to investigate the properties of the raw materials used in developing filaments. The processing parameters of printing also affect the performance and the mechanical properties of the printed object. A list of different variables related feeding material, processing parameters and printer machine are given in Table 1.3.

Table 1.3: Different variables that can affect the mechanical properties of the object to be printed.

Feeding material variables	processing parameters	Machine variables
<ul style="list-style-type: none"> Density and thermal characteristics of the raw materials 	<ul style="list-style-type: none"> Environmental conditions 	<ul style="list-style-type: none"> Model of the printer machine
<ul style="list-style-type: none"> Rheological properties 	<ul style="list-style-type: none"> Build orientation 	<ul style="list-style-type: none"> Diameter of extrusion nozzle
<ul style="list-style-type: none"> Concentration and miscibility of the raw materials used 	<ul style="list-style-type: none"> Extrusion temperature 	<ul style="list-style-type: none"> Software used
<ul style="list-style-type: none"> Diameter of the filament 	<ul style="list-style-type: none"> Infill density and pattern 	
<ul style="list-style-type: none"> Uniformity of the diameter of the filament 	<ul style="list-style-type: none"> Raster angle and width Layer thickness Amount of deposited material 	

It is one of the major advantages of FDM printing that its feeding material i.e., filament can be developed using hot-melt extrusion (HME) technique. In this process, material is fed through a barrel with rotating screws on a shaft at the required temperature. After rotating through the barrel, material is extruded through a nozzle die in the form of filaments^{31, 32}. A detailed illustration of the HME process in the manufacturing of the filament is shown in Figure 1.3.

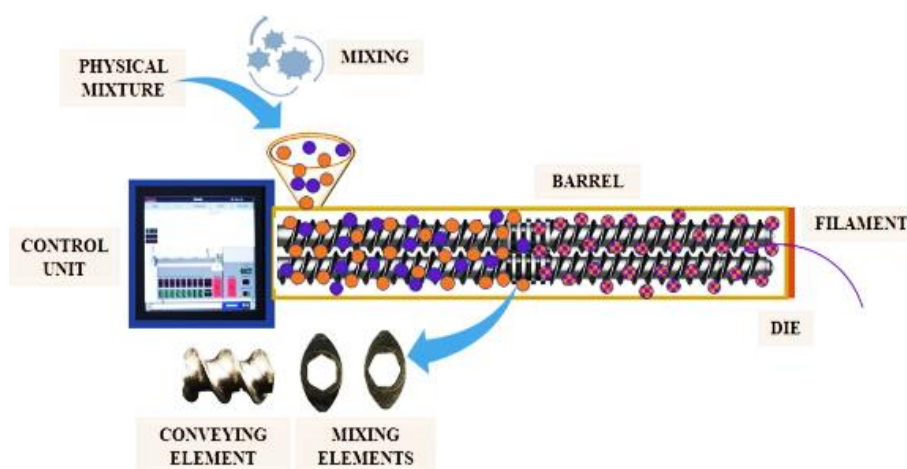


Figure 1.3: Schematic presentation of HME process for filament production.

Although HME and FDM are two separate techniques but require synchronisation i.e., if the former process does not work consequently, the later will also disrupt and the quality of the drug product will be compromised. The critical quality parameters of a drug product manufactured *via* HME-FDM coupling include mechanical properties of filaments, concentration of the active pharmaceutical ingredient (API), distribution of API, melt viscosity and FDM process parameters while printing. To check these parameters, process analytical technology tools (PAT) can be utilised for the process control and real-time monitoring ^{27, 33, 34}.

This process has been accepted by many researchers as a suitable method of developing filaments. Zhang et al., 2017, were successful in developing extended-release drug delivery system of acetaminophen by using HME coupled with FDM printing. Various polymers ethyl cellulose, HPMC, HPC Soluplus and Eudragit L100 were used for this purpose ³⁵. Likewise, Pereira GG et al., 2020 ³⁶, has also investigated various polymers that are suitable for HME-FDM coupled process. Recently, a literature review has been published explaining the suitability of HME coupled with FDM printing ³⁷. These research reports provide evidence that HME is a suitable process of developing filaments for FDM printing and provide an insight on suitable polymers and PAT tools for analysis purposes.

The key step of FDM printing is the extrusion process ³⁰ in which filament is inserted into the extruder and feeding gears drive the filament down to extrude through the nozzle basically acting as a piston. Therefore, melt viscosity and strength of the filament are the major properties of the filament among others for successful printing. For this purpose, the filament should be of optimum strength i.e., have enough toughness so that can be rolled up on the spool and enough stiffness so that can be pushed through the nozzle. However, filament should not be too brittle otherwise it will break when feeding through gears and will be difficult to collect on the spool. In the same manner, filament should not be too soft otherwise it will bend and would not roll through feeding gears.

Overall, the melt viscosity of the filament should be kept low because it helps in determining the drop in the pressure in the nozzle while extruding and the force required to push the melted material through the extruder nozzle. Nevertheless, the melt viscosity should not be too low that instead of extruding filament as a continuous rod it will extrude in the form of droplets. The extruded layers on the build plate should solidify rapidly to prevent structure

collapsing. However, very rapid solidification result in poor adhesion between the printed layers^{30, 38}. The surface roughness of the filament should also be considered while printing. Filament with moderate surface roughness provide essential friction that is required to push the filament through feeding gears³⁹ On the contrary, printing with filament having high surface roughness will be difficult due to high friction³⁵. To adjust the surface roughness of the filament a filler³⁹ to overcome the roughening, a non-melt drug⁴⁰ or blending of flexible materials³⁵ can be added for smoothening purposes. Moreover, the uniform size of the filament throughout its length is also important for precise dosing and fine structure of the object during printing⁴¹⁻⁴⁵. This is due to the fact that FDM printer deposit calculated amount of filament which is based on the diameter of the filament and is usually 1.75 mm for FDM printer⁴¹. The swelling properties of the polymer used, pulling speed and size of the die are used to determine the diameter of the extruded filament. All these factors should be kept in consideration and using a calibration device while extruding using HME can help in achieving filament of uniform size^{29, 46, 47}. A summary related to the key physicochemical properties of filaments intended for 3D printing applications are summarised in Table 1.4.

Table 1.4: key physicomechanical properties of filaments intended for 3D printing applications.

Criterion	Risk	Validation method	Required values	Proposed solution	References
Diameter	Unable to load the filament	Use of digital Vernier calliper, ultrasonic screw gauges, laser micrometre	1.75-3 mm	Choose right size of the nozzle	29
Diameter uniformity	Printing error Varying feed rate Deformed prints	Visual inspection Digital Vernier calliper	Diameter should be consistent throughout the length	Lubricants should be used	48
Stiffness	Difficult to collect the filament on the spool Difficult to exit from the print head	Mechanical analysis Texture and flexure testing	~ 1000 N/m	Using polymer blends helps	30, 35
Brittleness	Does not allow proper loading of the filament Can break inside the extruder or during printing	Tensile and torsional strength	~0.15-0.2% Pa (10^4)	Use plasticisers	49
Softness	Can easily compress between the driving gears and leads to printing failure	Tensile strength and shore hardness	-	Decrease the amount of plasticiser	48, 49

The extrusion process which requires temperature can act as a limitation when dealing with pharmaceutical products. It can potentially cause thermal degradation of the drug. Though the researchers have reduced the printing temperature 200-230 °C to 100-170 °C when using polyvinyl alcohol (PVA) and polylactic acid (PLA) but the thermal degradation of drug was still observed ³⁸.

There is another major limitation regarding feeding material for FDM printing i.e. the pharmaceutical grade polymers approved by the FDA have poor thermoplasticity and requires particular mechanical properties as mentioned above. Acrylonitrile butadiene styrene (ABS), PVA, PLA and polycaprolactone (PCL) are commonly used and commercially available filaments for FDM printing. These polymers have good flexibility, stiffness and thermoplasticity. Nevertheless, PCL and PLA are not very suitable polymeric material when developing pharmaceutical dosage forms and ABS has toxicity. PVA is highly soluble in water and was therefore used to print oral dosage form. Drug was loaded into PVA filament by soaking the filament in the drug solution followed by the process of drying. This resulted in very low drug loading; however, it was overcome by using hot-melt extrusion method to prepare drug loaded filaments with high drug loading.

Since 2015, many research studies have focused on the application of pharmaceutical grade polymers in FDM 3D printing. Most of the pharmaceutical polymers were successfully printed into various dosage forms with immediate or controlled release behaviour such as hydroxypropyl cellulose (HPC) and Eudragit RL and RS ⁴⁰, PLA ^{50, 51}, PVA ^{52, 53}, polyvinylpyrrolidone (PVP) ⁵⁴, methacrylate, hydroxypropyl cellulose ⁵⁵, hydroxypropyl methylcellulose acetate succinate (HPMCAS) ⁵⁶, acrylonitrile butadiene styrene ⁵⁷, PCL ⁵⁸, ethyl cellulose ⁵⁹, hydroxypropyl methyl cellulose (HPMC) ³⁵ and ethyl vinyl acetate ²⁸.

Despite the limitations, FDM is a low-cost technology and since 2000, it has been the most used additive manufacturing worldwide. The extrusion techniques other than FDM involves printing via syringe-based tool-head. Fabrication of polypills containing five drugs in one tablet ⁶⁰ and bilayer tablets ⁶¹ have been reported via this technique, however, this technique is time consuming as it involves drying process post-printing and produce tablets of high friability ^{61, 62}. FDA granted 3D printed tablets available in the United States market are based on powder-bed printing technique ³⁹. The drawback is that tablets produced via this technique exhibit surface imperfections and poor mechanical properties ^{63, 64}.

FDM printing, on the other hand, offers objects with stable mechanical properties and yields tablets of less or negligible friability⁴⁰. This technique requires filament feeding to print objects. Loading of drugs into commercially available filaments and extrusion of drug-loaded filaments via hot-melt extrusion using pharmaceutical grade polymer has been explored^{65, 66}.

To aid the processing conditions of extrusion and printing, plasticisers such as polyethylene glycol, triacetin and triethyl citrate are frequently used^{67, 68, 69}. The inclusion of plasticiser into the polymer system increases the free volume between polymer chains thereby allowing the segments of the chain to rotate and move more freely thus improving the stretchability and flexibility⁷⁰.

However, the use of plasticisers in developing pharmaceutical dosage forms is not beneficial as it can affect the gastric motility which can alter the gastrointestinal transit time thus affecting the drug absorption. These findings become more important and serious where patients are on life-long pharmacotherapy for example in the case of chronic diseases. Long-term exposure to plasticiser will affect the drug absorption thus failing to achieve therapeutic effect resulting in poor patient compliance and adherence⁷¹.

The major constraints of this technique are the extremely limited number of FDM printable materials currently available and the use of plasticiser. The researchers have investigated the feasibility of pharmaceutical grade polymers for FDM printing and are using plasticisers^{40, 55, 72}. Food and Drug Administration has not listed any pharmaceutical polymer suitable for FDM printing. Moreover, the drug-loaded filaments feasible for FDM printing are not available commercially and researchers are loading drug onto ready-made plastic filaments such as PLA and ABS. Therefore, our aim is to investigate the feasibility of different polymers for hot-melt extrusion (HME) and for FDM printing and to develop plasticiser free filament for FDM printing of personalised drug delivery systems.

1.2. Aim and objectives

The aim of our research work is to understand and explore the novel technological and material insights for the development of personalised drug delivery systems. For this purpose, the research work was divided into two phases. Each phase consisted of literature search and experimental work.

Phase I: Proof of concept

- **Literature search:** To systematically review the role of 3D printing technology in developing personalised dosage forms, to investigate the which materials have been used by researchers for HME and FDM and to collect evidence whether any study have addressed drug absorption challenges caused by plastic induced gastric motility.
- **Experimental work:** Development and characterisation of plasticiser-free HPMC polymers-based filaments using HME intended for FDM printing.

Phase II: Proof validity

- **Literature search:** To systematically review the drug delivery routes available for the treatment of overactive bladder syndrome.
- **Experimental work:** Development of gastroretentive drug delivery system for overactive bladder syndrome.

The schematic illustrating the objectives is given in the Figure 1.4.

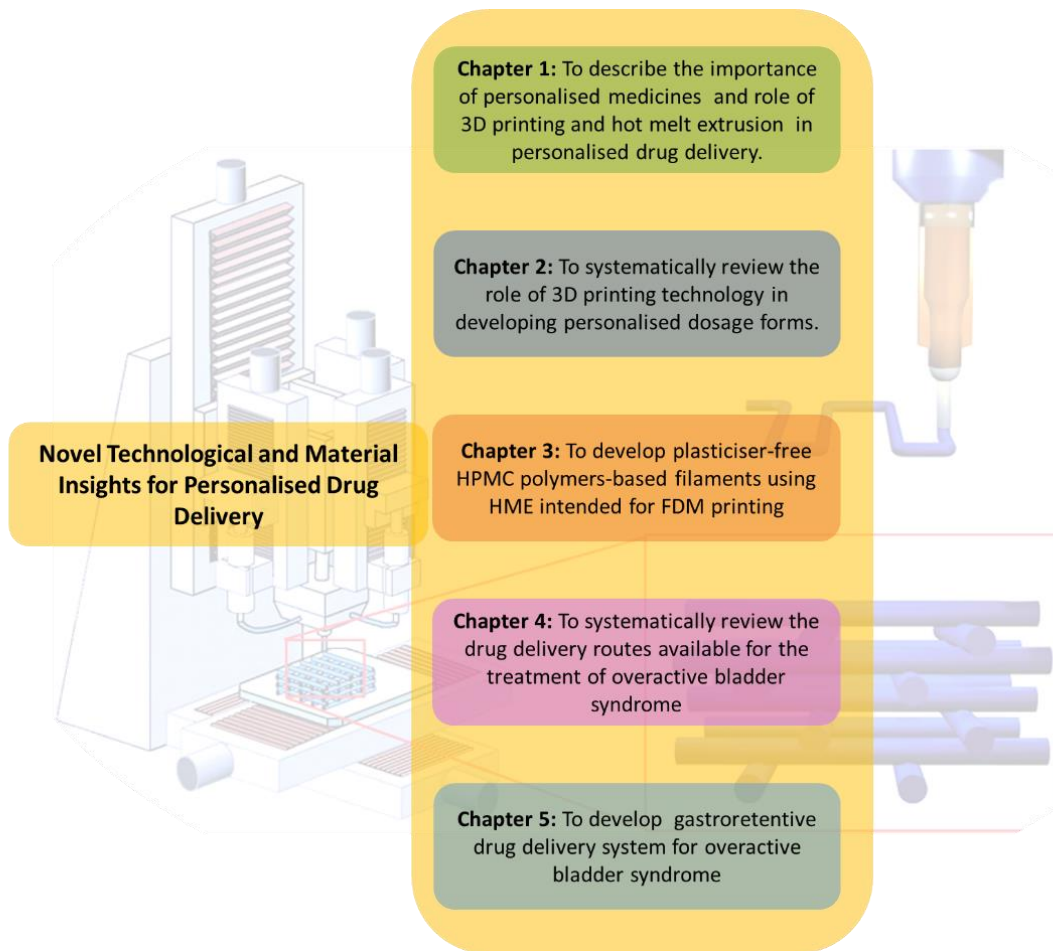


Figure 1.4: Schematic illustrating the aim and objectives of the thesis.

1.3. Thesis structure

Phase I: Proof of concept phase

This phase consisted of two parts i.e., literature search and the experimental work. In the first part a comprehensive systematic review was carried out to investigate the role of 3D printing technologies in developing personalised drug delivery system and to observe if there is any study addressing the effect of plasticiser induced gastric motility on drug absorption. The first part provided basis for the experimental work by confirming that none of the studies was addressing that problem. The second part then consisted of extrusion of plasticiser free filaments and tablet printing.

Chapter 2

An elaborative systematic review on the pharmaceutical applications of 3D printing technologies was conducted. This chapter describes the searching criteria, search terms, search engines used, the selecting criteria, data extraction, and quality assessment processes applied. The importance of personalised drug delivery and how 3D printing technologies can help in developing personalised drug delivery devices was thoroughly investigated. The different types of 3D printing technologies available and their principal mechanism were also explored. It provides an elaborative overview of pharmaceutical applications of 3D printing. The advantages and disadvantages of 3D printing technologies, the regulatory challenges the technology is facing, and the future aspects were also discussed.

Chapter 3

Three different grades of hydroxypropyl methyl cellulose were used in developing extended-release drug delivery system for the delivery of anti-diabetic drug, glipizide. The extrusion of plasticiser free filaments using hot melt extrusion and employment of those filaments in developing tablets using FDM has been explained in detail. The physicochemical characterisation of filaments and the developed tablet followed by *In vitro* and *in vivo* drug release studies were also carried out.

Phase II: Proof validity

To further strengthen and ensure validity of our concept, we targeted another chronic condition i.e., OAB. At first, a systematic review was carried out to find out which drug delivery administration route should be used and which drugs are used for the treatment of OAB. The literature search provided basis for the experimental work and gastroretentive floating drug delivery system for oral administration of gabapentin was developed using plasticiser free PEO filaments.

Chapter 4

A comprehensive systematic review was conducted on the various drug delivery strategies used in the practice to manage overactive bladder (OAB). A brief overview of what is overactive bladder syndrome and how it affects the quality of life was provided. The searching criteria, search terms, search engines used, the selecting criteria, data extraction, and quality assessment processes applied has been explained. The importance of different drug delivery routes used for the administration of the drugs and drugs used in the management of OAB were investigated.

Chapter 5

The absorption related challenges of gabapentin, an effective drug for the treatment of OAB, were addressed by developing gastroretentive floating drug delivery system with extended drug release via FDM printing using plasticiser-free PEO filaments. Tablets were printed with varying infill density and shell number to develop intragastric floating tablets. The physicochemical characterisation of the filaments and the printed tablets, the *in vitro* floating and drug release testing and the pharmacokinetic parameters were also studied.

References

1. M. M. Reidenberg, *Clinical Pharmacology & Therapeutics*, 2003, **74**, 197.
2. D. J. Crommelin, G. Storm and P. Luijten, *International journal of pharmaceuticals*, 2011, **415**, 5.
3. A. T. Florence and V. H. Lee, *International journal of pharmaceuticals*, 2011, **415**, 29.
4. A. T. Florence, *An introduction to clinical pharmaceuticals*, Pharmaceutical press, 2010.
5. Z. Khizer, M. R. Akram, R. M. Sarfraz, J. S. Nirwan, S. Farhaj, M. Yousaf, T. Hussain, S. Lou, P. Timmins and B. R. Conway, *Polymers*, 2019, **11**, 1095.
6. J. S. Cohen, *Journal of the American Pharmacists Association*, 2002, **42**, 160.
7. R. Tutton, *Social Science & Medicine*, 2012, **75**, 1721.
8. H. Kadry, T. A. Al-Hilal, A. Keshavarz, F. Alam, C. Xu, A. Joy and F. Ahsan, *International Journal of Pharmaceuticals*, 2018, **544**, 285.
9. N. Sandler, A. Määttänen, P. Ihalainen, L. Kronberg, A. Meierjohann, T. Viitala and J. J. J. o. p. s. Peltonen, 2011, **100**, 3386.
10. M. Alomari, F. H. Mohamed, A. W. Basit and S. Gaisford, *International Journal of Pharmaceuticals*, 2015, **494**, 568.
11. J. S. Cohen, *Postgraduate medicine*, 1999, **106**, 163.
12. A. Herxheimer, *The Lancet*, 1991, **337**, 346.
13. R. W. Pies, *The Journal of clinical psychiatry*, 1995.
14. K. Beebe and A. D. Kennedy, *Computational and structural biotechnology journal*, 2016, **14**, 97.
15. K. Wening and J. Breikreutz, *International journal of pharmaceuticals*, 2011, **404**, 1.
16. B. M. Wu, S. W. Borland, R. A. Giordano, L. G. Cima, E. M. Sachs and M. J. Cima, *Journal of Controlled Release*, 1996, **40**, 77.
17. K. Sanderson, *Pharm J*, 2015, **294**, 598.
18. Y. E. Choonara, L. C. du Toit, P. Kumar, P. P. Kondiah and V. Pillay, *Expert review of pharmacoeconomics & outcomes research*, 2016, **16**, 23.
19. C. L. Ventola, *Pharmacy and Therapeutics*, 2014, **39**, 704.
20. A. Gebhardt, *Carl Hanser, München*, 2007.
21. A. Popelka, P. Sobolčiak, M. Mrlík, Z. Nogellova, I. Chodák, M. Ouederni, M. A. Al-Maadeed and I. Krupa, *Emergent Materials*, 2018, **1**, 47.
22. C. Bosqué, *Rapid Prototyping Journal*, 2015.
23. M. B. Hoy, *Medical reference services quarterly*, 2013, **32**, 93.
24. J. Goole and K. Amighi, *International journal of pharmaceuticals*, 2016, **499**, 376.
25. S. C. Ligon, R. Liska, J. r. Stampfl, M. Gurr and R. Mülhaupt, *Chemical reviews*, 2017, **117**, 10212.
26. S. S. Crump, *Journal*, 1992.
27. S. C. Ligon, R. Liska, J. r. Stampfl, M. Gurr and R. J. C. r. Mülhaupt, 2017, **117**, 10212.
28. N. Genina, J. Holländer, H. Jukarainen, E. Mäkilä, J. Salonen and N. Sandler, *European Journal of Pharmaceutical Sciences*, 2016, **90**, 53.

29. A. Melocchi, F. Parietti, G. Loreti, A. Maroni, A. Gazzaniga and L. Zema, *Journal of Drug Delivery Science and Technology*, 2015, **30**, 360.
30. M. Alhijaj, P. Belton and S. Qi, *European Journal of Pharmaceutics and Biopharmaceutics*, 2016, **108**, 111.
31. M. A. Repka, S. Bandari, V. R. Kallakunta, A. Q. Vo, H. McFall, M. B. Pimparade and A. M. Bhagurkar, *International journal of pharmaceutics*, 2018, **535**, 68.
32. R. Censi, M. R. Gigliobianco, C. Casadidio and P. Di Martino, *Pharmaceutics*, 2018, **10**, 89.
33. Z. Rahman, S. F. B. Ali, T. Ozkan, N. A. Charoo, I. K. Reddy and M. A. Khan, *The AAPS journal*, 2018, **20**, 1.
34. S. M. Dadou, Z. Senta-Loys, A. Almajaan, S. Li, D. S. Jones, A. M. Healy, Y. Tian and G. P. Andrews, *International journal of pharmaceutics*, 2020, **584**, 119382.
35. J. Zhang, X. Feng, H. Patil, R. V. Tiwari and M. A. Repka, *International journal of pharmaceutics*, 2017, **519**, 186.
36. G. G. Pereira, S. Figueiredo, A. I. Fernandes and J. F. Pinto, *Pharmaceutics*, 2020, **12**, 795.
37. D. K. Tan, M. Maniruzzaman and A. Nokhodchi, *Pharmaceutics*, 2018, **10**, 203.
38. A. Goyanes, U. Det-Amornrat, J. Wang, A. W. Basit and S. Gaisford, *Journal of controlled release*, 2016, **234**, 41.
39. M. Sadia, A. Sośnicka, B. Arafat, A. Isreb, W. Ahmed, A. Kelarakis and M. A. Alhnan, *International journal of pharmaceutics*, 2016, **513**, 659.
40. K. Pietrzak, A. Isreb and M. A. Alhnan, *European Journal of Pharmaceutics and Biopharmaceutics*, 2015, **96**, 380.
41. J. J. Water, A. Bohr, J. Boetker, J. Aho, N. Sandler, H. M. Nielsen and J. Rantanen, *Journal of Pharmaceutical Sciences*, 2015, **104**, 1099.
42. R. O. Williams III, A. B. Watts and D. A. Miller, *Formulating poorly water soluble drugs*, Springer, 2016.
43. B. Wang, D. Wang, S. Zhao, X. Huang, J. Zhang, Y. Lv, X. Liu, G. Lv and X. Ma, *European Journal of Pharmaceutical Sciences*, 2017, **96**, 45.
44. Y. Kojo, S. Matsunaga, H. Suzuki, H. Sato, Y. Seto and S. Onoue, *European Journal of Pharmaceutical Sciences*, 2017, **97**, 55.
45. C. Yewale, H. Tandel, A. Patel and A. Misra, in *Applications of Polymers in Drug Delivery*, Elsevier, 2021, pp. 131.
46. A. Melocchi, F. Parietti, A. Maroni, A. Foppoli, A. Gazzaniga and L. Zema, *International journal of pharmaceutics*, 2016, **509**, 255.
47. A. Maroni, A. Melocchi, F. Parietti, A. Foppoli, L. Zema and A. Gazzaniga, *Journal of Controlled Release*, 2017, **268**, 10.
48. E. Fuenmayor, M. Forde, A. V. Healy, D. M. Devine, J. G. Lyons, C. McConville and I. Major, *Pharmaceutics*, 2018, **10**, 44.
49. L. K. Prasad and H. Smyth, *Drug development and industrial pharmacy*, 2016, **42**, 1019.

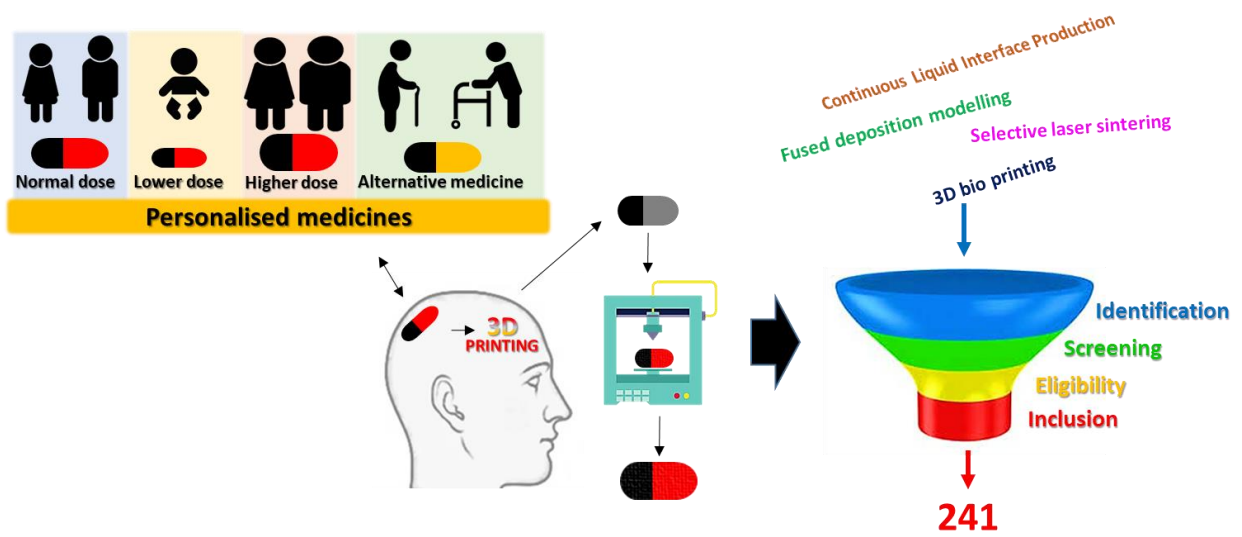
50. A. Goyanes, J. Wang, A. Buanz, R. Martínez-Pacheco, R. Telford, S. Gaisford and A. W. J. M. p. Basit, 2015, **12**, 4077.
51. A. Goyanes, H. Chang, D. Sedough, G. B. Hatton, J. Wang, A. Buanz, S. Gaisford and A. W. Basit, *International journal of pharmaceuticals*, 2015, **496**, 414.
52. M. Adamkiewicz and B. Rubinsky, *Cryobiology*, 2015, **71**, 518.
53. J. A. Baird and L. S. Taylor, *Advanced Drug Delivery Reviews*, 2012, **64**, 396.
54. T. C. Okwuosa, D. Stefaniak, B. Arafat, A. Isreb, K.-W. Wan and M. A. Alhnan, *Pharmaceutical research*, 2016, **33**, 2704.
55. L. Ruiz-Cantu, A. Gleadall, C. Faris, J. Segal, K. Shakesheff and J. Yang, *Biofabrication*, 2016, **8**, 015016.
56. A. Goyanes, F. Fina, A. Martorana, D. Sedough, S. Gaisford and A. W. Basit, *International journal of pharmaceuticals*, 2017, **527**, 21.
57. Z. Wang, J. Wang, M. Li, K. Sun and C.-j. Liu, *Scientific reports*, 2014, **4**, 5939.
58. J. Holländer, N. Genina, H. Jukarainen, M. Khajeheian, A. Rosling, E. Mäkilä and N. Sandler, *Journal of pharmaceutical sciences*, 2016, **105**, 2665.
59. W. Kempin, C. Franz, L.-C. Koster, F. Schneider, M. Bogdahn, W. Weitschies and A. Seidlitz, *European Journal of Pharmaceutics and Biopharmaceutics*, 2017, **115**, 84.
60. S. A. Khaled, J. C. Burley, M. R. Alexander, J. Yang and C. J. Roberts, *Journal of controlled release*, 2015, **217**, 308.
61. S. A. Khaled, J. C. Burley, M. R. Alexander and C. J. Roberts, *International journal of pharmaceuticals*, 2014, **461**, 105.
62. W. Katstra, R. Palazzolo, C. Rowe, B. Giritlioglu, P. Teung and M. Cima, *Journal of controlled release*, 2000, **66**, 1.
63. W. E. Katstra, R. D. Palazzolo, C. W. Rowe, B. Giritlioglu, P. Teung and M. J. Cima, *Journal of Controlled Release*, 2000, **66**, 1.
64. D.-G. Yu, C. Branford-White, Y.-C. Yang, L.-M. Zhu, E. W. Welbeck and X.-L. Yang, *Drug Development and Industrial Pharmacy*, 2009, **35**, 1530.
65. A. Goyanes, A. B. Buanz, G. B. Hatton, S. Gaisford and A. W. Basit, *European Journal of Pharmaceutics and Biopharmaceutics*, 2015, **89**, 157.
66. J. Skowyra, K. Pietrzak and M. A. Alhnan, *European Journal of Pharmaceutical Sciences*, 2015, **68**, 11.
67. A. Goyanes, U. Det-Amornrat, J. Wang, A. W. Basit and S. Gaisford, *Journal of Controlled Release*, 2016, 234, 41.
68. R. Beck, P. Chaves, A. Goyanes, B. Vukosavljevic, A. Buanz, M. Windbergs, A. Basit and S. Gaisford, *International journal of pharmaceuticals*, 2017, 528, 268.
69. W. Kempin, C. Franz, L.-C. Koster, F. Schneider, M. Bogdahn, W. Weitschies and A. Seidlitz, *European Journal of Pharmaceutics and Biopharmaceutics*, 2017, 115, 84.
70. Z. Khizer, M. R. Akram, R. M. Sarfraz, J. S. Nirwan, S. Farhaj, M. Yousaf, T. Hussain, S. Lou, P. Timmins and B. R. Conway, *Polymers*, 2019, **11**, 1095.

71. H. Lim and S. W. Hoag, *AAPS PharmSciTech*, 2013, 14, 903.
72. A. L. Sarode, H. Sandhu, N. Shah, W. Malick and H. Zia, *European Journal of Pharmaceutical Sciences*, 2013, **48**, 371.

CHAPTER 2

3D printed patient centric medicines: a systematic review

Graphical abstract



Notes for readers

- 3D printing is an additive manufacturing technique which facilitates the transformation of a 3D digital model to a physical model through layer-by-layer printing.
- Over the past few years, 3D printing technologies have brought evolution in the pharmaceutical manufacturing sector with enormous potential of providing digital dosage form designing and patient centric medicines.
- The aim of this review was to identify the research studies contributing to the practicability of 3D printing technologies in developing novel personalised drug delivery devices.
- The review was conducted following preferred reporting items for systematic reviews and meta-analyses guidelines. A total of 241 studies were included and were further categorised according to the types of 3D printing technologies.
- The review found that various technologies (extrusion-based, Vat polymerisation, powder bed fusion and jetting techniques) have been used and their pharmaceutical applications are promising and commendable, nevertheless, the outcomes illustrated the marked potential of fused deposition modelling (FDM), an extrusion-based technology.
- The review has comprehensively outlined the role of these technologies which will be helpful for researchers in the future. The merits and demerits were tabulated and an insight into the limitations, excipients employed, and regulatory challenges were also discussed which concludes that despite making hefty achievements, 3D printing technologies must face regulatory and technical challenges before mainstream adoption in the pharmaceutical industry.

2. 3D printed patient centric medicines: a systematic review

2.1. Introduction

3D printing is steering the course of traditional manufacturing of pharmaceutical products toward the production of digital and personalised drug delivery devices to treat patients individually with better therapeutic outcomes ^{1, 2}. It is because of the advantages that 3D printing resides over conventional manufacturing methods such as on-demand manufacturing, ability to design and print complex but sophisticated solid dosage forms, adjustment of doses as per patient's requirement, overall customisation of the medicines, high acceptability and cost-effectiveness, that "one-size-fits-all" approach is coming to its expiration ¹.

Moreover, 3D printing is a highly flexible manufacturing method that could improve the whole process of medicine development. Due to its ability to readily adjust doses, it could be beneficial in the initial phases of drug development such as preclinical studies. These studies consist of *in vivo* testing of drugs involving wide range of doses with the purpose of investigating various parameters including safety, toxicology, efficacy, tolerability and pharmacokinetic parameters ³. All these beneficial prospects of 3D printing point towards the accelerated development of this modernised manufacturing technology over the coming years with the goal of improving the quality of patient's life.

In the recent years, researchers have shown great interest in utilising 3D printing technology in the development of various drug delivery devices ⁴. This chapter describes the pharmaceutical applications of 3D printing technologies and how these technologies has been used to develop drug delivery devices with complex geometry, accommodating multiple drugs in a single dosage form, drug delivery devices with multi-release kinetics, dose adjustment by varying size of the dosage form, to minimise the side effects and maximise the therapeutic effect. It also provides an overview of the various materials that has been used in the development of drug delivery devices via 3D printing. This chapter also highlights the main 3D printing technologies that are commonly used for the development of pharmaceutical products. The overall aim of this review is to report the advancements in pharmaceutical products developed via 3D printing technologies that are facilitating advances required for personalised drug delivery. In addition to this, we also aimed to observe that if there is any

study that is addressing the effect of plasticiser induced gastric motility on the drug absorption while using plasticiser in the pharmaceutical formulation to aid the process of HME and FDM printing.

Although 3D printing technology presents countless economic and medical advantages, nevertheless, there are regulatory and technical challenges that restricts the regular commercialisation of the 3D printed products. Subsequently, a continuous refinement and novelty in 3D printing methods are required to overcome the challenges and limitations to facilitate personalised and on-demand drug delivery devices for health care in the future. This review, therefore aimed at collating the literature focused on 3D printing technologies employed to manufactured patient centric medicines using systematic approach using PRISMA (preferred reporting items for systematic reviews and meta-analyses) guidelines. Moreover, this review presents the advantages, limitations, regulatory challenges of 3D printing technologies and also discusses the future prospects and outlook of 3D printing in pharmaceutical dosage form manufacturing.

2.2. Methodology

2.2.1. Search plot, information sources and screening process

The search plot, which includes identification, screening, eligibility, and inclusion as its key determinants. A systematic search of published research studies from January 2004 to April 2021 was carried out. An inclusive search plot based on EMBASE, PubMed, MEDLINE and Scopus and Google Scholar databases was established. The primary authors conducted the search using the following search terms; “3D printing” AND “3D printing in drug delivery” OR “3D printing in pharmacy” OR “3D printed medicine”. Titles and abstracts of the resultant studies were screened, and the studies irrelevant to the rationale of the current systematic review were excluded. The full texts of the remaining studies were then screened thoroughly, and their eligibility was assessed.

2.2.2. Study selection

The primary investigators independently evaluated the suitability of eligible studies. The full text was screened against the rationale of the systematic review by two reviewers. Any disagreements and differences of opinion among reviewers over the eligibility of a particular

study were resolved through a comprehensive mutual discussion. To be included, a study must include the use of 3D printing technology for the development of drug delivery system, active pharmaceutical ingredient, and the subsequent drug release testing. Any study that did not fulfil this criterion was excluded. The studies that were employing 3D printing in developing drug delivery devices but did not contain any active pharmaceutical ingredient for the *in vitro* or *in vivo* drug release studies were excluded.

2.2.3. Data extraction and collection

The data was extracted from all the eligible studies using a form adopted from Khizer et al., 2021⁵, Table 2.1. The extracted information was subsequently tabulated using Microsoft Word 2019 following an already published method⁵⁻⁸. The extracted information includes active pharmaceutical ingredient used, drug delivery route, *in vitro/in vivo* studies, excipients, and study characteristics.

Table 2.1: Form used for the data extraction from eligible studies.

Study parameters	Description
Study ID	
Active pharmaceutical ingredient (API)	
Drug delivery route	
Investigation type (<i>in-vitro</i> or <i>in-vivo</i> , <i>animal model</i>)	
Used excipients	
Study characteristics	
Reference	

2.2.4. Risk of bias assessment

To assess the risk of bias in the studies included in the current systematic review, various well-established tools or criteria were investigated (Table 2.2). After a thorough check, none of those well-established criteria fully fitted to the rationale and scope of our systematic review, albeit they all were substantial and well-detailed. In this case, a personalised approach was adopted i.e., a customised bias assessment criterion was developed based on the standard quality assessment criteria that matched with the rationale of our systematic review for

evaluating primary research papers from different fields⁹⁻¹¹ adopting the redundancy and mapping approach^{7, 12, 13}. The customised criterion, given in the Tables 2.3 and 2.4, was applied for assessing the risk of bias in the included studies. The risk of bias was assessed in research rationale, methodology, results, discussion of results and conclusion sections of each study. The primary author carried out initial investigation individually; however, the final recommendation to each study was assigned after detailed discussion and the results are summarised in the Tables 2.5-2.8.

Table 2.2: List of various quality assessment and risk of bias assessment tools considered.

Number	Risk of bias/quality assessment frameworks
1	Academy of Nutrition & Dietetics/American Dietetic Association Quality Criteria Checklist
2	Critical Skills Appraisal Program (CASP) Checklists
3	Clinical Trials Assessment Measure
4	Cochrane Back Review Group Methods 2009
5	Cochrane Effective Practice and Organisation of Care (EPOC) Tools
6	Cochrane Handbook
7	Cochrane Risk of Bias Tool
8	Cochrane Risk of Bias Tool 2.0
9	Downs and Black
10	GRADE approach
11	Jadad Scale
12	Joanna Briggs Institute Critical Appraisal Tools
13	Kratochwill et al. (2010) recommended criteria
14	Mixed Methods Appraisal Tool (MMAT)
15	Modified Coleman Methodology Scores
16	National Health and Medical Research Council (Australian Government) Scale
17	NICE Checklists (National Institute for Health and Care Excellence)
18	National Heart, Lung, and Blood Institute (NHLBI) Quality Assessment Tools
19	OSTEBA statements (Basque Office for Health Technology Assessment)
20	Oxford Center for Evidence-based Medicine Levels of Evidence (CEBM)
21	PEDro (Physiotherapy Evidence Database) Scale
22	Rosendal scale
23	SIGN (Scottish Intercollegiate Guidelines Network) Checklist for Cohort Studies
24	Standard quality assessment criteria for evaluating primary research papers from a variety of fields
25	STROBE (Strengthening The Reporting of Observational Studies in Epidemiology)
26	Tool for the assessment of Study quality and reporting in Exercise (TESTEX)

Table 2.3: Detailed description of risk of bias assessment process.

Study area	Description	Reviewer's judgement
Research rationale	Explanation of research rationale including aim and objectives, allowing sufficient knowledge to facilitate the decision-making process.	Was research rationale (hypothesis and/or aim and/or objectives) adequately described?
Description of methodology	Methodology of the experiments are described adequately allowing sufficient knowledge to facilitate the decision-making process and there are probable chances of replication.	Was research methodology adequately/sufficiently described?
Characterisation and testing	Characterisation and testing techniques are relevant and described in sufficient detail that there are probable chances of replication.	Were research characterisation and testing techniques adequately/sufficiently described?
Description of results	Results are described in sufficient detail, allowing sufficient knowledge to facilitate the decision-making process.	Were results adequately/sufficiently described?
Description of discussion	Results are plausibly discussed, allowing sufficient knowledge to facilitate the decision-making process.	Were results discussed adequately/sufficiently described?
Description of conclusions	Conclusions are described in accordance with set hypothesis, allowing sufficient knowledge to facilitate the decision-making process.	Were conclusions adequately/sufficiently described and relevant to rationale?
Other source of bias	Any other important concerns not addressed on the described key areas of the present tool.	Was study free of any unexpected problem?

Table 2.4: Summary of an approach for assessing the risk of bias within and across studies.




Risk of bias	Sign	Interpretation	Within study	Across study
Low		Probable bias evidence implausible to seriously affect the findings with no impact on confidence	All major areas have low risk of bias	Most of the studies are found to have low risk of bias, not impact the result interpretation process.
Unclear		Probable bias evidence to raise doubts regarding findings with mild to moderate impact on confidence	One or more areas of the study has unclear risk of bias.	Most of the studies are found to have low/or unclear risk of bias, not impact the result interpretation process.
High		Probable bias evidence seriously affecting the findings with high impact on confidence	One or more areas of the study has high risk of bias.	High proportion of studies have high risk of bias, sufficiently impacting the result interpretation process.

Table 2.5: Assessment of risk of bias for studies based on extrusion technique included in the systematic review

Study ID	Risk of bias parameters					
	Research rationale	Description of methods	Characterisation and testing	Description of results	Discussion	Overall conclusions
(Masood, 2007) ¹⁸	+	+	+	+	+	+
(Goyanes et al., 2014) ¹⁹	+	+	+	+	+	+
(Goyanes, Buanz, et al., 2015) ²⁰	+	+	+	+	+	+
(Chai et al., 2017) ²¹	+	+	+	+	+	+
(Kimura et al., 2019) ²²	+	+	+	+	+	+
(Lamichhane et al., 2019) ²³	+	+	+	+	+	+
(Q. Li et al., 2018) ²⁴	+	+	+	+	+	+
(Boetker et al., 2016) ²⁵	+	?	+	+	+	+
(Khizer et al., 2019) ²⁶	+	+	+	+	+	+
(Shi et al., 2021) ²⁷	+	+	+	+	+	+

(Korte & Quodbach, 2018) ²⁸	+	+	+	+	+	+
(Kadry et al., 2018) ²⁹	+	+	+	+	?	+
(Christos I Gioumouxouzis et al., 2017) ³⁰	+	+	+	+	+	+
(Tagami et al., 2017) ³¹	+	+	+	+	+	?
(Melocchi et al., 2016) ³²	+	+	+	+	+	+
(Öblom et al., 2019) ³³	+	+	+	+	+	+
(Isreb et al., 2019) ³⁴	+	+	+	+	+	+
(Saviano et al., 2019) ³⁵	+	+	?	+	+	+
(Yan Yang et al., 2018) ³⁶	+	+	+	+	?	+
(J. Zhang, W. Yang, et al., 2017) ³⁷	+	+	+	+	+	?
(Skowyra et al., 2015) ³⁸	+	+	+	+	+	+
(Korte et al., 2018) ³⁹	+	+	?	+	+	+
(Cerda et al., 2020) ⁴⁰	+	+	+	+	+	+
(Ayyoubi et al., 2021) ⁴¹	+	+	+	?	+	+
(Goyanes, Martinez, et al., 2015) ⁴²	+	+	+	+	+	+
(Xiaowen Xu et al., 2019) ⁴³	+	+	+	+	+	+
(Tan et al., 2020) ⁴⁴	+	+	+	+	+	+
(Q. Li et al., 2017) ⁴⁵	+	?	+	+	+	+

(Goyanes, Wang, et al., 2015) ⁴⁶	+	+	+	+	+	+
(Sadia, Arafat, et al., 2018) ⁴⁷	+	+	+	+	+	+
(Smith et al., 2018) ⁴⁸	+	+	+	+	?	+
(Arafat, Wojsz, et al., 2018) ⁴⁹	+	+	+	+	?	+
(Genina et al., 2017) ⁵⁰	+	+	+	+	+	+
(Markl et al., 2017) ⁵¹	+	+	?	+	+	+
(Goyanes, Chang, et al., 2015) ⁵²	+	+	+	?	+	+
(Okwuosa et al., 2017) ⁵³	+	+	+	+	+	+
(Christos I. Gioumouxouzis et al., 2020) ⁵³	+	+	+	+	+	+
(Fina et al., 2020) ⁵⁴	+	+	+	+	+	+
(Christos I Gioumouxouzis, Chatzitaki, et al., 2018) ⁵⁵	+	+	+	+	+	+
(Goyanes et al., 2017) ⁵⁶	+	?	+	+	?	+
(Goyanes, Kobayashi, et al., 2016) ⁵⁷	+	+	+	+	+	?
(Pereira et al., 2019) ⁵⁸	+	+	+	+	+	+
(Okwuosa et al., 2016) ⁵⁹	+	+	+	+	+	+
(Sadia et al., 2016) ⁶⁰	+	+	+	+	+	+
(Sadia, Isreb, et al., 2018) ⁶¹	+	+	+	+	?	+
(Christos I Gioumouxouzis, Baklavaridis, et al., 2018) ⁶²	+	+	+	?	+	+

(Pietrzak et al., 2015) ⁶³	+	+	+	+	+	+
(Goyanes et al., 2019) ⁶⁴	+	+	?	+	+	+
(Ong et al., 2020) ⁶⁵	+	+	+	?	+	+
(Solanki et al., 2018a) ⁶⁶	+	+	+	+	+	+
(Kempin et al., 2018) ⁶⁷	+	+	+	+	+	+
(Kollamaram et al., 2018) ⁶⁸	+	+	+	+	+	+
(Beck et al., 2017) ⁶⁹	+	?	+	+	?	+
(Melocchi et al., 2018) ⁷⁰	+	+	+	+	?	+
(Verstraete et al., 2018a) ⁷¹	+	+	+	+	+	+
(Yajuan Sun & Soh, 2015) ⁷²	+	+	+	+	?	+
(Melocchi et al., 2015) ⁷³	+	+	+	+	?	+
(Maroni et al., 2017) ⁷⁴	+	+	+	+	+	+
(Goyanes, Det-Amornrat, et al., 2016) ⁷⁵	+	+	?	+	+	+
(J. Zhang, X. Feng, et al., 2017) ⁷⁶	+	+	+	?	+	+
(Okwuosa et al., 2018) ⁷⁷	+	+	+	+	+	+
(Arafat, Qinna, et al., 2018) ⁷⁸	+	+	+	+	+	+
(Jamróz et al., 2017) ⁷⁹	+	+	+	+	+	+
(Ehtezazi et al., 2018) ⁸⁰	+	+	+	+	+	+

(Hussain et al., 2020) ⁸¹	+	+	+	+	+	+
(Alhijaj et al., 2016) ⁸²	+	?	+	+	?	+
(Jensen et al., 2014) ⁸³	+	+	+	+	?	+
(Weisman et al., 2015) ⁸⁴	+	+	+	+	+	+
(Weisman et al., 2018) ⁸⁵	+	+	+	+	+	+
(Tappa et al., 2019) ⁸⁶	+	+	+	+	+	+
(Costa et al., 2015) ⁸⁷	+	+	+	+	+	+
(Farto-Vaamonde et al., 2019) ⁸⁸	+	+	+	+	+	+
(Chou et al., 2016) ⁸⁹	+	+	?	+	+	+
(Lim et al., 2016) ⁹⁰	+	+	+	?	+	+
(Hung et al., 2016) ⁹¹	+	+	+	+	+	+
(Chou et al., 2017) ⁹²	+	+	+	+	+	+
(C. Wang et al., 2017) ⁹³	+	+	+	+	+	+
(S. Li et al., 2017) ⁹⁴	+	?	+	+	?	+
(T. W. B. Kim et al., 2017) ⁹⁵	+	+	+	+	?	+
(Visscher et al., 2018) ⁹⁶	+	+	+	+	+	+
(Rajzer et al., 2018) ⁹⁷	+	+	+	+	+	+
(Govender et al., 2018) ⁹⁸	+	+	+	+	+	+

(Schmid et al., 2021) ⁹⁹	+	+	+	+	?	+
(X. Li et al., 2018) ¹⁰⁰	+	+	+	+	+	+
(Andersen et al., 2013) ¹⁰¹	+	+	?	+	+	+
(Sandler et al., 2014) ¹⁰²	+	+	+	?	+	+
(Water et al., 2015) ¹⁰³	+	+	+	+	+	+
(Ballard et al., 2017) ¹⁰⁴	+	+	+	+	+	+
(Horst et al., 2017) ¹⁰⁵	+	+	+	+	+	+
(Liang et al., 2018) ¹⁰⁶	+	+	+	+	?	+
(Holländer et al., 2016) ¹⁰⁷	+	+	+	+	?	+
(Arany et al., 2020) ¹⁰⁸	+	+	+	+	+	+
(Shi et al., 2020) ¹⁰⁹	+	+	+	+	+	+
(Genina et al., 2016) ¹¹⁰	+	+	+	+	+	+
(Tappa et al., 2017) ¹¹¹	+	+	+	+	?	+
(Fu et al., 2018) ¹¹²	+	+	+	+	+	+
(Luzuriaga et al., 2018) ¹¹³	+	+	+	+	+	+
(Pozzoli et al., 2016) ¹¹⁴	+	+	+	+	+	+
(Muwaffak et al., 2017) ¹¹⁵	+	+	+	?	+	+
(Misra et al., 2017) ¹¹⁶	+	+	+	+	+	+

(Glatzel et al., 2016) ¹¹⁷	+	+	+	+	+	+
(D. Yu et al., 2008) ¹¹⁸	+	+	+	+	+	+
(M. Zhu et al., 2011) ¹²²	+	+	+	+	+	+
(Shim et al., 2014) ¹²³	+	?	+	+	+	+
(J. Zhang, Zhao, Zhu, Huang, et al., 2014) ¹²⁴	+	+	+	+	+	+
(Shim et al., 2015) ¹²⁵	+	+	+	+	+	+
(S. J. Lee et al., 2016) ¹²⁶	+	+	+	+	+	+
(Y. Zhang et al., 2017) ¹²⁷	+	+	+	?	+	+
(Lin et al., 2018) ¹²⁸	+	+	+	+	+	+
(Song et al., 2015) ¹²⁹	+	+	+	+	+	+
(Gao et al., 2015) ¹³⁰	+	+	+	+	+	+
(Rattanakit et al., 2012) ¹³¹	+	?	+	+	+	+
(El Aita et al., 2019) ¹³²	+	+	+	+	+	+
(Tagami et al., 2021) ¹³³	+	+	+	+	+	+
(Khaled, Alexander, Irvine, et al., 2018) ¹³⁴	+	+	+	+	+	+
(Siyawamwaya et al., 2018) ¹¹⁹	+	+	+	?	+	+
(Gupta et al., 2015) ¹³⁵	+	+	+	+	+	+
(Do et al., 2017) ¹³⁶	+	+	+	+	+	?
(Holländer et al., 2018) ¹³⁷	+	+	+	+	+	+

(Maver et al., 2018) ¹³⁸	+	?	+	+	?	+
(R. Chang et al., 2010) ¹³⁹	+	+	+	+	+	+
(Snyder et al., 2011) ¹⁴¹	+	+	+	+	+	+
(King et al., 2013) ¹⁴²	+	+	+	+	+	+
(Zhao et al., 2014) ¹⁴³	+	+	+	?	+	+
(Dai et al., 2016) ¹⁴⁴	+	+	+	+	+	+
(Knowlton & Tasoglu, 2016) ¹⁴⁵	+	+	+	+	+	+
(Nguyen et al., 2016) ¹⁴⁶	+	+	+	+	+	+
(Homan et al., 2016) ¹⁴⁷	+	+	+	+	?	+
(Q. Gu et al., 2016) ¹⁴⁸	+	+	+	+	?	+
(Tarafder et al., 2016) ¹⁴⁹	+	+	+	+	+	+
(Ahlfeld et al., 2017) ¹⁵⁰	+	+	+	+	+	+
(C. Wu et al., 2011) ¹⁵¹	+	+	+	+	?	+
(J. Zhang, Zhao, Zhu, Zhu, et al., 2014) ¹⁵²	+	+	+	+	+	+
(M. Zhu et al., 2015) ¹⁵³	+	+	+	+	+	+
(K. Li et al., 2015) ¹⁵⁴	+	+	+	+	+	+
(Pei et al., 2018) ¹⁵⁵	+	+	+	+	+	+
(Min et al., 2015) ¹⁵⁶	+	+	+	+	+	+
(H. Wang et al., 2016) ¹⁵⁷	+	+	+	+	+	+

(Y. Wu et al., 2020) ¹⁵⁹	+	+	+	+	?	+
(Y. S. Zhang et al., 2016) ¹⁶⁰	+	+	+	+	?	+
(Y. Wang et al., 2018) ¹⁶¹	+	?	+	+	+	+
(Seoane-Viaño et al., 2020) ¹⁶²	+	+	+	+	?	+
(Liaskoni et al., 2021) ¹⁶³	+	+	+	+	+	+
(Khaled et al., 2014a) ¹⁶⁴	+	+	+	+	+	+
(M. Cui et al., 2019) ¹⁶⁵	+	+	+	+	+	+
(Tagami et al., 2019) ¹⁶⁶	+	+	+	+	v+	+
(Z. Wang et al., 2020) ¹⁶⁷	+	+	+	+	+	+
(Herrada-Manchón et al., 2020) ¹⁶⁸	+	?	+	+	?	+
(Khaled et al., 2015a) ¹⁶⁹	+	+	+	+	+	+
(Khaled et al., 2015b) ¹⁷⁰	+	+	+	+	?	+
(Khaled, Alexander, Wildman, et al., 2018) ¹⁷¹	+	+	+	?	+	+
(El Aita et al., 2020) ¹⁷²	+	+	+	+	?	+
(Yan Yang et al., 2020) ¹⁷³	+	+	+	+	?	+
(Algahtani et al., 2020) ¹⁷⁴	+	+	+	+	+	+
(Aita et al., 2020) ¹⁷⁵	+	+	+	+	+	+
(Cheng et al., 2021) ¹⁷⁶	+	+	+	+	?	+
(Fang et al., 2021) ¹⁷⁷	+	+	+	?	+	+

(Kuźmińska et al., 2021) ¹⁷⁸	+	+	+	+	?	+
(Johannesson et al., 2021) ¹⁷⁹	+	+	+	+	+	+
(Elbadawi et al., 2021) ¹⁸¹	+	+	+	+	+	+
(Yi et al., 2016) ¹⁸²	+	?	+	+	?	+
(Souza et al., 2017) ¹⁸⁴	+	+	+	+	+	+

Table 2.6: Assessment of risk of bias for studies based on vat polymerisation included in the systematic review.

Study ID	Risk of biasness parameters					
	Research rationale	Description of methods	Characterisation and testing	Description of results	Discussion	Overall conclusions
(J.-H. Lee et al., 2012) ¹⁸⁶	+	+	+	+	+	+
(Chi et al., 2014) ¹⁸⁷	+	+	+	+	+	+
(El Merhie et al., 2016) ¹⁸⁸	+	+	+	+	?	+
(J. Wang et al., 2016) ¹⁸⁹	+	+	+	+	+	+
(Healy et al., 2019) ¹⁹⁰	+	+	+	+	+	+
(Xiaoyan Xu et al., 2020) ¹⁹¹	+	+	+	+	+	+
(Goyanes, Det-Amornrat, et al., 2016) ⁷⁶	+	+	+	+	+	+
(Martinez et al., 2017) ¹⁹²	+	+	+	?	+	+
(Castro et al., 2015) ¹⁹³	+	+	+	+	+	+
(W. Zhu et al., 2016) ¹⁹⁴	+	+	+	+	+	+
(Parry et al., 2017) ¹⁹⁵	+	+	+	+	+	+
(Gittard et al., 2011) ¹⁹⁶	+	?	+	+	?	+
(Pere et al., 2018) ¹⁹⁷	+	+	+	+	+	+

(Johnson et al., 2016) ¹⁹⁸	+	+	+	+	+	+
(Caudill et al., 2018) ²⁰⁰	+	+	+	+	+	+
(Bloomquist et al., 2018) ²⁰¹	+	+	+	+	+	+
(Gittard et al., 2010) ²¹²	+	+	+	+	+	+
(T. Y. Huang et al., 2015) ²¹³	+	+	+	+	+	+
(Ma et al., 2016) ²¹⁶	+	+	+	+	+	+
(Yuanyuan Sun et al., 2016) ²¹⁷	+	+	+	+	?	+
(Lim et al., 2017) ²¹⁸	+	+	?	+	+	+
(Stanojević et al., 2021) ²¹⁹	+	+	+	+	+	+

Table 2.7: Assessment of risk of bias for powder bed fusion studies included in the systematic review.

Study ID	Risk of bias parameters					
	Research rationale	Description of methods	Characterisation and testing	Description of results	Discussion	Overall conclusions
(Cheah et al., 2002) ²²⁶	+	+	+	+	+	+
(Fina et al., 2017) ²²⁷	+	+	?	+	+	+
(Fina, Madla, et al., 2018) ²²⁸	+	+	+	+	+	+
(Fina, Goyanes, et al., 2018) ²²⁴	+	+	+	+	+	+
(Awad et al., 2019) ²²⁹	+	+	+	+	+	+
(Awad et al., 2020) ²³⁰	+	+	+	+	+	+
(Ngo et al., 2018) ²³¹	+	+	+	+	+	+
(B. M. Wu et al., 1996) ²³²	+	+	+	+	+	+
(Katstra et al., 2000) ²³³	+	?	+	+	?	+
(Rowe et al., 2000) ²³⁴	+	+	+	+	+	+
(Wang et al., 2006) ²³⁵	+	+	+	+	+	+
(Yu et al., 2007) ²³⁶	+	+	+	+	+	+

(D.-G. Yu, C. Branford-White, Y.-C. Yang, et al., 2009; DG Yu et al., 2008) ²³⁷	+	+	+	+	+	+
(D. G. Yu et al., 2009) ²³⁸	+	+	+	+	+	+
(Infanger et al., 2019) ²³⁹	+	+	+	+	+	+
(Shi et al., 2019) ²⁴⁰	+	+	+	+	+	+
(D.-G. Yu, C. Branford-White, Z.-H. Ma, et al., 2009) ²⁴¹	+	+	+	+	+	+
(G. Wu et al., 2014) ²⁴²	+	+	+	+	+	+
(Gbureck et al., 2007) ²⁴³	+	+	+	+	+	+
(W. Wu, Zheng, Guo, Sun, et al., 2009) ²⁴⁴	+	+	+	+	+	+
(W. Wu et al., 2016) ²⁴⁵	+	+	?	+	+	+
(Tarafder et al., 2014) ²⁴⁶	+	+	+	?	+	+
(Maher et al., 2017) ²⁴⁹	+	+	+	+	+	+

Table 2.8: Assessment of risk of bias for studies based on jetting technique included in the systematic review.

Study ID	Risk of biasness parameters					
	Research rationale	Description of methods	Characterisation and testing	Description of results	Discussion	Overall conclusions
(W. Huang et al., 2007) ²⁵²	+	+	+	+	+	+
(W. Wu, Zheng, Guo, & Huang, 2009) ²⁵³	+	+	+	+	+	+
(Vorndran et al., 2010) ²⁵⁴	+	?	+	+	?	+
(Y. Gu et al., 2012) ²⁵⁵	+	+	+	+	?	+
(Planchette et al., 2016) ²⁵⁶	+	+	+	+	+	+
(Acosta-Vélez et al., 2017) ²⁵⁷	+	+	+	+	+	+
(Kyobula et al., 2017) ²⁵⁸	+	+	+	+	+	+
(Elizabeth A. Clark et al., 2020) ²⁵⁹	+	+	+	+	+	+
(Meléndez et al., 2008) ²⁶⁰	+	+	+	+	+	+
(Buanz et al., 2011) ²⁶¹	+	+	+	+	+	+
(Varan et al., 2017) ²⁶²	+	+	+	+	+	+
(Sandler et al., 2011) ²⁶³	+	+	+	+	+	+

(Genina et al., 2012) ²⁶⁴	+	+	+	+	+	+
(Scoutaris et al., 2011) ²⁶⁵	+	+	+	+	+	+
(B. K. Lee et al., 2012) ²⁶⁶	+	+	+	?	+	+
(Tarcha et al., 2007) ²⁶⁷	+	+	+	+	+	+
(Matsusaki et al., 2013) ²⁶⁸	+	+	+	+	+	+
(Raijada et al., 2013) ²⁷⁰	+	+	+	+	+	+
(Hirshfield et al., 2014) ²⁷¹	+	?	+	+	?	+
(Hsu et al., 2015) ²⁷²	+	+	+	+	?	+
(Uddin et al., 2015) ²⁷³	+	+	+	+	+	+
(Wickström et al., 2015) ²⁷⁴	+	+	+	+	+	+
(Wickström et al., 2017) ²⁷⁵	+	+	+	+	+	+
(Içten et al., 2017) ²⁷⁶	+	+	+	+	+	+
(Clark et al., 2017) ²⁷⁷	+	+	+	+	+	+
(Anderson et al., 2013) ²⁸⁰	+	+	+	+	+	+
(M. Cui et al., 2021) ²⁸¹	+	+	+	+	+	+
(S.-Y. Chang et al., 2020) ²⁸²	+	+	+	+	+	+
(Inzana et al., 2015) ²⁸³	+	+	+	+	+	+

(Xi et al., 2016) ²⁸⁴	+	+	+	+	+	+
(Lind et al., 2017) ²⁸⁵	+	+	+	+	+	+
(Yikun Yang et al., 2017) ²⁸⁸	+	+	+	+	+	+
(J.-C. Wang et al., 2017) ²⁸⁹	+	+	+	+	+	+
(B. Wang et al., 2018) ²⁹⁰	+	+	+	+	+	+

2.3. Results and discussion

The research studies identified through databases were 25,660 at first. After removing the duplicates and applying eligibility criteria 241 studies were included in this systematic review. Figure 2.1 summarises the process of study selection. The included 241 research studies met the inclusion criteria and were then further categorised according to the types of 3D printing technologies present. After categorisation, the summarised characteristics of all the eligible studies were tabulated. Of 241, 162 articles were based on extrusion-based techniques, 22 articles belonged to vat polymerisation, 23 articles were of powder bed fusion and 34 articles belonged to the jetting techniques (Figure 2.2). Based on the number of research articles, we found that extrusion-based printing techniques are the most widely used techniques, particularly fused deposition modelling (FDM) and paste extrusion, in the drug delivery followed by jetting techniques, powder bed fusion and vat polymerisation. We also found out that any study that used the plasticiser to aid the printing process did not address the effect of plasticiser induced gastric motility and how it affects the drug absorption eventually.

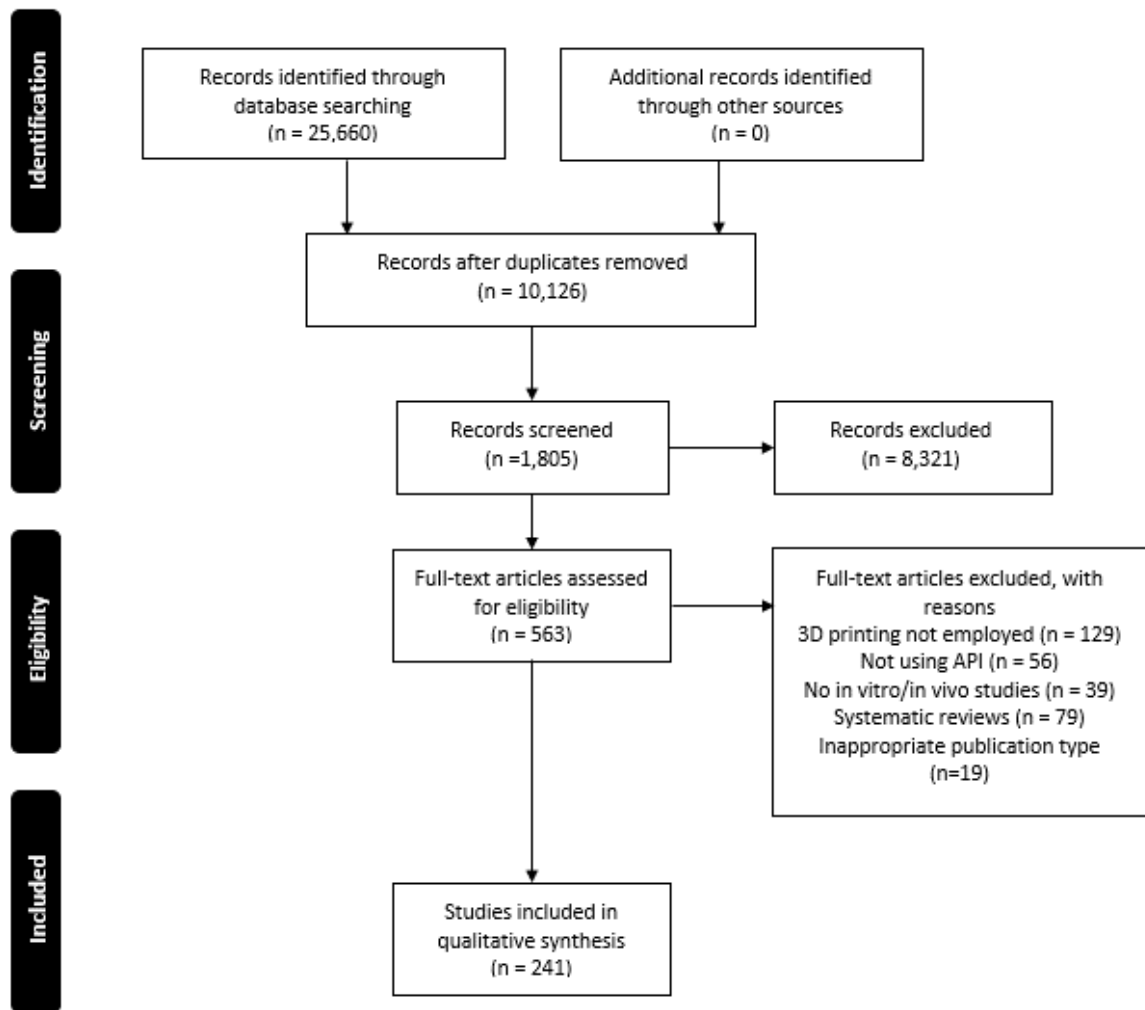


Figure 2.1: Illustration depicting the selection process of eligible studies.

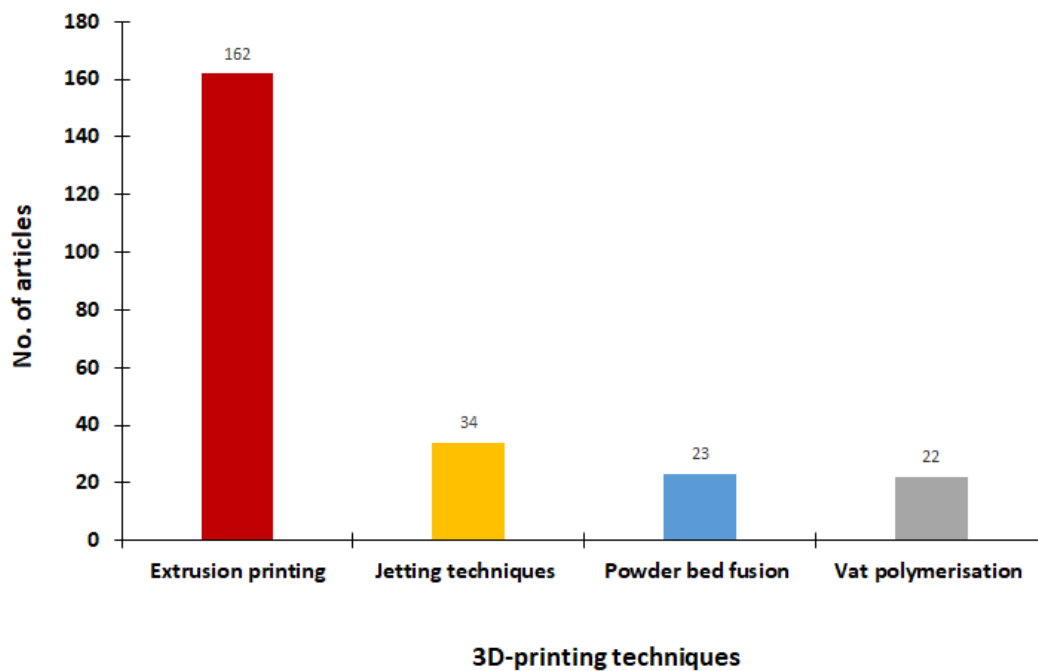


Figure 2.2: Distribution of studies based on the used 3D printing technology.

The overall assessment of risk of bias in the included studies is given in the Figure 2.3 (a). The studies showed low risk of bias in general. However, among all areas, there was 20% unclear bias in the discussion section, 8% in results and methodology section, 5% in testing and 2% in conclusion section.

Figure 2.3 (b) shows the risk of assessment of bias in extrusion-based research studies. The figure shows that generally, there was low risk of bias among these studies. There was 2% unclear bias in the conclusion section, 16% in the discussion, 6.5% in the results, 3.5% in the testing and 6% in the methodology section. Similarly, there was low risk of bias in vat polymerisation studies. However, 1.5% unclear was seen in the discussion section and 0.5% unclear bias was seen in each result, testing and methodology sections, Figure 2.3 (c).

Among research studies based on powder bed fusion technique, there was 1% unclear bias in the testing section whereas the unclear bias in the methodology, results and discussion section was same, 0.5%, Figure 2.3 (d). There was no unclear bias in rationale and conclusion

section. Likewise, Figure 2.3 (e) shows the risk of bias in research studies based on jetting techniques. There was no unclear bias in the rationale, testing and conclusion sections. However, there was 2% unclear bias in the discussion section, 0.5% in the results and 1% in the methodology section.

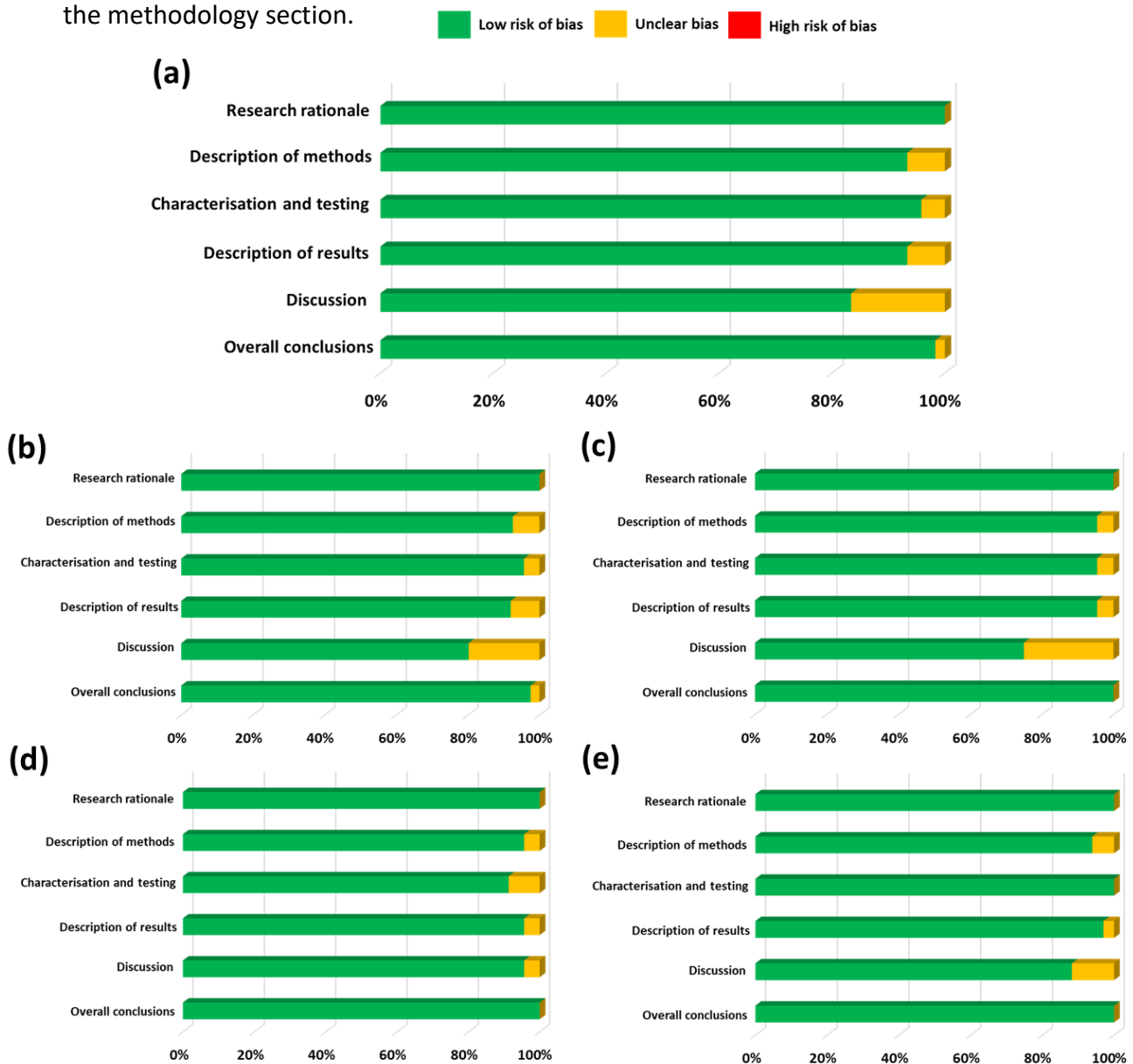


Figure 2.3: Assessment of risk of bias for (a) overall distribution of bias among each study included in the systematic review (b) extrusion-based studies (c) vat polymerisation studies (d) powder bed fusion studies (e) jetting technique studies.

The included 241 research studies were also categorised as per their publication year. Figure 2.4 represents the overall trend throughout the years, it shows that the actual rise in the number of research studies begin from 2015 and is increasing onwards.

Figure 2.5 shows the number of the model drugs that has been frequently used in the research studies. The figure shows that the paracetamol is the most frequently used drug followed by theophylline and dyes.

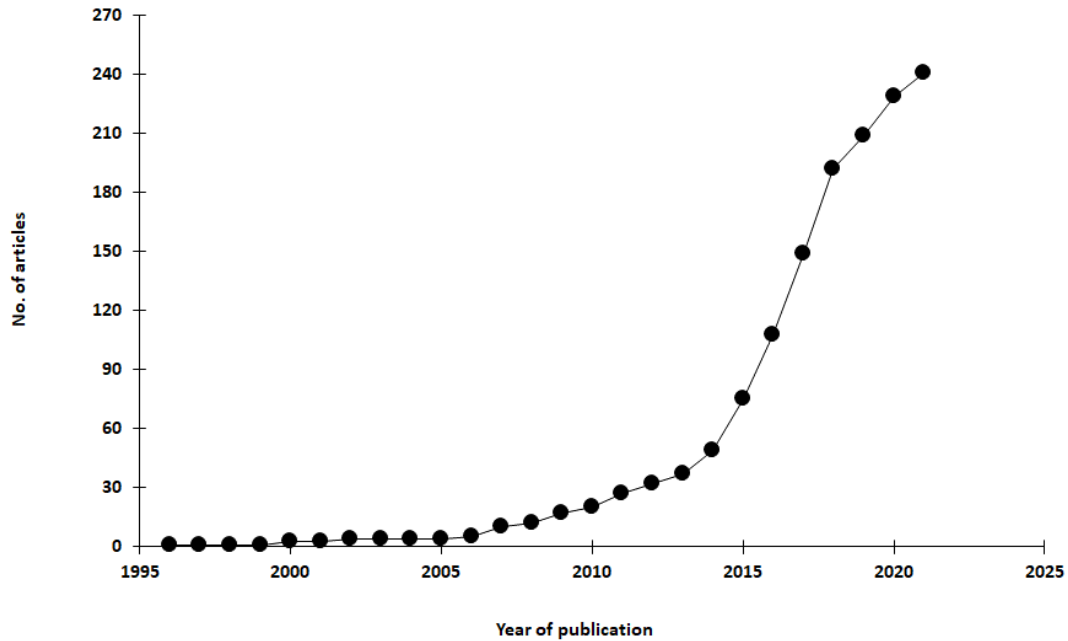


Figure 2.4: Overall trend of research studies across the years.

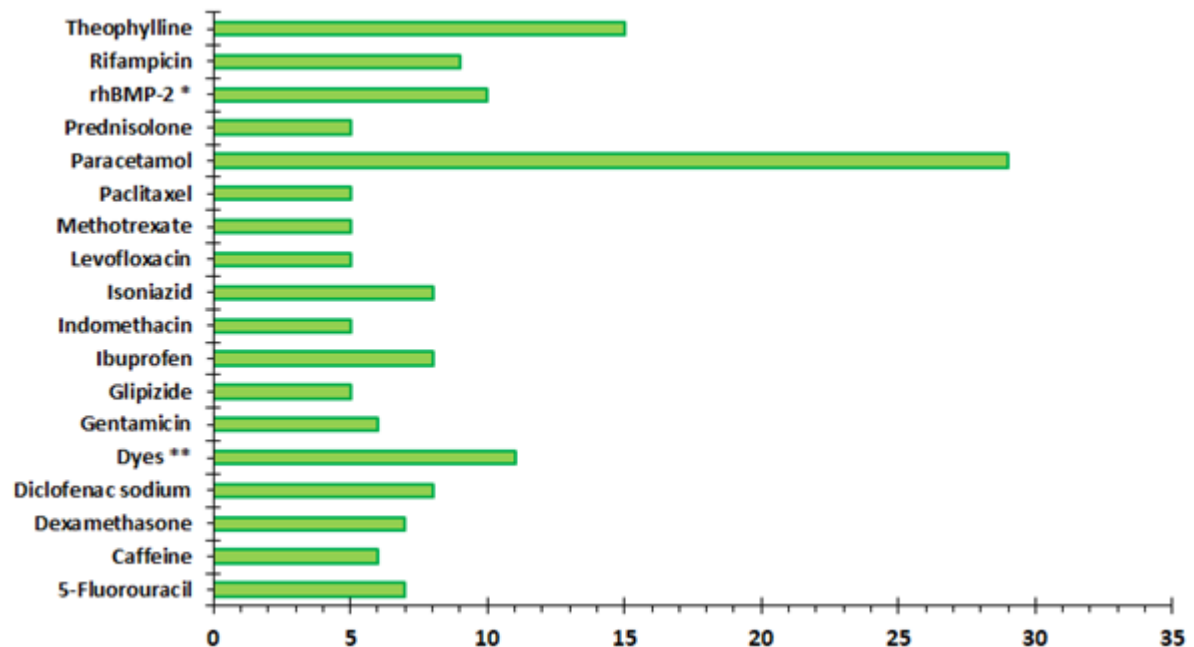


Figure 2.5: Distribution of frequently used model drugs.

(*recombinant human bone morphogenetic protein-2, **methylene blue dye, orange G, fluorescein, rhodamine B, alizarin, brilliant blue).

2.3.1. Key findings of the current systematic review

2.3.1.1. Extrusion-based 3D printing

Extrusion-based 3D printing involves layer-by-layer deposition of fed materials such as polymer solutions, pastes, dispersions, molten and semi-molten polymers through a moveable nozzle and is controlled by the computer. Three major types of extrusion-based printing include (a) fused deposition modelling, (b) pneumatic extrusion and (c) paste extrusion ^{14, 15}.

Figure 2.6 shows bar chart of extrusion-based printing techniques based on the number of research articles. In this systematic review, 162 of the 241 included studies fell in the category of extrusion-based technique out of which 19 are of pneumatic extrusion, 42 are paste extrusion and 101 belongs to FDM.

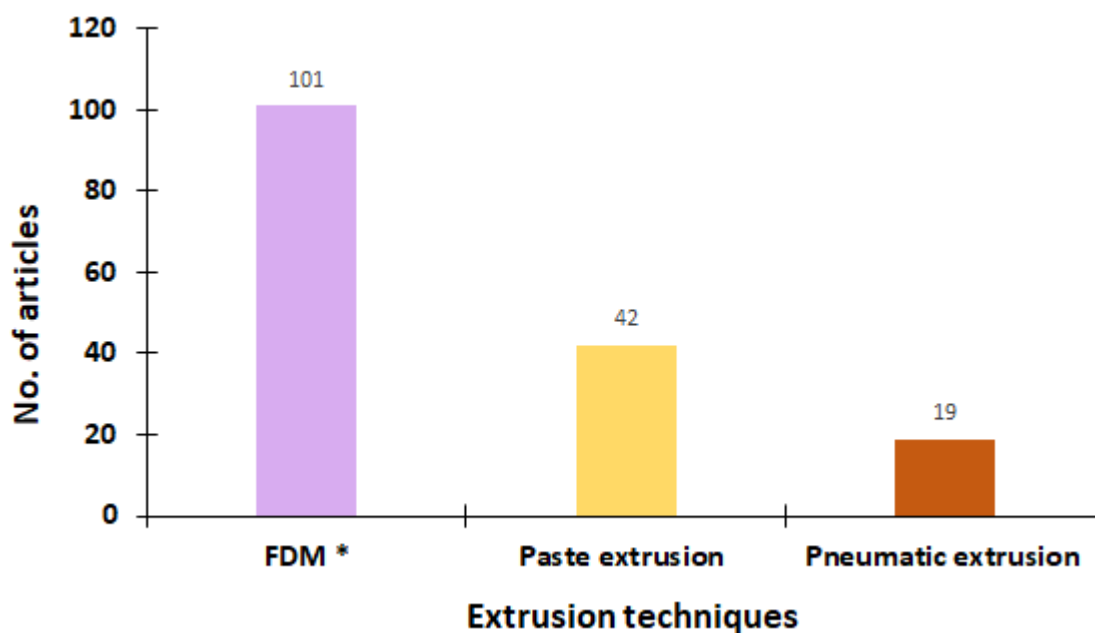


Figure 2.6: Distribution of included studies based on extrusion-based printing techniques. (*Fused deposition modelling).

2.3.1.1.1. FDM and its applications

FDM is a digitally controlled technique comprising feeding, melting, extrusion and layer by layer deposition of the filaments through a nozzle of the temperature-controlled print head as is graphically illustrated in the Figure 2.7¹⁶. The temperature of the print head is adjusted according to the polymer used e.g. for amorphous and semi-crystalline polymers the temperature is set above the glass transition temperature and the melting temperature, respectively^{14, 17}.

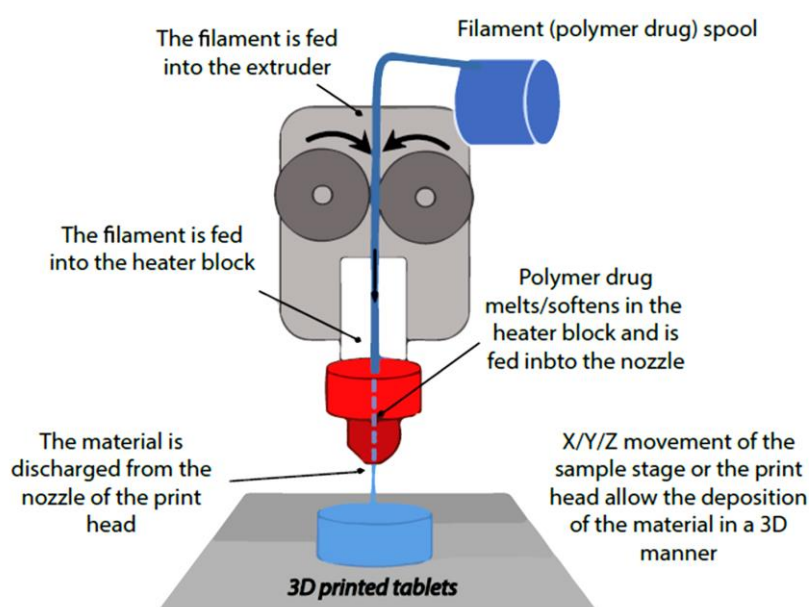


Figure 2.7: Schematic illustration depicted the working principle of FDM, reproduced with permission from¹⁶.

Many research groups have employed FDM in developing drug delivery devices namely tablets, capsules, discs, and scaffolds etc. Depending on the design model, these devices are able to accommodate more than one active ingredient with varying release profiles. Several applications of FDM printing in drug delivery are noted below.

The digital control of FDM process parameters has made fabrication of polymer-based controlled release drug delivery devices relatively simple and easy as compared to traditional manufacturing methods which can be expensive, require high initial investment and often have problems in process control. Furthermore, FDM provides digital control over process parameters such as infill density, infill pattern, raster angle and raster gap and possess several

advantages including minimum material wastage, comparatively cheap, safe and a non-toxic process. These features were demonstrated in a study from 2007 in which FDM was used to develop acrylonitrile butadiene styrene (ABS) based controlled release cylindrical drug delivery devices. To mimic the drug flow, methylene blue dye was used as a model drug to study the drug release behaviour. It was reported that FDM process parameters such as raster gap and raster angle played a basic role in controlling the drug release and structure of the device and control over porosity was of utmost importance in controlling the drug release. An increase or decrease in raster gap resulted in increased or decreased porosity. A device with raster angle of 0-90° and raster gap of 0.0762 mm resulted in controlled release of drug over a period of 64 hours, thereby allowing the researchers to conclude that digital control of FDM parameters can result in devices with optimised drug release characteristics ¹⁸.

Another study investigated the impact of different infill densities on drug release behaviour. Polyvinyl alcohol (PVA) filament was soaked in absolute ethanol for drug loading and 0.29% loading of fluorescein, a model drug, was achieved. *In vitro* dissolution testing of tablets printed with 10%, 50% and 90% infill density was carried out. Tablets with 10% infill density showed complete release of drug within 6 hours, whereas complete dissolution of 50% and 90% infill tablets took 15 hours and 20 hours, respectively, indicating that infill density has a considerable effect on the drug release ¹⁹. In a study conducted by Goyanes *et al.* in 2014, PVA filaments loaded with two model drugs 4-aminosalicylic acid (4-ASA) and 5-aminosalicylic acid (5-ASA) were developed for printing of tablets with modified release dissolution profiles. Drug was loaded into ready-made PVA filaments by soaking the filaments in the solution containing drug and ethanol. 0.06% of 5-ASA and 0.25% w/w of 4-ASA were loaded into filaments. The printing process turned out to be effective for 5-ASA, whereas thermal degradation occurred in 4-ASA. The *in vitro* dissolution profile revealed that 50% drug release from all the tablets with different infill densities (10%, 50%, 90%) containing 5-ASA was achieved in a period of 1 hour and total drug release in less than 4 hours. However, tablets with a low infill percentage exhibited rapid drug release. Additionally, the effect of infill density was more prominent on the dissolution profiles of tablets with 4-ASA. Tablets with 10% infill density showed total release of drug within 4 hours of dissolution. On the other hand, tablets with 50% and 90% infill density exhibited sustained release ²⁰.

Likewise, digital control of infill density in a study conducted by Chai *et al.* resulted in the development of a floating drug delivery system along with the sustained release of drug. Different infill densities were examined to achieve optimal floating and hydroxypropyl cellulose (HPC) was used to achieve sustained release of drug. The main objective of the floating drug delivery system was to increase the gastric residence time of drug, thereby improving bioavailability and increasing drug absorption. According to this study, it was reported that the formulation which contained 0% infill, 2 shells, and 10% domperidone, displayed optimal floating properties. The optimised formulation floated for approximately 10 hours *in vitro* and for more than 8 hours *in vivo*. The relative bioavailability, which was $222.49 \pm 62.85\%$ for fabricated floating tablets, was compared with marketed tablets. After administration of a single oral dose of 20 mg Motilium® in rabbits, C_{max} (mean peak plasma concentration) of domperidone for Motilium® was reported to be 596.167 ± 143.132 ng/ml, whereas for fabricated floating tablets, it was 505.983 ± 43.175 ng/mL. T_{max} for Motilium® was 1.5 hours, while for fabricated floating sustained release delivery system, t_{max} was 5 hours. It was concluded from the *in vivo* results that the fabricated floating tablets showed significant sustained release of drug ($p < 0.05$) and correlated with *in vitro* floating results ²¹.

Floating system is effective for increasing bioavailability of drugs having window for absorption. Kimura *et al* reported that the increase in the outer shell thickness of tablets resulted in prolonged floating and delayed release of itraconazole showing zero-order drug release ²². Tablets with different infill density and open and closed systems were printed using FDM containing HPMCAS as carrier polymer and pregabalin as a model drug. It was reported that tablets printed with low infill density and an open system showed faster drug release in comparison to open and closed systems with high infill density. Formulation printed with partially open layer on the top and completely closed bottom showed zero-order drug release ²³. Another study developed and evaluated hydroxypropyl methyl cellulose (HPMC) based gastro-floating tablets with different infill densities (30%, 50% and 70%) using different grades (K4M and E15) of HPMC and polyvinyl pyrrolidone (PVP) K30. The floating time of tablets possessing lower infill density (30%) was greater than the tablets with higher infill density (50%). Tablets with 50% infill density displayed optimal floating time and drug release characteristics ²⁴.

Boetker *et al.*, utilised different concentrations (20% and 40%) of HPMC along with polylactic acid (PLA) to fabricate discs possessing modified drug release characteristics containing nitrofurantoin as a model drug. The drug release rate was dependent on the HPMC loading i.e. the nitrofurantoin release rate from discs containing 40% HPMC was greater than discs containing 20% HPMC due to the higher content of water-soluble excipient in 40% HPMC discs²⁵. HPMC filaments were extruded via HME without using any plasticiser to print the matrix tablets. Filaments were extruded using different grades of HPMC varying in viscosity. It was reported that the higher the viscosity of the polymer, higher will be the swelling of the matrix tablet and drug release will be decreased. During *in vivo* studies in rabbits, an extended drug absorption profile was observed. It was concluded that the matrix tablets can be printed without using plasticiser and viscosity of the polymer greatly plays a vital role in defining the release profile²⁶. HME was coupled with FDM to print the sustained release tablets. It was reported that using different release modifiers (PVA, Soluplus®, Eudragit® RL PO/RS PO, HPMC K4M/E10M/K100M, Kollidon® vinyl acetate 64 (VA 64)/17PF/30) can result in controlled drug release for 24 hours²⁷.

Oblong-shaped tablets with sustained release profiles were developed using Eudragit® RL as a polymer with the employment of FDM printing which allows simultaneous dose adaption and estimation of drug release. Dissolution studies showed that tablets with a denser network or higher infill density exhibited slower drug release, thus demonstrating the effect infill density has on the drug release pattern which may be exploited to develop modified release formulations²⁸. Drug delivery devices with different types of drug release profiles i.e. immediate, sustained, pulsatile and chronotherapeutic (outer-layer composed of drug-free filament while inner core composed of drug-loaded filaments) were fabricated (Figure 2.8). Filaments containing only drug (diltiazem) and polymer (HPMC) with no additional excipients were extruded to fabricate tablets and a base and cap were also printed. The effect of different infill patterns and infill densities were also evaluated. During *in vitro* dissolution tests, an immediate release profile was observed in tablets (with or without base and cap) with 25% infill density. Increased infill density and various infill patterns resulted in extended drug release. Tablets with hexagonal pattern showed fastest drug release whereas a diamond infill pattern resulted in the slowest drug release. Tablets with no drug in the outer shells and 50% infill density showed no drug release initially but later on showed immediate-release.

Tablets with two-phase drug release showed 50% of the drug being released in the first 1.5 hours, then no release for 2 hours followed by drug release for 6 hours. Moreover, the in-vivo (rats) data also showed satisfactory correlation with in-vitro findings²⁹.

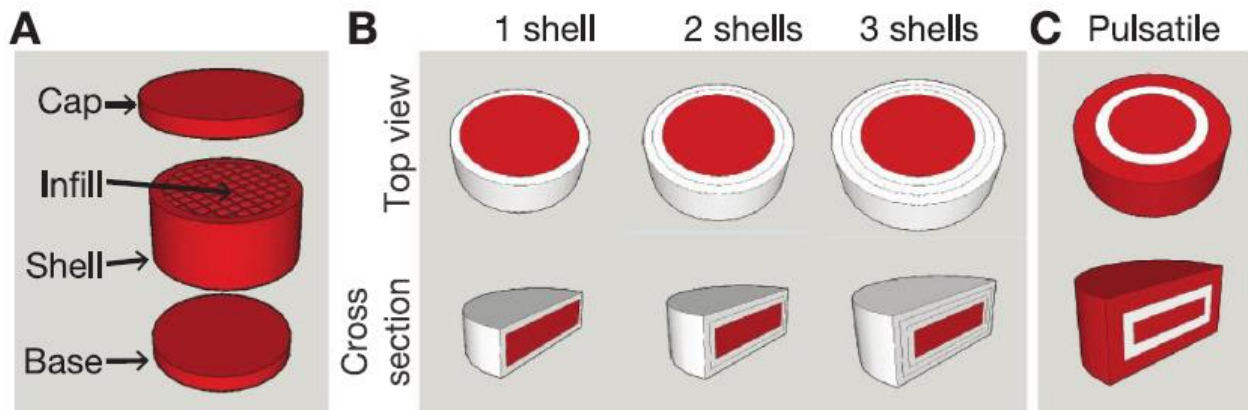


Figure 2.8: Dosage from design (A) infill patterns, base, caps and shell of the designed tablets (B) Chrono-controlled release tablets (C) Pulsatile-release tablets, reproduced with permission from²⁹.

PVA and PLA were used to fabricate a controlled release drug delivery system. The inner structure of the tablet consisted of hydrochlorothiazide, PVA and mannitol, whereas the outer part was made up of PLA (Figure 2.9). The resulting formulations followed zero-order drug release kinetics. Qualitative assessment of the dissolution mechanism of printed tablets was also conducted employing time lapsed X-ray micro focus computed tomography (4D μ CT). 4D μ CT image sequence revealed detachment of the PLA compartment followed by gradual erosion of PVA which agrees with *in vitro* dissolution studies³⁰.

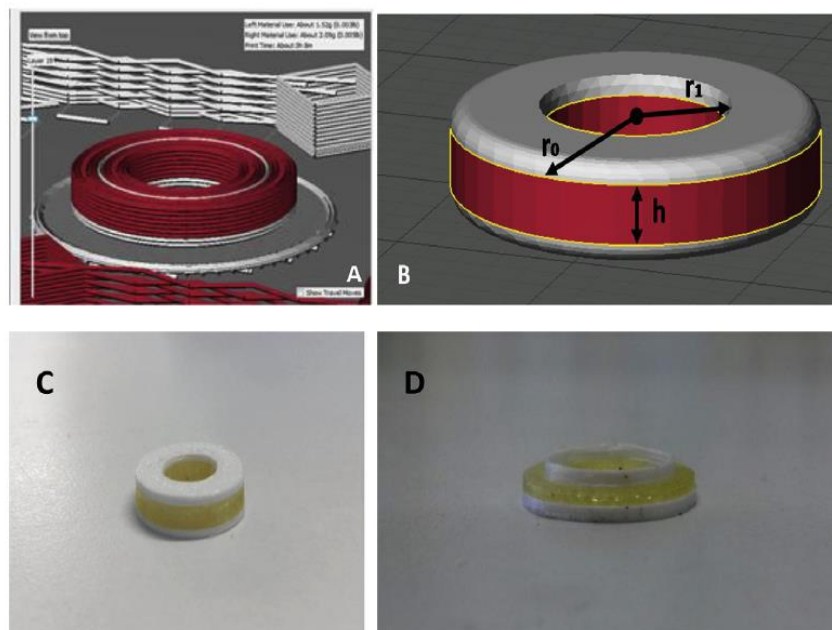


Figure 2.9: (A) STL model of three-compartment tablet with hollow cylinder (B) Demonstrating dimensions of tablets (C) FDM printed formulation (D) Half-printed formulation with inner binding PLA ring, reproduced with permission from ³⁰.

The impact of infill density and other printing parameters, such as flow rate from the nozzle of the FDM printer and temperature, on the characteristics of a printed formulation were also studied by Tagami *et al.* who developed curcumin-loaded PVA filaments to print the tablets. It was reported that the increase in temperature affected the colour of FDM printed tablets due to thermal degradation of curcumin, thus emphasising the importance of optimal selection of temperature. It was also suggested that increasing the printing speed might prevent this degradation by reducing the exposure time to the heated nozzle. Lower infill density resulted in tablets with floating capabilities, whereas high infill density caused the tablets to sink down during dissolution testing. Moreover, the drug release was faster from the low infill density tablets ³¹.

Widely used polymers of pharmaceutical grade and of different aqueous solubility i.e. readily soluble (PEO, Kollicoat® IR), insoluble (ethyl cellulose, Eudragit® RL), enteric soluble (Eudragit® L, HPMCAS) and erodible/swellable (hydrophilic cellulose derivatives, PVA, Soluplus®) were used for the development of filaments loaded followed by printing of discs. Upon investigation, the discs performed as erodible/swellable, promptly soluble, gastro-resistant and insoluble slowly-permeable layers in accordance with the nature of the polymer used. Therefore, it was concluded that the selected polymers were suitable for FDM printing and

for producing modified drug release profiles when loaded with active pharmaceutical ingredient ³².

HPC, PEO and Eudragit polymers were used to print tablets containing 30% w/w isoniazid. Among all formulations, PEO tablets showed fastest drug release. A sustained release of drug was observed with HPC tablets. Tablets containing both Eudragit and HPC released 80% of drug in 334 minutes ³³.

PEO of different molecular weights (100000, 200000, 300000, 600000, 900000) were employed in printing oral dosage forms with a radiator like design of dosage form using theophylline as a model drug. The extruded PEO filaments were of variable mechanical resistance. PEO filaments with 200000-600000 molecular weight were compatible with the printing process. Moreover, the radiator design of dosage form resulted in accelerated drug release ³⁴.

Saviano *et al.*, reported the effect of particle size of polymer on formulation processes including mixing, extrusion and printing. The PVA particle size in the range of 200-600 μm were suitable for homogeneous mixing of polymer and drugs, extrusion of filaments and printing process. 10% and 35% ciprofloxacin concentrations were used in the formulation. All formulations showed complete release of drug in 270 minutes ³⁵.

Ethyl cellulose (EC) was used to develop sustained release tablets along with other materials that are widely used to modify the drug release including HPMC, PVA, xanthan gum and sodium alginate. The effect of different printing parameters including printing temperature, speed, layer height, infill density, thickness of the outer shell and infill pattern were evaluated. Figure 2.10 shows an STL model of a tablet with 25% infill density. Drug release studies showed that the addition of a release modifier affected the drug release pattern, as the drug release from hydrophilic matrix was limited (cumulative drug release at 24 h (Q_{24h}) =17.8%) in the absence of a modifier. With the addition of release modifiers, HPMC and sodium alginate, the amount of drug release increased within a period of 24 hours (Q_{24h} = 83% and 80.3%, respectively), whereas with xanthan gum and PVA, the drug release was incomplete (Q_{24h} = 54.3% and 42%, respectively). However, HPMC was optimal in modifying the drug release. In addition, it was also reported that infill density, thickness of the outer shells, release modifiers and drug content affected the drug release pattern. Additionally, the quality

and shape of the printed product was affected by the printing temperature, speed, thickness of outer shells and layer height ³⁶.

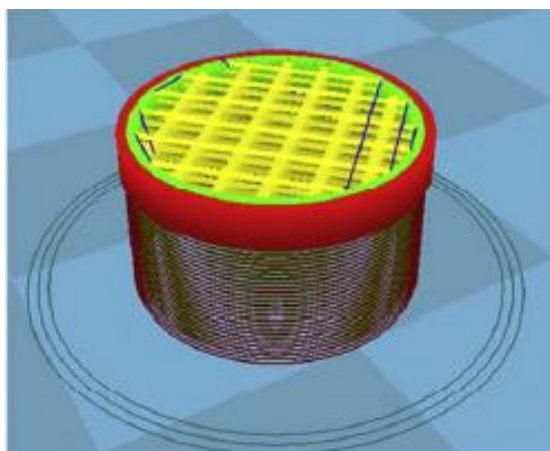


Figure 2.10: Schematic illustration of STL model of tablet with 25% infill density. Reproduced with permission from ³⁶.

HPMC based acetaminophen matrices were developed to study the impact of the thickness of the outer shell on drug release properties from the printed matrices. The study concluded that the thickness of the outer shells has a noticeable impact on the drug release kinetics. During dissolution testing, thick and tight outer shells act as a barrier contributing to slow formation of a hydrogel and constant control of the drug release rate from HPMC matrices. Moreover, it was reported that the impact of the thickness of the outer shell in controlling the drug release was greater than the impact of infill density ³⁷.

PVA filaments loaded with prednisolone were developed to fabricate ellipse shaped tablets with extended drug release properties. The mass of the tablets was controlled digitally by adjusting the volume of the designed template of device using a software. Precision of dose control was in the range of 88.7% and 107%. Dissolution testing showed that tablets were able to extend the drug release up to 24 hours ³⁸.

Controlled release tablets of theophylline were printed using Eudragit RL as a polymer along with two plasticisers to investigate the effect of a lipophilic plasticiser (stearic acid) and hydrophilic plasticiser (PEG 4000) on drug release. The formulation with stearic acid showed a faster drug release in comparison to the formulation containing PEG. The PEG formulation released $85.93 \pm 0.98\%$ of the drug, whereas the stearic acid formulation released only 10.66

± 1.60% after 120 minutes. After 24 hours, the stearic acid formulation released only 50% of the drug, whereas the drug was completely released from the PEG formulation. In conclusion, the formulation containing stearic acid prolonged the drug release while the formulation with PEG did not succeed in prolonging the drug release due to PEG 4000 increasing water solubility while stearic acid is insoluble in water ³⁹.

Passive diffusion method was applied to load drug onto PVA filaments to develop sustained release tablets of nifedipine. The stiffness and surface roughness of filament affected passive diffusion loading of drug onto filaments. 3% w/w drug loading was achieved and tablets showed sustained release of the drug over 24 hours ⁴⁰.

Passive diffusion and hot melt extrusion techniques were used for drug loading. Kollidon VA64 and ethyl cellulose were used to extrude drug loading filaments via hot melt extrusion. The drug loading via hot melt extrusion was 13 times higher than passive diffusion. The printed formulations showed biphasic drug release profile ⁴¹.

Manufacturing of tablets with different shapes is a difficult task to perform with traditional methods. However, in a study conducted by Goyanes *et al.*, FDM allowed the development of tablets with five different geometries i.e. cube, pyramid, cylinder, sphere and torus (Figure 2.11). This study demonstrated that the geometrical shape affects the drug release and is dependent on the ratio of surface area to the volume and not on the surface area. Drug release was investigated in three different ways i.e. by keeping the surface area, surface area/volume ratio and weight constant. The drug release order observed by keeping the surface area constant was as follows; pyramid > torus > cube > sphere > cylinder and with constant surface area/volume ratio it was cube > sphere > torus > cylinder > pyramid. With constant weight of tablets, drug release profiles were very similar ⁴².



Figure 2.11: Images of 3D printed tablets fabricated at constant (A) surface area (B) surface area/mass ratio (C) mass with different geometries, reproduced with permission from ⁴².

The impact of using different internal geometries (horn, reversed horn and cylinder) on controlling the drug release was investigated by printing tablets with PVA and paracetamol. The dissolution studies showed gradually increasing, gradually decreasing and constant drug release profiles for tablets with horn, reversed horn and cylinder geometries, respectively which concludes that drug release can be controlled by manipulating internal geometry of tablet ⁴³. A drug delivery device that can be fully customised was printed with the help of FDM. The device can be customised in number of ways e.g. varying dose, size, shape, release profiles, duration and can accommodate multiple drugs. The method turned out to be efficient, inexpensive and simple and is feasible for on-demand medication ⁴⁴.

FDM has also allowed printing of such designs of drug delivery devices, which are quite difficult by conventional methods. Such an innovative design of drug delivery device with controlled release profile was introduced by Li *et al.* in which researchers have accommodated a small tablet within a larger tablet with the help of a two-nozzle FDM printer, thus making a two-chamber tablet- DuoTablet. Three different DuoTablets, each containing varying concentrations of glipizide in the internal core and external layer, were printed:

- i. 4.76% in the internal core and 2.18% in the external layer

- ii. 2.18% in the outer layer only
- iii. 4.76% in the internal core only

In vitro dissolution tests reported that the formulation showed controlled release for about 5 hours in accordance with the Korsmeyer–Peppas model. Initially, the content of glipizide in the outer layer was released followed by the release of glipizide from the inner core. The external layer released approximately 90% glipizide in the first two hours. The release from the inner core took place after a lag time of 85 minutes during dissolution testing. The uniformity and thickness of the external layer governed the lag time ⁴⁵. Similarly, in another study, a duo-caplet (Figure 2.12) was designed that accommodated a capsule within a large capsule resulting in a two-chamber device. Each chamber consisted of two different drugs, paracetamol and caffeine. Dissolution studies showed that the release of both model drugs was concurrent and did not rely on drug solubility instead the drug release profile was dependent on the macrostructure of the duo-caplet. Moreover, the release of drug from the inner chamber was dependent on the thickness of the outer layers of the caplet. Such designs enable researchers to attain desired drug release patterns ⁴⁶.

FDM has not only provided digital control over process parameters but has also enabled researchers to bring innovation to the internal structure of drug delivery devices to aid the drug release. Inclusion of perforated channels of varying width, length and alignment in caplets was reported by Sadia *et al.*, to facilitate the drug release with hydrochlorothiazide used as the model drug (Figure 2.13). The perforated channels inside the caplets showed an increase in surface area/volume ratio. In addition, the change in length and width of perforated channels also had an impact on the drug release. Caplets with a channel width of ≥ 0.6 mm displayed an immediate release pattern. However, the caplets containing multiple short channels (8.6mm) were more effective in facilitating the drug release as compared to long channels (18.2mm) ⁴⁷.

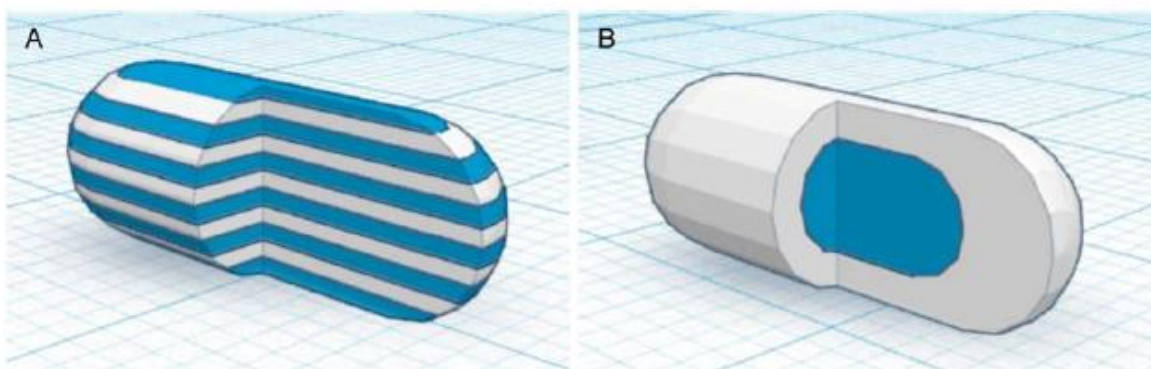


Figure 2.12: 3D design of printed formulations (A) halved multilayer device (B) halved DuoCaplet, reproduced with permission from ⁴⁶.

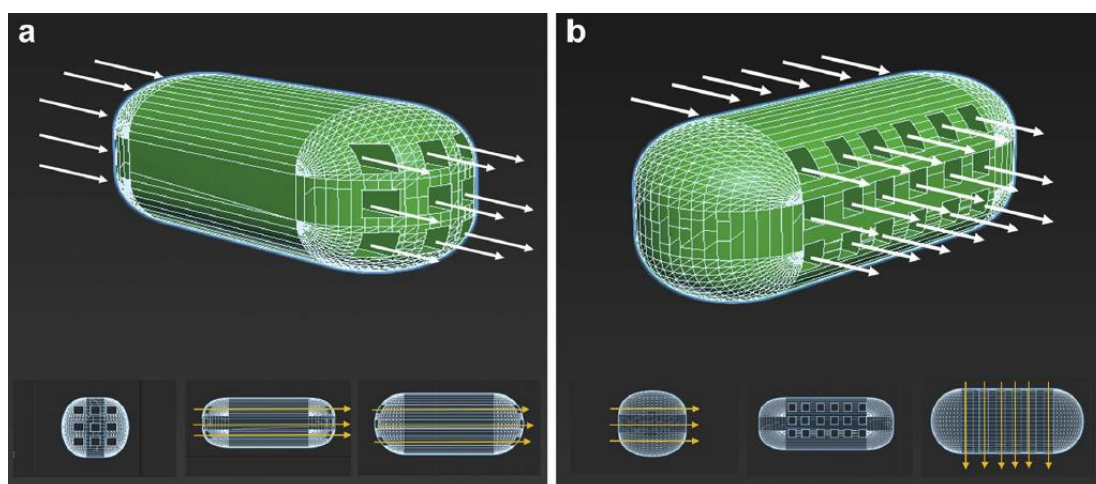


Figure 2.13: Digital design representing perforating square sectioned channels in capsule design (a) parallel to long axis (b) at right angle with long axis with frontal, side and top view of channelled tablet designs. Reproduced with permission from ⁴⁷.

Thin-walled drug free capsules without macroscopic defects were printed by using zoning process which involves modification of 3D printer files by creating discrete zones. These capsules were then filled with liquid formulation of metformin HCl. It was reported that the liquid formulation was not dripped from thin-walled FDM printed capsules having discrete zones. Moreover, visible defects were seen on the capsules without discrete zones. It was concluded that such kind of approach is useful for the delivery of temperature sensitive drugs and suitable for the delivery of liquid formulation ⁴⁸.

Arafat *et al.* also proposed the concept of facilitating drug release by incorporating built-in gaps in the tablet. Figure 2.14 shows a schematic of a tablet design containing blocks/gaps in comparison with a solid non-block tablet. Tablets with 1 mm gaps disintegrated within a time of 4 minutes and 86.7% of theophylline was released within a period of 30 minutes, thus meeting the criteria of immediate release drug products set by the USP ⁴⁹.

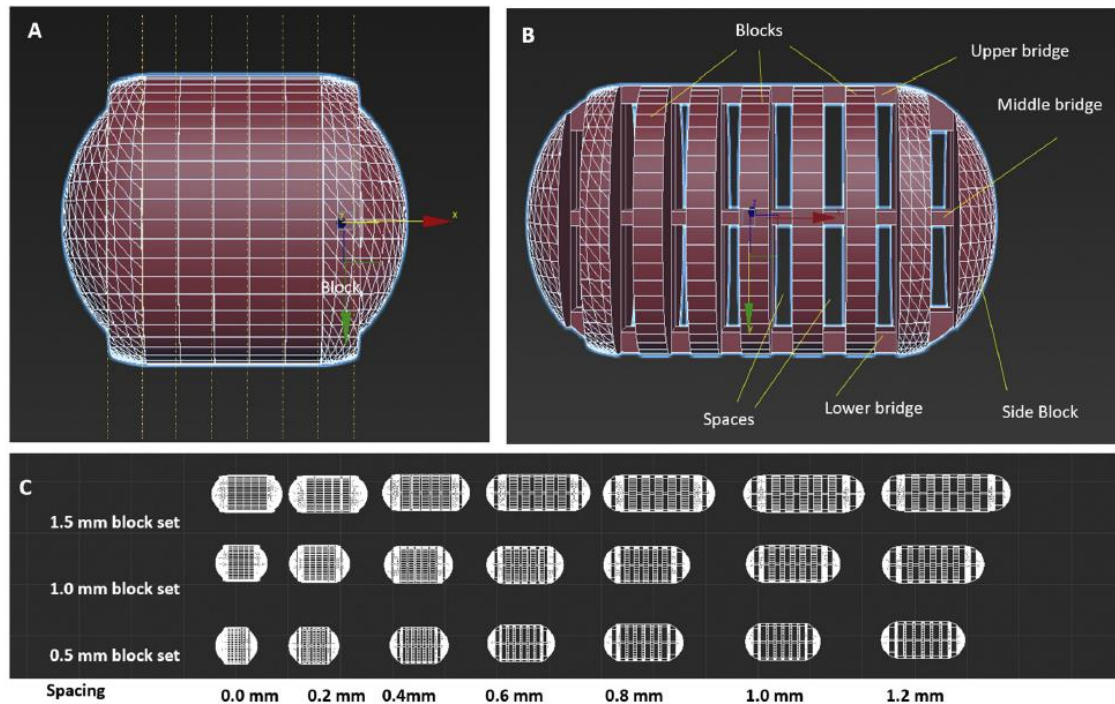


Figure 2.14: Digital schematic showing comparison of multi-block unit with non-block design (A) Solid-block tablet (B) Tablet with 9 block units joined together by 3 bridges (C) three sets of tablets with different block size (0.5, 1 and 1.5 mm), reproduced with permission from ⁴⁹.

Dual-compartmental dosage units (dcDUs) were fabricated to accommodate drug loaded filaments, prepared via hot-melt extrusion (HME). PLA was used to develop a two-compartment shell. The printing was paused after the shell was printed to fill the compartment with weighed extruded drug-loaded (either isoniazid or rifampicin) filaments manually and subsequently, a cap of PVA polymer was printed to close the shell. The bottom of the shell was also filled with weighed drug loaded filaments and some of these formulations were physically sealed. *In vitro* pH transfer dissolution testing and *in vivo* studies reported modified drug release pattern from dcDUs. *In vitro* dissolution tests revealed that the

outcome of sealing was effective resulting in effective delay of drug release. While the effect of sealing was not prominent during *in vivo* studies carried out in rats⁵⁰.

A two-compartment tablet loaded with self-nanoemulsifying drug delivery system was developed and micro computed tomography and terahertz pulse imaging techniques were employed to examine the printing accuracy and resolution of the inner structure of 3D printed tablets. These techniques revealed that some of the structures comprising PVA were larger than the computer aided design templates. The drug release from the two-compartment dosage unit was compared with the gelatine capsules and it was observed that there was sufficient delay in the release of drug from two-compartment formulations. Initially, 80% of the saquinavir was released from the outer compartment followed by the release of halofantrine from inner compartment that took place after approximately 240 minutes⁵¹.

To attain targeted delivery of drugs to the intestinal region, budesonide loaded PVA caplets were fabricated and coated with an enteric polymer (Eudragit® L100) to modify the drug release and this method resulted in desired drug release pattern. There was no drug release in acidic environment whereas at alkaline pH (7.2) approximately 80% of the total drug was released within 8 hours⁵².

A combination of PVP and a methacrylic polymer, Eudragit L100-55, was used to develop gastric resistant tablets. The inner core of the tablet was made up of PVP and was loaded with the drugs as shown in Figure 2.15, which was then encapsulated in a methacrylic polymer. Tablets were printed with three model drugs, (theophylline, budesonide and diclofenac sodium). Such design of the tablet resulted in desired drug release. In acidic pH, there was almost no drug release while in alkaline pH, more than 80% of all the drugs were released within 8 hours⁵³.

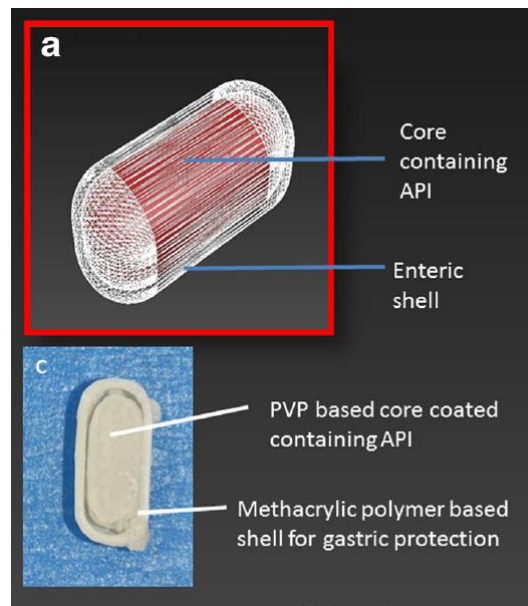


Figure 2.15: Digital design of the 3D printed tablet with enteric shell. Reproduced with permission from ⁵³.

An osmotically controlled tablet was printed, by encapsulating the core of the tablet with a cellulose acetate coating shell. The core was composed of PVA, diltiazem and osmogens such as NaCl and mannitol. All the formulations showed sustained release of the drug which proved that osmotic formulation can be 3D printed to provide sustained release of the drug ⁵⁴.

By simple modification in dosage form design it was possible to achieve series of zero drug release profiles for 16 to 48 hours. This was achieved by creating a shell around the core of the tablets. The use of different shell designs and infill density made it easy to manipulate the drug release according to the requirements ⁵⁵.

pH-sensitive polymethacrylate tablets were manufactured for the targeted (colonic) and controlled delivery of 5-fluorouracil (5-FU). FDM allowed printing of hollow tablets to accommodate chitosan-coated alginate beads loaded with 5-FU. Dissolution testing revealed that the controlled release of 5-FU beads encased within the polymethacrylate tablet was pH-dependent. The polymethacrylate matrix acted as a barrier which enabled targeted (colonic) delivery of 5-FU alginate beads ⁵⁶.

Researchers have also introduced 3D printed tablets capable of achieving enteric dissolution without an outer coating of enteric polymer. For this purpose, different grades (HG, LG and MG) of HPMCAS were used to develop enteric printlets with 50% w/w drug loading

(paracetamol). *In vitro* dissolution test revealed that drug release was dependent on some factors that include inner structure of the tablets, polymer composition and drug loading. Printlets developed using polymers with lower pH threshold resulted in faster drug release. HPMC LG showed fastest release followed by MG and HG. Initially, all the tablets resulted in slow drug release (less than 10%) in acidic pH (1.2) complying with the USP criteria whereas the drug release was fastest in the alkaline pH⁵⁷.

Commercially available PVA filaments were utilised to extrude drug-loaded filaments. In total, four filaments, two of paracetamol with drug loading of 4.3% and 8.2% and two of caffeine with drug loading of 4.7% and 9.5% were successfully extruded. All the caplets resulted in 100% drug release in less than 480 minutes. Independent of change in the pH of the dissolution media, the drug release started in acidic medium simulating gastric conditions and continued in the bicarbonate buffers (intestinal conditions). The drug release profile from formulations containing caffeine was moderately faster than formulations with paracetamol. Furthermore, it was also reported that there was no relationship between drug release rate and microstructure of the caplets⁵⁸.

Multi-layered tablets containing 4 drugs in one dosage forms were printed via FDM using PVA. The drugs were layered on the top of each other in a sequence. Two types of layer sequencing were used based on the solubility of drugs, the most soluble drugs lisinopril dihydrate and amlodipine besylate were printed in external layers and low solubility drugs were accommodated in internal layers of the device and vice versa. It was reported that the drug release was dependent on the layer position of drug in the tablet and a biphasic drug release profile was obtained i.e. initially the drug release was faster but later on became slow. This effect was more prominent in tablets with soluble drugs on the external layers⁵⁹.

Nearly, 70% of oral dosage forms account for immediate release tablets. Researchers have investigated the feasibility of various polymers resulting in the successful fabrication of immediate release tablets. PVP was used to fabricate immediate release tablets of two model drugs, theophylline and dipyridamole. *In vitro* dissolution testing showed that the formulation achieved more than 85% release of theophylline and dipyridamole in a period of 30 minutes

⁶⁰.

Eudragit EPO and tri-calcium phosphate (TCP) were used to develop immediate release caplets of four model drugs (theophylline, captopril, prednisolone, and 5-ASA). The disintegration time of all the formulations was less than 15 minutes. Dissolution data showed that more than 85% of drug was released in a time of 30 minutes for all model drugs ⁶¹. Another study by Sadia *et al.*, has also reported the use of Eudragit EPO along with Triethylcitrate (TEC) and TCP for immediate release of combination of drugs, hydrochlorothiazide and enalapril maleate from bilayer oval-shaped tablets ⁶². Moreover, research study by Gioumouxouzis *et al.*, not only reported the combination of two anti-diabetic drugs but also achieved two different dissolution profiles i.e. immediate (glimepiride) and sustained (metformin) from a bilayer dosage form hence increasing the patient compliance. Eudragit[®] RL and PVA were used as carrier polymers along with a plasticiser, poly ethylene glycol (PEG) 400. According to the dissolution testing, the dissolution of glimepiride was 87.04% after 75 minutes, exhibiting immediate release while for metformin it was 86.98% in 480 minutes, exhibiting sustained release ⁶³.

Different methacrylic (Eudragit RL, RS and E) and cellulose polymers (HPC SSL) and their combinations were also investigated to achieve immediate and sustained drug release. Plasticisers, triethyl citrate and triacetin, were also used to facilitate processing and to increase the mechanical properties of filaments. An easy to swallow caplet was designed and 50% w/w drug (theophylline) loading was achieved. The inclusion of Eudragit RL polymer resulted in the extended release of theophylline over 16 hours in a dissolution test. However, tablet matrix composed of Eudragit E and HPC SSL showed immediate release and the majority of theophylline was released in 25 minutes. The mixture of Eudragit RL and Eudragit RS resulted in slow release of theophylline ⁶⁴. FDM technology was modified to print the tablets using powder mixture or pellets instead of filaments. A single screw extruder was employed to achieve this goal. Different grades (UL, SSL, SL and L) of HPC were used to prepare powder mixtures using itraconazole as a model drug. Tablets were successfully prepared using this method. Tablets printed with ultra-low molecular weight grade HPC showed faster drug release as compared to other HPC grades ⁶⁵.

Modified release tablets were printed with abuse deterrent and alcohol resistant properties ⁶⁶. Evaluation of different polymers (Kollidon[®] VA64, Kollicoat[®] IR, Affinisol[™]15 cP, and HPMCAS) and their combinations revealed that a 1:1 mixture of Affinisol[™]15 cP and Kollidon[®]

VA64 and 10% drug loading is optimal for the fabrication of immediate release drug delivery devices via FDM. Dissolution testing of tablets (60% infill density) at pH 2 showed nearly 90% release of haloperidol within 45 minutes, whereas tablets with 100% infill density released 85% drug in 120 minutes. In contrast, the rate of dissolution was relatively rapid in pH 6.8 with nearly 70% and 80% drug release in 60 and 120 minutes, respectively, from tablets with 60% infill, whereas tablets with 100% infill took almost 3 hours to achieve complete drug release (more than 80%). The higher porosity in the 60% infill tablets was responsible for the faster drug release⁶⁷. FDM has proven to be suitable for the printing of thermolabile drugs for example pantoprazole sodium sesquihydrate. The commonly used PVP and PEG were investigated as carrier polymers. Tablets fabricated with PVP showed fastest drug release (10 min) than tablets formulated with PEG (29 min). This study showed that FDM is suitable technique while dealing with thermos-sensitive drugs and PVP is preferable in formulating immediate release tablets than PEG⁶⁸.

To overcome the problem of thermal degradation of drug (4-ASA) reported by Goyanes et al.,²⁰ Kollidon (VA64 and 12PF) was used as a matrix forming carrier polymer to print immediate release tablets with drugs (ramipril and 4-ASA) having low melting temperature. Both drugs were printed at 90 °C. The singular or combinatorial use of Kollidon VA64 with Kollidon 12 PF resulted in immediate drug release profile. More precisely, the *in vitro* dissolution testing showed that the combination of polymer exhibited rapid drug release as compared to the single use of polymer. Drug release was 100% within 20-30 minutes. Moreover, no thermal degradation of drugs was reported. This study concluded that appropriate selection of excipients and temperature can overcome such problems i.e. thermal degradation of drug⁶⁹.

The storage, stability, shipping and delivery of nanocapsules is challenging due to the risk of microbial contamination. FDM printed tablets loaded with suspension of deflazacort polymeric nanocapsules were developed to address this issue. Polymeric materials like Eudragit® RL100 and polycaprolactone (PCL) were used to print tablets and mannitol was used as a channelling agent. Release constant for Eudragit tablets with channelling agent was faster compared to PCL tablets whereas similar release rates were observed for Eudragit and PCL tablets without channelling agent. Moreover, tablets having 50% infill density showed rapid drug release with high drug loading. It was concluded that this approach has proven to be

useful in converting suspension of nanocapsules to solid dosage forms that ensures its chemical stability ⁷⁰.

3D printed capsular device has also been investigated for the delivery of dietary supplements using HPC as a carrier polymer. Images of the 3D printed capsular device with different size and shapes are shown in Figure 2.16. The devices were filled and assembled manually. The printed devices showed the two-pulse release of caffeine, in compliance with the swellable nature of the polymer ⁷¹.



Figure 2.16: FDM printed middle and hollow parts of dual compartment device, reproduced with permission from ⁷¹.

Although FDM has shown great potential in fabricating controlled/sustained and immediate release dosage forms, tablets with complex geometrical shapes, tablets with discrete zones, built-in gaps, tablet within a tablet etc., the range of polymeric excipients is limited to PLA, PCL, PVA methacrylic/cellulose polymers. Moreover, the drug load is often below 30% w/w with the exception of few research studies that printed caplets with 50% w/w drug loading. Therefore, researchers have investigated thermoplastic polyurethanes (TPUs) that allow fabrication of filaments with high drug loads (up to 70% w/w) without facing HME processing issues or burst-release and also has the potential to delay the drug release. Different grades of TPU were examined using two model drugs metformin HCL and theophylline. TPU with high cross-over values $T_{\tan \delta}=1$ and high shore hardness ($> 41D$) was found to be suitable for higher drug loading, enabling 60% w/w drug loading. Metformin HCl being freely soluble was used with Tecoflex™ EG-72D grade of TPU, which is hydrophobic. Hydrophilic grade, Tecophilic™ SP-60D-60 of TPU was used with slightly soluble theophylline. *In vitro* dissolution tests showed

that all TPU-based formulations containing drugs of varying aqueous solubility successfully prolonged the drug release over a period of 24 hours ⁷².

An impermeable hollow container of tablet shape was printed using PLA by 3D printer. A polymer solution (the mixture of 4-Pentenoic anhydride (PNA), pentaerythritol tetrakis (3-mercaptopropionate) (PETMP), 3, 5- dioxo-1,8-dithiooctane (an ethylene glycol-based dithiol, EGDT)), containing orange dye was poured onto polydimethylsiloxane (PDMS) mould. For cross-linking purposes, this mixture was then exposed to ultraviolet light for 10 minutes. This cross-linked polymer was then removed from the mould and inserted into a PLA container. After insertion, another layer of polymer solution without dye was poured onto the top to avoid burst release of dye and was then again cured by ultraviolet light for 10 minutes. The final size of the tablets was 11 mm × 7.5 mm × 5.5 mm with a 1.1 mm thick coating of PLA. Tablets containing five different shapes of moulds were fabricated. After immersion in phosphate buffered solution, the dye started to release after 10 hours. Depending on the shape of the mould used, different release profiles were observed including constant, pulsed, decreasing and increasing release profiles. A series of release profiles including constant, decreasing and increasing were also observed from a single tablet concluding that the tablet can be customised to achieve desired release profile. Furthermore, two moulds one of which contained orange dye and the other contained blue dye were prepared and inserted into one tablet. The results revealed that one of the dyes showed increased release and the other showed a decreasing profile, as was expected. For further customisation of the release profile, two pieces of polymer were inserted manually away from the bottom of the container and at different heights. The release profiles of the two dyes were again as expected, five pulses that were out of the phase ⁷³.

The likelihood of developing oral capsules capable of producing pulsatile release by FDM 3D printing from HPC filaments was reported. The capsular devices were manually filled and amassed exhibited the two-pulse release of acetaminophen, in accordance with the nature of the polymer. It was noticed that these assembled capsular devices showed a lag phase before a swift release of the drug. The ability of these capsules to release drug and their morphological changes on contact with water were comparable to the delivery systems developed by injection moulding ⁷⁴.

Injection moulding is a non-3D printing technique that has been proven to be suitable for the manufacturing of capsules with complex geometry with cavities, curvature and details in the order of hundreds of microns. For the purpose of comparing injection moulding and FDM, multi-functional versatile capsular delivery platform composed of isolated compartments were fabricated using both techniques (Figure 2.17⁷⁵). These capsules were loaded either with two or more model drugs or with varying dose of one model drug to achieve multiple release profiles. Compartment halves composed of readily soluble (KIR), enteric (hydroxypropyl methyl cellulose acetate succinate (HPMCAS)), swellable or erodible (HPMC) polymers containing acetaminophen and with wall thickness of 600 or 1200 μm , were developed and assembled. The desired two-pulse release pattern was achieved, consistent with the attributes of the carrier polymers. The drug release pattern from moulded capsular devices was also consistent with the printed devices. On comparison, even though the printed and moulded devices had similar composition and wall thickness, the latter was less resistant to deformation⁷⁵. FDM was also compared with another 3D printing technology, stereolithography (SLA). An anti-acne drug (salicylic acid) loaded patches were fabricated by both techniques. The diffusion tests revealed that the drug diffusion rate is faster in SLA patches than the patches made with the FDM⁷⁶.

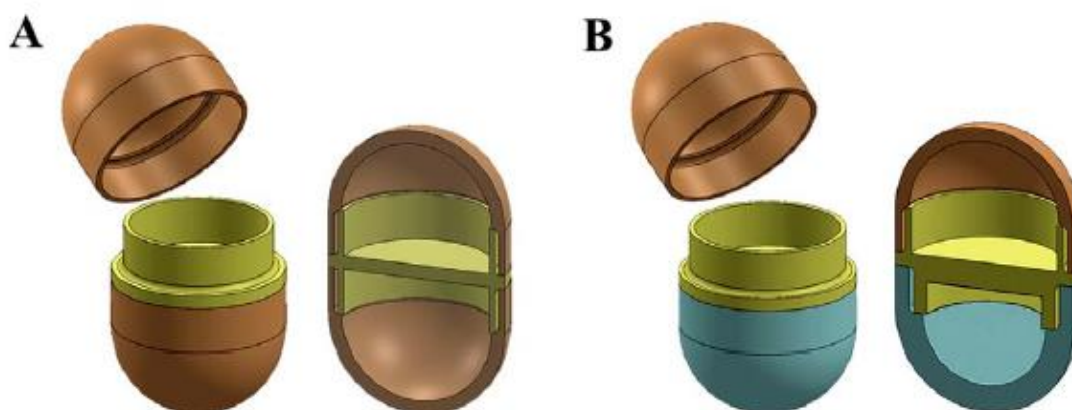


Figure 2.17: Cross-section and isometric views of dual compartment devices with (A) same or (B) different thickness, reproduced with permission from⁷⁵.

FDM printed tablets were compared with tablets developed using directly compressed mill-extruded tablets and tablets prepared from physical mixture. It was noticed that the printed

tablets had smooth surfaces and an extended drug release rate due to its tight internal structure, high density and hardness. In contrast, faster drug release patterns were observed with physical mixture tablets and directly compressed mill-extruded tablets⁷⁷.

The use of FDM in combination with liquid dispensing has also been reported. FDM was used to fabricate shells composed of different polymers including Eudragit RL and EPO for sustained and immediate release, respectively. These polymeric shells were then filled with the suspension of dipyridamole and theophylline with the help of a liquid dispenser. The optimal thickness of the outer shell to modify the release and contain the liquid drug suspension within the shells was discovered to be 1.6mm. This study reported that the dose and release behaviour of the drug can be controlled digitally by manipulating the volume dispensed and shell thickness using a software⁷⁸.

The warfarin tablets available in the market are usually of limited doses. This results in the splitting or cutting of tablets available in the market to modify the dose according to the requirements resulting in dose variation. To overcome these problems, ovoid shaped capsular devices with 200 or 400 µg warfarin doses were developed via FDM to achieve accurate dose delivery of the drug. *In vitro* drug release studies were conducted in a fasted state simulated gastric fluid and was in accordance with the British pharmacopoeia criteria for warfarin tablets with all tablets showing more than 80% dissolution after 45 minutes. Furthermore, 3D printed devices were compared with an aqueous solution of warfarin during *in vivo* studies performed in rats. *In vivo* studies showed that 3D printed warfarin dosage forms were as effective as their liquid formulation in increasing plasma concentration after administration of a double dose of warfarin (184% vs. 192% respectively). FDM printed devices presented a lower C_{max} of 200 µg and 400 µg for warfarin tablets (1.51 and 3.33 mg/mL) as compared to the liquid formulation (2.5 and 6.44 mg/mL). T_{max} was greater for FDM printed 200 µg and 400 µg warfarin devices at 6 and 3.7 hours respectively, whereas for the liquid formulation it was 4 and 5 hours for 200 µg and 400 µg tablets, respectively. The longer T_{max} was due to the slower transit time of large oral units in rats. Such effects are not present in humans where gastric fluids are in abundance⁷⁹.

Solid oral dosage forms that disintegrate or dissolve rapidly in the mouth are categorised as orodispersible dosage forms. Such dosage forms are recommended for patients with dysphagia resulting in improved patient compliance. The most used method for the

preparation of orodispersible films is solvent casting method but other methods such as HME, 2-dimensional (2D) printing techniques and electrospinning can also be used. Various polymers are available to be used as film formers and many of them can be used in FDM for the fabrication of orodispersible films. Jamróz *et al.*, utilised PVA (water soluble) for the preparation of orodispersible films containing aripiprazole (poor aqueous solubility). The properties of FDM printed films were compared with the casted films. Due to the amorphous state of aripiprazole and the greater surface area, the printed films exhibited a rapid dissolution rate of more than 95% in 15 minutes and for casted films, the dissolution rate was 75%. It was also reported that the high concentration of PVA was responsible for the amorphous state of aripiprazole in printed films⁸⁰. Single-layered fast dissolving films (SLFDFs) and multi-layered fast dissolving films (MLFDFs) were developed containing PVA and paracetamol at 130 °C. Depending on the formulation and design, SLFDFs presented shortest disintegration time of 42 ± 7 seconds, and for MLFDFs it was 48 ± 5 seconds⁸¹. Fast-dissolving tablets of captopril were developed using HPC filaments and sodium starch glycolate and croscarmellose sodium as superdisintegrants. It was reported that the tablets showed rapid disintegration during *in vitro* analysis, in addition, the *in vivo* results were also correlated with *in vitro* results⁸². Different combinations of polymer blends were investigated to develop a solid dispersion containing felodipine. Different polymers including tween 80, PEG and PEO were used with either Soluplus or Eudragit EPO to fabricate solid dispersions. These solid dispersions were then compared with a standard dispersion composed of PVA. The drug loading was 10% and it was observed that the drug was molecularly dispersed. Solid dispersions composed of Eudragit EPO showed bulk disintegration, whereas dispersions with Soluplus disintegrated in a 'peeling style', layer by layer⁸³.

Apart from for the development of oral dosage forms (tablets and capsules), FDM has also been utilised for the development of scaffolds, implants, discs, constructs, vaginal rings and wearable mouth guards for effective and safe delivery of drugs. FDM was combined with other novel technologies including thermal-induced phase separation (TIPS) and lyophilisation, to modify the scaffolds printed with FDM. These scaffolds were investigated for bone repair. FDM printed PCL scaffolds were infused with a mixture of 1, 4-dioxane, water and PCL and then exposed to the TIPS procedure followed by lyophilisation. These scaffolds were incorporated with bone morphogenic protein-2 (BMP-2). This procedure resulted in a

nano-porous structure protected by the printed microstructure. A cranial bone defect model in pigs was utilised to carry out *in vivo* studies in pigs. Modified nano-structured PCL scaffolds did not produce promising results in comparison to unmodified scaffolds which displayed improved osseointegration and osteoconductivity after 8 and 12 weeks during *in vivo* studies⁸⁴.

For localised and sustained delivery of antibiotic (gentamicin) and chemotherapeutic drugs, (methotrexate) constructs (discs, catheters, and beads) were developed. The combination of methotrexate, gentamicin and PLA resulted in an enhanced and efficient drug delivery. Filaments extruded with gentamicin retained their anti-bacterial property and FDM printed constructs with these filaments resulted in the inhibition of bacteria on culture plates and the constructs containing PLA and methotrexate inhibited the growth of cancer cells. These constructs can be fabricated with different infill density that range from 10-100% and resolution (50-400 microns) to approach patient specific treatment⁸⁵. PCL was also investigated for the same purpose by printing catheters containing gentamicin sulphate and methotrexate separately and it was discovered that both catheters followed the same pattern of release. *In vitro* tests showed burst release of drug in the first few hours followed by steady and sustained release of drugs. The sustained release of drugs from both catheters was observed even after 5 days⁸⁶. PLA constructs (pins, screws and bone plates) with or without drugs were printed with 100% infill density. The flexural strength of drug loaded constructs was lower than the constructs with no drugs. The constructs loaded with gentamicin showed effective bacterial inhibition and XTT assay indicated the presence of chemotherapeutic properties in methotrexate constructs⁸⁷.

Controlled release dexamethasone loaded scaffolds were prepared using different concentrations of PCL and poloxamine PCL: poloxamine and binary mixtures were prepared at 100:0, 90:10 and 80:20 wt%. The scaffolds utilized were loaded with a higher concentration of dexamethasone (1 mg/ g) in order to facilitate the monitoring of the slowly released drug. It was revealed that 80:20 samples with lower porosity showed an increased degradation rate while the opposite was observed in 100:0 samples with higher porosity and slow degradation rate. As a consequence, samples of 90:10 showed greater drug release with optimum degradation rate and porosity followed by 100:0 and 80:20 samples⁸⁸.

Two different methods of drug loading into filaments were investigated using dexamethasone or prednisolone as a model drug. The first method consisted of soaking of PLA filaments in drug solution which were then used for printing scaffold while second method involved printing of scaffold at first which was then soaked in drug solution. The first method resulted in sustained release irrespective of choice of drug whereas second method showed rapid drug release which concludes that drug loading method is significant in defining drug release profiles ⁸⁹.

A biocompatible scaffold was fabricated to improve tendon graft healing. For this purpose, bolts for bone anchoring were developed by FDM using PLA polymer. Whereas nanofibrous membranes laden with collagen were prepared by electrospinning using a biodegradable material, poly (lactic-co-glycolic acid) (PLGA). Varying ratio of PLGA and collagen was used. *In vitro* studies reported that the PLGA-collagen laden nanofibrous membranes were hydrophilic, stable and suitable for animal studies. Nanofibrous membranes containing 67/33 ratio of PLGA/collagen were selected for *in vivo* studies in rabbits. These studies showed that the bolts have sufficient durability and stability for bone healing. Collagen loaded nanofibrous membranes resulted in increased cell attachment and tissue invasion thus enhancing bone healing ⁹⁰.

Scaffolds with holes of varying diameters were printed to achieve zero-order drug release kinetics using carbamazepine as a model drug. Scaffolds with diameters of 1, 1.5 and 2 mm were fabricated, and it was found that the rate of drug release was directly proportional to the diameter of the holes i.e. drug release increased as the size of the holes increased. The number and diameter of holes also affected the drug release, for instance, when the number of holes was 4 in scaffold, the drug release rate was 0.0048 mg/min, 0.0065 mg/min and 0.0074 mg/min for holes of 1, 1.5 and 2 mm in diameter, respectively. However, when the number of holes was increased to 12, the drug release rate also increased to 0.0021 mg/min, 0.0050 mg/min and 0.0092 mg/min for holes of 1 mm, 1.5 mm and 2 mm in diameter, respectively ⁹¹.

Composite scaffolds of various shapes and dimensions were printed using cryogenic FDM printer for cartilage repair (Figure 2.18 ⁹²). The printing ink was composed of dispersion of nanoparticles of polyurethane (PU), hyaluronan and bioactive agents e.g. a small drug molecule Y27632 or transforming growth factor β (TGF β 3). Y27632 [(1R, 4r)-4-((R)-1-

aminoethyl)-N-(pyridin-4-yl) cyclohexanecarboxamide, $C_{14}H_{21}N_3O$, $247.34 \text{ g mol}^{-1}$] is an inhibitor for Rho-associated coiled-coil containing protein kinase (ROCK) which increases the differentiation of chondroprogenitors but its effect on mesenchymal stem cells (MSCs) depends on the cell density and morphology. Two types of scaffolds were fabricated containing;

- i- PU, hyaluronan, TGF β 3 (concentration of TGF β 3 = 5-20 ng/ml)
- ii- PU, hyaluronan, Y27632 (concentration of Y27632 = 25 ppm)

In vitro, TGF β 3 was released slowly from the scaffolds without losing bioactivity and resulted in self aggregation and chondrogenic differentiation of MSCs after 3 days. Slow and sustained release of Y27632 was also observed for at least 8 days where MSCs aggregated after 3 days. Both scaffolds showed remarkable chondrogenesis of MSCs, however, scaffolds with Y27632 were preferable because less hypertrophy was observed with these scaffolds. Also, the release of Y27632 may efficiently induce the chondrogenesis of aggregated MSCs without using any growth factor. These scaffolds were implanted in rabbit's knees to carry out *in vivo* tests which revealed the vital role of these scaffolds in repairing the cartilage. The compliant nature of the scaffolds allowed them to fit into the shape of the defect and avoids disengagement. The degradation rate of biodegradable PU scaffolds was faster *in vivo* than that *in vitro* ⁹².

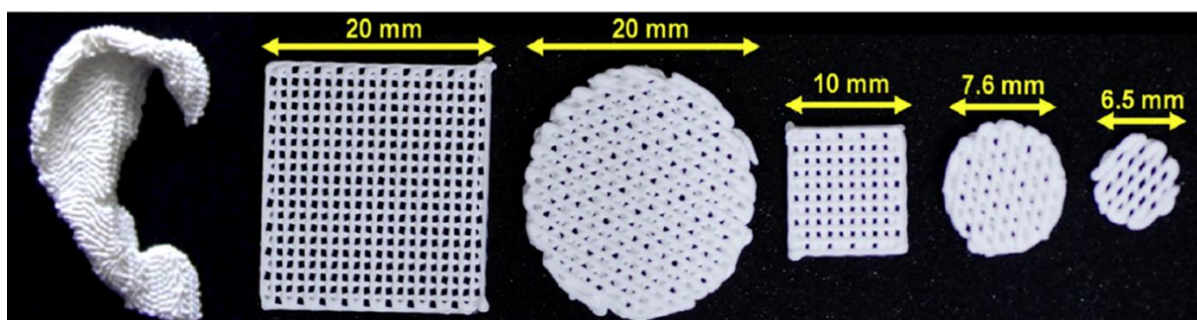


Figure 2.18: 3D printed scaffolds with various dimensions and shapes, reproduced with permission from ⁹².

A biocompatible scaffold loaded with antibiotics (vancomycin and ceftazidime) was developed for treating the femoral metaphyseal comminuted fracture. A PLA cage was printed for bone fixation, whereas PLGA nanofibrous membranes were loaded with

antibiotics to treat infection. *In vitro* studies showed that the scaffold could sustain the release of antibiotics for more than 3 weeks. Nanofibrous membranes released high concentrations of antibiotics well above their minimum inhibitory concentration for more than 30 days. *In vivo* studies carried out in rabbits also displayed the same pattern of sustained and gradual release of drugs for more than 3 weeks⁹³.

Water in oil emulsion procedure was used to develop biodegradable nanocomposite scaffolds loaded with recombinant human bone morphogenetic protein-2 (rhBMP-2) and nanoparticles of calcium phosphate with adjustable osteoinductivity and osteoconductivity. PLLA polymer solution (oil phase) was used with deionised water containing rhBMP-2 (water phase) with calcium phosphate nanoparticles. An FDM printer was modified to a cryogenic printer for the printing of the scaffolds. *In vitro* studies showed that the mechanical properties of printed scaffolds were comparable to the properties of cancellous bone of human. Sustained release of rhBMP-2 and Ca²⁺ ions from printed scaffolds along with improved osteogenic differentiation, cell attachment, viability and proliferation were also reported⁹⁴.

Phenyl-alanine based poly ester urea (PEU) was used to develop scaffolds loaded with osteogenic growth peptide or bone morphogenetic protein-2 (BMP-2). The presence of growth peptide resulted in increased mesenchymal stem cells osteogenic differentiation⁹⁵.

An orthopaedic liner comprising PLA and tetracycline for the treatment of joint infections was developed. *In vitro* studies concluded that the elution rate of tetracycline from a cube shaped reservoir with 10% infill density was higher than a cube with 20% infill density. The digital control of infill density resulted in the desired elution rate⁹⁶.

FDM was combined with a salt-leaching technique to develop scaffolds with porosity. The introduction of micro porosity and increased surface area resulted in prophylactic release of cefazolin for up to 3 days. *In vitro* studies showed that there were no cytotoxic effects at optimal cefazolin concentration of 100 µg/ml against 3T3 fibroblasts. Moreover, the formation of a blood clot was also not affected⁹⁷.

Otolaryngologists are currently facing issues with fixing the nasal cartilage implant with needle and threads. For this purpose, poly (L-lactic acid) (PLLA) biocompatible scaffolds for structural support of the nasal system were fabricated with FDM. Nanofibrous membranes containing gelatine and osteogenon were loaded on to the surface of scaffolds with the help

of electrospinning. It was observed that the concentration of gelatine affected the properties of nanofibrous membranes. During bioactivity tests, PLLA scaffolds showed mineralisation due to the presence of drug and gelatine on their surfaces. The presence of gelatine also accounted for the increased cell adhesion ⁹⁸.

Biocompatible scaffolds were printed with PLA for the delivery of hydrophilic in-situ formed sodium indomethacin. PAA (poly acrylic acid)-PVA hydrogel was incorporated into scaffolds loaded with sodium indomethacin to improve the structural strength and to provide support to damaged tissues. Drug release studies showed that, initially, the drug release was rapid due to weakly bound highly hydrophilic sodium indomethacin causing 65.23% of the drug to be released within the first 60 minutes. Following this, a sustained release was observed due to matrix swelling, with 83.36% drug released after 8 hours. The results concluded that the release pattern is suitable for prolonged healing of damaged tissues ⁹⁹.

Supercritical fluid technology was used to load the drug, ibuprofen, onto printed PLA scaffolds of varying pore sizes. It was observed that the dissolution rate decreased with the decrease in pore size which concluded that dissolution rate can easily be changed by changing the pore size. The supercritical fluid technology was able to develop controlled release dosage forms that can be tailored ¹⁰⁰.

A combination of polymer (PLA), plasticiser (PEG) and ceramic (nano hydroxyapatite) was used to fabricate a scaffold for bone regeneration which was then loaded with dexamethasone. *In vitro* studies showed that the initial stages of cell proliferation were not affected by dexamethasone but later, the release of dexamethasone resulted in improved mineralisation and phosphatase secretion. *In vivo* studies in rats also confirmed that these scaffolds helped in accelerating bone regeneration ¹⁰¹.

Hydrogels loaded with cell or drugs are commonly used in tissue engineering. FDM has been utilised by Andersen et al., to develop a hydrogel composed of hydroxyethyl cellulose, alginate and hyaluronic acid and loaded with small interfering RNA (siRNA) for effective tissue development. Such composition provides optimal printability, serum stability and cell biocompatibility to the gel. Mesenchymal cells were also seeded onto these hydrogels and when introduced to spinal cord's cells these gels resulted in sequence specific and localised gene slicing ¹⁰².

Bacteria have a survival strategy to colonise surfaces and grow as biofilm communities embedded in gel-like polysaccharide matrices. For example, a catheter for urinary tract provides ideal environment for the development of bacterial species and thus produce complications in the treatment of patients. To address this issue, FDM was utilised in the development of anti-microbial devices by using an anti-microbial API for instance, nitrofurantoin. Three types of sample discs were printed: (1) discs only with PLA (2) nitrofurantoin was added externally on the top of printed PLA discs and (3) nitrofurantoin was incorporated into PLA before printing the discs. It was reported that it is more effective to incorporate nitrofurantoin into structures instead of adding the drug on the top. Bacterial attachment was highest in samples containing only PLA and samples with external addition of nitrofurantoin also showed biofilm formation. On the other hand, samples with incorporated nitrofurantoin resulted in 86% inhibition of biofilm colonisation ¹⁰³.

Different loadings, 10% and 30%, of nitrofurantoin in PLA discs were also investigated. Drug release from these discs was dependent on drug loading i.e. higher drug loading resulted in higher drug release. Discs with 30% loading of nitrofurantoin were able to prevent the planktonic and surface associated growth of *Staphylococcus aureus* in a period of 7 days. However, discs with 10% drug loading only prevented surface-associated growth ¹⁰⁴.

Anti-bacterial 3D printed meshes loaded with gentamicin were fabricated in a layer by layer manner. The introduction of printed meshes to the culture media with *Escherichia. coli* resulted in inhibition of bacterial growth in a zone with an area size of $1.1 \pm 0.1 \text{ cm}^2$, whereas for culture media with *Staphylococcus aureus*, growth inhibition was achieved in a zone with an area size of $1.2 \pm 0.1 \text{ cm}^2$. Furthermore, meshes without gentamicin did not affect bacterial growth ¹⁰⁵.

Bioactive potential of pure oleo gum resins from olibanum, benzoin and myrrha was evaluated to develop bioactive discs using FDM. These resins were charged with 10% nanoparticles of metal oxides MoO_3 , Cu_2O , P25 and TiO_2 . The tested biopolymers showed the characteristics of commercially available semi-crystalline polymers. Anti-bacterial and anti-fungal tests showed that surface associated growth was prevented with discs containing the pure state of oleo gum resin while discs charged with metal oxides had increased bacteriostatic effect ¹⁰⁶.

Wearable oral drug delivery devices with tuneable release characteristics and customisable designs were developed and first in-human study was carried out. The objective of this study was to treat oral diseases by localised and sustained delivery of drugs. Wearable mouth guards were designed on the basis of dentition impressions using intraoral scans and printed using two biodegradable polymers; PLA and PVA. Two types of filaments were extruded to print mouth guards including chlobetasol propionate loaded PLA filaments and vanillic acid loaded PLA: PVA (9:1 w/w) filaments. Drug release kinetics showed sustained release of chlobetasol propionate over 14 days, while vanillic acid was rapidly released with 71% of the drug released in 10 days. In this study, polymer composition was also used to achieve the desired drug release profile instead of changing infill pattern, infill density or shape of the device. Images of the mouth guards before and after *in vitro* dissolution are shown in Figure 2.19. However, the human volunteers experienced discomfort while wearing mouth guards with vanillic acid due to its low quality because of the low resolution of FDM ¹⁰⁷.

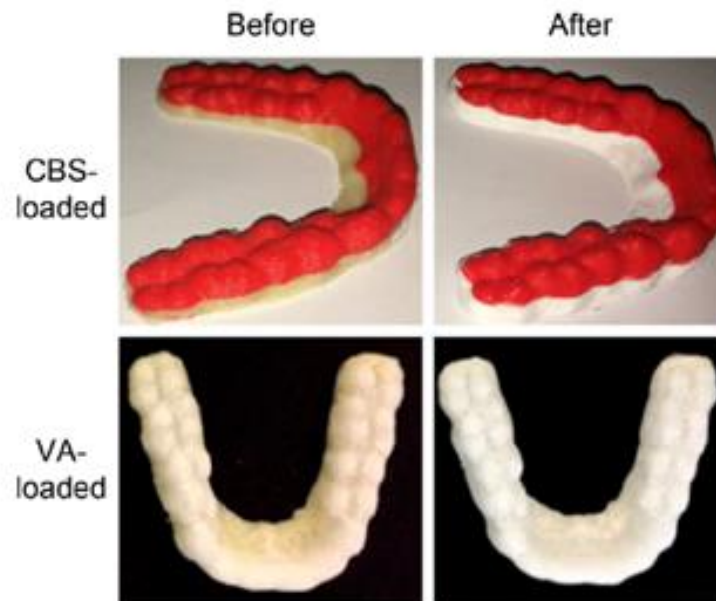


Figure 2.19: Images of the CBS (chlobetasol propionate)-loaded and VA (vanillic acid)-loaded mouth guards before and after the in vitro dissolution study, reproduced with permission from ¹⁰⁷.

Since 1960, implantable drug delivery systems have been studied. These implants are usually manufactured as intravaginal rings (IVR), rods and intrauterine system (IUS) using injection moulding and extrusion. The polymers used for the manufacturing of these drug delivery devices have to be non-biodegradable or should have a very slow degradation rate and also be non-swellable. Commercially available IVR and IUS are composed of non-degradable polymers such as ethyl vinyl acetate (EVA) or polydimethylsiloxane (PDMS), however PCL is a potential alternative of thermoplastic materials for manufacturing of drug implants through 3D printing due to its slow degradation rate. The properties of the polymer allow long sustained release from drug delivery devices, as well as remarkable biocompatibility and high permeability to many drugs.

To investigate the potential of PCL in the fabrication of implantable drug delivery systems, T-shaped intrauterine devices for controlled release of indomethacin were printed with FDM. PCL filaments with drug loading of 5%, 15% and 30% were developed separately using HME followed by printing of intrauterine devices. Drug release studies of 3 prototypes (1-2 weeks old) showed an initial burst release phase followed by slow diffusion of drug. The prototype with 5% drug showed faster drug release compared to the others, whereas the slowest release was observed with the prototype containing 30% drug¹⁰⁸.

FDM was investigated for the development of personalised implantable drug delivery system. It was reported that the varying diameter and infill densities affected the drug release from the printed device. The drug release was increased with increase in diameter whereas increase in infill percentage hindered the dissolution. The type of polymers (PMMA, PLA, antibacterial PLA, polyethylene terephthalate glycol) did not affect the dissolution significantly, however, the highest drug release was observed from PMMA after 24 hours. MTT assay confirmed that the printed implants were nontoxic and cytocompatible¹⁰⁹.

A drug delivery device controlled by the remote was printed for cancer treatment. At first, a reservoir was printed which was then fitted with the magnetic bar. The use of varying magnetic fields allowed tuning of the drug release. The position of the magnetic bar in the reservoir affected the drug release i.e. when placed at the bottom, only 10 % drug was released in 12 hours whereas when placed at the side of the device 50% drug was released in 20 minutes. The device was also able to inhibit cell growth during *in vitro* cell culture test¹¹⁰.

12 different grades of EVA were investigated as drug carrier polymer for FDM printing of T-shaped intrauterine system and subcutaneous rods. Of these, only five grades were revealed to be suitable for FDM printing. Filaments were extruded with 5% and 15% indomethacin drug loading. *In vitro* drug release concluded that drug release from filaments with 5% drug loading was faster than the filaments with 15% drug loading. The developed FDM printed intrauterine system and subcutaneous rods with 5% drug resulted in faster drug release than those devices printed with 15% drug loaded filaments. Overall, the drug release from the filaments was lower than the prototypes because of the difference of the state of API. In filaments most of the drug was crystalline whereas in printed constructs the drug was amorphous ¹¹¹.

3D printed constructs were developed for intrauterine hormonal delivery. Oestrogen and progesterone were coated on PCL pellets and were extruded to obtain the filaments. These filaments were used as stock material for FDM to get the intrauterine device. *In vitro* assay showed that printed constructs resulted in increased luciferase activity depicting the presence of a bioactive agent and No detrimental effects were observed. Moreover, extended release of hormones was observed over a period of one week ¹¹².

Vaginal rings of different shapes (O, Y and M) Figure 2.20 were printed for sustained delivery of hormones. PEG 4000 was mixed with progesterone to form a solid dispersion. The dispersion was cut into pieces to mix with a mixture of PLA: PCL (8:2) and tween 80 to extrude filaments followed by printing of rings. No thermal degradation of progesterone was observed during printing. Due to the higher surface area/volume ratio and unique shape, O-shaped vaginal rings had a higher dissolution rate than other Y and M-shaped rings. However, all the rings resulted in sustained release of progesterone for a period of 7 days. It was reported that the mechanism of diffusion was responsible for sustained release of progesterone ¹¹³.

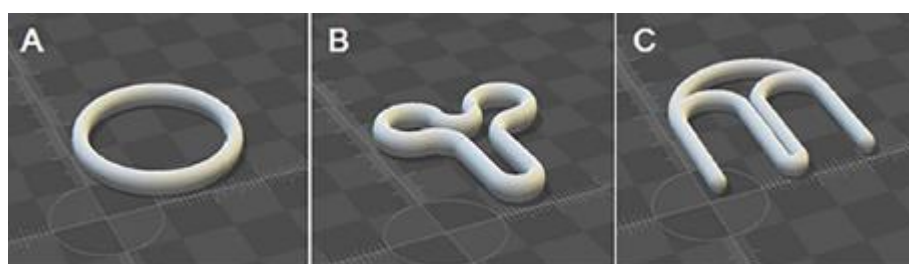


Figure 2.20: STL model of vaginal rings (A) O-shaped (B) Y-shaped (C) M-shaped, reproduced with permission from ¹¹³.

Microneedles of different lengths were fabricated for more effective transdermal delivery of drug. Digital control over various parameters shape, length and density helped in designing microneedles with desired characteristics. PLA filaments were utilised to print microneedle arrays. The arrays were placed in 5 molar KOH solution for etching and for fluorescein loading, the arrays were then placed in acetone solution containing fluorescein (2mg/ml). Penetration testing of printed arrays on parafilm and porcine skin showed that 92% and 84% of the needles pierced the parafilm and porcine, respectively, without getting broken after applying transverse pressure. A single array containing 25 microneedles delivered 3.23 μg of drug. Approximately 50% of the drug was released in a period of 4 hours ¹¹⁴.

An ABS expansion chamber lined with RPMI 2650 nasal cell epithelia was designed and printed to study drug permeation, deposition and transport over nasal epithelia of commercially available/new aerosol nasal products after being actuated. Seeding density and culture time affected the mucus production in RPMI 2650 nasal cell line. 2.50×10^6 cell/ml was found to be the optimal seeding density for mucus production. Commercially available Rhinocort nasal spray containing budesonide suspension was used to carry out the drug permeation and deposition experiments. After actuation of Rhinocort spray into the expansion chamber, initially, $47.3 \pm 5.0\%$ of the drug was transported across nasal epithelia. After 4 hours of the experiment, $14.4 \pm 4.9\%$ of budesonide was found on the surface of the cells, whereas $2.5 \pm 1.6\%$ was present inside the cells, indicating low binding of drug with RPMI 2650 nasal cell epithelia in the expansion chamber ¹¹⁵.

Anti-bacterial wound dressings were developed with PCL comprising different metals e.g. silver, zinc and copper. FDM technique allowed nose shaped wound dressings customisable

to patient' needs. Inductively coupled plasma atomic emission spectroscopy technique was used to test metal release from wound dressings. The release of all the metals was rapid in the first 24 hours followed by slow and sustained release for up to 72 hours. Thermal activity tests showed that wound dressings with silver and copper metals had the most effective bactericidal properties. Moreover, it was reported that increase in the thickness of the wound dressing and loading of metals could have improved outcomes ¹¹⁶.

Graphene incorporated PCL was used as feed material for a commercially available FDM printer to print a cardiac stent. This stent was loaded with niclosamide and IP6 (inositol phosphate 6) to regulate normal blood flow. Improved mechanical properties of printed stent were observed during *in silico* examination. *In vitro* tests of 120 hours reported non-toxic behaviour of stent towards cell growth. Anti-blood coagulation testing using the blood from a pig showed that niclosamide and IP6 drugs had no role in blood coagulation. Results from an *ex vivo* study concluded that these stents are plausible to use in real patients ¹¹⁷.

An automatic robotic system for anti-microbial testing was developed combining FDM printing technology with ink-jet technology. Fresh agar solution from the robot was deposited on a petri dish with kanamycin and tetracycline to evaluate the anti-bacterial properties of these drugs. Instead of a circular pattern, lanes of agar resulted in increased spatial resolution. Deposition of 37.1 µg of kanamycin showed 24.2 ± 0.68 mm zone of inhibition while deposition of 43.5 µg of tetracycline showed 27.5 ± 3.4 mm inhibition zone ¹¹⁸.

The research studies cited above show that the type of pharmaceutical dosage form mostly fabricated *via* FDM, irrespective of the delivery route, were tablets/capsule/discs followed by scaffolds and implants as shown in Figure 2.21. These studies demonstrate that FDM is a suitable method for preparing solid dosage forms approaching personalised drug delivery.

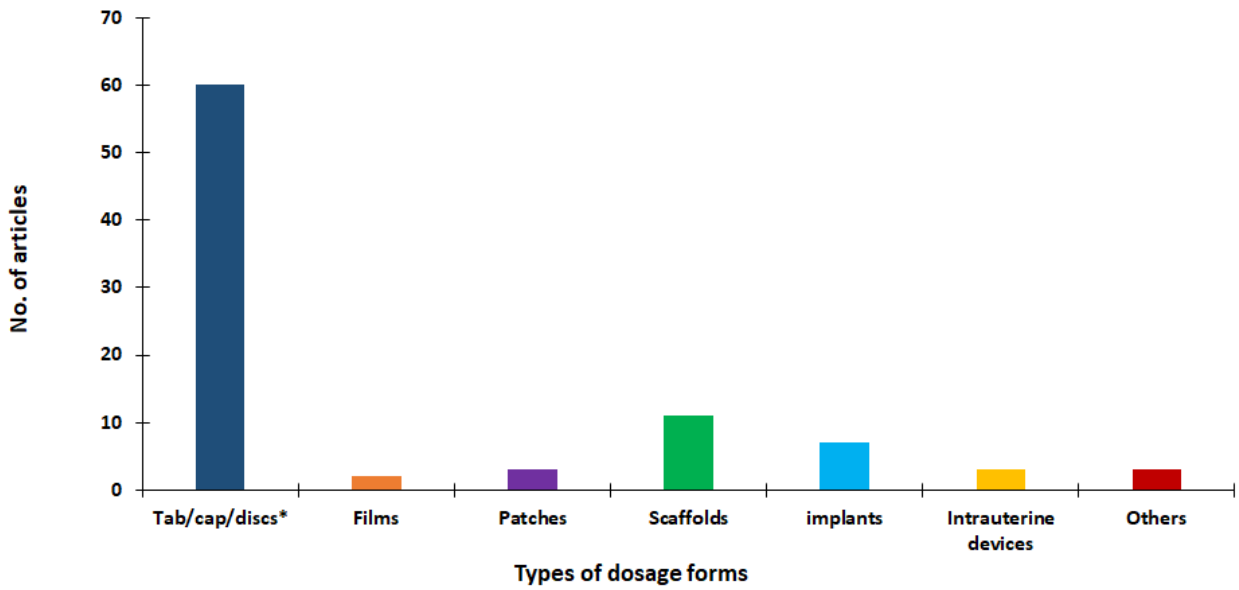


Figure 2.21: Distribution of pharmaceutical dosage forms developed using FDM technique.

*(*Tablets/capsules/discs. Others include wearable mouth guard, microneedle array, expansion chamber wound dressings, stent, bioactive mesh, antimicrobial testing robotic setup).*

2.3.1.1.2. Pneumatic extrusion and its applications

Compressed gas is utilised as a driving force for extrusion in this system (Figure 2.22¹¹⁹) Air and nitrogen are commonly used compressed gases for pneumatic extrusion but nitrogen is preferable for the printing of biological inks where sterility is required and furthermore, this system is suitable for variety of viscoelastic inks^{120, 121}. However, the use of air or nitrogen as a compressed gas has made this system difficult to build and operate in comparison to other extrusion systems that are driven by motors. The applications of pneumatic extrusion in drug delivery are described below.

Artificial bone scaffolds are the most promising material for repairing bone defects lesion. Using conventional manufacturing technologies, e.g. membrane lamination, fibre bonding, solvent casting and particulate leaching, it is difficult to fabricate customised scaffolds with specially designed functional gradient. To provide a suitable artificial bone scaffold for use in the repair of cranio-maxillofacial bone defects and to observe the process of osteogenesis, the development of porous scaffolds composed of poly lactide-co-glycolide (PLGA)/ TCP using low-temperature rapid-prototyping technology was explored and the scaffold was loaded with rhBMP-2. The implantation of printed scaffolds in goats with cranial defects resulted in preliminary repair after 12 weeks and complete repair in 24 weeks. The slow release of rhBMP-2 resulted in the induction of a new bone¹²².

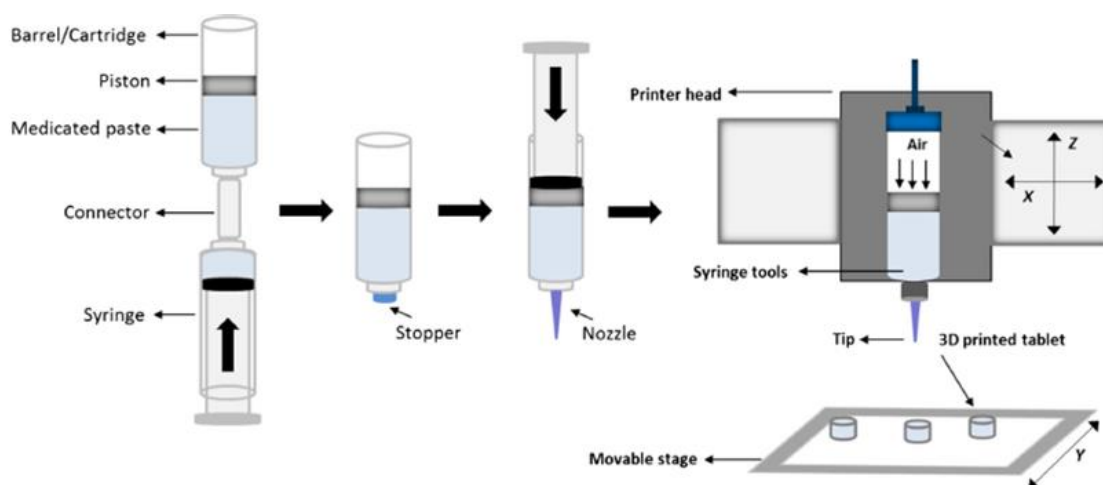


Figure 2.22: Schematic diagram illustrating working principle of pneumatic extrusion, reproduced with permission from¹¹⁹.

Controlled drug release systems have always been preferred for optimised delivery of anti-tuberculosis drugs. PLGA has gained much attention to be used as a carrier polymer for pulmonary delivery of micro-particles of anti-tuberculosis drugs. However, acidic degradation of PLGA significantly decreases pH values when PLGA microspheres embedded into defected bone cavities and can lead to the *tubercle bacillus* bacterium developing drug resistance. Therefore, mesoporous silica nanoparticles are a good choice for sustained and localised delivery of anti-tuberculosis drugs without decreasing pH values. Thus, a composite scaffold composed of mesoporous silica nanoparticles and β -TCP was developed for the delivery of isoniazid and rifampicin for the treatment of osteoarticular tuberculosis therapy. *In vitro* and *in vivo* (rabbit) studies showed sustained release of both drugs from the composite scaffold. The bactericidal action of isoniazid and rifampicin at concentrations of 0.025-0.05 $\mu\text{g}/\text{ml}$ and 0.005-0.5 $\mu\text{g}/\text{ml}$ against *Mycobacterium tuberculosis* was greater than their effective levels. For more than 42 days the concentration of both drugs stayed above the effective level of concentration and no significant injury to kidney and liver was detected ¹²³.

The fabrication method of scaffolds for the sustained delivery of rhBMP-2 described by Park *et al.* and Lee *et al.* involved use of a toxic organic solvent which can pose health risks. The dipping method does not result in consistent loading of rhBMP-2 and can cause wastage of rhBMP-2, thus only non-toxic and clinically relevant biomaterials and efficient processes were used to develop scaffolds for sustained delivery of rhBMP-2. Two types of scaffolds composed of PLGA, PCL, rhBMP-2 and collagen and the other with gelatine were fabricated. *In vitro* test showed that the outbreak release of rhBMP-2 from scaffold composed of PCL, PLGA and gelatine did not cause osteogenic differentiation of turbinates-derived mesenchymal stromal cells of humans at a dose of 5 $\mu\text{g}/\text{ml}$. After 4 and 8 weeks of implantation of the collagen-scaffold in rabbit with diaphyseal defect, long-term release of rhBMP-2 showed exceptional bone healing properties without inducing inflammation. In contrast, short-term release of rhBMP-2 from gelatine-scaffold induced inflammation after 4 weeks of implantation. In conclusion, these materials and the extrusion process were effective in developing controlled release rhBMP-2 scaffolds ¹²⁴.

Mesoporous bioactive glass (MBG) has enhanced degradation, drug delivery properties and bone-forming bioactivity than usual bioactive glass. Recently, it has been reported that incorporation of bioactive inorganic components such as strontium, which is an important

trace element in human bone, could improve biological and physicochemical properties of MBG. To evaluate this, strontium containing mesoporous bioactive glass (MBG) scaffolds were developed for bone regeneration. The results from the *in vitro* assay showed that the scaffolds displayed a slow rate of ion dissolution and an increase in strontium substitution significantly improved the potential of the scaffolds to maintain the pH. Additionally, the scaffolds had the ability to provoke cell differentiation and proliferation of osteoblasts. The study concluded that the mesoporous structure of the scaffolds resulted in sustained release of dexamethasone thus making it suitable for bone regeneration ¹²⁵.

The chronic stage of osteomyelitis becomes untreatable with intravenous delivery of antibiotics. To overcome this, a PCL-PLGA scaffold loaded with tobramycin was developed. Drug release studies resulted in slow and sustained release of tobramycin for a period of 35 days. *In vivo* studies carried out in rats showed that the scaffold not only mitigated the infection caused oedema and inflammation, but also aided in the formation of new bone after 8 weeks of implantation ¹²⁶.

Porous scaffolds composed of PCL were printed to enhance cell differentiation during bone regeneration. Extruded PCL scaffolds were grafted with 100 ng/ml of rhBMP-2 (PCL100) and 500 ng/ml of rhBMP-2 (PCL500). These grafted scaffolds were then coated with polydopamine. After 28 days of *in vitro* release examination, it was observed that the grafting resulted in the sustained release of rhBMP-2. Furthermore, the osteoconductive and cell proliferation ability of PCL500 scaffolds was better than the PCL100 scaffolds ¹²⁷.

A bio-ceramic scaffold composed of β -TCP was developed and coated with silver nanoparticles dispersed in graphene oxide to retain its antibacterial activity for application in bone tissue engineering. The resulting scaffolds showed exceptional antibacterial properties against *Escherichia. coli* in an *in vitro* assay. In addition, the scaffolds augmented the bone related gene expression and alkaline phosphatase activity leading to increased osteogenic differentiation of bone marrow stromal cells of rabbits. Hence, the study revealed that scaffolds with osteogenic and antibacterial activity would be suitable for bone defects while preventing bacterial infections ¹²⁸.

A tissue scaffold comprising a non-steroidal anti-inflammatory drug (NSAID) was produced for the regeneration of bone via pneumatic extrusion. For this purpose, bone cells were enclosed

in the fibrous alginate hydrogel and few of these hydrogels were coated with a layer of chitosan to improve the biocompatibility and retention of the drug. Cell viability testing showed that the growth of bone cells accelerated, however, initially the number of cells in the coated sample were lower than the number of cells in uncoated samples but later on after day 4 the number cells increased and were higher than that in uncoated samples. The slow and steady release of diclofenac resulted in inhibition of tumour necrosis factor- α (TNF- α) secretion and interleukin-6 from macrophages. The chitosan coating increased the efficacy and retention of drug release and also played a vital role in protecting the bone cells from noxious compounds after the depletion of drug ¹²⁹.

Cyclosporine A causes serious side effects after systemic administration, therefore sometimes it is not suitable to deliver sufficient dosage of the drug after xenogeneic cell transplantation. To overcome this issue, a drug carrier was developed for local and sustained delivery of cyclosporine A. This was achieved by loading cyclosporine A into microspheres of PLGA, which were then incorporated into 8% w/w alginate hydrogel. A frame network composed of PCL and PLGA was also developed to bear the load of the whole structure. The *in vitro* release profile measured using a dialysis method showed rapid release of cyclosporine from the hydrogel on day 1 followed by sustained release of the drug for a period of 4 weeks, leading to 75% of the drug being released over 28 days. The release of the drug also prevented increase in interleukin secretions. The immunomodulatory effect of these drug carriers was also evaluated by implanting the drug carrier seeded with human lung fibroblast cell line in BALB/c mouse, subcutaneously. A significant suppression of T-cell mediated rejection was reported for a period of 4 weeks ¹³⁰.

Built-in micro channels were introduced in cell-laden hydrogel structures by controlling the crosslinking time to deliver nutrients for the growth of the cells (fibroblasts). Such kind of structures were printed on the basis of the fusion of filaments of sodium alginate that are hollow and serve as building blocks. The process of fusion depends on the crosslinking time as it is difficult to control the sequence of crosslinking time for forming un-gelled alginate that results in fused structures. The concentrations of calcium chloride and sodium alginate were evaluated to control the crosslinking time. It was reported that the smaller distance between adjoining hollow alginate filaments and highly concentrated sodium alginate solution resulted in structures with high-strength. Green fluorescein protein (EGFP, molecular weight = 27KD)

was easily diffused in the printed alginate filament confirming that hollow filaments were capable of nutrient delivery. Perfusion tests showed smooth perfusion of purple and red dyes through the channels from inlet to outlet. Viability analysis showed successful encapsulation of L929 mouse fibroblasts in hollow alginate filaments. After one day of culturing, the majority of the cells were alive, concluding that the printing method was biocompatible ¹³¹.

To provide sustained long-term drug release, biodegradable structures using PVA and PLGA loaded with dexamethasone-21-phosphate disodium salt were fabricated via extrusion printing and two types of devices with different drug encapsulation designs were prepared. In the first design, dexamethasone was dissolved in PVA and the solution was printed in square patterns on casted PLGA film which was then then rolled into a cylindrical scroll. The second structure was printed in a layer by layer manner in which PLGA solution was printed, upon which dexamethasone/PVA solution was printed, upon which a layer of PLGA solution was printed again. The same procedure was used to develop two- and three-layer structures, separately. *In vitro* drug release studies were carried out on both devices for a period of 4 months. Rolled and sealed devices showed continuous release of dexamethasone, whereas long-term release (more than 100 days) of dexamethasone was observed with layer by layer implants. Moreover, the release rate decreased with an increase in PLGA content in the layer by layer implant ¹³².

Copolymers PVA-PEG and PVP-PVA were used for the formulation of immediate release tablets of levetiracetam. The disintegration time of PVA-PEG and PVP-PVA tablets was 95 ± 10 s and 130 ± 20 s. The copolymers were effective in producing immediate release tablets ¹³³.

Drug loaded gummies were printed using gelatine and HPMC. The amount of gelatine greatly affected the strength of gummies and addition of HPMC helped in printing smoothly. 85% of the drug was released within 15 minutes ¹³⁴.

Extrusion-based 3D printing was employed to print tablets of different geometries; solid, ring and mesh, with high drug loading (more than 80% w/w) of paracetamol. A schematic diagram of these tablets is shown in Figure 2.23. The *in vitro* dissolution profile showed distinct release patterns for all formulations. Tablets with a mesh structure showed immediate release by releasing 70% of drug within the first 15 minutes. On the other hand, tablets with a ring and

solid design exhibited 25% and 12% drug release in the same time period, respectively, hence it was reported that the surface area had a great influence on drug release. Mesh tablets had a higher surface area leading to rapid water absorption than solid or ring tablets. A correlation between drug release and surface area/volume ratio was also observed i.e. the higher surface area/volume ratio resulted in faster drug release. Thus, one formulation could yield different release patterns to achieve and optimise personalised dosing ¹¹⁹.

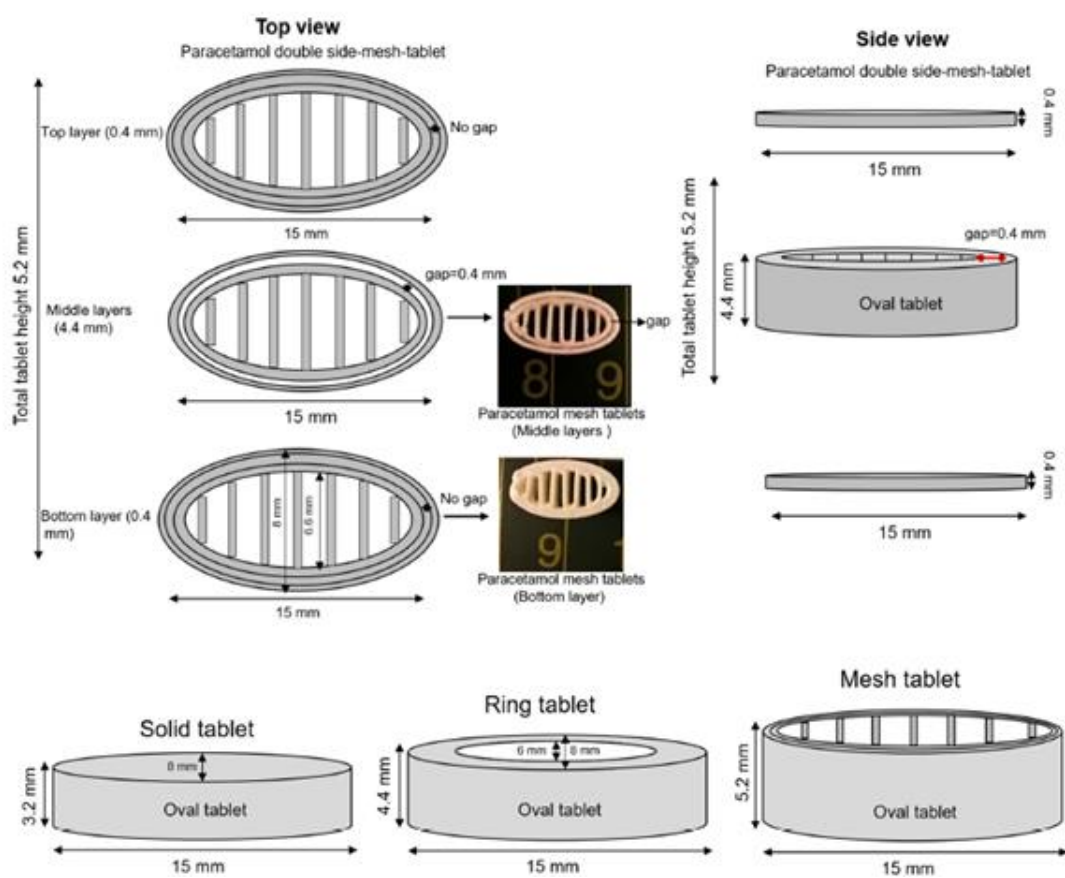


Figure 2.23: Schematic illustration of tablets with solid, ring and mesh geometries along with their top view and side view, reproduced with permission from ¹¹⁹.

Humic acid and polyquaternium 10 complex were investigated as drug carriers for the controlled delivery of three anti-HIV-1 drugs: emtricitabine, tenofovir disoproxil fumarate and efavirenz. Prism-shaped rectangular tablets with 24 layers were fabricated with each layer consisting of 6.3 mg of tenofovir disoproxil fumarate, 4 mg of efavirenz and 12.5 mg of

emtricitabine. Upon investigation, hydrogen bonding was observed between drugs and drug carrier indicating an increase in drug solubility. *In vitro* drug release tests showed controlled release of all drugs for the first 12 hours, particularly emtricitabine and tenofovir disoproxil fumarate, whereas efavirenz exhibited controlled release for a period of 24 hours. *In vivo* studies carried out in pigs showed that the majority of all the drugs released in alkaline pH. The complexation of humic acid-polyquaternium 10 complex was responsible for the controlled release of drug. *In vitro-in vivo* correlation studies indicated that the *in vitro* tests showed slow release of drug initially but C_{max} was achieved more rapidly¹³⁵.

Extrusion-printing was employed for the fabrication of capsules with programmed release of payload molecules (biomolecules, food dyes or enzymes) (Figure 2.24). Furthermore, these capsules were stimuli-responsive which was achieved by loading the polymer shell with gold nanorods that allows highly selective photo thermal rupture and triggered temporal release of the bio molecular payload. For this purpose, at first, 2D multiplexed arrays of aqueous cores comprising 0.1 to 10 mg/ml concentration of payload molecule (horseradish peroxidase, type I) dissolved in a solution of PVA and ethylene glycol were printed onto hydrophobic solid substrate like siliconized glass slides. After printing, aqueous cores were coated with PLGA solution containing plasmonic gold nanorods to form a shell which is stimuli-responsive. These capsules were then irradiated with a laser wavelength according to the absorption peaks of nanorods for selective rupture of capsules. Image and quantitative analysis confirmed that capsules were ruptured only when irradiated with an analogous laser wavelength. Furthermore, the release rate of the biomolecule was dependent on the number of lasers irradiated over the ruptured capsules. Laser irradiated rupture also provided control over temporal release of payload biomolecules. The presence of plasmonic gold nanorods played a vital role in making the capsules stimuli-responsive as the capsules without plasmonic gold nanorods did not rupture when irradiated with corresponding laser. The size of the nanorods also determined the rupture of capsules as was demonstrated when capsules with nanorods of 10 nm in diameter resulted in incomplete rupture whereas capsules with 25 nm nanorods were fully ruptured. However, the development of 3D multiplexed arrays requires printing of an aqueous core without solid substrate. For this purpose, a water in oil emulsion-based ink, as an aqueous core, containing red dye (rhodamine B isothiocyanate-dextran) and green dye ((poly (fluorescein isothiocyanate allylamine hydrochloride)), were

incorporated directly and dispersed into PLGA solution containing plasmonic gold nanorods. After this, 10% PLGA solution was coated to form a shell around the emulsion-based ink to prevent the release of the aqueous core. 40%wt solution of Pluronic F-127 in water was used to prepare a thin layer of hydrogel and the emulsion-based ink was directly printed on this hydrogel in a layer-by-layer function to print a capsule shaped structure with multiple layers. When exposed to the corresponding laser wavelength, these capsules ruptured and released fluorescein dyes ¹³⁶.

To imitate the blood vessel system during tissue fabrication, PLGA and alginate were utilised to print tubes via extrusion printing, which were used for the sequential delivery of fluorophores. The inner core of the tubes was made up of PLGA (1% w/v) loaded with 0.8 mg/ml of Rhodamine B enclosed in an alginate (4% w/v) shell loaded with fluorescein (0.025 mg/ml). Biocompatibility assays of these tubes were conducted by incubating the tubes with bone marrow stromal stem cells and human embryonic kidney (HEK293) cell line, which showed that no cytotoxicity was observed. *In vitro* release studies showed immediate release of the majority of fluorescein from alginate within a period of 24 hours. No rhodamine release was observed during the first 24 hours and later sustained release was observed for the next three to four days ¹³⁷.

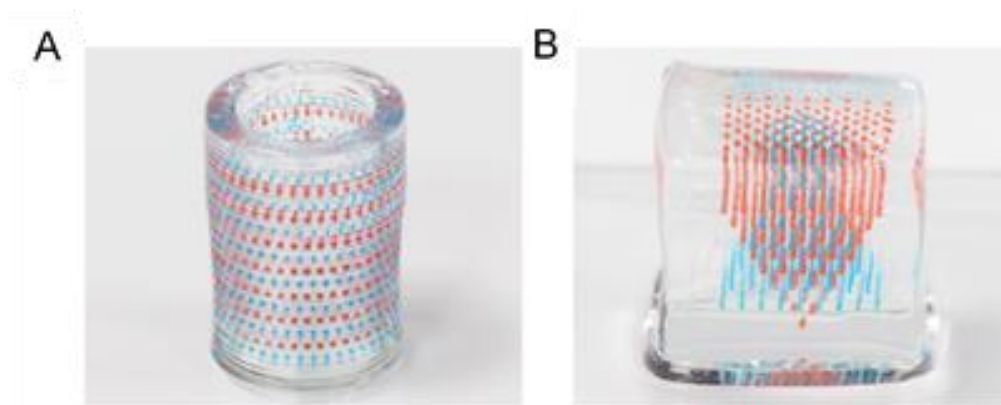


Figure 2.24: 3D printed multiplexed capsule arrays (A) cylindrical and (B) square hydrogel matrices, reproduced with permission from ¹³⁶.

Intrauterine devices were designed and printed using PDMS as a carrier polymer. Figure 2.25 shows the 3D printed grid structures. Devices were cured with ultra-violet (UV) light during and after printing process and afterwards, degree of swelling was determined to measure the extent of curing. It was reported that degree of swelling decreased with increased curing of devices using UV light. Devices were loaded with 1% and 1.5% of prednisolone. *In vitro* drug release tests showed that intrauterine devices containing 1% of drug exhibited cumulative drug release of 9.5-11%, whereas for devices with 1.5% drug loading, it was 10.4-11%. After a period of 28 days, the cumulative amount of drug was highest in the device containing a high amount of drug loading irrespective of pore size ¹³⁸.

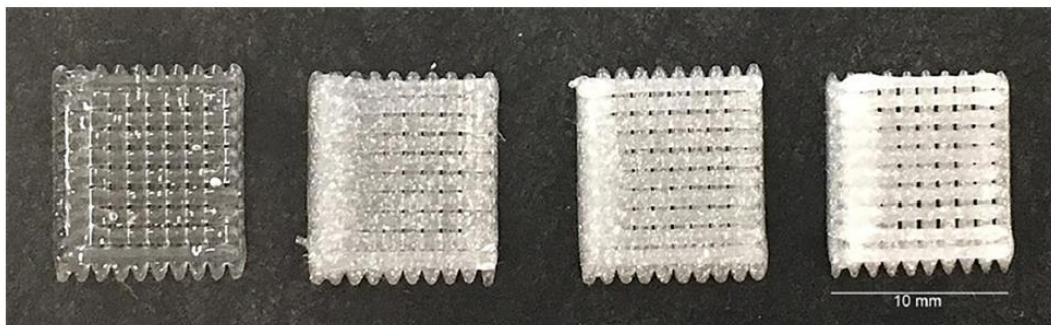


Figure 2.25: Picture of 3D printed grid structures, from left placebo grid 0.5, 0.5%. 1% and 1.5% drug containing grids, reproduced with permission from ¹³⁸.

Extrusion printing was compared with electrospinning technique by comparing the properties of extruded wound dressings with the properties of dressings prepared by electrospinning. For the extrusion process, 1:1 ratio of carboxy methyl cellulose (CMC) and alginate hydrogel was used to print the dressing along with the addition of two drugs: diclofenac sodium and lidocaine. Post-printing, CaCl_2 was used for crosslinking to print homogeneous layers of dressings, thus ensuring stability of porosity. Upon investigation, it was observed that both of the drugs had no effect on the stability of the hydrogel formulation during printing and sustained release of both drugs for 2 days was observed during drug release tests. On the other hand, for the preparation of nanofibres via electrospinning, poly ethylene oxide (PEO)/CMC formulation was used. It was observed that the size of nanofibers with diclofenac sodium was less homogeneous, whereas homogeneous nanofibers were obtained with

lidocaine. The drug release profile of nanofibers was also quite different from extruded dressings with 90% of both drugs from nanofibres released in a period 30 minutes ¹³⁹.

The research studies cited above show the great potential of pneumatic extrusion printing in the fabrication of drug delivery devices of different types. The type of pharmaceutical dosage forms mostly fabricated via pneumatic extrusion, irrespective of the delivery route, were scaffolds followed by tablets and hydrogels and implants as shown in the Figure 2.26.

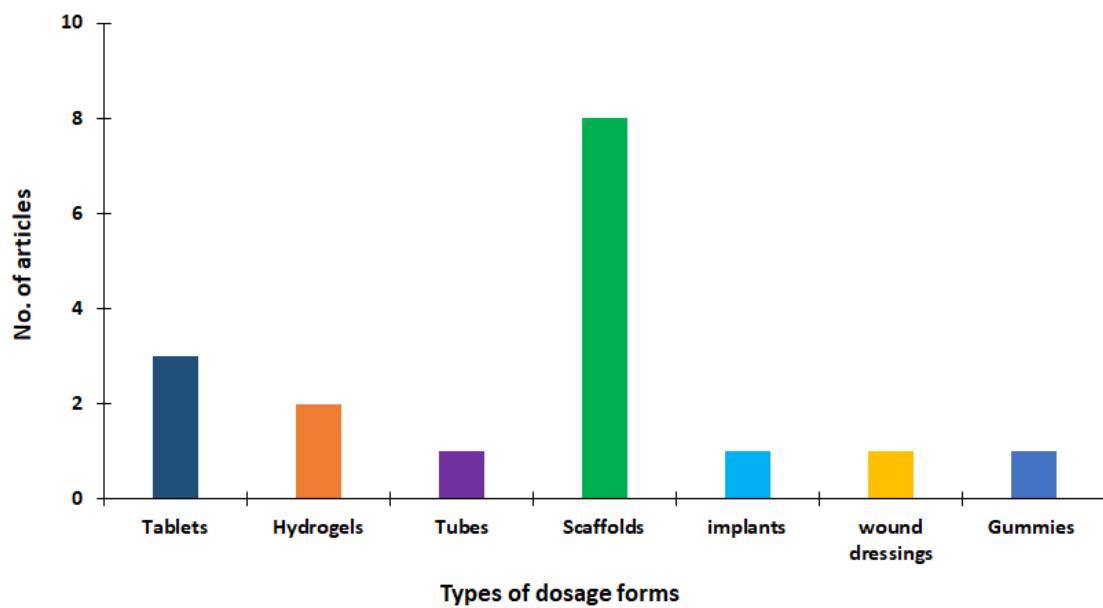


Figure 2.26: Distribution of pharmaceutical dosage forms developed using pneumatic extrusion.

2.3.1.1.3. Paste extrusion and its applications

In paste extrusion, the piston and the material are physically contacted with each other as shown in the schematic diagram (Figure 2.27 ¹⁴⁰) and thus, there is a constant volume displacement and therefore provides better control of the extrusion rate. However, there is one limitation with this system i.e., it takes time to start and stop the process which can lead to inaccurate printing. On the other hand, paste extrusion has been utilised to print cellular materials critical for organ on a chip model or cell laden drug testing systems. Paste extrusion is also considered one of the most biocompatible 3D printing techniques for cellular work, as it does not use elevated temperatures ¹⁵. Applications of paste extrusion in fabrication of different dosage forms and to provide personalised dosing are detailed below.

Bio-fabrication of micro-organs onto a microfluidic device lined with liver cells, hepatocytes that imitates the microenvironment of the cell was fabricated for evaluation of drug metabolism in an *in vitro* model using PDMS and different concentrations of alginate. Under persistent perfusion flow, biological characterisation of the device was carried out to check the suitability of the device for *in vitro* evaluation of drug metabolism. It was reported that different concentrations of alginate (1.5%, 2.25% and 3%) had no effect on the conversion of the drug from EFC (7-ethoxy-4-trifluoromethyl coumarin) to HFC (7-hydroxy-4-trifluoromethyl coumarin) during drug metabolism. On the other hand, the device showed a 26% increase in metabolic conversion of HFC during the drug perfusion study ¹⁴¹.

Another microfluidic chip was reported by Sander *et al.*, ¹⁴² who described an *in vitro* model to study and evaluate multi-cellular drug conversion and to observe the radiation shielding effect of amifostine. Epithelial cells and hepatocytes were embedded in Matrigel and then were sealed in the microfluidic chip. Fluorescence-based cytotoxicity tests showed that cells remained viable for 48 hours after temperature-controlled printing. Micronuclei count was carried out to determine the damage done to the cells. Micronuclei count reported that hepatocytes treated with drug showed reduced radiation damage as compared to hepatocytes without treatment of drug.

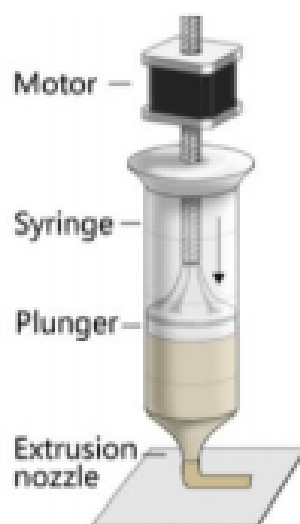


Figure 2.27: Schematic diagram illustrating working principle of paste extrusion, reproduced with permission from ¹⁴⁰.

A human breast cancer model was developed for *in vitro* screening of anti-cancer drugs. Such models help in understanding the initiation and progression of breast cancer and to define targeted therapeutics more efficiently. The developed human breast cancer model consisted of breast cancer lesions. These lesions were surrounded by endothelial cells, mammary fibroblasts and adipose tissue and had an advantage of distinguishing different cell types and measuring the effect of small molecules on cancer cells, simultaneously. During culture testing, bio-printed neotissues remained viable for 14 days. To measure the biological response of anti-cancer drugs (cisplatin, paclitaxel, methotrexate, and tamoxifen) mammary neotissues were fabricated directly into multi-well plates. Upon interaction with cancer and stromal cells, the bio-printed neotissues retained their compartmentalised structures. Adipocytes differentiation and endothelial network formation were observed after bio printing of the stromal compartment. Cancer cells incorporated into 3D bio printed structures were less susceptible to toxicity induced by tamoxifen as compared to isolated 2D cancer cells ¹⁴³.

An *in vitro* cervical tumour model was constructed by bio-printing of Hela cells and fibrinogen/alginate/gelatin hydrogels using paclitaxel as a model drug. Different parameters including matrix metalloproteinase protein expression, cell proliferation and chemoresistance of 3D printed models were measured and were compared with 2D models and it was revealed that the 3D printed models showed 90% cell viability. A higher proliferation rate

and formation of cellular spheroids of HeLa cells were reported in 3D printed models whereas 2D model showed monolayer sheet of cells. Higher chemo-resistance and protein expression of HeLa cells were also observed in 3D printed models as compared to 2D models. Therefore, 3D printed cell laden models help in providing evolution in cancer study ¹⁴⁴.

An *in vitro* model laden with glioma stem cells was printed for studying cell biology, drug resistance, glioma genesis and susceptibility of anti-cancer drugs. Fibrinogen/gelatine/alginate hydrogels were used to print the cell laden model that could imitate the extracellular matrix. High cell proliferation activity and 86.92% survival rate of glioma stem cells were reported. The glioma stem cells exhibited differential potential and inherent characteristics of stem cells ¹⁴⁵.

Liver tissues were directly printed onto a microfluidic device for drug screening applications. The resulted device showed promising long-term culture of bio-printed spheroids and the printed cells showed viability after printing. Acetaminophen was used as a model drug to test drug toxicity. Decrease in metabolic activity was reported after a period of 6 days in culture and a decrease in activity and density of the cell was also observed. The device was also capable of automatic testing of multiple drugs in an efficient manner, thus making it a suitable device for drug screening applications before carrying out clinical trials ¹⁴⁶.

Multicellular model of human liver tissue accommodating primary human parenchymal (hepatocyte) and non-parenchymal (endothelial and hepatic stellate) cell populations were bio-printed to study human drug response in particular for drug induced liver injury. Trovafloxacin was used as a model drug to assess the ability of model in detecting trovafloxacin-induced toxicity at clinical doses ($\leq 4\mu\text{M}$). However, the drug induced toxicity was dose dependent and strong toxicity was only observed in rodent models when trovafloxacin was administered with lipopolysaccharide. These findings reported that the inflammation in the liver due to trovafloxacin was mediated by Kupffer cells, a myeloid cell type present in the liver. Thus the combination of bio printing and primary cells derived from patients could be beneficial in studying human drug response more efficiently ¹⁴⁷.

Occurrence rates of acute kidney injury are increasing due to excessive use of prescription drugs. Although 25% of acute renal failure observed in the clinic is drug induced, predicting nephrotoxicity in preclinical *in vitro* or animal studies remains difficult. Hence, there is an

urgent need of kidney tissue models that can detect drug toxicity in human and serve as building blocks for human kidneys and nephrons. While renal injury can take place in any location, the convoluted proximal (PT) tubule gets damaged most frequently. For this purpose, organ-on-a chip, bio-printing and 3D cell culture were used in combination to design and print 3D convoluted renal PT models. These PT models are composed of open lumen architecture seeded with proximal tubule epithelial cells, embedded in extracellular matrix and enclosed within perfusable tissue chips where they were exposed to physiological shear stress. Direct imaging and diffusion permeability tests were used to analyse the effects of different concentrations of cyclosporine A, a nephrotoxin. Increased functional properties and epithelial morphology was reported in 3D convoluted PTs. Immunostaining imaging revealed cyclosporine A-induced damage that includes broken cell-cell junction and areas devoid of cells were exposed at 50 μM cyclosporine A. These cell devoid areas became more prominent at 100 μM cyclosporine A. The epithelial barrier was disrupted on introduction of cyclosporine A and was dependent on dose. Epithelial barrier permeability was increased by 4 and 6-fold when exposed to 50 μM and 100 μM cyclosporine A, respectively. Overall, these results indicated that these constructs can be used qualitatively and quantitatively to assess nephrotoxicity and this method can be a suitable means of producing on demand human kidney tissue models ¹⁴⁸.

A human neural stem cell laden model was created for the investigation of disease, function and development of the human neural system. For this purpose, a polysaccharide-based bio ink consisting of agarose carboxymethyl-chitosan and alginate was used. Stable cross-linking was used to gel the bio ink to form a porous scaffold. The scaffold was encapsulated with stem cells for *in situ* differentiation and expansion. Differentiated neurons established active networks that increase the calcium response upon induction of bicuculline and were gamma-aminobutyric acid expressing ¹⁴⁹.

Connective tissue growth factor and transforming growth factors were encapsulated onto PLGA microspheres. These microspheres were then embedded into microfibers made up of PCL to print temporomandibular joint disc scaffolds for tissue regeneration. *In vitro*, the printed scaffolds loaded with growth factors induced multiphase production of fibro cartilaginous tissues from mesenchymal stem cells. To perform *in vivo* studies, the scaffold was implanted in rabbits after perforating the disc of temporomandibular joint.

Consequently, the scaffold did not induce arthritic changes on condyles of temporomandibular joint and enhanced the healing of perforated disc ¹⁵⁰.

Vascular endothelial growth factor laden hydrogel strands comprising alginate-gellan gum was combined with oil-based calcium phosphate cement paste to print a biphasic scaffold for bone healing. It was reported that the swelling of hydrogel within the structure of the scaffold did not result in blockage of macro pores. Rats with defective femur bone were used to carry out the *in vivo* studies. These studies revealed the chemotactic behaviour of vascular endothelial growth factor towards cells indicating the need of gradient distribution of vascular endothelial growth factor for the movement of endothelial cells inside the structure of the porous scaffold. The gradual spread of growth factor encouraged the cells to flourish inside the scaffold ¹⁵¹.

This technique provides precise layer by layer control over the architecture of scaffolds by plotting under mild conditions. This advantage makes this technique a preferable choice for the fabrication of scaffolds. For applications in bone regeneration, MBG scaffolds with controllable pore structure were fabricated. MBG powder was mixed with PVA solution to prepare an injectable paste. The results reported greater toughness and mechanical strength when compared with the polyurethane scaffolds. The scaffolds exhibited good apatite mineralisation ability and highly controllable pore structure. Drug release tests showed burst release of dexamethasone with approximately 75% of drug released from the scaffold in the first 2 days followed by sustained and slow release up to 10 days ¹⁵².

Scaffolds consisting of PCL and MBG were loaded with nanoparticles of Fe₃O₄ for local delivery of anticancer drug, doxorubicin and to induce hyperthermia. The scaffolds with 60% porosity resulted in mineralisation of human bone marrow mesenchymal stem cells, increased alkaline phosphatase activity and osteogenesis related gene expression and cell proliferation. The scaffolds had exceptional ability of magnetic heating and inclusion of Fe₃O₄ nanoparticles into the scaffold did not affect their ability of apatite mineralisation. *In vitro* drug release showed that 30% of the drug was released on the first day followed by slow and sustained release of drug for up to 10 days. The scaffold proved to be useful for the local delivery of anticancer drug with improved osteogenic activity¹⁵³.

Composite scaffolds containing isoniazid and rifampicin were fabricated for the treatment of osteoarticular tuberculosis. Mesoporous silica nanoparticles and MBG were coated with poly (3-hydroxybutyrate-co-3-hydroxyhexanoate) (PHBHHx) to develop scaffolds loaded with drugs. *In vitro* and *in vivo* (rabbits) studies showed that the printed scaffolds had properties comparable to the properties of commercially available calcium phosphate scaffolds. These 3D printed scaffolds showed more extended release of anti-tuberculosis drugs than commercial scaffolds ^{154, 155}.

Another study also reported a combination of MBG with metal organic frameworks for sustained delivery of isoniazid. The resulted scaffolds were biocompatible with compressive strength of 3-7 MPa and scaffolds showed good apatite forming ability during *in vitro* analysis. Metal organic frameworks degradation controlled the release rate of drug which lead to the scaffolds displaying rapid release of drug initially, followed by sustained release of drug ¹⁵⁶.

Scaffolds containing dimethyloxallyl glycine were developed to initiate the process of osteogenesis and angiogenesis in the bone defects. *In vitro* release profile showed initial burst release of drug in the first three days followed by sustained release of drug. *In vivo* studies were carried out in male rats to evaluate the performance of these scaffolds. It was reported that the scaffolds showed an excellent ability of enhancing osteogenesis and angiogenesis. The formation of vessels was stimulated by the microfil perfusion with the delivery of dimethyloxallyl glycine ¹⁵⁷.

Wang *et al.*, used hydroxyapatite to fabricate a scaffold for the delivery of rhBMP-2 with collagen to improve osteoconductivity. After printing the scaffolds, they were sintered in a 1.4 kW, 2.45 GHz microwave furnace which is a volumetric heating phenomenon with short processing period and high heating rate. It provides various advantages including cost reduction, improved properties, finer microstructure, time and energy savings ¹⁵⁸. *In vitro* studies reported that the scaffold could release rhBMP-2 for more than 21 days. The increased osteoconductivity was also reported for induction of human mesenchymal stem cells. *In vivo* studies reported that scaffold exhibited excellent bone regeneration capacity ¹⁵⁹.

Calcium phosphate cement-based scaffolds coated with the 5-fluorouracil were successfully developed for bone cancer treatment. The scaffolds showed complete drug release within 2 hours and were able to inhibit the cell growth during *in vitro* cell culture test ¹⁶⁰.

Bio-printing was used for the fabrication of hydrogel fibrous scaffolds embedded with endothelial cells to engineer endothelialized myocardial tissues. Controlled anisotropy was used to seed cardiomyocytes on to endothelial bed to produce myocardium capable of generating synchronised and spontaneous contraction. Cardiac organoids were also embedded in the device to make it a complete platform for drug screening and for evaluation of drug toxicity of cardiovascular drugs ¹⁶¹.

Although shape memory hydrogels have wide applications in tissue engineering and drug delivery, the fabrication of these hydrogels is still challenging. Pluronic F127 diacrylate macromer and sodium alginate were combined to form shape memory hydrogels with methotrexate as a model drug. The results showed that 3D printing of these hydrogels displayed a rapid release rate of drug in comparison with conventional hydrogels ¹⁶².

Rectal suppositories of the tacrolimus were developed using coconut oil and gelucire 44/14 as lipid excipients. Liquid excipients were feasible to print and the suppositories showed 50% of the drug release within first hour. The *in vitro* disintegration time of the suppositories was less than 10 minutes. However, these results were different from the *in vivo* results carried in rats due to lower amount of the liquid present in rat's colon and thus delayed the disintegration process ¹⁶³.

Sustained release drug implants of lidocaine using PCL were successfully printed and the drug release followed Korsmeyer-Peppas model ¹⁶⁴.

Guaifenesin bilayer tablets were fabricated to imitate the drug release profile of commercially available guaifenesin tablets and to provide personalised drug delivery. Different concentrations of HPMC (14%, 10%, 6% and 8%) along with other excipients that act as disintegrants such as microcrystalline cellulose and sodium starch glycolate, were used to prepare bilayer tablets containing guaifenesin. 3D printed drugs were compared with the commercial tablets of guaifenesin. The dissolution profile of all the tablets with different concentrations of HPMC showed sustained release of drug for a period of 12 hours with initial rapid release of the drug in the first 20 minutes due to the presence of disintegrants. The dissolution profile of tablets with 14% w/w HPMC showed close similarity with the release of drug from commercial guaifenesin tablet ¹⁶⁵.

The effect of printing parameters such as outline and grid width values on drug release studies was investigated. Tablets were composed of HPMC K100 as carrier polymer and glipizide as model drug. It was reported that the use of different outline values had no significant impact on dissolution behaviour. The tablets with different outline values showed more than 95% cumulative drug release in nearly 8 hours. On the other hand, the drug release was faster with increase in grid width values due to increase in surface area ¹⁶⁶.

HPMC was used to prepare the hydrogel required for printing of tablets. Different amounts of hydrogel 30%, 40% and 50% were incorporated into the printer. The weight and hardness of the tablets were decreased when the amount of hydrogel was increased in the printer ink and the drug dissolution was delayed ¹⁶⁷.

3D printed niosomal-hydrogel containing cryptotanshinone was developed for the topical treatment of acne. The entrapment efficiency was observed between 67-71% and the drug release from the hydrogel followed Korsmeyer-Peppas model. Higher rate of transdermal flux was observed during permeation studies. The hydrogel also showed anti-acne effect without any skin irritation in rats during *in vivo* studies ¹⁶⁸.

3D printing was successful in developing drug loaded gummies, a more suitable and acceptable dosage form for children. The printed gummies were quite appealing to the eyes and showed complete release of drug in 120 minutes. In addition the results of uniformity of the drug content and dose accuracy were also satisfactory ¹⁶⁹.

A polypill was designed to increase patient compliance, thereby minimising multiple intake of medicines. A polypill containing 5 drugs with immediate and sustained release profiles for cardiovascular treatment regimen was printed. Two drugs, aspirin and hydrochlorothiazide, were printed in the top layer of the tablet for immediate release, whereas other three compartments containing pravastatin, atenolol and ramipril were included for the purpose of achieving a sustained release profile. The *in vitro* dissolution profile showed 75% immediate release of hydrochlorothiazide and aspirin within a period of 30 minutes due to the presence of sodium starch glycolate that acts as a disintegrant. Conversely, 69%, 81% and 66% of atenolol, pravastatin and Ramipril, respectively, was released in a sustained manner in a period of 720 minutes due to the presence of HPMC ¹⁷⁰.

Khaled, *et al.* also fabricated a polypill using extrusion technique containing three different drugs nifedipine, glipizide and captopril. Drug release kinetics showed that captopril exhibited zero order drug release whereas nifedipine and glipizide showed first order release ¹⁷¹.

The fabrication of a tablet with maximum drug loading is usually challenging using conventional tablet compression methods. On the other hand, 3D printing has proven to be very promising for high drug loading in tablets. Tablets containing 80% w/w paracetamol with immediate release pattern were printed with chemical and physical properties that followed the USP criteria. Disintegration testing resulted in disintegration of tablets within 6 seconds and most of the drug was released within 5 minutes ¹⁷².

Immediate release tablets of levetiracetam were printed with precise dispensing of the drug. Tablets were printed with different number of layers. All the printed formulations disintegrated in 3 minutes. The dissolution was dependent on the number of layers i.e. the drug release decreased with increase in the number of layers ¹⁷³.

Gelatine-based pastes, a thermo-sensitive material, were successfully used in printing immediate and prolonged release tablets of ibuprofen and diclofenac sodium, respectively. The additives like HPMC and microcrystalline cellulose were added to improve the printability. It was also reported that computational fluid dynamics simulation was helpful in understanding the printing process ¹⁷⁴.

The core tablet for immediate release of the drug was encapsulated with a surrounded shell to achieve sustained drug release. The drug release profile followed Korsmeyer-Peppas model and was affected by the space between the core tablet and the shell ¹⁷⁵.

HPMC, polyvinyl acetate-PVP copolymer and silicon dioxide were used as polymer matrix for sustained release tablets of levetiracetam. It was reported that changes in infill design and amount of HPMC can affect the dissolution profile of the drug, higher amount of HPMC decrease the drug release ¹⁷⁶.

Sustained release tablets of theophylline were successfully developed using various doses of the drug (0, 75, 100 and 125 mg) and along with different concentrations (8, 110 and 12%) of methyl cellulose. During *in vitro* dissolution test it was reported that tablets were able to

sustained the release for 12 hours. It was due to the cross-linked structure of methylcellulose that was able to embed the drug and thus resulted in the sustained release of drug ¹⁷⁷.

Controlled release tablets with zero-order release profiles of various model drugs (glipizide, theophylline, gliclazide, puerarin, lornoxicam) having varying solubility were investigated. It was reported that using drugs with solubility 9.45 µg/mL to 8.34 mg/mL and drug loading from 3% to 43% w/w zero-order release profiles can be achieved without changing 3D printing parameters. It was concluded that this platform has the potential of developing zero-order release system using model drugs with different solubilities and drug loadings. were developed. ¹⁷⁸.

Paste extrusion usually involves a drying process after printing, however, recently it has been reported that the use of glycerol monostearate, a fatty glyceride, can eliminate the need of drying process after printing. It not only acted as plasticiser and a lubricant but also provided aid in solidifying at room temperature. The tablets showed sustained drug release for 12 hours which was affected by Eudragit RS: RL polymer ratio. Increasing amount of Eudragit RS in comparison to RL resulted in further delay of drug release ¹⁷⁹.

Emulsified gels were used for printing lipid tablets of fenofibrate. Soybean oil, polyethoxylated castor oil and croscarmellose sodium were added as excipients. The tablets were successfully printed and disintegrated in less than 15 minutes ¹⁸⁰.

Oral films using natural polymers pullulan were developed. It was reported that the addition of HPMC improved the mechanical properties of the films ¹⁸¹.

For the local and controlled delivery of the chemotherapeutic drug 5-fluorouracil, PLGA and PCL were used to develop patches. *In vitro* drug release testing showed that the patches were able to control the release for a period of 4 weeks. *In vivo* studies in mice showed that the patches suppressed the growth of subcutaneous pancreatic cancer xenografts with very few side effects ¹⁸².

This printing technique has also enabled direct writing of magnetised cells to develop 3D printed cell models. It involves magnetisation and aggregation of cells at first which is carried out by incubating cells in a biocompatible assembly composed of poly-L-lysine, iron oxide and gold. Afterwards, magnetic forces are employed to aggregate cells in 3D patterns like hollow

rings, rings and spheroids in a multi-well plate. After aggregation, cells interact with each other to build extracellular matrix in order to replicate tissue environment ^{183, 184}.

Using this platform, an *in vitro* model for the evaluation of human uterine contractility was designed and printed. Magnetic 3D bio printing was employed to print human myometrium cells into shape of rings. When these rings, lined with human cells, were exposed to indomethacin and nifedipine the contraction was inhibited. However, the inhibition was dependent on dose of indomethacin and nifedipine. The effect of ibuprofen on the contractility of rings was also observed. Ibuprofen had no effect on uterine contractions ¹⁸⁴.

The above-mentioned studies clearly show that paste extrusion is pragmatic in building organ on a chip models, cell laden models and scaffolds Figure 2.28 depicts that paste extrusion was mostly employed in the development of tablets followed by scaffolds, organ on a chip model and cell laden models. Table 2.9 shows the summarised characteristics of all the extrusion-based research articles. The table briefly describes the model drug, carrier polymer, plasticiser and results of the studies.

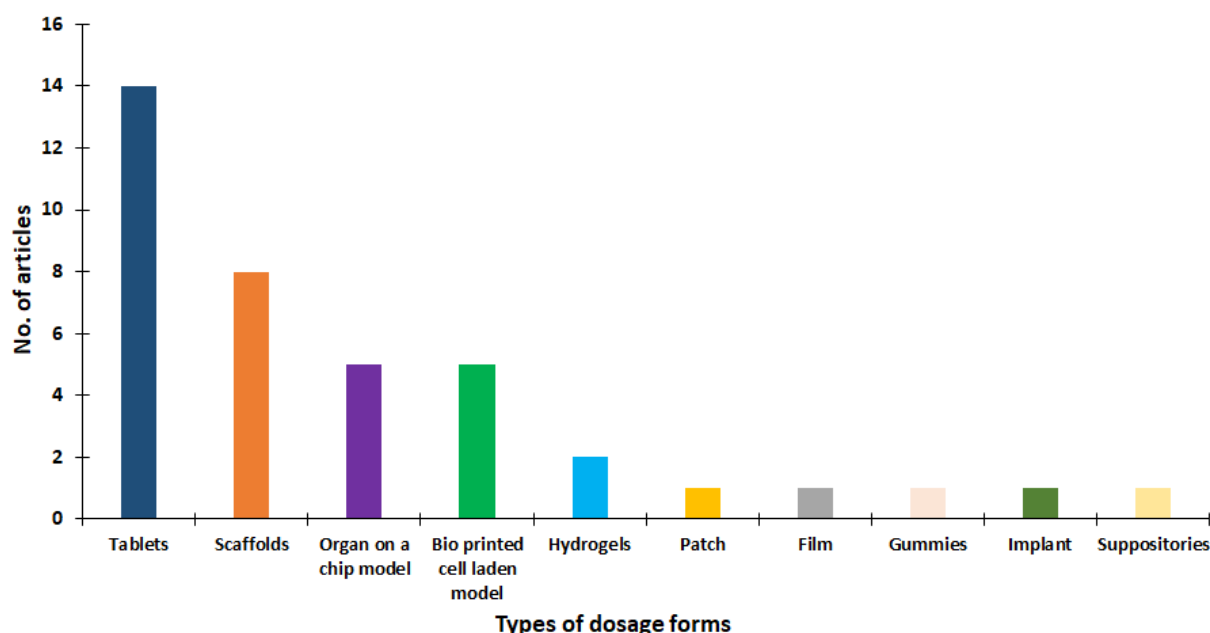


Figure 2.28: Distribution of pharmaceutical dosage forms developed using paste extrusion technique.

Table 2.9: Summarised characteristics of eligible studies used extrusion printing techniques for developing medicines.

Active ingredient	Dosage forms	<i>In vitro/In vivo</i>	Carrier materials	Plasticiser	Printing technique	Study characteristics	References
Methylene blue dye	Implants	<i>In vitro</i>	..	ABS	FDM	ABS based controlled release cylindrical drug delivery devices were developed. FDM process parameters such as raster gap and raster angle play a basic role in controlling the drug release and structure of the device.	18
Fluorescein	Tablets	<i>In vitro</i>	PVA	..	FDM	Tablets with different (10%, 50% and 90%) infill densities were fabricated. 10% infill tablets showed complete drug release in 6 hours whereas 50% and 90% showed complete drug release in 15 hours and 20 hours, respectively.	19
4-ASA and 5-ASA	Tablets	<i>In vitro</i>	PVA	..	FDM	FDM printing was suitable for fabrication of tablets containing 5-ASA but for 4-ASA there was thermal degradation. The drug and infill density affected the dissolution profiles of tablets.	20

Domperidone	Tablets	<i>In vitro and in vivo</i>	HPC	..	FDM	A floating drug delivery system combined with sustained release of drug was developed. The optimised formulation, which contains 0% infill, 2 shells, and 10% domperidone, exhibited sustained release. Floating capabilities were different <i>in vivo</i> and <i>in vitro</i> studies.	21
Itraconazole	Tablets	<i>In vitro</i>	HPMC, PVP	-	FDM	The increase in the outer shell thickness of tablets resulted in prolonged floating and delayed release of itraconazole showing zero-order drug release.	22
Pregabalin	Tablets	<i>In vitro</i>	HPMCAS	PEG 400	FDM	Tablets with different infill density and open and closed systems were printed using FDM. It was reported that tablets printed with low infill density and an open system showed faster drug release in comparison to open and closed systems with high infill density.	23
Dipyridamole	Tablets	<i>In vitro</i>	HPMC K4M and E15, PVP K30	..	FDM	Gastro-floating tablets with different infill densities were developed. The floating time of tablets having lower infill density (30%) was longer than the tablets with higher infill density (50%).	24

Nitrofurantoin	Discs	<i>In vitro</i>	PLA, HPMC	..	FDM	Modified release discs were fabricated with varying amount of HPMC loading. Higher loading of HPMC resulted in highly concentrated release of nitrofurantoin.	25
Glipizide	Tablets	<i>In vitro and in vivo</i>	HPMC	-	FDM	Filaments were extruded using different grades of HPMC varying in viscosity. Matrix tablets with higher viscosity resulted in higher swelling, low erosion of matrix, decreased drug release during in vitro studies. Extended drug absorption profile during in vitro studies.	26
Ibuprofen	Tablets	<i>In vitro</i>	PVA, Soluplus®, Eudragit® RL PO/RS PO, HPMC K4M/E10M/K100 M, Kollidon® vinyl acetate 64 (VA 64)/17PF/30	PEG 6000	FDM	HME was coupled with FDM to print the sustained release tablets. It was reported that using different release modifiers can result in controlled drug release for 24 hours.	27
Theophylline	Oblong-shaped tablets	<i>In vitro</i>	Eudragit® RL PO,	Stearic acid	FDM	Sustained release oblong-shaped tablets were developed which allows dose adaption and estimation of drug release at the same time. Dissolution studies showed that tablets with high infill density exhibited slower drug release.	28

Diltiazem	Tablets	<i>In vitro and in vivo</i>	HPMC	..	FDM	Filaments containing only drug and polymer with no additional excipients were extruded to fabricate tablets. Infill density and infill patterns affect the drug release profile.	29
Hydrochlorothiazide	Tablets	<i>In vitro</i>	PVA, Mannitol, PLA	..	FDM	Controlled release hydrochlorothiazide tablets were fabricated via FDM. These tablets exhibited zero-order kinetics in the dissolution test.	30
Curcumin	Tablets	<i>In vitro</i>	PVA	..	FDM	Printing parameters affect the characteristics of formulation. Increase in temperature resulted in change of colour of tablets. Change in infill density affected the dissolution properties.	31
Acetaminophen, Furosemide	Discs	<i>In vitro</i>	EC, HPC, HPMC, HPMCAS, Eudragit® L 100-55, EDR L, and Eudragit® RL PO, PEO, PVA, Kollicoat® IR, Soluplus®, Glycerol	PEG 400 and 8000, TEC	FDM	The suitability of commercially available polymers of pharmaceutical grade for FDM printing was evaluated. Drug loaded discs fabricated with tested polymers were evaluated. The polymers turned out to be suitable for FDM printing.	32
Isoniazid	Tablets	<i>In vitro</i>	HPC, PEO, Eudragit RS PO, RL PO and L 100	-	FDM	HPC, PEO and Eudragit polymers were used to print tablets containing 30% w/w isoniazid. Among all formulations, PEO tablets showed fastest drug release. A sustained release of drug was observed with HPC tablets. Tablets containing both Eudragit and HPC released 80% of drug in 334 minutes.	33

Theophylline	Oral dosage form	<i>In vitro</i>	PEO	PEG 6000	FDM	The extruded PEO filaments were of variable mechanical resistance. PEO filaments within range of 200000-600000 molecular weight were compatible with the printing process. Moreover, the radiator design of dosage form resulted in accelerated drug release.	34
Ciprofloxacin hydrochloride	Tablets	<i>In vitro</i>	PVA	Dibutyl Sebacate	FDM	The PVA particle size in the range of 200-600 μm were suitable for homogeneous mixing of polymer and drugs, extrusion of filaments and printing process. All formulations showed complete release of drug in 270 minutes.	35
Ibuprofen	Tablets	<i>In vitro</i>	HPMC K100-LV, EC, PVA, Xanthan gum, Sodium alginate	..	FDM	Sustained release tablets with EC and other release modifiers were developed. HPMC turned out to be optimal in modifying the drug release. Infill density, thickness of the outer shells, release modifiers and drug content also affect the drug release pattern.	36
Acetaminophen	Tablets	<i>In vitro</i>	HPMC E5, Soluplus®	..	FDM	HPMC based controlled release tablets were fabricated. Different infill densities and varying thickness of the outer shells affected the drug dissolution profile. Tablets with thick outer shells resulted in sustained release of drug.	37

Prednisolone	Tablets	<i>In vitro</i>	PVA filaments	..	FDM	Tablets with extended drug release characteristics were fabricated. Dissolution testing showed that tablets were able to extend the release up to 24 hours.	38
Theophylline	Tablets	<i>In vitro</i>	Eudragit RL	PEG 4000, stearic acid	FDM	Formulation containing stearic acid prolonged the drug release while formulation with PEG did not succeed in prolonging the drug release. The reason is PEG 4000 has increased water solubility while stearic acid is insoluble in water.	39
Nifedipine	Tablets	<i>In vitro</i>	PVA filaments	..	FDM	Passive diffusion method was applied to load drug onto filaments to develop sustained release tablets. 3% w/w drug loading was achieved and tablets showed sustained release of the drug over 24 hours.	40
Nifedipine	Tablets	<i>In vitro</i>	PVA filaments, Kollidon VA64, EC	..	FDM	Passive diffusion and hot melt extrusion techniques were used for drug loading. Kollidon VA64 and ethyl cellulose were used to extrude drug loading filaments via hot melt extrusion. The drug loading via hot melt extrusion was 13 times higher than passive diffusion. The printed formulations showed biphasic drug release profile.	41

Paracetamol	Tablets	<i>In vitro</i>	PVA	..	FDM	Change in geometrical shape of tablet affects the drug release. The drug release rate of cube shaped tablets was fastest followed by torus, cylinder and pyramid shaped tablets.	42
Paracetamol	Tablets	<i>In vitro</i>	PVA	-	FDM	Tablets were printed with different internal geometries. The dissolution studies showed gradually increasing, gradually decreasing and constant drug release profiles for tablets with horn, reversed horn and cylinder geometries, respectively which concludes that drug release can be controlled by manipulating internal geometry of tablet.	43
Acetaminophen, phenylephrine HCl and diphenhydramine HCl	Tablets	<i>In vitro</i>	ABS filaments, carnauba wax, sodium alginate and croscarmellose sodium	..	FDM	A drug delivery device that can be fully customised was printed with the help of FDM. The device can be customised in number of ways e.g. varying dose, size, shape, release profiles, duration and can accommodate multiple drugs.	44

Glipizide	Tablets	<i>In vitro</i>	PVA	..	FDM	A smaller tablet was accommodated within a larger tablet containing different amounts of drug. The formulation showed controlled release for about 8 hours in accordance with the Korsmeyer–Peppas model.	45
Paracetamol and Caffeine	Capsules	<i>In vitro</i>	PVA	..	FDM	A duo-caplet, capsule within a large capsule, was designed. In vitro dissolution studies showed that the release of both model drugs was concurrent and was not relying on drug solubility instead the drug release was dependent on the macrostructure of the duo-caplet.	46
Hydrochlorothiazide	Tablets	<i>In vitro</i>	PVP, Eudragit E	TEC	FDM	Perforated built-in channels were introduced in caplets to accelerate drug release from polymethacrylate tablets. Caplets having multiple short channels (8.6mm) were more effective in facilitating the drug release as compared to the caplets having longer channels (18.2mm).	47
Metformin HCl	Capsules	<i>In vitro</i>	PLA filament, PVA, HEC	PEG 400	FDM	Capsules with discrete zones were introduced. No drip of drug filling was observed from these capsules. There were visible defects on the capsule without discrete zones.	48

Theophylline	Tablets	<i>In vitro</i>	HPC	..	FDM	Gaps were incorporated into the tablets to facilitate the drug release. Tablets with 1mm gaplet spaces disintegrated within a time of 4 minutes and 86.7% of drug was released within a period of 30 minutes.	49
Isoniazid, Rifampicin	Capsule	<i>In vitro and in vivo</i>	PEO, PLA, PVA	..	FDM	HME- extruded filaments loaded with API were incorporated into dual-compartmental dosage units fabricated with PVA and PLA. <i>In vitro</i> and <i>in vivo</i> studies exhibited modified drug release patterns.	50
Carbamazepine, Halofantrine, Saquinavir	Cylindrical tablets	<i>In vitro</i>	PVA, PLA	..	FDM	A tablet containing two compartments loaded with self-nanoemulsifying drug delivery system was developed. The drug release was compared with the gelatine capsules and it was observed that there was ample delay in the release of API from two-compartment formulations.	51
Budesonide	Caplets	<i>In vitro</i>	PVA, Eudragit® L100	TEC	FDM	Drug loaded PVA caplets were fabricated to attain targeted delivery. There was no drug release in acidic environment whereas in alkaline pH approximately 80% of the total drug was released within 8 hours.	52
Theophylline, Budesonide, Diclofenac sodium	Tablets	<i>In vitro</i>	PVP and Methacrylic acid co-polymer	TEC	FDM	Gastric resistant tablets, inner core made up of PVP encapsulated in methacrylic polymer were developed. In acidic pH there almost, no drug release while in alkaline pH more than 80% of all the drugs was release within a period of 8 hours.	53

Diltiazem	Tablets	<i>In vitro</i>	PVA, PVP K30, cellulose acetate	..	FDM	An osmotically controlled tablet was printed, by encapsulating the core of the tablet in a shell. All the formulations showed sustained release of the drug which proved that osmotic formulation can be 3D printed to provide sustained release of the drug.	54
Paracetamol	Tablets	<i>In vitro</i>	HPC, HEC, PEO, ABS white filament	D-mannitol	FDM	The core of the tablet was printed with a surrounding shell to attain zero order release. The device was able to show zero-order drug release in the time spans of 16 to 48 hours.	55
5-Fluorouracil	Tablets	<i>In vitro</i>	PLA filaments, Eudragit® L 100-55, Eudragit® S100	TEC	FDM	A pH- responsive, targeted and controlled release hollow tablets containing alginate beads loaded with 5-FU were developed. Dissolution test revealed that the formulation was in accordance with the pH values and could enable targeted (colonic) delivery of 5-FU alginate beads.	56
Paracetamol	Tablets	<i>In vitro</i>	HPMCAS (LG, MG, HG)	Methyl paraben	FDM	3D printed tablets capable of achieving enteric dissolution without an outer coating of enteric polymer were developed. All the tablets resulted in slow drug release in acidic pH whereas the drug release was fastest in the alkaline pH. HPMCAS LG showed fastest release in alkaline pH.	57

Paracetamol and caffeine	Caplets	<i>In vitro</i>	PVA	..	FDM	All the caplets resulted in 100% drug release in less than 480 minutes. The drug release profile from formulations containing caffeine was moderately faster than formulations with paracetamol.	58
Lisinopril dihydrate, indapamide, rosuvastatin calcium and amlodipine besylate	Tablets	<i>In vitro</i>	PVA	Sorbitol	FDM	Multi-layered tablets containing 4 drugs in one dosage forms were printed via FDM. It was reported that the drug release was dependent on the layer position of drug in the tablet and a biphasic drug release profile was obtained i.e. initially the drug release was faster but late on became slow.	59
Theophylline or Dipyridamole	Tablets	<i>In vitro</i>	PVP	TEC	FDM	FDM was used to fabricate immediate release tablets. The formulation achieved more than 85% release of theophylline and dipyridamole in a period of 30 minutes.	60

Theophylline, Captopril, Prednisolone, 5-ASA	Tablets	<i>In vitro</i>	Eudragit® PO, TCP	TEC	FDM	Immediate release tablets were fabricated with 4 different model drugs. The disintegration time of all the formulations was less than 15 minutes.	61
Enalapril maleate and hydrochlorothiazide	Tablets	<i>In vitro</i>	TCP, Eudragit EPO	TEC	FDM	A single bilayer tablet for flexible dose combinations and immediate release of two anti-hypertensive drugs was developed. Tablets only with methacrylate polymeric matrix yielded immediate drug release profile.	62
Metformin, Glimepiride	Tablets	<i>In vitro</i>	Eudragit® RL, PVA	PEG 400, CA monohydrate, TEC, PLA	FDM	The successful fabrication of a bilayer dosage form containing two anti-diabetic drugs resulted in the two different dissolution profiles i.e. immediate (glimepiride) and sustained (metformin). It was concluded that FDM printing is suitable in consolidating two or more APIs in one dosage form thus increasing patient compliance by minimising multiple administrations.	63
Theophylline	Tablets	<i>In vitro</i>	Eudragit® RL100, RS100, HPC	TEC, Triacetin	FDM	FDM was used to design a tablet that can ease swallowing. Different polymers were used to achieve desired drug release pattern. Linear relationship between printed volume and mass can be applied to adjust the dose digitally.	64

Itraconazole	Tablets	<i>In vitro</i>	HPC (UL, SSL, SL and L)	-	FDM	Tablets were successfully prepared using different grades of HPC. Tablets printed with ultra-low molecular weight grade HPC showed faster drug release as compared to other HPC grades.	65
Tramadol	Tablets	<i>In vitro</i>	HPC, PEO	D-mannitol	FDM	Modified release tablets were printed with abuse deterrent and alcohol resistant properties.	66
Haloperidol	Tablets	<i>In vitro</i>	Kollidon® VA64, Kollicoat® IR, HPMC HME 15 cP, HPMCAS MG	..	FDM	Dissolution rates of FDM printed immediate release tablets were observed. Dissolution testing at pH 2 of tablets with 60% infill density showed complete release of drug in 45 minutes whereas for tablets with 100% infill density there was complete release of drug in 120 minutes.	67
Pantoprazole sodium sesquihydrate	Tablets	<i>In vitro</i>	Poloxamer 407, PVP, Kollidon® VA64, Kollicoat® IR	PEG 6000 and 20,000, TEC	FDM	Immediate release tablets containing thermo-sensitive drug, pantoprazole sodium sesquihydrate were printed. Tablets fabricated with PVP showed fastest drug release (10 min) than tablets formulated with PEG (29 min).	68

Ramipril and 4-ASA	Tablets	<i>In vitro</i>	Kollidon VA64 and 12PF	PEG 1500	FDM	Immediate release tablets with drugs having low melting temperature were developed. Drug release was 100% within a period of 20-30 minutes. Moreover, it was reported that there was no drug degradation owing to suitable use of polymers capable of printing at lower temperatures.	69
Deflazacort	Tablets	<i>In vitro</i>	PCL, Eudragit® RL100 and RS100, Mannitol	PEG 6000, TEC	FDM	Drug-loaded nanocapsules were incorporated into FDM printed tablets. Tablets having 50% infill density exhibited rapid drug release with high drug loading.	70
Caffeine	Capsule	<i>In vitro</i>	HPC	..	FDM	Multi-compartment capsular systems for the delivery of dietary supplements were developed. Fabricated capsular devices met the pre-set elemental, microbiological and by-product specifications. Manually filled and assembled capsular devices showed the desired two-pulse release of caffeine.	71
Theophylline, Milled and unmilled, metformin HCL	Tablets	<i>In vitro</i>	..	TPU	FDM	TPU-based dosage forms were fabricated with 60% w/w drug loading. In vitro dissolution tests showed that all TPU-based formulation containing drugs of varying aqueous solubility successfully prolonged the drug release over a period of 24 hours.	72

Orange G, Brilliant blue G	Tablets	<i>In vitro</i>	PLA, PDMS	Ethylene glycol-based dithiol, EGDT	FDM	Hollow PLA tablets were fabricated to incorporate moulds of polymer solution containing dyes. Different shapes of moulds were investigated resulting in constant, pulsed decreasing and increasing release profiles proving that tablets with customised release profiles can be manufactured.	73
Acetaminophen	Capsules	<i>In vitro</i>	HPC, PLA filament,	PEG 1500	FDM	Oral capsules for pulsatile release of drug were fabricated. Manually assembled capsular devices showed a lag phase before expeditious and quantitative emancipation of the drug during the release test.	74
Acetaminophen	Capsule	<i>In vitro</i>	PLA, PVA, HPMC	PEG, Glycerine	FDM	Multi-compartmental capsular devices for controlled drug release were developed. The desired two-pulse release pattern was achieved consistent with the attributes of the carrier polymers.	75
Salicylic acid	Patch/Mask	<i>In vitro</i>	PCL	PEGDA 700, PEG 300	FDM and SLA	Anti-acne patches were fabricated with FDM and SLA. SLA printing resulted in high drug loading and high resolution of patches as compared to FDM.	76

Acetaminophen	Tablets	<i>In vitro</i>	HPC EF and LF, HPMC E5, EC N14, Soluplus, Eudragit® L100, PLA	..	FDM	FDM printed tablets were compared with directly compressed tablets. FDM printed tablets exhibited smooth surfaces and because of tight inner structures resulted in improved extended drug released rates.	77
Dipyridamole and Theophylline	Capsule	<i>In vitro</i>	Eudragit EPO, RL	TEC	FDM	FDM was used in combination with liquid dispensing. FDM fabricated polymeric shells were filled with drug suspension through liquid dispenser. The thickness of outer layer of the shell can modify the drug release according to the requirements.	78
Sodium warfarin	Tablets	<i>In vitro and in vivo</i>	Eudragit EPO	TEC	FDM	Capsular devices loaded with 200 or 400 µg warfarin dose were developed. FDM printed devices presented low C _{max} of warfarin (1.51 and 3.33 mg/mL) as compared to the liquid formulation (2.5 and 6.44 mg/mL).	79
Aripiprazole	Films	<i>In vitro</i>	PVA	..	FDM	ODFs were printed with FDM and compared with casted films. The printed films exhibited a rapid dissolution rate, more than 95% in 15 minutes and for casted films dissolution rate was 75%.	80

Paracetamol	Films	<i>In vitro</i>	PEO, PVA	PEG 4,000 and 30,000	FDM	Two types of FDFs; single layered and multiple layered were developed. Single layered films disintegrated in shorter time 42 ± 7 seconds whereas multiple layered disintegrated in 48 ± 5 seconds.	81
Captopril	Tablets	<i>In vitro and in vivo (rabbits)</i>	HPC, Sodium starch glycolate, croscarmellose sodium	PEG 6000	FDM	Personalised fast dissolving tablets were developed for the treatment of hypertension. The tablets showed rapid disintegration and <i>in vivo</i> results were in accordance with <i>in vitro</i> results.	82
Felodipine	Discs	<i>In vitro</i>	Polysorbate (Tween 80), PEO 100,000, Soluplus, Eudragit® EPO and PVA	PEG 4000	FDM	Different combinations of polymer blends were investigated to develop a solid dispersion. The process of disintegration affected the drug release rates. Solid dispersions composed of Eudragit EPO exhibited bulk disintegration whereas dispersions with Soluplus disintegrated in a 'peeling style', layer by layer.	83
Bone morphogenic protein-2 (BMP-2)	Functionalised scaffold	<i>In vitro and in vivo</i>	PCL	..	FDM	Scaffolds loaded with BMP-2 were printed for bone repair. Modified scaffolds showed improved osseointegration and osteoconductivity after 8 and 12 weeks during <i>in vivo</i> studies.	84

Gentamicin sulphate or Methotrexate	Discs, Catheters, beads	<i>In vitro</i>	PLA	..	FDM	Constructs (discs, catheters, beads) for sustained delivery of antibiotic and chemotherapeutic drugs were developed. Constructs loaded with gentamicin resulted in inhibition of bacteria on culture plates. The constructs containing PLA and methotrexate inhibited the growth of cancer cells.	85
Gentamicin sulphate or Methotrexate	Catheters	<i>In vitro</i>	PLA pellets	..	FDM	Catheters containing gentamicin sulphate and methotrexate were printed separately. Both catheters followed the same pattern of release. <i>In vitro</i> test showed burst release of drug in the first few hours followed by steady and sustained release of drugs. The sustained release of drugs from both catheters was observed even after 5 days.	86
Gentamicin and methotrexate	Pins, screws and bone plates	<i>In vitro</i>	PLA	-	FDM	PLA constructs with or without drugs were printed with 100% infill density. The flexural strength of drug loaded constructs was lower than the constructs with no drugs. The constructs loaded with gentamicin showed effective bacterial inhibition and XTT assay indicated the presence of chemotherapeutic properties in methotrexate constructs.	87

Dexamethasone	Scaffold	<i>In vitro</i>	Poloxamine 908, PCL	..	FDM	Samples containing PCL and poloxamine at ratio of 90: 10, showed greater drug release with optimum degradation rate and porosity followed by 100:0 and 80:20 samples.	88
Prednisolone and dexamethasone	Scaffold	<i>In vitro</i>	PLA filaments	-	FDM	Scaffold printed with preloaded drug filaments showed sustained drug release whereas scaffolds loaded with drug after printing showed rapid drug release.	89
Collagen	Combination of bone cage and nanofibrous patch	<i>In vitro and in vivo</i>	PLGA nanofibers, PLA bolt	..	FDM	A biocompatible scaffold was fabricated to improve tendon graft healing. <i>In vivo</i> studies showed that bolts have sufficient durability and stability for bone healing. Collagen laden nanofibrous membranes resulted in escalating cell attachment and tissue invasion thus enhancing bone healing.	90
Carbamazepine	Scaffold	<i>In vitro</i>	..	ABS filament	FDM	Scaffolds with holes of varying diameters were printed to achieve the zero-order drug release kinetics. Drug release was increased with the increase in size of the holes.	91

Transforming growth factor- β (GF β 3) or a small molecule drug Y27632	Composite scaffolds	<i>In vitro and in vivo</i>	PCL diol, PU, PLGA, HLA	..	FDM	<i>In vitro</i> , TGF β 3 was released slowly from the scaffolds without losing bioactivity and resulted in self aggregation and chondrogenic differentiation of MSCs after 3 days. Slow and sustained release of Y27632 was also observed for at least 8 days.	92
Vancomycin and Ceftazidime	Combination of bone cage and nanofibrous patch	<i>In vitro and in vivo</i>	PLGA nanofibers, PLA bolt	..	FDM	PLA cage was printed for bone fixation where as PLGA nanofibrous membranes were loaded with antibiotics to treat infection. <i>In vitro</i> studies showed that scaffold could sustain the release of antibiotics for more than 3 weeks.	93
Recombinant human bone morphogenetic protein -2 (rhBMP-2)	Scaffold	<i>In vitro</i>	PLA	..	FDM	Mechanical properties of printed scaffolds were comparable to the properties of cancellous bone of human. Sustained release of rhBMP-2 and Ca ²⁺ ions from printed scaffolds along with improved osteogenic differentiation, cell attachment, viability and proliferation were also reported.	94
Osteogenic growth peptide (OGP) or BMP-2	Functionalised scaffold	<i>In vitro</i>	PEU	..	FDM	The presence of growth peptide on printed scaffolds resulted in increased mesenchymal stem cells osteogenic differentiation.	95

Tetracycline	Implants	<i>In vitro</i>	PLA	..	FDM	<i>In vitro</i> studies concluded that the elution rate of tetracycline from a cube shaped reservoir with 10% infill density was higher than cube with 20% infill density.	96
Cefazolin	Scaffold	<i>In vitro</i>	PCL	..	FDM	The introduction of micro porosity and increased surface area resulted in prophylactic release of cefazolin for up to 3 days. <i>In vitro</i> studies showed that there were no cytotoxic effects at optimal cefazolin concentration of 100 µg/ml against 3T3 fibroblasts.	97
Osteogenon	Scaffold	<i>In vitro</i>	PLLA filaments	..	FDM	During bioactivity test, PLLA scaffolds showed mineralisation due to the presence of osteogenon and gelatine on their surfaces. Presence of gelatine also accounted for increased cell adhesion.	98
Sodium indomethacin	Scaffold	<i>In vitro</i>	PCL, PVA-PAA	..	FDM	Drug release studies showed that initially, the drug release was rapid, later on sustained release was observed due to matrix swelling, with 83.36% drug release after 8 hours.	99
Ibuprofen	Scaffolds	<i>In vitro</i>	PLA	..	FDM	Supercritical fluid technology was used to load the drug onto printed scaffolds of varying pore sizes. It was observed that the dissolution rate decreased with the decrease in pore size which concluded that dissolution rate can easily be changed by changing the pore size.	100

Dexamethasone	Scaffold	<i>In vitro and in vivo</i>	PLA	PEG	FDM	Initial stages of cell proliferation were not affected by dexamethasone but later the release of dexamethasone resulted in improved mineralisation and phosphatase secretion.	101
siRNA	Implants	<i>In vitro and ex vivo</i>	Alginate powder	..	FDM	Carbohydrate gels containing different small-interfering (si) siRNA were deposited onto an implant. Mesenchymal cells were also seeded on these implants. When introduced to spinal cord's cells these implants resulted in localised gene silencing.	102
Nitrofurantoin	Circular discs	<i>In vitro</i>	PLA	..	FDM	Medical devices capable of inhibiting of biofilm colonisation were developed. It was reported that it is more effective to incorporate nitrofurantoin into structures instead of adding the drug on the top of the sample.	103
Nitrofurantoin	Implantable discs	<i>In vitro</i>	PLA, HA	..	FDM	Drug release from the developed discs was dependent on drug loading. Higher drug release was resulted with higher drug loading.	104
Gentamicin	Hernia meshes/Bioactive mesh	<i>In vitro</i>	PLA filament	..	FDM	The introduction of printed meshes to the culture media with <i>Escherichia. coli</i> resulted in inhibition of $1.1 \pm 0.1 \text{ cm}^2$ zone whereas for culture media with <i>Staphylococcus. aureus</i> zone of inhibition was $1.2 \pm 0.1 \text{ cm}^2$.	105

Oleo-gum-resins of <i>Boswellia papyrifera</i> , <i>Comiphorra myrrha</i> and <i>Styrax benzoin</i>	Bioactive discs	<i>In vitro</i>	Oleo gum resin and nanoparticles of TiO ₂ , P25, Cu ₂ O, and MoO ₃	..	FDM	Bioactive discs of oleo gum resin of pure state and charged with metal oxides were prepared. Discs with charged metal oxides exhibited increased bacteriostatic effect.	106
Chlobetasol propionate and vanillic acid	Wearable mouth guard	<i>In vitro and in vivo</i>	PLA, PVA	..	FDM	Drug release kinetics showed sustained release of chlobetasol propionate over 14 days. On contrary, vanillic acid was rapidly released reaching 71% in 10 days.	107
Indomethacin	T-shaped intrauterine devices	<i>In vitro</i>	PCL filaments	..	FDM	Drug release studies of 3 prototypes (1-2 weeks old) showed initial burst release phase followed by slow diffusion of drug.	108
Diclofenac sodium	Implants	<i>In vitro</i>	PLA, antibacterial PLA, PMMA, polyethylene terephthalate glycol	..	FDM	FDM is suitable in developing personalised medication for surgeries. It was reported that varying diameter and infill density affected the drug release whereas the impact of using types of polymers was not quite significant. MTT assay confirmed the nontoxicity of the implants.	109

5-fluorouracil	Implants	<i>In vitro</i>	PLA, PDMS	..	FDM	A magnetic field-triggered device was printed for the cancer treatment. The position of the magnetic bar in the reservoir affected the release of the drug. when placed at the bottom, only 10 % drug was released in 12 hours whereas when placed at the side of the device 50% drug was released in 20 minutes.	110
γ-indomethacin	Intrauterine devices, Subcutaneous rod	<i>In vitro</i>	EVA	..	FDM	The resulted FDM printed intrauterine system and subcutaneous rods with 5% drug resulted in faster drug release than those devices printed with 15% drug loaded filaments.	111
Oestrogen and progesterone	Intrauterine devices	<i>In vitro</i>	PCL	..	FDM	Printed constructs resulted in increased luciferase activity depicting the presence of bioactive agent. No detrimental effects were observed. Moreover, extended release of hormones was observed over a period of one week.	112
Progesterone	Vaginal rings	<i>In vitro</i>	PCL	PEG	FDM	The shape of rings affected the dissolution rate. Due to higher surface area/volume ratio and unique shape, O-shaped vaginal rings had increased dissolution rate than other Y and M-shaped rings.	113

Fluorescein	Microneedles array	<i>In vitro and ex vivo</i>	PLA	..	FDM	Successful penetration of printed arrays in porcine skin was reported. Approximately 50% of drug was released in a period of 4 hours.	114
Rhinocort nasal spray (Budesonide suspension)	Expansion chamber	<i>In vitro and ex vivo</i>	..	ABS	FDM	After actuation of Rhinocort spray into printed expansion chamber, initially, $47.3 \pm 5.0\%$ of drug was transported across nasal epithelia. After 4 hours of experiment, $14.4 \pm 4.9\%$ of budesonide was found on the surface of the cells whereas $2.5 \pm 1.6\%$ was present inside the cells.	115
Copper sulphate (II) pentahydrate, Zinc oxide, Silver nitrate	Wound dressings	<i>In vitro</i>	PCL	..	FDM	The release of all the metals from printed dressings was rapid in first 24 hours followed by slow and sustained release for up to 72 hours. Thermal activity test showed that wound dressings with silver and copper metals had the most effective bactericidal properties.	116
Niclosamide, inositol phosphate (IP6)	Stent	<i>In vitro and ex vivo</i>	PCL, graphene nanoplatelets	..	FDM	<i>In vitro</i> test of 120 hours reported non-toxic behaviour of stent towards cell growth. Anti-blood coagulation test using real blood of pig showed that niclosamide and IP6 drugs had no role in blood coagulation.	117

Kanamycin, Tetracycline, Polymixin B	Antimicrobial testing robotic setup	<i>In vitro</i>	PLA	..	FDM	During culture assay, deposition of 37.1 µg of kanamycin showed 24.2 ± 0.68 mm zone of inhibition while deposition of 43.5 µg of tetracycline showed 27.5 ± 3.4 mm inhibition zone.	118
rhBMP-2	Composite scaffolds	<i>In vivo</i>	PLGA, TCP	..	PnE	Active artificial bone composed of PLGA and TCP were developed to observe the process of osteogenesis. Implantation of scaffold in goats resulted in complete repair of cranial defect after 24 weeks of surgery.	122
Isoniazid, Rifampicin	Composite scaffolds	<i>In vitro and in vivo</i>	TCP, MSNs coating	..	PnE	<i>In vitro</i> and <i>in vivo</i> (rabbit) studies showed sustained release of both drugs, isoniazid and rifampicin, from the composite scaffold. The bactericidal action of isoniazid and rifampicin at concentrations of 0.025-0.05 µg/ml and 0.005-0.5 µg/ml against <i>Mycobacterium tuberculosis</i> was greater than their effective levels.	123
rhBMP-2	Composite scaffolds	<i>In vitro and in vivo</i>	PLGA, PCL	..	PnE	Two scaffolds containing PCL/PLGA/rhBMP-2/collagen and PCL/PLGA/rhBMP-2/gelatine were developed implanted into rabbits. The release of rhBMP-2 from scaffold with collagen showed ideal bone healing characteristics whereas the release of rhBMP-2 from scaffold with gelatine induced inflammation.	124

Dexamethasone	Composite scaffolds	<i>In vitro</i>	Non-ionic block copolymer EO ₂₀ PO ₇₀ EO ₂₀ (Mw = 5800), MBG, PVA	..	PnE	Strontium containing MBG scaffolds for bone regeneration were developed. The scaffolds showed sustained release of drug and the ability to provoke differentiation and proliferation of cells of osteoblast.	125
Tobramycin	<i>Antibiotic-loaded scaffolds</i>	<i>In vitro and in vivo</i>	PCL, PLGA	..	PnE	Scaffold was developed to treat chronic osteomyelitis. <i>In vitro</i> test showed sustained release of drug. <i>In vivo</i> studies showed that scaffold mitigated the oedema and inflammation due to infection.	126
rhBMP-2	<i>Bio-porous scaffolds</i>	<i>In vitro</i>	PCL	..	PnE	Polydopamine coated PCL scaffolds were grafted with 100 ng/ml (PCL100) and 500 ng/ml (PCL500) of rhBMP-2 to enhance cell differentiation. PCL500 scaffolds showed better cell proliferation than PCL100 scaffold during <i>in vitro</i> tests.	127
Silver nanoparticles	<i>Bio ceramic scaffolds</i>	<i>In vitro</i>	TCP, GO, PVA	..	PnE	β-TCP scaffold coated with silver nanoparticles disperse in graphene oxide was developed. The resulted scaffold had antibacterial activity and increased osteogenic activity suitable for bone defects.	128

Diclofenac	<i>Scaffold</i>	<i>In vitro</i>	Chitosan, Sodium alginate	..	PnE	Chitosan coating around the scaffold comprising bone cells enclosed in fibrous alginate hydrogel increased the efficacy and retention of drug release. Slow and steady release of drug helped in healthier bone regeneration.	129
Cyclosporine A	<i>Hydrogel loaded with CsA</i>	<i>In vitro and in vivo</i>	PLGA, PVA, PCL	..	PnE	Drug carriers were developed for local delivery of cyclosporine A. <i>In vitro</i> drug release test showed rapid release of cyclosporine from hydrogel on day 1 followed by sustained release of drug for a period of 4 weeks. In 28 days, 75% of drug was released from hydrogel.	130
Green fluorescence protein (EGFP, MW 27KD)	<i>Hydrogel</i>	<i>In vitro</i>	Sodium alginate	..	PnE	Hollow filaments of alginate were developed for the delivery of nutrients. Filaments were biocompatible in use and produced structures of high strength with high concentration of sodium alginate.	131

Dexamethasone-21-phosphatedisodium salt	<i>Implants</i>	<i>In vitro</i>	PVA, PLGA	..	PnE	Implants were fabricated for treating bone defects. Dexamethasone was successfully encapsulated within PLGA/PVA structure. The release of drug was monitored for 4 months. Implants with layered structure showed long term release.	132
Levetiracetam	<i>Tablets</i>	<i>In vitro</i>	PVA-PEG, PVP-PVA	-	PnE	Copolymers PVA-PEG and PVP-PVA were used for the formulation of immediate release tablets. The disintegration time of PVA-PEG and PVP-PVA tablets was 95 ± 10 s and 130 ± 20 s. The copolymers were effective in producing immediate release tablets.	133
Lamotrigine	<i>Gummies</i>	<i>In vitro</i>	Gelatine, reduced syrup, HPMC	..	PnE	Drug loaded gummies were printed using gelatine and HPMC. The amount of gelatine greatly affected the strength of gummies and addition of HPMC helped in printing smoothly. 85% of the drug release was within 15 minutes.	134
Paracetamol	<i>Tablets</i>	<i>In vitro</i>	PVP K25, starch	..	PnE	Tablets with three different structures; solid, ring and mesh were fabricated. Each tablet gave distinct drug release profile. Mesh tablets showed 70% drug release within first 15 minutes whereas ring and solid tablets showed 25% and 12% drug release, respectively.	119

Efavirenz, Tenofovir disoproxil fumarate, and Emtricitabine	Tablets	<i>in vitro and in vivo</i>	Humic acid, HECE, CAP	..	PnE	HA-PQ10 complex was used as a bio ink to formulate tablets containing three anti-HIV-1 drugs. <i>In vitro</i> and <i>in vivo</i> studies resulted in controlled release of all the drugs due to complex nature of HA-PQ10.	135
Multiplexed gradients/Payload biomolecules	Capsules	<i>In vitro</i>	PLGA	..	PnE	Stimuli-responsive capsules comprising plasmonic gold nanorods and biomolecule were developed. Laser irradiation of corresponding wavelength ruptured the capsules thus releasing biomolecules. Number of laser irradiation controlled the biomolecule release.	136
Fluorescein, Rhodamine B (model chemical entities)	Tubes	<i>In vitro</i>	Sodium alginate, PLGA	..	PnE	Tubes intimating blood vessel system were developed for sequential delivery of fluorophores. Fluorescein was released immediately in 24 hours. After 24 hours sustained release of rhodamine B was observed.	137
Prednisolone	Implants/ inserts/ intrauterine devices	<i>In vitro</i>	PDMS	..	PnE	Intrauterine devices fabricated via FDM were cured with UV light. <i>In vitro</i> drug release test showed that intrauterine devices containing 1% of drug exhibited cumulative drug release of 9.5-11% whereas for devices with 1.5% drug loading it was 10.4-11%.	138

Diclofenac sodium, Lidocaine	<i>Wound dressings</i>	<i>In vitro</i>	CMC	..	PnE	CMC and alginate hydrogel containing two drugs was used to prepare dressings. <i>In vitro</i> release test showed the sustained release of drugs for 2 days.	139
7-ethoxy-4-trifluoromethyl coumarin	<i>Organ-on-a-chip model</i>	<i>In vitro</i>	PDMS, alginate solution	..	PE	A micro-organ device as an <i>in vitro</i> drug metabolism model was developed using PDMS and varying alginate concentrations. Encasing hydrogel-based tissue constructs in delineate design patterns that bio mimics the cell's natural microenvironment for augmented biological functionality.	141
Amifostine	<i>Organ-on-a-chip model</i>	<i>In vitro</i>	Matrigel	..	PE	Epithelial cells and hepatocytes were embedded in Matrigel and then were sealed in microfluidic chip. Micronuclei count reported that hepatocytes treated with drug showed reduced radiation damage as compared to hepatocytes without treatment of drug.	142
Cisplatin, paclitaxel, methotrexate, and tamoxifen	<i>Bio printed cell laden model</i>	<i>In vitro</i>	Endothelial cells	..	PE	The developed human breast cancer model was consisted of breast cancer lesions. During culture test, bio-printed neotissues remained viable for 14 days. Upon interaction of drugs with cancer and stromal cells, the bio-printed neotissues retained their compartmentalised structures.	143

Paclitaxel	<i>Bio printed cell laden model</i>	<i>In vitro</i>	Gelatine-alginate-fibrinogen solution	..	PE	3D printed models showed 90% cell viability. Higher proliferation rate and formation of cellular spheroids of Hela cells were also reported.	144
Temozolomide	<i>Bio printed cell laden model</i>	<i>In vitro</i>	Gelatine-alginate-fibrinogen solution	..	PE	Fibrinogen/gelatine/alginate hydrogels were used to print the cell laden model that could imitate the extracellular matrix. High cell proliferation activity and 86.92% survival rate of glioma stem cells were reported.	145
Acetaminophen	<i>Organ-on-a-chip model</i>	<i>In vitro</i>	PDMS, PMMA Gelatine methacryloyl hydrogel	..	PE	The printed cells on model showed viability after printing. Decrease in metabolic activity was reported after a period of 6 days in culture. Decrease in activity and density of cell was also observed.	146
Trovafloxacin, Levofloxacin	<i>Bio printed cell laden model</i>	<i>In vitro</i>	Novogel 2.0 hydrogel	..	PE	Liver tissue model was printed to assess the human drug response. The drug induced toxicity was dose dependent. Strong toxicity was only observed in rodent models when trovafloxacin was administered with lipopolysaccharide.	147
Cyclosporine A	<i>Organ-on-a-chip model</i>	<i>In vitro</i>	Silicone elastomer, Pluronic F127	..	PE	Increased functional properties and epithelial morphology was reported in 3D convoluted proximal tubules. Epithelial barrier was disrupted on introduction of cyclosporine A and was dependent on dose. Epithelial barrier permeability was increased by 4 and 6 fold when exposed to 50 μ M and 100 μ M cyclosporine A, respectively.	148

Bicuculline	<i>Bio printed cell laden model</i>	<i>In vitro</i>	Alginate, Carboxymethyl-chitosan, and Agarose.	..	PE	Scaffold was encapsulated with stem cells for <i>in situ</i> differentiation and expansion. Differentiated neurons established active networks that increase the calcium response upon induction of bicuculline and were gamma-aminobutyric acid expressing.	149
rhBMP-2, CTGF, TGF	<i>Cylindrical scaffold</i>	<i>In vitro and in vivo</i>	PLGA, PVA, PCL	..	PE	Scaffold loaded with growth factors were developed. In vitro assay showed that scaffold induced multiphase production of tissues from mesenchymal stem cells. In vivo studies showed enhanced healing of perforated discs after implanting scaffold.	150
VEGF	<i>Hydrogel loaded scaffolds</i>	<i>In vitro, ex and in vivo</i>	Tween 80, Alginate powder, Gellan gum	..	PE	Combination of CPC paste, and VEGF laden hydrogel strands was used to develop a scaffold for bone healing. The chemotactic behaviour of VEGF towards cells caused the cells to migrate inside the cells thus encouraging the cells to grow.	151
Dexamethasone	<i>Scaffold</i>	<i>In vitro</i>	PVA, MBG	..	PE	Implants with increased mechanical strength and toughness were fabricated for bone regeneration. 75% drug release was observed in first 2 days followed by slow release up to 10 days.	152

Doxorubicin	<i>Composite scaffolds</i>	<i>In vitro and ex vivo</i>	Non-ionic block copolymer EO20PO70EO20, PCL, MBG	..	PE	PCL/MBG scaffold with inclusion of Fe ₃ O ₄ nanoparticles were developed for local delivery of anticancer drug and to induce hyperthermia. The resulted scaffold showed sustained release of drug with exceptional magnetic heating ability.	153
Isoniazid and Rifampicin	<i>Composite scaffolds</i>	<i>In vitro and in vivo</i>	MBG, mesoporous silica nanoparticles	..	PE	Scaffolds loaded with anti-tuberculosis drugs were developed for osteoarticular tuberculosis. <i>In vitro</i> and <i>in vivo</i> studies resulted in sustained release of drugs.	154
Isoniazid and Rifampicin	<i>Composite scaffolds</i>	<i>In vivo</i>	MBG	..	PE	Scaffolds loaded with anti-tuberculosis drugs were developed for osteoarticular tuberculosis. <i>In vivo</i> studies resulted in sustained release of drugs.	155
Isoniazid	<i>Scaffold</i>	<i>In vitro</i>	PCL, Pluronic	..	PE	MBG-MOF scaffolds showed good apatite forming ability in vitro. The dissolution profile showed sustained release of drug from scaffold.	156

Dimethyloxallyl glycine	<i>Scaffold</i>	<i>In vitro and in vivo</i>	Poly(3-hydroxybutyrate-co-3-hydroxyhexanoate), PCL	..	PE	Scaffolds with dimethyloxallyl glycine enhanced osteogenesis and angiogenesis during in vivo studies. Drug was released in a sustained manner for about four weeks.	157
rhBMP-2	<i>Scaffold</i>	<i>In vitro, ex and in vivo</i>	Chitosan	..	PE	<i>In vitro</i> studies reported that printed scaffold could release rhBMP-2 for more than 21 days. The increased osteoconductivity was also reported for induction of human mesenchymal stem cells. <i>In vivo</i> studies reported that scaffold exhibited excellent bone regeneration capacity.	159
5-fluorouracil	Scaffolds	<i>In vitro</i>	Calcium phosphate cement, Soluplus	PEG	PE	CPC based scaffolds coated with the drug were successfully developed for the bone cancer treatment. The scaffolds showed complete drug release in within 2 hours and were able to inhibit the cell growth during in vitro cell culture test.	160

Doxorubicin	<i>Organ-on-a-chip model</i>	<i>In vitro</i>	Gelatine meth acryloyl hydrogel, Alginate	..	PE	Printed myocardial tissues were capable of generating synchronised and spontaneous contraction. Device proved to be suitable for screening of cardiovascular drugs.	161
Methotrexate	<i>Hydrogels</i>	<i>In vitro</i>	Sodium alginate, Pluronic F127	..	PE	Shape memory hydrogels were developed to use as a drug carrier. The resulted hydrogels exhibited rapid release of drug and were biocompatible.	162
Tacrolimus	Suppositories	<i>In vitro and in vivo (rats)</i>	Gelucire 44/14, coconut oil	..	PE	Liquid excipients were feasible to print. The suppositories showed 50% of the drug release within the first hour. The in vitro and in vivo disintegration times were different due to the lower amount of liquid in rat' colon.	163
Lidocaine	Implants	<i>In vitro</i>	PCL	..	PE	Sustained release drug implants were successfully printed and the drug release followed Korsmeyer-Peppas model.	164

Guaifensen and HCL	Tablets	In vitro	HPMC, PAA	..	PE	3D printed tablets with were compared with commercial tablets of guaifenesin. 3D printed tablets were comparable to the commercial tablets. All formulations showed sustained release of drug for a period of 12 ours.	165
Glipizide	Tablets	In vitro	HPMC K100 and E15, PVP	-	PE	The effect of printing parameters such as outline and grid width values on drug release studies was investigated. The tablets with different outline values showed more than 95% cumulative drug release in nearly 8 hours. On the other hand, the drug release was faster with increase in grid width values due to an increase in surface area.	166
Naftopidil	Tablets	In vitro	HPMCs	-	PE	Various amounts of prepared hydrogel were incorporated into the printer for printing of tablets. The weight and hardness of the tablets were decreased when the amount of hydrogel was increased in the printer ink and the drug dissolution was delayed.	167

Cryptotanshinone	Hydrogel	<i>In vitro and in vivo (rats)</i>	Tween 80, cholesterol, glycerine, sodium polyacrylate 700	..	PE	Niosomal-hydrogel was developed for the topical treatment of acne. The drug release from the hydrogel followed Korsmeyer-Peppas model. The hydrogel also showed anti-acne effect without any skin irritation in rats during <i>in vivo</i> studies.	168
Ranitidine hydrochloride	Gummies	<i>In vitro</i>	Xanthan gum, carrageenan, corn starch and gelatine	..	PE	3D printing was successful in developing drug loaded gummies, a more suitable and acceptable dosage form for children. The printed gummies were quite appealing to the eyes and showed complete release of drug in 120 minutes.	169
Aspirin, Hydrochlorothiazide, Atenolol, Pravastatin sodium, Ramipril	Tablets	<i>In vitro</i>	HPMC, PVP	PEG 6000	PE	A polypill containing 5 different drugs for cardiovascular treatment regimen was developed. Tablet showed immediate release for two of 5 drugs whereas the other three drugs exhibited sustained release.	170

Captopril, Nifedipine, Glipizide	Tablets	<i>In vitro</i>	HPMC	PEG 6000	PE	Polypill containing three different drugs was developed. Captopril exhibited zero order whereas other two drugs showed first order drug release during in vitro dissolution test.	171
Paracetamol	Tablets	<i>In vitro</i>	PVP, Croscarmellose sodium	..	PE	Tablets with high drug loading (80% w/w) were developed. The printed tablets exhibited desired immediate release pattern.	172
Levetiracetam	Tablets	<i>In vitro</i>	PVA-PEG, Kollicoat® IR	..	PE	Immediate release tablets of levetiracetam were printed with precise dispensing of the drug. Tablets were printed with different number of layers. All the printed formulations showed disintegration time of 3 minutes. The dissolution was dependent on the number of layers i.e. the drug release decreased with increase in the number of layers.	173
Ibuprofen and diclofenac sodium	Tablets	<i>In vitro</i>	HPMC, gelatine, MCC	..	PE	Gelatine-based pastes, a thermo-sensitive material, were successfully used in printing immediate release and prolonged release tablets of ibuprofen and diclofenac sodium, respectively. The additives like HPMC and microcrystalline cellulose were added to improve the printability. It was also reported that computational fluid dynamics simulation was helpful in understanding the printing process.	174

Propranolol HCL	Tablets	<i>In vitro</i>	Cellulose acetate, D-mannitol	PEG 6000	PE	The core tablet for immediate release of the drug was encapsulated with a surrounded shell to achieve sustained drug release. The drug release profile Korsmeyer-Peppas model and was affected by the space between the core tablet and the shell.	175
Levetiracetam	Tablets	<i>In vitro</i>	PVP-PVAc copolymer, HPMC, silicon dioxide	..	PE	Sustained release tablets with varying infill design and the amount of HPMC were printed. The results indicated that higher amount of HPMC decreased the drug release.	176
Theophylline	Tablets	<i>In vitro</i>	Methyl cellulose	..	PE	Sustained release tablets of theophylline were successfully developed using various doses of the drug and along with different concentrations of methyl cellulose.	177
Glipizide, theophylline, gliclazide, puerarin, lornoxicam	Tablets	<i>In vitro</i>	HPC, polyoxyethylene	..	PE	Controlled release tablets with zero-order release profiles of various model drugs having varying solubility were investigated. It was reported that using drugs with solubility 9.45 µg/mL to 8.34 mg/mL and drug loading from 3% to 43% w/w zero-order release profiles can be achieved without changing 3D printing parameters.	178

Theophylline	Tablets	<i>In vitro</i>	Eudragit® RL and RS, glycerol monostearate	..	PE	The tablets containing fatty glyceride to eliminate the need of post-printing drying process, were printed and showed sustained drug release for 12 hours which was affected by Eudragit RS: RL polymer ratio. Increasing amount of Eudragit RS in comparison to RL resulted in further delay of drug release.	179
Fenofibrate	Tablets	<i>In vitro</i>	Soybean oil, polyethoxylated castor oil and Tween 85, methyl cellulose, croscarmellose sodium	..	PE	Emulsified gels were used for printing lipid tablets of fenofibrate. The tablets were successfully printed and disintegrated in less than 15 minutes.	180
Caffeine	Films	<i>In vitro</i>	Pullulan, HPMC	..	PE	Oral films using natural polymer were developed. It was reported that the addition of HPMC improved the mechanical properties of the films.	181
5-fluorouracil	Patch	<i>In vitro and in vivo</i>	PCL, PLGA	..	PE	Patches were developed for controlled and local delivery of chemotherapeutic drug. Patches were able to release the drug in a controlled manner for a period of 4 weeks.	182

Ibuprofen, nifedipine, indomethacin	<i>Bio-printed cell laden model</i>	<i>In vitro and ex vivo</i>	Commercially Available Human Uterine Smooth Muscle Cells	..	PE	Based on the smooth muscle cells physiology, bio printed hollow myometrial rings were found to contract immediately after printing. Exposure to tocolytic compounds, indomethacin and nifedipine, clinically used for inhibition of the myometrial contractions, affected the contraction in myometrial rings in a dose-dependent manner.	184
-------------------------------------	-------------------------------------	-----------------------------	--	----	----	---	-----

2.3.1.2. Vat Polymerisation

Vat polymerisation is one of the highest resolution additive manufacturing technique. The high-resolution printing enables printing of highly personalised drug delivery devices with such shapes that are critical for transdermal drug delivery systems and implants. Various polymers can be used to develop immediate or extended release drug delivery systems¹⁵. Vat polymerisation includes the following techniques: (a) stereolithography (SLA), (b) digital light processing (c) 2-photon polymerisation (2PP) and (d) continuous liquid interface production (CLIP).

Among 241 selected articles, 22 research articles belong to vat polymerisation, out of which 13, 4, 3, and 2 are further categorised into SLA, DLP, CLIP and 2PP respectively (Figure 2.29).

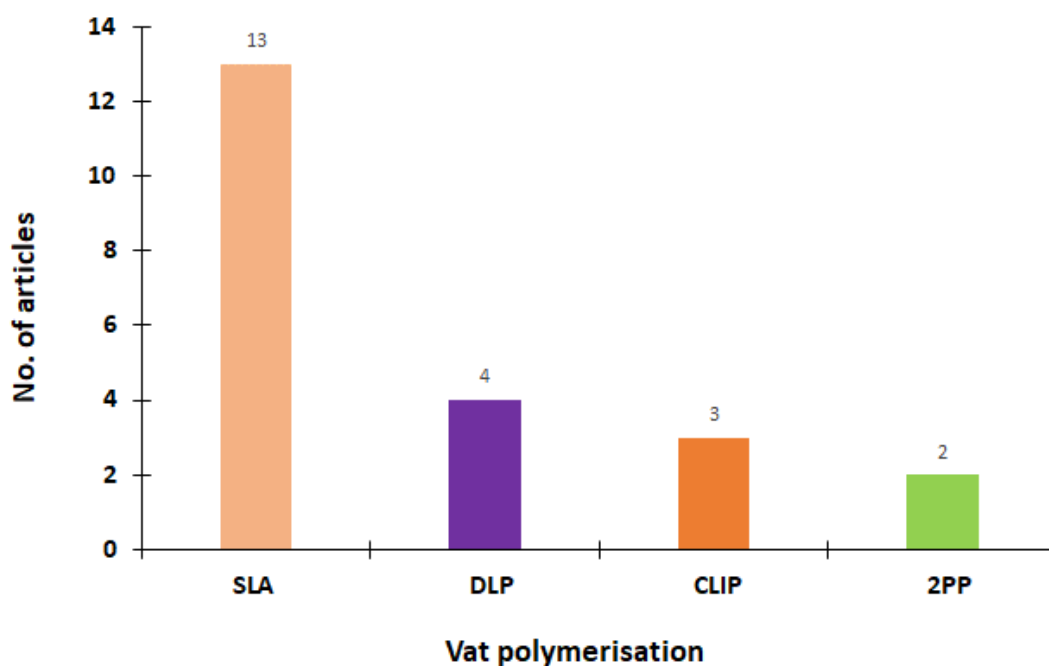


Figure 2.29: Distribution of included studies based on vat polymerisation-based techniques.

Stereolithography (SLA); Continuous liquid interface production (CLIP); Digital light processing (DLP); 2-photon polymerisation (2PP).

2.3.1.2.1. SLA and its applications

The SLA process (Figure 2.30 ¹⁸⁵) also involves printing in a layer by layer manner. A set of coordinates is used to present the slice information to define the tilted angle of two mirrors which also guide the position of laser beam along the plane. In addition, by controlling the laser intensity the exposure of dose can be adjusted for every pixel of the layer separately. This enables SLA to process grayscale patterns and the technique is flexible enough to combine with printing methods ¹⁵.

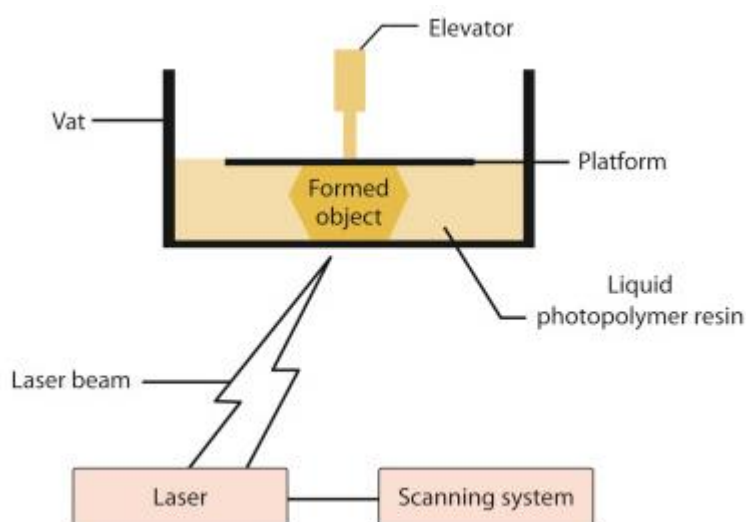


Figure 2.30: Schematic diagram illustrating working principle of stereolithography, reproduced with permission from ¹⁸⁵.

Several applications of SLA in providing safe, effective and tailored drug dose according to patient's requirements are described.

Drug delivery management is of the utmost importance in ocular diseases such as diabetic retinopathy, glaucoma, retinitis pigmentosa and age-related macular degeneration to prevent blindness. Intraocular injections, oral medications and biodegradable implants are used to provide lifelong treatment to treat these incurable diseases. Implants with pump systems dispense drugs from an internal reservoir, thus providing control over drug delivery rate and volume. Therefore, an implantable device for ocular delivery of corticosteroid fluocinolone acetonide was printed using PDMS and microchannels were incorporated between the top and bottom layer of the device. Different configurations of microchannels

were evaluated for diffusion properties as the movement of the drug concentration across microchannels was due to the concentration gradient. In 38 seconds, flow field reached at the end of the channel. Sustainable diffusion rates with fully developed flow took place at nearly 150 seconds. Experimental analysis showed that each microchannel configuration exhibited a different rate of drug diffusion. Channel design of osmotic I and II resulted in the optimal diffusion rate required for ocular drug delivery ¹⁸⁶.

Reconstitution of lyophilised drugs is a practical challenge in demanding environments like rural areas, disaster zones and battlefield support. Biological drugs are usually stored in their lyophilised forms in sealed glass vials to avoid hydrolysis. These vials require reconstitution upon administrations. Reconstitution involves dilution injection into vials, manual shaking and confirm homogeneity by visual look. For effective reconstitution of drugs with large payloads (like biological and antibiotic drugs in order of tens of milligrams) and APIs with low solubility, numerical model should be considered. Portable packaging for rapid reconstitution of lyophilised drugs was developed using stereolithography technique. Computational fluid dynamic technique was employed to design and revamp the microfluidics for rapid mixing and integrating physical properties of drugs and diluents. Experimental results were in accordance with the computational fluid dynamics indicating effective reconstitution of tissue plasminogen activator. Experimental study also demonstrated that structural dimensions and physical properties of diluent and drugs can result in desired release kinetics of drugs ¹⁸⁷.

A nebulising device with variable frequency was printed using SLA to evaluate aerosol deposition of gentamicin in maxillary sinuses of the nasal replica model. It was reported that the effect of acoustic airflow due to the variable frequency resulted in excellent deposition of gentamicin into maxillary sinuses of nasal replica. The deposition of the drug was dependent on the frequency sweep of acoustic airflow. Shorter sweep cycle resulted in increased deposition indicating that imposing acoustic airflow with frequency sweep can result in improved and more targeted deposition ¹⁸⁸.

To investigate the feasibility of SLA in developing drug-loaded tablets with modified-release characteristics, torus shaped tablets containing 4-ASA and paracetamol were printed using polyethylene glycol diacrylate (PEGDA) and PEG 300 (Figure 2.31). The tablets containing thermally labile drugs were printed without any degradation. Furthermore, dissolution testing revealed sustained release of drugs, although a change in the ratio of the PEG and

PEGDA affected the drug release rate. Paracetamol tablets with 35% PEGDA achieved 100% drug release after a period of 10 hours, whereas tablets with 65% and 95% PEGDA resulted in 84% and 76% of drug release, respectively, after 10 hours. Tablets containing 4-ASA also followed the same pattern ¹⁸⁹.

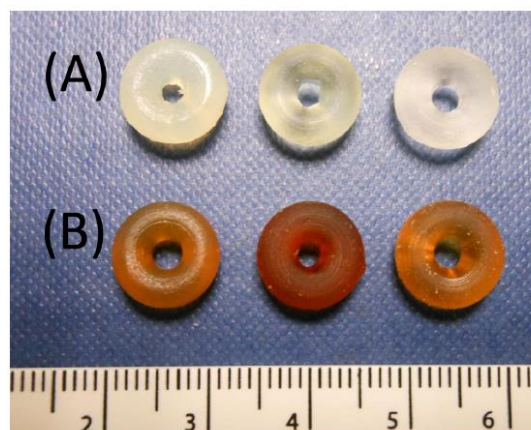


Figure 2.31: Images of 3D printed tablets loaded with (A) paracetamol (B) 4-ASA with different percentages of PEG/PEGDA, reproduced with permission from ¹⁸⁹.

SLA is not only suitable for developing personalised dosage forms but it also has been reported as a digital technology fitted for bulk manufacturing of pharmaceutical dosage forms. Healy et al., were able to print 28 dosage forms in one print process using SLA. The photopolymer solution was prepared using PEGDA/PCL along with Irgacure TPO as a photoinitiator and paracetamol and aspirin were used as model drugs. During a 24-hour drug release studies, both drugs showed sustained release. The dimensions of the printed tablets were significantly different from the targeted which could be attributed to the incorporation of two different drugs ¹⁹⁰.

A polypill containing four anti-hypertensive drugs irbesartan, atenolol, hydrochlorothiazide and amlodipine was printed to improve the patient compliance and reduce the pill burden. The tablets were successfully printed; however, the study reported the drug-photopolymer reaction between primary amine group of amlodipine and diacrylate group of photocurable resin. Such interaction can lead to degradation of the drug which would ultimately diminish the therapeutic effect. It was concluded that photocurable resins should be carefully selected for SLA printing ¹⁹¹.

Hydrogels cross-linked with PEGDA possessing varying water content were fabricated for the controlled release of ibuprofen. Riboflavin was also added to the formulation as a photo initiator and 10% w/w of drug was loaded into the hydrogels with water content up to 30%. The dissolution profile showed that drug release rates were dependent on the content of water and had a direct correlation i.e. higher content of water in hydrogel resulted in faster release of drug¹⁹².

A 3D-printed scaffold loaded with transforming growth factor (TGF- β 1) was fabricated for osteochondral defects. A nano ink comprising crystalline nano hydroxyapatite and core shell of PLGA loaded with growth factor was formulated to print the porous scaffold. Increased osteogenic differentiation, cell proliferation and adhesion of human bone-marrow derived mesenchymal stem cell was observed along with sustained release of growth factor during *in vitro* assay¹⁹³.

In breast cancer, bone is the common location of metastasis. Therefore, to examine the breast cancer bone invasion, a 3D printed nanocomposite matrix containing fluorouracil was developed. In comparison with 2D cell culture, cell growth on 3D printed scaffolds had an increased migration capacity and spheroid morphology. Spheroid assemblage was increased when bone marrow mesenchymal stem cells were cultured with tumour cells. Moreover, the 3D printed nanocomposite matrix had greater drug resistance of breast cancer cells as compared to 2D culture. The results suggested that the printed nanocomposite matrix was able to imitate the environment surrounding tumour cells, thus making it a suitable tool to study breast cancer bone invasion and for analysing sensitivity of drug as reported by Zhu, Holmes *et al.*,¹⁹⁴.

To improve bone regeneration after rupture of the anterior cruciate ligament, a bio absorbable porous scaffold with suitable pull out strength was fabricated using poly propylene fumarate loaded with rhBMP-2 microspheres and coated with carbonate hydroxyapatite by Parry, Olthof *et al.*,¹⁹⁵. The synergistic effect between microspheres and coating with carbonate hydroxyapatite resulted in a decrease in initial burst release of rhBMP-2 from 17% to 6-7%. The cumulative release also decreased from 32% to 16-19%.

Microneedles are miniaturized lancet shaped devices that are used to penetrate the keratinised stratum corneum layer of the epidermis which blocks the transport of active

pharmaceutical ingredients through the skin. The introduction of metals for the treatment of wounds or other skin conditions has been investigated. Keeping this in view, an acrylate-based polymer was used to develop microneedle arrays with a coating of silver and zinc oxide as bactericidal for wound treatment. The microneedles exhibited anti-bacterial activity against two bacteria *Staphylococcus epidermidis* and *Staphylococcus aureus* during agar assay

196.

Transdermal delivery of insulin was achieved by fabricating microneedle arrays via SLA. FDA approved class I resin dental SG was employed to print the cone and pyramid shaped microneedles using a stereolithography technique. Ink jet printing was used to print or coat insulin solution onto these microneedles using xylitol, mannitol and trehalose as an insulin carrier and, post printing, the microneedle arrays were cured with a UV laser to improve mechanical properties. Skin penetration studies did not report any breakage of microneedle and it was also reported that all carriers were suitable to keep the insulin in its native form, but xylitol exhibited the best performance. *In vitro* profile showed both cone and pyramid shaped microneedle arrays exhibited rapid release of insulin within a period of 30 minutes

197.

2.3.1.2.2. CLIP and its applications

Continuous liquid interface production (CLIP) (Figure 2.32 ¹⁹⁸) involves inhibition of polymerisation by using an oxygen permeable film closer to the UV surface and therefore does not required recoating step for each layer ¹⁹⁹. Furthermore, CLIP is comparatively faster than traditional DLP, hence allowing production of objects with features below 100 μm at z-axis growth rates of 30 cm h^{-1} ¹⁴. Applications of CLIP in drug delivery are noted below.

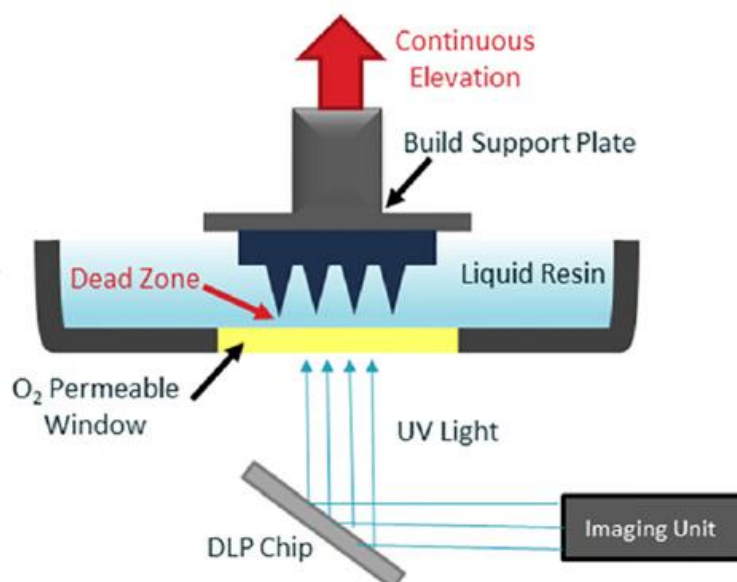


Figure 2.32: Schematic diagram illustrating working principle of CLIP, reproduced with permission from ¹⁹⁸.

Pyramid shaped microneedle patches were fabricated using a trimethylolpropane triacrylate resin because of its low viscosity and fast reaction. Microneedles are useful for the transdermal delivery of drugs that is difficult for drugs using conventional routes. The resin was used to establish a method for the evaluation of microneedles. After this, PEGDA, PCL-tMa and polyacrylic acid was used to fabricate microneedles for the delivery of therapeutics. The microneedles were loaded with a drug surrogate, rhodamine B base. In vitro release of rhodamine B in phosphate buffer saline showed that PCL based microneedles released 0.5 wt% of rhodamine B for more than a period of one week whereas PEG based microneedles released 5 wt%. Penetration testing showed successful penetration of all microneedles into murine skin during *ex vivo* analysis thus making this technology a suitable method for the fabrication of microneedles ¹⁹⁸.

For spatial delivery of proteins, microneedle patches were fabricated. PEG based microneedles were coated with a solution of proteins such as lysozyme, ovalbumin and bovine serum albumin. Microneedles were dipped into the solution containing proteins without reaching to the base of the patch and it was reported that proteins retained their activity after coating process. Penetration testing reported rapid release of proteins into porcine skin. Additionally, *in vivo* studies were carried out in live mice which demonstrated a sustained release of proteins in the skin for more than 72 hours ²⁰⁰.

CLIP was used to fabricate controlled release drug delivery devices with complex geometry using liquid resins. *In vitro* drug release studies showed that the geometry of the device i.e. changes in the size of the unit cell that build scaffolds, can adjust the release of rhodamine B (drug surrogate) while keeping the drug loading constant. In addition, the composition of the polymer matrix and density of crosslinks can also adjust the release of rhodamine B. PEG based hydrophilic matrices showed an increase in drug release and swelling of the device as the crosslink density increased, whereas the drug release and swelling of PCL based matrix did not depend on the crosslink density and it was also reported that devices were biocompatible. By keeping in view all the observations made with the drug surrogate, the efficiency of the devices was also evaluated with clinically relevant drugs - docetaxel and dexamethasone 21-acetate. The devices showed controlled and sustained release of docetaxel and dexamethasone 21-acetate in compliance with the evaluations made with drug surrogate ²⁰¹.

2.3.1.2.3. 2PP and its applications

2PP uses a pulsed titanium: sapphire laser attached with computer-controlled mirrors to direct the beam within photo resin vessel and during the process builds support-free microscopic structures ²⁰² (Figure 2.33 ²⁰³).

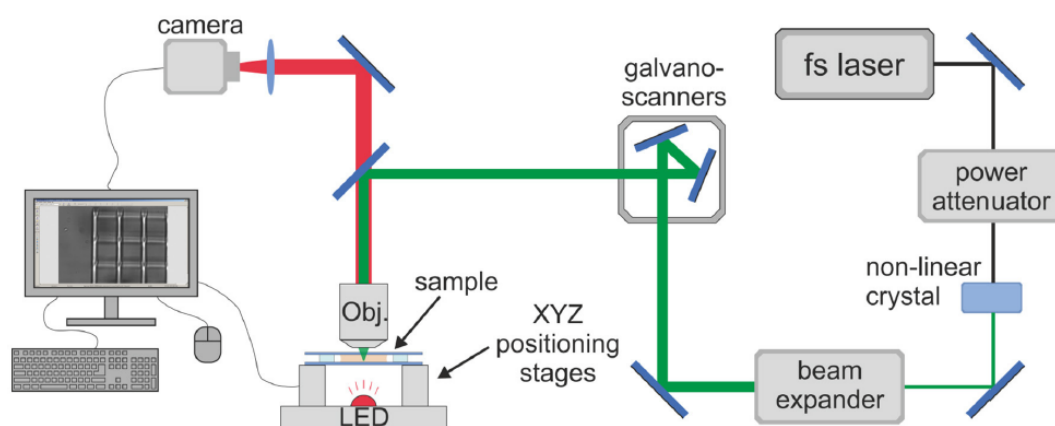


Figure 2.33: Schematic diagram illustrating working principle of 2PP, reproduced with permission from ²⁰³.

2PP may also be referred to as two photon- absorbed photo polymerisation ²⁰⁴, two-photon induced polymerisation ²⁰⁵, two-photon lithography ²⁰⁶, two-photon laser scanning

lithography²⁰⁷, multiphoton-excited microfabrication²⁰⁸, 3-D multiphoton lithography²⁰⁹, 3D laser lithography²¹⁰, or simply direct laser writing²¹¹.

Gittard, *et al.* conducted out an experiment with the aim to reduce the risk of skin infections associated with transdermal drug delivery by introducing antibacterial properties into the microneedle device. PEGDA 600 with a photo-initiator was used to fabricate microneedle arrays containing gentamicin sulphate. This 3D printing technique was good in maintaining uniformity of microneedle arrays. Gentamicin sulphate inhibited the growth of *Staphylococcus aureus* and a 26.8 mm circular zone of inhibition was reported during agar plating assay²¹².

Cell injection therapies often get neglected because of the non-targeted delivery and less control over the delivery site. Micro-transporters that can efficiently collect and deliver the cells to the targeted location were developed using 2PP. Sodium alginate with calcium carbonate nanoparticles suspension was used to encapsulate K562 leukaemia cells which were then loaded into micro-transporters. To evaluate the performance of cell loaded micro-transporters, a microfluidic channel was fabricated. The channel consisted of three branches mimicking the capillary network system. The micro-transporters then released the cells into the main branch from where the cells were navigated into further branches. The rotating frequency of the micro-transporters delivered the cells without forming large clusters²¹³.

2.3.1.2.4. DLP and its applications

SLA and DLP are quite similar techniques that utilise light to cross-link a photo resin in a selective and layer by layer manner and build free-standing object as shown in Figure 2.34²¹⁴. However, DLP is unique from SLA in that DLP each layer is selectively exposed to light all-at-once instead of point-by-point²¹⁵. It is also known as dynamic mask photolithography because it closely resembles classical lithography. Applications of DLP in drug delivery are listed below;

An *in vitro* hepatic model consisting of hexagonal units of liver and supporting cells was developed using a 3D bio printing method. The model can enhance functional and structural characteristics of human induced pluripotent stem cell-derived hepatic progenitor cells (hiPSC-HPCs) thus helping in early drug screening and liver disease studies ultimately approaching personalised medicine. The printed model resulted in functional and phenotypic

improvements of hiPSC-HPCs within weeks during culture assay. In addition, an increase in cytochrome P450 induction, metabolic secretion gene expression level specifically related to liver and better morphological organisation was also reported ²¹⁶.

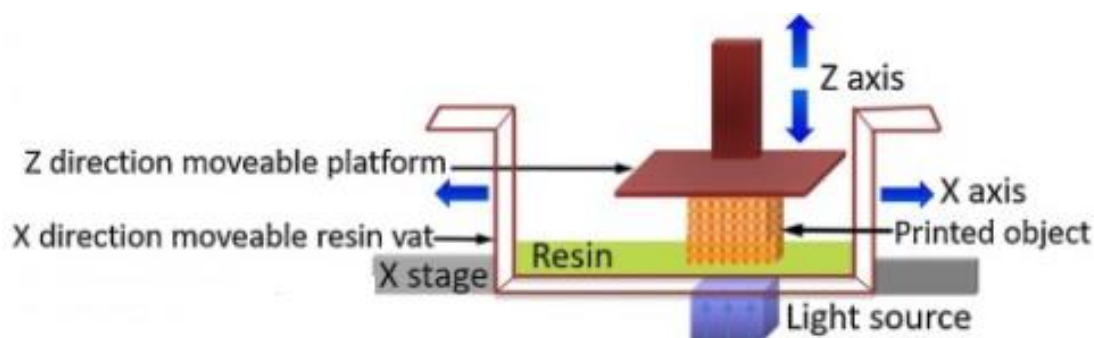


Figure 2.34: Schematic diagram illustrating working principle of DLP, reproduced with permission from ²¹⁴.

Non-dissolvable suppositories were fabricated using silicone elastomers. Four analgesics (ketoprofen, lidocaine HCl, ibuprofen sodium, and diclofenac sodium) at 1%, 5% and 10% drug loading were kneaded into two kinds of silicone polymers, Silastic1 Q7- 4720 and MED-4901. It was found that the mechanical properties of suppositories can be tuned by varying drug-polymer combinations. MED-4091 silicone formulations with 1% and 5% w/w diclofenac sodium turned were revealed to be the optimal formulations with sustained drug release and biocompatibility at cellular level, thus were chosen to fabricate suppositories. In 30 days, 96% cumulative drug release from 1% suppository was observed ²¹⁷.

Oral administration of NSAIDs can cause side effects in people suffering from trigger finger where traditional splints are not useful. To overcome this, microneedle splints were developed for the effective delivery of diclofenac sodium through the wavy surface of the skin of triggered finger. It was reported that printed microneedle splints were biocompatible with human dermal cell lines and 64% penetration efficiency was achieved with human cadaver skin. *In vitro* drug release testing showed higher drug penetration through the skin within a period of 0.5 hours ²¹⁸.

Release rate from the tablets can be tailored by changing the dimensions of the tablet and drug loading. This was achieved by keeping the diameter constant and varying the thickness

(0.75-3 mm) and drug loading (5, 10, 15 and 20%). Tablets with decreased thickness i.e. 0.75 and 1 mm and drug loading up to 15% showed immediate release of the drug. Whereas tablets with increased thickness showed prolonged release of the drug. In conclusion, DLP is an effective printing technique in developing tablets with immediate and prolonged release tablets ²¹⁹.

The above-mentioned studies of vat polymerisation show that the most fabricated type of pharmaceutical dosage form were tablets followed by microneedles patches and scaffolds. This technique is also useful in developing cell laden models, micro transporter, and nanocomposite matrix ophthalmic implants etc. (Figure 2.35). The summarised characteristics of research articles using vat polymerisation techniques are listed in Table 2.10 The table briefly describes the model drug, carrier polymer, plasticiser and results of the studies.

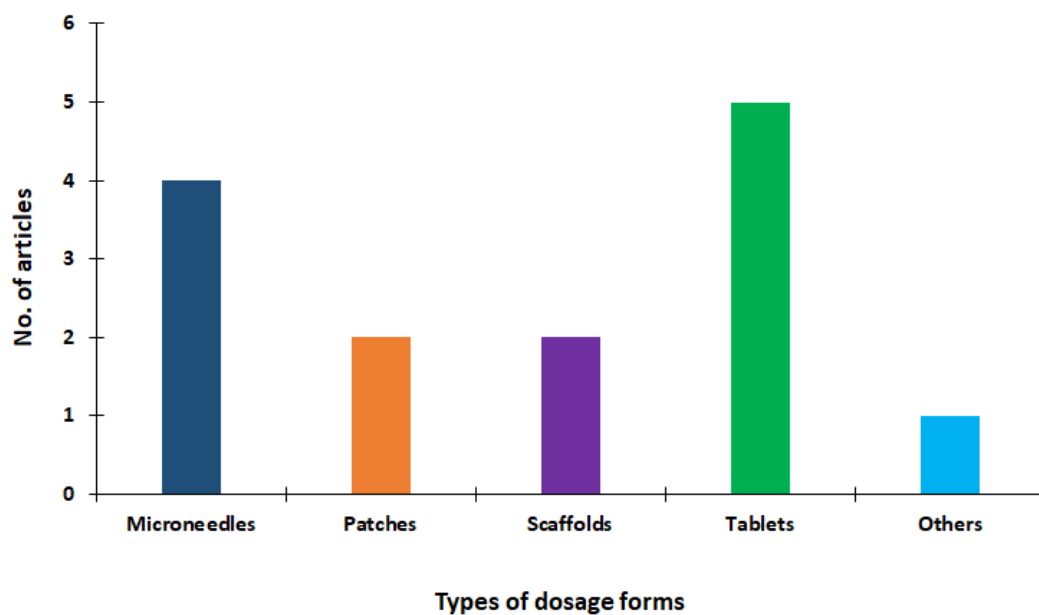


Figure 2.35: Distribution of pharmaceutical dosage forms developed using Vat polymerisation techniques.

(Others include hydrogel, nebulising device, ophthalmic implant, bio printed cell laden model, micro transporter, suppository and nanocomposite matrix)

Table 2.10: Summarised characteristics of eligible studies used vat polymerisation printing techniques for developing medicines.

Active ingredient	Dosage forms	<i>In vitro/In vivo</i>	Carrier materials	Plasticiser	Printing technique	Study characteristics	References
Corticosteroid fluocinolone acetonide	Ophthalmic implant	<i>In vitro</i>	Poly (methyl acrylate-Co-2-Hydroxyethyl acrylate), PDMS	..	SLA	Implantable devices for ocular drug delivery with different microchannel configuration were developed. Channel design of osmotic I and II resulted in optimal drug diffusion rate.	186
Tissue plasminogen activator	Injection	<i>In vitro</i>	..	Resin, light-polymerizable acrylic plastic (VisiJet® Clear,)	SLA	Packages for rapid reconstitution of lyophilised drug were developed. The printed product resulted in increased and effective reconstitution of tissue plasminogen activator.	187
Gentamicin	Nebulising device	<i>In vitro</i>	Non-porous resin, human plastinated cast	..	SLA	A nebulising system of variable frequency for deposition of gentamicin into nasal replica model was developed. Acoustic airflow with variable frequency resulted in deposition of drug into maxillary sinuses of model.	188
4-ASA and paracetamol	Tablets	<i>In vitro</i>	..	PEGDA, PEG 300	SLA	Torus shaped tablets were developed with thermally labile drugs. Printing of tablets occurred without drug degradation. In vitro release profile showed sustained release of drugs. Change in concentration of PEGDA affected the drug release.	189

Paracetamol and aspirin	Tablets	<i>In vitro</i>	PCL triol, Irgacure TPO	PEGDA	SLA	28 dosage forms were printed in one printing process. During a 24-hour drug release studies, both drugs showed sustained release. The dimensions of the printed tablets were significantly different from the targeted which could be attributed to the incorporation of two different drugs.	190
Irbesartan, atenolol, hydrochlorothiazide and amlodipine	Tablets	<i>In vitro</i>	..	PEGDA, PEG 300	SLA	The tablets were successfully printed; however, the study reported the drug-photopolymer reaction between primary amine group of amlodipine and diacrylate group of photocurable resin. It was concluded that photocurable resins should be carefully selected for SLA printing.	191
Salicylic acid	Patch/Mask	<i>In vitro</i>	PCL	PEGDA 700, PEG 300	SLA and FDM	Anti-acne patches were fabricated with FDM and SLA. SLA patches showed accelerated drug release than patches made with FDM.	76
Ibuprofen	Hydrogels	<i>In vitro</i>	..	PEGDA 700, PEG 300	SLA	Hydrogels or controlled release of drug were developed. Water content of hydrogel determined the release rate of drug from hydrogels. Faster release of drug resulted from hydrogels with higher water content.	192

Growth-factor β 1	Scaffolds	<i>In vitro</i>	PLGA	PEGDA	SLA	A porous scaffold loaded with growth factor was developed for osteochondral defects. The resulted scaffold exhibited sustained release of growth factor along with increased cell proliferation and adhesion.	193
Fluorouracil	Nanocomposite matrix	<i>In vitro</i>	HA nanoparticles	PEGDA, PEG	SLA	A nanocomposite matrix for studying breast cancer bone invasion was developed. The resulted model. This model presented increased drug sensitivity of breast cancer cells as compared to 2D cell culture.	194
rhBMP-2	Composite scaffolds	<i>In vitro</i>	PLGA, PPF, Carbonate hydroxyapatite coating	..	SLA	A bio-absorbable porous scaffold for bone regeneration coated with carbonate hydroxyapatite was fabricates. In vitro results showed decrease in cumulative release of rhBMP-2.	195
Silver and zinc oxide	Microneedle array structures	<i>In vitro and ex vivo</i>	Photosensitive acrylate polymer, eShell 200	..	SLA	Microneedle were coated with metals to provide antibacterial activity for wound treatment. The resulted microneedles had effective antibacterial properties against <i>S. epidermidis</i> and aureus.	196

Insulin	Microneedle arrays	<i>In vitro</i>	Class I resin Dental SG, Trehalose, mannitol, Xylitol	..	SLA	Microneedle arrays coated with insulin were developed for transdermal delivery of insulin. Xylitol was the best insulin carrier. <i>In vitro</i> studies resulted in rapid release of insulin from all arrays within 30 minutes.	197
Fluorescein, Rhodamine B (model chemical entities)	Microneedle patches	<i>In vitro and ex vivo</i>	PAA, PCL-tMa	PEGDA	CLIP	Microneedle patches were fabricated for the delivery of therapeutics. Penetration test showed successful penetration of microneedles into murine skin. Microneedles with PCL released 0.5wt% drug whereas PEG based released 5wt%.	198
Bovine serum albumin Ovalbumin, and Lysozyme	Patches	<i>In vitro and in vivo</i>	..	PEG 350	CLIP	Microneedle patches coated with proteins were fabricated. The insertion of microneedles into live mice resulted in sustained release of proteins for over 72 hours.	200
Progesterone, hydrocortisone, dexamethasone-21-Acetate, paclitaxel, bicalutamide, acetaminophen, ibuprofen, acetylsalicylic acid, and salicylic acid	Cylindrical devices	<i>In vitro</i>	PCL	PEGDMA 750, 550, PEGMEMA 500, 360, HEMA, PMA, PEGDME	CLIP	Controlled release drug delivery devices were fabricated using PEG and PCL for the composition of matrix. The device showed controlled and sustained release of drugs during <i>in vitro</i> drug release test.	201
Gentamicin sulphate	Microneedles	<i>In vitro</i>	..	PEGDA 600	TPP	Microneedles with anti-microbial properties were developed. The anti-microbial properties of printed microneedles were confirmed with inhibition of <i>S. aureus</i> during an agar plating assay.	212

K562 leukaemia cells (ATCC)	Micro transporter	<i>In vitro</i>	Sodium alginate ..	TPP	Micro-transporter was developed for the targeted and triggered delivery of cells. The printed device could steer the cells into smaller tubes without forming large clusters.	213
Rifampicin	Hepatic model	<i>In vitro</i>	Gelatine meth acryloyl, Glycidal methacrylate-hyaluronic acid	DLP	In vitro hepatic model consisting of hepatic cells was developed for early drug screening and to study hepatic diseases. The increased cytochrome P450 induction, metabolic secretion and gene expression levels were reported in 3D culture during in vitro testing.	216
Diclofenac sodium, Lidocaine hydrochloride, Ketoprofen	Suppositories	<i>In vitro</i>	Silastic® Q7-4720 and MED-4901 silicone polymers, IPA	SLA/DLP	The mechanical properties of the drug laden silicone elastomers and the rate of drug release from the elastomers can be tuned by varying drug-polymer combinations. The silicone elastomers containing 1% (w/w) and 5% (w/w) diclofenac sodium were the optimal formulations with prolonged drug release and biocompatibility at cellular level.	217
Diclofenac sodium	Microneedle splint	<i>In vitro</i>	3DM-castable resin	DLP	Microneedle array that acts as a splint to immobilise the affected trigger finger and delivers NSAIDs trans dermally. <i>In vitro</i> test showed high drug penetration into human cadaver skin was observed within 0.5 hour.	218

Atomoxetine	Tablets	<i>In vitro</i>	..	PEGDA and PEG 400	DLP	The aim was to develop immediate and prolonged release tablets by varying thickness and drug loading. Tablets with decreased thickness showed immediate release while tablets with increased thickness showed prolonged release of the drug.	219
-------------	---------	-----------------	----	----------------------	-----	--	-----

2.3.1.3. Powder bed fusion

Powder bed fusion (PBF) is one of the first generations of commercialised additive manufacturing processes. PBF utilises thermal energy to fuse certain areas on the powder bed. Briefly, the energy source fuses the powder after each layer feeding, which results in the construction of the 3D structure via layer-by-layer deposition. PBF can further be categorised according to the process used which includes selective laser melting (SLM) and selective laser sintering (SLS), which was the first PBF process developed and commercialised ²²⁰. The differences are their powder fusing mechanisms and material options. SLM fully melts the material and forms a homogeneous part. It is a single material process since the melting points of different materials are not be the same, but alloyed powders can be used. However, for SLS, the laser heats the powder to a point that it can molecularly fuse together at the surface ²²¹.

In this systematic review, we found 23 articles out of 241 that belong to this category of 3D printing. Precisely, 7 articles are of SLS, 15 of powder bed printing and only one belongs to selective laser melting as shown in the Figure 2.36.

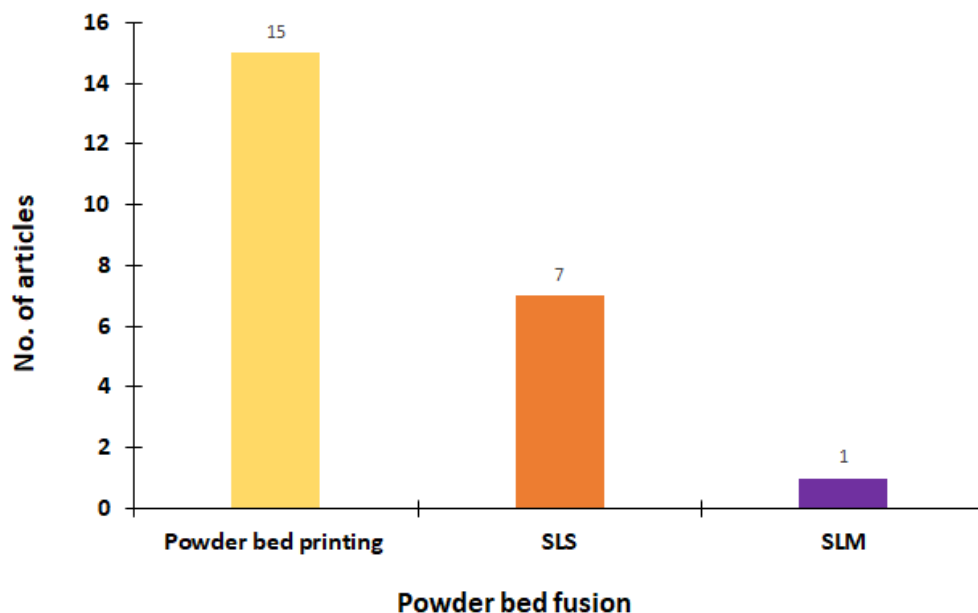


Figure 2.36: Distribution of included studies based on powder bed fusion techniques.

2.3.1.3.1. SLS and its applications

The principle mechanism of SLS is shown in Figure 2.37²²². It involves deposition, solidification of the powder followed by lowering of the build platform by one-layer thickness. These steps are repeated continuously until the final layer is printed. The solidification process is done via using a laser source and the powder deposition is carried out using a roller²²³.

In addition, SLS has several advantages including minimised wastage of material as the unsintered powder remains loose and could be reused and promotes the use of recycling feedstock. These benefits prove the cost-effectiveness of the technology in comparison with other technologies with SLS found to be more economical than SLA, FDM and injection moulding²²⁴.

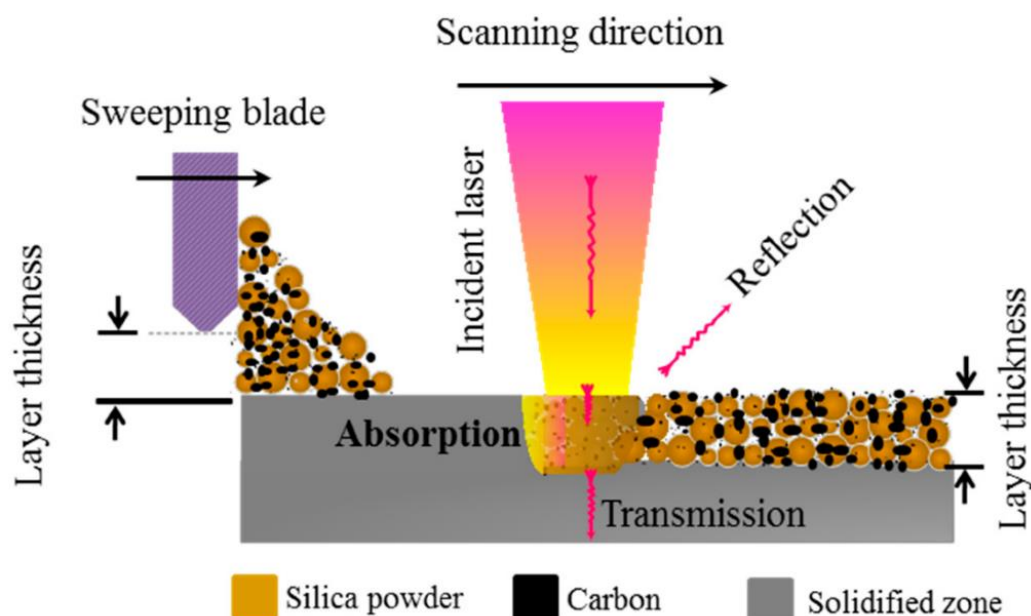


Figure 2.37: Schematic diagram illustrating working principle of SLS, reproduced with permission from²²².

Series of interconnected pores is one of the most important criteria necessary in the macrostructure of drug delivery devices that allows the drug to be embedded before implantation and diffuse into the biological environment once implanted. Digital control of process parameters in rapid prototyping techniques makes manipulation of macrostructure and porosity of drug delivery devices quite easy²²⁵. To investigate the feasibility of SLS,

cylindrical composite structures with an internal network of interconnected pores were developed to be utilised as drug delivery devices. These structures consisted of a porous matrix core and a dense shell and the role of laser power, pore density and interconnectivity in controlling the drug release were investigated. It was observed that the loading of methylene blue dye into the device decreased when the laser power setting was increased. Higher pore densities were observed in the devices printed at 10160 mm/s as compared to the devices printed at 5080 mm/s. In addition, the printing of devices at lower scanning speed resulted in decreased pore density which led to poor pore interconnectivity causing blockage of pathways for diffusion, thus inhibiting the release of methylene blue dye. Moreover, the structure of the dense walls was able to control the release from the device. The selection of optimal parameters of the process can lead to the achievement of desired release rate of drug²²⁶.

SLS was used to fabricate tablets with two polymers Eudragit L100-55 and Kollicoat IR to investigate the immediate and modified release characteristics. The paracetamol release from formulations printed with Kollicoat was not dependent on pH and instead the drug release was dependent on drug content. Conversely, Eudragit formulations showed pH-dependent drug release and was not reliant on drug loading which resulted in the complete release of drug within 12 hours²²⁷.

Cylindrical tablets with enhanced drug release rates were fabricated by using HPMC E5, Kollidon VA 64 and 5% paracetamol (Figure 2.38). The dissolution profile showed that increase in laser scanning speed resulted in accelerated drug release. HPMC formulation printed at a laser speed of 100 mm/s showed complete release of drug after a period of four hours. The HPMC formulations fabricated at 200 and 300 mm/s showed complete drug release in approximately 3 hours and 2 hours, respectively. Tablets containing Kollidon also followed the same pattern²²⁸.

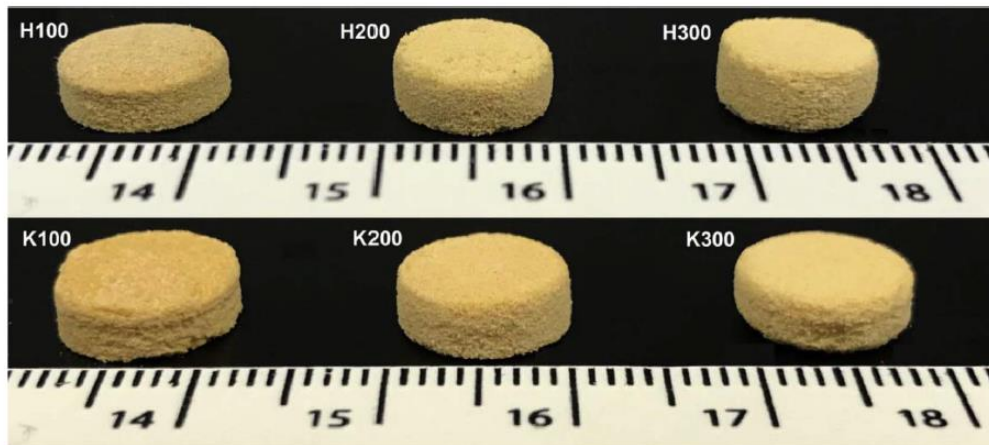


Figure 2.38: Images of HPMC and Kollidon printlets (scale is in cm), reproduced with permission from ²²⁸.

This technique is capable of producing objects with high detailed structures, therefore, 3D gyroid lattice constructs were created using SLS. Cylindrical printlets and gyroid lattices with modified release drug characteristics were developed using four different polymers (PEO, Eudragit L, RL and EC). Each cylindrical printlet and gyroid lattice was composed of 5% paracetamol, 92% polymer and 3% candurin gold sheen. Every formulation exhibited a different drug release behaviour due to the polymer. 60% of the drug was released within the first 2 hours and complete release of the drug occurred in the following next 4 to 5 hours from the cylindrical formulations containing PEO as polymer. Cylindrical formulations containing Eudragit L released only 16% of the drug in acidic pH and rapid release of drug was observed in intestinal pH resulting in complete dissolution in a period of 12 hours. EC cylindrical formulations exhibited only 20% of drug release in a period of 24 hours. 95% of drug was released at a constant rate after an initial burst from cylindrical Eudragit RL formulations. In case of gyroid lattice printlets, PEO exhibited rapid drug release and was dissolved completely within a period of 10 minutes. Eudragit RL formulations showed complete dissolution within 120 minutes. An increase in the surface area resulted in increased dissolution and most of the drug was released in acidic pH from Eudragit L. EC formulations showed four times increased drug release than cylindrical devices ²²⁴.

Miniprintlets of 1- and 2-mm in diameter containing two active ingredients namely paracetamol and ibuprofen were printed with biphasic drug profiles. Kollicoat polymer was

used for immediate release of ibuprofen and ethyl cellulose was used for sustained release of paracetamol. The drug release was reduced with increase in diameter ²²⁹.

To help the visually impaired patients in identifying their medications, orally disintegrated tablets were printed with moon and braille patterns. These patterns did not affect the mechanical and dissolution properties of the tablets, all the tablets were disintegrated within 5 seconds without any water in-take. This approach is useful in reducing medication error and can increase patient adherence ²³⁰.

Like other rapid prototyping technologies, SLS has also been used to fabricate biocomposite scaffolds with a controlled drug release profile. Generally, such kind of delivery systems are loaded with different anti-inflammatory and anti-biotic drugs internally and externally and are used for treating infections such as osteomyelitis and ophthalmic inflammation associated with surgical procedures. Polymethyl methacrylate (PMMA) is a bio-stable polymer and is suitable carrier polymer for local delivery of drugs due to its remarkable compatibility with human tissue and existing use for medical implants.

Ngo, *et al.* developed a biocomposite scaffold for the local delivery of NSAID (flurbiprofen) using PMMA and β -TCP. Carbon dioxide in the super critical state acts as a non-toxic solvent, was used in this study to load the drug in the scaffold. The drug loading increased with an increase in pressure while keeping the temperature constant. Higher temperature also resulted in higher drug loading. The soaking of the scaffold in ethanolic solution resulted in 50% drug release within a period of four hours. The parameters of supercritical carbon dioxide could control the drug release ²³¹.

2.3.1.3.2. Powder bed printing and its applications

Figure 2.39²²¹ shows the schematic diagram of powder bed printing which is very much similar to other techniques. It also has numerous applications in drug delivery which are listed below.

In 1996, a model device was designed to explain control of drug release profiles by controlling microstructure, position and composition using methylene blue and alizarin yellow dyes. The top and bottom of the tabular device were composed of relatively non-resorbable PCL while PEO was used for internal layers. It was reported that the position of the dye in the drug delivery device could control the dye release. In addition, the controlled release of dye could also be achieved by altering the composition of the polymer matrix and the microstructure within the drug delivery device. The resulted device with symmetrical position of dyes had walls of varying thickness while keeping the composition of the wall constant. The resulted device with asymmetrical position of dyes had walls of varying thickness while keeping the composition of the wall constant. This device resulted in immediate release of methylene blue dye while yellow dye was released after lag time of 4 hours²³².

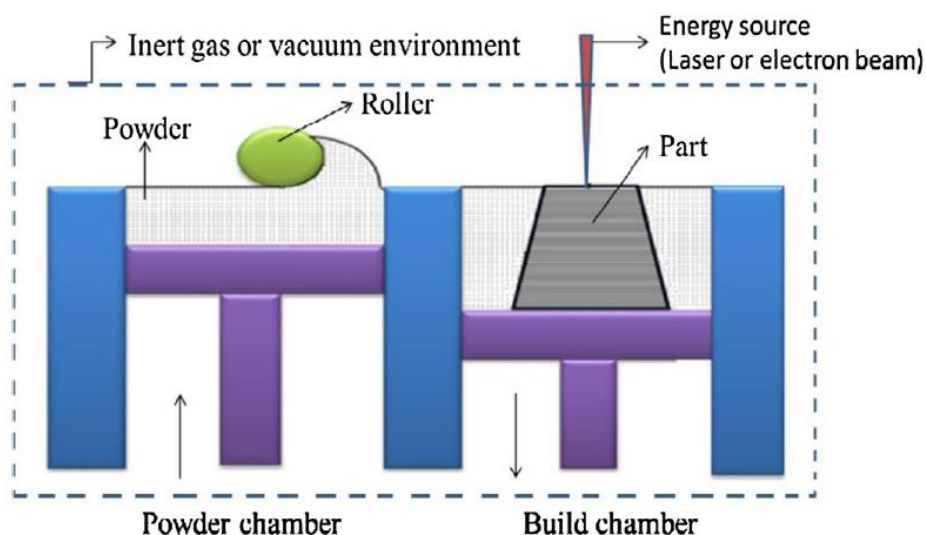


Figure 2.39: Schematic diagram illustrating working principle of powder bed printing. Reproduced with permission from²²¹.

Tablets with complex geometry and varying densities were fabricated. Tablets had two types of drug release mechanisms i.e. erosion and diffusion, chlorpheniramine maleate was used as model drug. To prepare tablets with erosion mediated drug release, 8.9% to 17.9% of polymer content was used. The increase in polymer content resulted in decrease in drug release with the change of lag time between 25 and 50 minutes. Whereas for tablets with diffusion mediated drug release, 9% to 16.7% polymer content was used. The release rate decreased with increase in polymer content. No change in lag time was also reported ²³³.

Four types of tablets with different release patterns were fabricated using Eudragit and Kollidon SR as polymers and chlorpheniramine maleate and diclofenac as model drugs. Immediate-extended release tablets showed pH-dependent drug release, immediate release of chlorpheniramine maleate at acidic pH was observed after 10 minutes followed by extended release of drug within a period of 7 hours. Breakaway tablets were composed of three sections that separates the two drugs. In simulated gastric fluid, separated sections eroded in 35 to 40 minutes. Enteric dual pulsatory tablets contained diclofenac in two separate sections. These tablets showed two pulse release at 1 hour and 8 hours during dissolution testing. Dual pulsatory tablets with two different pH solubility sections showed immediate erosion of one section to release diclofenac within the first 30 minutes and 5 hours later the second section was eroded ²³⁴.

Another study reported the use of Kollidon SR to make the inner core of the tablet with immediate release of the drug surrounded by a drug free HPMC shell. The types of formulations prepared included i.e. 8-hour, 12-hour and 16-hour formulations containing 20/80 ratio of HPMC/Kollidon SR with an aqueous pseudoephedrine hydrochloride binder. The dissolution profiles of all the formulations were in accordance with the desired and targeted release profiles. The release rate was adjusted according to the desired release pattern by altering the ratio of polymers used and printing parameters were kept constant. It was reported that an increase in HPMC content in the polymer blend increased the drug release rate. Formulations with a target of 8 and 12 hours achieved approximately 100% drug release within the targeted time and 16-hour formulations released 75% of the drug in a period of 12 hours following near zero-order release kinetics. Moreover, *in vivo* studies were also carried out in adult human males which revealed that *in vivo* plasma concentration values were in consistent with the *in vitro* data ²³⁵.

Investigation of different release retardation materials like EC, sodium lauryl sulphate, stearic acid and Eudragit RS-100 with acetaminophen as a model drug was carried out by fabricating tablets via powder bed printing. Figure 2.40 shows a schematic diagram of the tablet with material gradient. Drug release kinetics showed that tablets containing EC gradient resulted in linear release of drug via an erosion mechanism in a period of 12 hours. Tablets with other release gradient materials e.g. sodium lauryl sulphate, stearic acid and Eudragit RS-100, also showed 79%, 97% and 97% linear drug release in a period of 5, 10 and 13 hours, respectively

236.

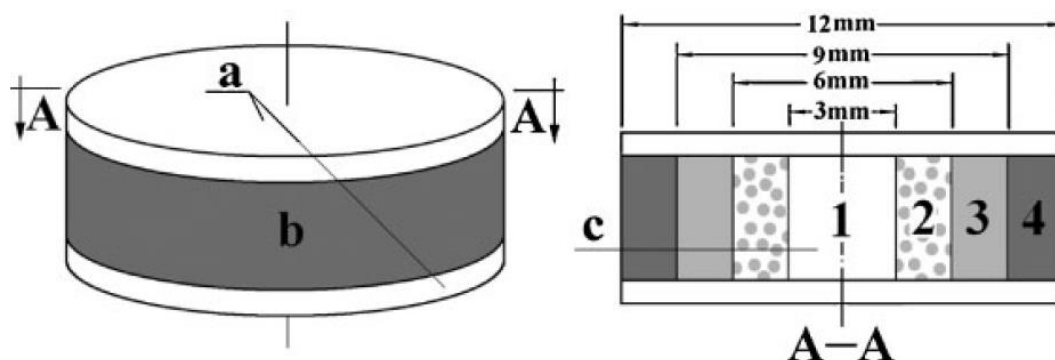


Figure 2.40: Schematic of tablet representing material gradients (a) barrier layer (b) region containing drug (c) retarded release material, reproduced with permission from ²³⁶.

Loose powder of PVP K30 and acetaminophen along with other excipients were used for the fabrication of fast disintegrating tablets via powder bed printing. The schematic diagram of fast disintegrating tablet is shown in Figure 2.41. The average wetting and disintegration time of six printed tablets was 51.7 ± 7.5 seconds and 21.8 ± 5.4 seconds, respectively. All the tablets showed disintegration and wetting times within the acceptable range defined by United States Pharmacopoeia ²³⁷.

Yu, Shen *et al.* also prepared fast disintegrating tablets using PVP K30. The printed tablets showed acceptable pharmacotechnical properties apart from friability. During friability testing, a total mass loss of 3.55% was observed. During *in vitro* testing, the tablets showed rapid disintegration and wetting time and dissolution testing showed complete release (98.5%) of drug within 2 minutes ²³⁸.

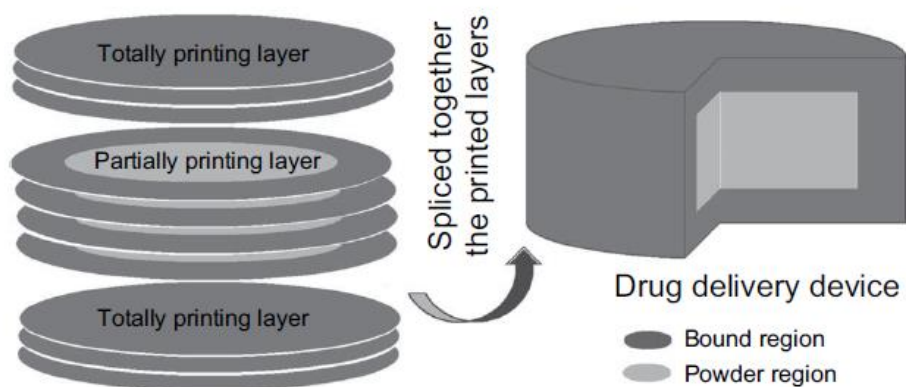


Figure 2.41: Schematic diagram of fast disintegrating tablet, reproduced with permission from ²³⁷.

Different grades of HPC were used as a solid binder in powder bed printing to prepare the formulation with 70% caffeine being used as a model drug. The particle size and viscosity of the polymer affects the friability, disintegration and the dissolution of the tablets. High viscosity HPC resulted in slower disintegration and dissolution whereas faster disintegration and dissolution was observed with low viscosity HPC ²³⁹.

Vinyl polymer, carbohydrate and CaSO₄ were used a carrier powder with 2-pyrrolidone as binder for the ink. Tablets of 10 mm and 13 mm in diameter were printed and coated with drug solution. 13 mm tablets showed better dissolution than 10 mm tablets. All formulations showed sustained release of drug for over 2 hours ²⁴⁰.

Powder bed printing has also shown its potential in fabricating tablets of unusual shapes. Doughnut-shaped drug delivery devices were developed with multiple layers using HPMC and EC and acetaminophen via powder bed printing. All of the tablets resulted in acceptable mechanical and pharmacotechnical properties. Drug release studies showed that all of the drug delivery devices showed linear drug release profiles irrespective of the printing parameters values and no initial burst of drug release was observed. It was also noted that the time required for total drug release decreased as the diameter of the inner hole increased ²⁴¹.

Wu *et al.* also fabricated doughnut-shaped (DST), multilayer doughnut-shaped (MDST) and columnar shaped tablets (CST) using PLLA (Figure 2.42). During *in vitro* testing, the initial burst release of isoniazid was observed and after 30 days, the concentration of isoniazid in all tablets was more than the effective bacteriostatic concentration. The drug concentration of the multilayer doughnut tablet fluctuated from 6th day of release but later on became stable. Drug concentration of doughnut shaped and columnar shaped tablets decreased gradually and the rate of decrease in concentration was faster in DST than CST ²⁴².

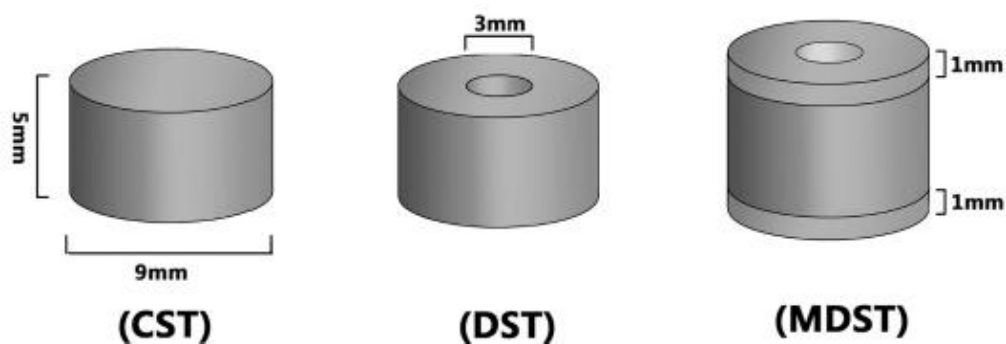


Figure 2.42: Isoniazid-PLLA implant ideograph. CST: columnar shaped tablet, DST: doughnut-shaped tablet, MDST: multilayer doughnut shaped tablet, reproduced with permission from ²⁴².

Implants are a suitable mode for local delivery of antibiotics without increasing serum levels. Gbureck, *et al.* fabricated an implant with multiple antibiotics for the treatment of osteomyelitis. Desorption and adsorption kinetics of antibiotics were studied. Monetite, hydroxyapatite and brushite were used to study the adsorption of tetracycline, ofloxacin and vancomycin. It was reported that there was a non-linear relationship between the amount of drug adsorbed and the immersion time, whereas a linear relationship was observed between the adsorption of drugs and the drug concentration. During *in vitro* dissolution testing, ofloxacin and vancomycin showed rapid release into PBS solution within a period of 1 to 2 days, whereas tetracycline showed a slow release with 25% release after 5 days. Moreover, an increase in polymer content resulted in delayed drug release ²⁴³.

Implants with complex geometry and loaded with isoniazid and rifampicin were fabricated via powder bed printing for the treatment of bone tuberculosis. *In vitro* and *in vivo* (rabbits)

results were correlated with each other. Both studies showed controlled release behaviour of both drugs. Drugs were positioned in an order of isoniazid-rifampicin-isoniazid-rifampicin and both studies showed ordered release of drugs as they were sequenced ²⁴⁴.

A multilayer implant loaded with levofloxacin and tobramycin was fabricated for the treatment of chronic osteomyelitis. *In vitro* studies showed sequenced release of drugs as they were positioned in the device i.e. tobramycin-levofloxacin-tobramycin-levofloxacin. *In vivo* studies were carried out in rabbits in which no reoccurrence of osteomyelitis was observed after giving treatment with the printed scaffolds for 2 months ²⁴⁵.

Excellent bioactivity of calcium phosphates and compositional similarities to bone mineral are the reasons for their wide use and preferred choice for hard tissues, such as teeth or bone repair, replacement, regeneration, or augmentation. Sustained and controlled release of drugs or osteogenic factors from scaffolds are required over a desired period of time for an effectual treatment. However, to avoid the initial burst release from scaffolds composed of TCP and alendronate as a model drug, coating of PCL on TCP-scaffolds was investigated. TCP fabricated scaffolds were then sintered at 1250 °C in a conventional muffle furnace for 2 hours. PCL coating resulted in controlled release of alendronate, whereas the scaffolds without the coating of PCL showed burst release of alendronate. Moreover, the PCL coating also protected the structural integrity of the scaffolds from the harsh environment. Histomorphology showed bone formation after 6 weeks in rats during *in vivo* studies ²⁴⁶.

2.3.1.3.3. SLM and its application

The SLM process, illustrated in Figure 2.43 ²⁴⁷, involves a layer with 30-100 mm in thickness and 20-45 mm in diameter, of spherical metal powder that is uniformly spread over a metal platform and a laser beam scan across it. The laser beam melts the powder and fuses with layer beneath it followed by descending of the platform and the process is repeated until the part is printed ²⁴⁸. The application of SLM in drug delivery is as follows.

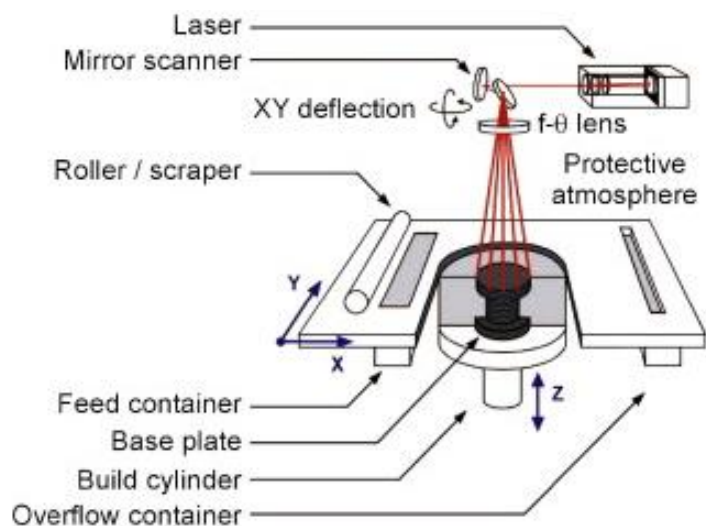


Figure 2.43: Schematic diagram illustrating working principle of selective laser melting. Reproduced with permission from ²⁴⁷.

Titanium (Ti) possesses excellent bio integration with human osteoblasts and is therefore the most preferred and commonly used material for implant fabrication and is also corrosion resistant. Unfortunately, these implants face many challenges for longevity and integration when inserted in the human body, especially in the case of bone carcinoma. To improve the process of osseointegration, manipulation of the surface topography of an implant is an effective way which may be achieved with the use of nanotubes that allows fabrication of implants with desired topography. Maher, *et al.* used titanium alloy to fabricate implants for the local delivery of anti-cancer drugs - doxorubicin hydrochloride and tumour necrosis factor related apoptosis-inducing ligand (Apo2L/TRAIL) - to increase the implant's capability of releasing drug and to reduce severe adverse effects caused which can be caused by the systemic administration of these drugs. At first, titanium wafers were printed on a 3D-SLM machine in the shape of square of strips ($1.5 \times 1.5 \text{ cm}^2$). An electrochemical cell with controlled temperature was used to carry out electrochemical anodization of 3D printed Ti-implants to create surface Titania nanotubes. For loading of two anti-cancer drugs (doxorubicin and Apo2L/TRAIL), drug solutions were placed on the surface of Ti-implants with Titania tubes separately and allowed to dry at room temperature under vacuum for 2 hours. The implants showed two-phase drug release behaviour, an initial burst release for the first few hours (% cumulative release of doxorubicin and Apo2L/TRAIL after 6 hours was 40% and 70%, respectively) followed by slow release of doxorubicin for 16 days and 4 days for Apo2L/TRAIL. The growth of fibroblasts was also studied on Ti-implants with Titania tubes to

confirm that these implants will allow cell proliferation and adhesion. Examination via light microscope revealed no sign of cell death, confirming the compatibility of implants. When doxorubicin-loaded implants were incubated with luciferase-expressing cells for 24 hours, the cells viability was reduced to $16.4 \pm 2\%$, indicating ample drug release for anticancer therapy.

On the other hand, cell viability was considerably lower than all implants containing Apo2L/TRAIL which demonstrates the effective release of Apo2L/TRAIL and also shows that the presence of fibroblasts did not prevent the drug release. In conclusion, this method proves that Titania nanotubes 3D-Ti implants have a potential to be utilised as a device together for bone fracture support and localised drug properties ²⁴⁹.

These research studies depicted that powder bed fusion is mostly used to fabricate tablets followed by implants, scaffolds and others (resorbable devices, gyroid lattices, cylindrical disc matrices, and shell core structure) (Figure 2.44). The summarised characteristics of research studies using powder bed fusion techniques are listed in the Table 2.11. The table briefly describes the model drug, carrier polymer, plasticiser and results of the studies.

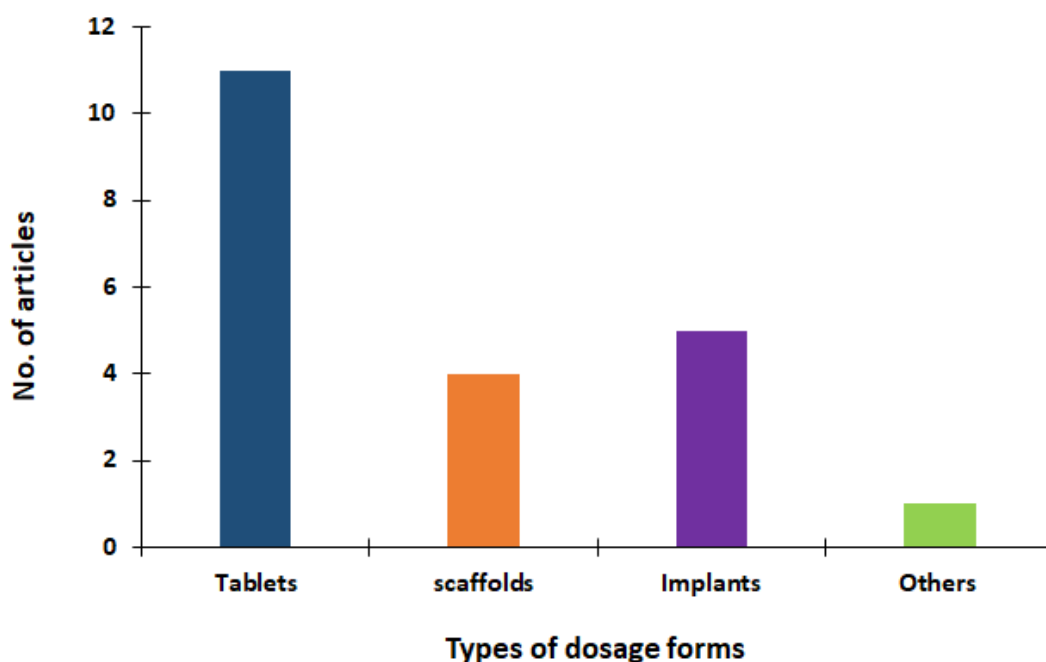


Figure 2.44: Bar chart representing the distribution of pharmaceutical dosage forms developed using powder bed fusion techniques. (*others include resorbable devices, gyroid lattices, cylindrical disc matrices, and shell core structure*).

Table 2.11: Summarised characteristics of eligible studies used powder bed fusion printing techniques for developing medicines.

Active ingredient	Dosage forms	<i>In vitro/In vivo</i>	Carrier materials	Plasticiser	Printing technique	Study characteristics	References
Methylene blue dye	Shell core structure	<i>In vitro</i>	PA	..	SLS	Controlled release delivery devices were fabricated. It was reported that dense wall, laser power and interconnectivity can alter the drug release according to the requirement.	226
Paracetamol	Tablets	<i>In vitro</i>	Kollocoat IR Eudragit®L100	..	SLS	The effect of two polymers on drug release was investigated. Tablets with Kollocoat showed pH-independent release whereas tablets with Eudragit showed pH dependent release.	227
Paracetamol	Tablets	<i>In vitro</i>	HPMC, Kollidon® VA 64	..	SLS	Tablets with enhanced drug release were fabricated. It was reported that drug release increased with increase in laser scanning speed for both polymers.	228
Paracetamol	Gyroid lattices	<i>In vitro</i>	Eudragit® L 100-55, Eudragit® RL, EC, PEO	..	SLS	Gyroid lattices with modulate drug release characteristics were fabricated using four different polymers. Each polymer exhibited different drug release pattern during in vitro dissolution behaviour.	224

Paracetamol and ibuprofen	Tablets	In vitro	EC, Kollicoat instant release	-	SLS	Miniprintlets of 1- and 2-mm diameter containing two active ingredients were printed with biphasic drug profiles. Kollicoat polymer was used for immediate release of ibuprofen and ethyl cellulose was used for sustained release of paracetamol. The drug release was reduced with increase in diameter.	229
Paracetamol	Tablets	<i>In vitro</i>	Kollidon VA64, Candurin® Gold Sheen	..	SLS	To help the visually impaired patients in identifying their medications, orally disintegrated tablets were printed with moon and braille patterns. These patterns did not affect the mechanical and dissolution properties of the tablets, all the tablets were disintegrated within 5 seconds without any water in-take. This approach is useful in reducing medication error and can increase patient adherence.	230
Flurbiprofen	Scaffold	<i>In vitro</i>	PMMA, TCP	..	SLS	Scaffold for the local delivery of drug was fabricated. In vitro test showed that 50% of drug was released into ethanolic solution from the scaffold.	231

Methylene blue and alizarin yellow	Resorbable devices	<i>In vitro</i>	PCL, PEO	..	PBP	Controlled release drug delivery devices were fabricated. It was reported that composition polymer matrix, thickness of walls and position of dye in the device can control the release of dye.	232
Chlorpheniramine maleate and fluorescein disodium salt	Tablets	<i>In vitro</i>	Eudragit® E-100, Eudragit RLPO	..	PBP	Tablets with two types of release mechanism were fabricated. For erosion and diffusion mediated tablets the drug release rate decreased with increase in polymer content.	233
Chlorpheniramine maleate and Diclofenac	Tablets	<i>In vitro</i>	Eudragit (L, E, RL, L 100), Kollidon SR	..	PBP	Four types of tablets breakaway tablets, immediate-extended release tablets, enteric dual pulsatory and dual pulsatory tablets were fabricated. Each type of tablet exhibited different release pattern.	234

Pseudoephedrine hydrochloride	Cubes	<i>In vitro and in vivo</i>	Kollidon SR, HPMC	TEC	PBP	Three types of tablets 8, 12- and 16-hours formulations were fabricated to achieve drug release in a desired period. The tablets showed drug release profile within the target time.	235
Acetaminophen	Tablets	<i>In vitro</i>	Eudragit RS-100, HPMC, EC, PVP	Stearic acid	PBP	Different retardation materials were investigated by fabricating tablets. Dissolution profile showed linear release from EC tablets in 12 hours.	236
Acetaminophen	Tablets	<i>In vitro</i>	PVP K30, PVP	..	PBP	Fast disintegrating tablets were fabricated using loose powders. The resulted tablets showed disintegration time of 21.8 ± 5.4 seconds.	237
Acetaminophen	Tablets	<i>In vitro</i>	PVP K 30	..	PBP	Fast disintegrating tablets were prepared. The tablets showed complete drug release within 2 minutes during dissolution test.	238

Caffeine	Tablets	<i>In vitro</i>	HPC	-	PBP	The particle size and viscosity of the polymer affects the friability, disintegration and the dissolution of the tablets. High viscosity HPC resulted in slower disintegration and dissolution whereas faster disintegration and dissolution was observed with low viscosity HPC.	239
5-fluorouracil	Tablets	<i>In vitro</i>	CasO ₄ powder, Soluplus	..	PBP	Printed tablets of 10 mm and 13 mm in diameter were coated with drug solution. 13 mm tablets showed better dissolution than 10 mm tablets. All formulations showed sustained release of drug for over 2 hours.	240
Acetaminophen	Tablets	<i>In vitro</i>	HPMC, EC, PVP K30	..	PBP	Doughnut-shaped tablets were fabricated. It was reported that total drug release time was decreased with increase in the diameter of the inner hole.	241
Isoniazid	Implants	<i>In vitro</i>	PLLA	..	PBP	Columnar, doughnut and multilayer doughnut shaped tablets were fabricated. All types of tablets showed bacteriostatic effect.	242

Vancomycin hydrochloride, Ofloxacin, Tetracycline hydrochloride	Multi-drug implants	<i>In vitro</i>	Polylactide-polyglycolide	..	PBP	Implants loaded with multiple drugs were fabricated for the treatment of osteomyelitis. Slow release of tetracycline while rapid release of ofloxacin and vancomycin was reported.	243
Isoniazid and rifampicin	Implants	<i>In vitro and in vivo</i>	PDLLA	..	PBP	Drugs were placed in a sequence in the implant. <i>In vitro</i> and <i>in vivo</i> studies showed same results i.e. controlled and sequenced release of drugs as they were positioned.	244
Levofloxacin and Tobramycin	Implants	<i>In vitro and in vivo</i>	PDLLA	..	PBP	A multi-layer drug implant was fabricated. The resulted implant showed sustained, sequenced and controlled released of drugs.	245
Alendronate	Scaffolds	<i>In vitro and in vivo</i>	PCL, TCP	..	PBP	To evaluate the effect of AD release behaviour through PCL coating on bone formation using PCL-coated 3D printed interconnected porous tricalcium phosphate (TCP) scaffolds.	246

Doxorubicin hydrochloride and Tumour necrosis factor related apoptosis-inducing ligand (Apo2L/TRAIL)	Implants	<i>In vitro</i>	Titanium alloy powder material (Ti6Al4V)	EG	SLM	Titanium implants for local delivery of anti-cancer drug were fabricated. The drug release exhibited two-phase behaviour showing a burst release within the first few hours (% cumulative release of doxorubicin and Apo2L/TRAIL after 6 h was 40% and 70%, respectively) and slow release phase of 16 days (doxorubicin) to 4 days (Apo2L/TRAIL).	249
--	----------	-----------------	--	----	-----	--	-----

2.3.1.4. Jetting techniques

These techniques involve pushing of material or binder liquid through a nozzle and deposition onto a substrate. It also allows printing of different materials on the same subject by using multiple print heads¹⁵. This 3D printing technique includes the following techniques: (a) inkjet printing, (b) drop on demand printing, (c) material and binder jetting and (d) electro hydrodynamic e-jetting.

34 research articles belong to this category of 3D printing technique among 241 articles. In all jetting techniques, ink jet printing is the most commonly used technique in fabricating drug delivery devices followed by drop on demand, E-jetting and material and binding jetting (Figure 2.45).

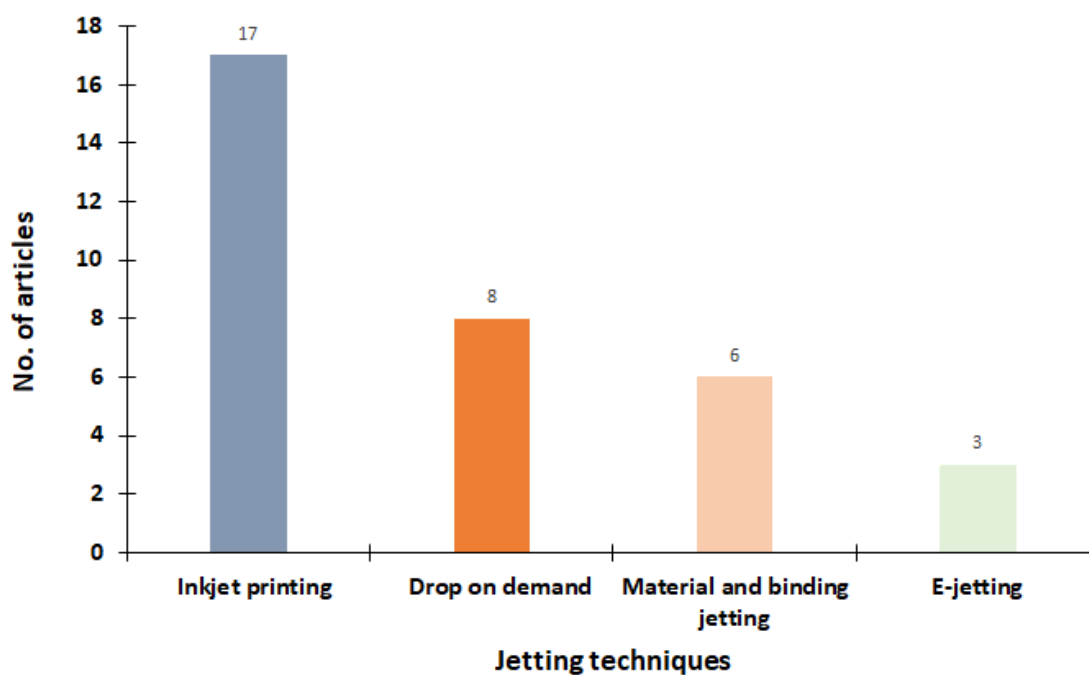


Figure 2.45: Distribution of included studies based on jetting techniques.

2.3.1.4.1. Inkjet printing and its applications

Inkjet printing is one of the most commonly used techniques and involves heating of liquid ink, a droplet of ink is then propelled out of the printing head using microscopic orifice ²⁵⁰. A schematic diagram of the working principle of the inkjet technique is illustrated in Figure 2.46 ²⁵¹. It is possible to build three-dimensional multi-material or multi-colour structures by using more than two print heads ¹⁴. Several applications of inkjet printing in drug delivery are detailed below.

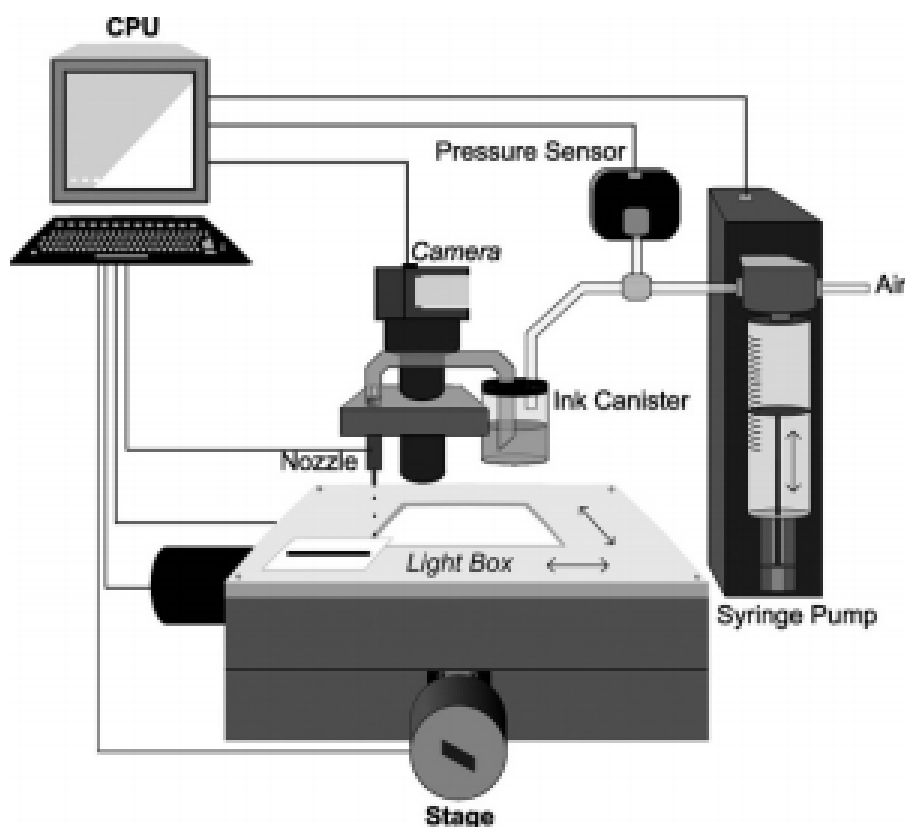


Figure 2.46: Schematic diagram illustrating working principle of inkjet printing, reproduced with permission from ²⁵¹.

Drug-loaded implants are an effective means of local delivery of drugs and certainly have advantages over systemic circulation. Sustained release of drug from implants when implanted near or in the target organ provide relatively high therapeutic efficacy and low systemic toxicity; however, implants with detailed microstructure and complex release profiles are difficult to fabricate with conventional methods. Therefore, inkjet printing was used to develop three types of implants containing levofloxacin which were named implant I, implant II and implant III. Implant I consisted of a homogeneous mixture of levofloxacin and PLA. Implant II was of capsule shape with an inner core that contained levofloxacin surrounded by PLA. Implant III was composed of two regions, upper and lower. Upper region encapsulated homogeneous mixture of levofloxacin and PLA and served as a reservoir system whereas, lower region was a matrix system composed of PLA which was loaded with levofloxacin. *In vitro* monitoring of the drug release profiles of these implants were carried out for 100 days and showed that implant II exhibited a higher daily dose than implant I excluding the initial burst release, and a maximum concentration of levofloxacin 11 µg/ml was achieved by implant II on the 20th day. Implant III showed a pulse release rate which started from day 5 followed by a steady release rate for next 25 days. Another pulse release from implant III was seen at day 50, which ended on the 80th day. In conclusion, the implants fabricated by the printing process showed a pulsed release profile which is more sophisticated as compared to implants prepared by conventional compression process ²⁵².

Likewise, an implant prototype containing rifampicin and levofloxacin was developed for bone infections and to carry out *in vivo* studies. The implant consisted of two regions; upper and lower. Both regions were composed of PLA; however, the upper region acted as a reservoir system containing rifampicin, whereas the lower region contained levofloxacin. *In vivo* studies revealed that levofloxacin started to release in the beginning and attained maximum concentration on day one. Conversely, rifampicin did not release in the beginning and was detected on 8th day. However, continuous release of both drugs was observed for more than 6 weeks and a higher concentration of levofloxacin and rifampicin was observed in muscle and bone than in artery blood ²⁵³.

To facilitate the drug release from the implant, tricalcium phosphate was mixed with HPMC or polymer solution of chitosan and was printed directly onto the tricalcium phosphate for

fabrication of a bioceramic implant used for the treatment of irregular bone defects. Diffusion of drug solution within the structure was reduced by modifying the polymer and it was found that the polymer modification with HPMC or chitosan hydrochloride affected the drug release kinetics and resulted in retardation of drug release rate from first order to zero order within a period of 3 to 4 days. The range of drug release rate was 0.68% to 0.96%, whereas the biological activity of rhBMP-2, vancomycin and heparin were between 1% and 18% and was reduced after spraying through nozzle of inkjet. Moreover, for vancomycin a further reduction of 11% was also observed ²⁵⁴.

Micro patterns of calcium-eluting and antibiotics on the surface of orthopaedic implants were introduced to improve cell growth and to prevent formation of biofilm colonies. Rifampicin was dissolved in PLGA with biphasic calcium phosphate solution. Nanoparticles of biphasic calcium phosphate solution were dispersed into PLGA matrix co-precipitated by PLGA and rifampicin. *In vitro* testing revealed that micro patterns greatly affected the release of rifampicin from the implant and the total release of rifampicin was observed within a period of one day. Implants were also effective against *Staphylococcus epidermidis*, thus preventing the formation of biofilm colonies ²⁵⁵.

Planchette, *et al.* used two inkjet technologies, piezoelectric- and solenoid valve-based inkjet printing to print medicines. For this purpose, three different solutions of PEG, sodium picosulphate and polymeric-nanosuspension consisting of PLGA nanoparticles treated with PEG were printed onto films of medical grade. Deviation $< \pm 2\%$ was observed when optimised printing parameters were used for dispensing of sodium picosulphate. A smooth surface texture was observed when films were printed with porous and hydrophilic substrates with deviation less than 12 μm , whereas cap-shaped-hemispherical dots were observed with non-porous and hydrophobic substrates due to decreased absorption and spreading. Therefore, PEG based hydrophilic coating solutions were used for homogeneous spreading and absorption of APIs onto substrates ²⁵⁶.

The combination of inkjet printing technique with direct compression method was illustrated to prepare dosage-controlled tablets. In this study, a 5.7 mg dose of ropinirole HCL containing bio ink was dispensed into blank tablets prepared by direct compression. *In vitro* release kinetics showed that within a period of 15 minutes, 60% of the drug was released from tablets and 80% of drug release was achieved within a period of 30 minutes. The high permeability

of drug loaded bio ink lead to immediate release kinetics suitable for achieving therapeutic effects instantly ²⁵⁷.

To investigate the effect of geometry on drug release and the capability of inkjet printing in developing tablets with complex geometry, tablets with a honeycomb architecture were designed and printed to modify the drug release without changing the composition. Fenofibrate was dissolved in beeswax to print the tablets with honeycomb architecture and tablets were successfully prepared. Traditional cylindrical tablets were also prepared for comparison purposes. *In vitro* drug release testing showed a higher drug release rate for the honeycomb tablets as compared to cylindrical tablets. Honeycomb tablets with 0.61 mm cell diameter showed optimum drug release profile, concluding that geometry has the potential of adjusting the drug release rate ²⁵⁸.

Solid dispersion tablets of various geometries including mesh, ring, thin film and cylinders were printed using PEGDA, Irgacure 2959 and N-vinyl-2-pyrrolidone matrix and carvedilol as model drug. All the printed devices released 80% of the drug within 10 hours. Comparatively, fastest release was observed from thin film followed by ring, mesh and slowest release was observed from cylinders ²⁵⁹.

Thermal inkjet printing has proven to be beneficial in studying the polymorphic nature of prednisolone. The prednisolone was mixed with ethanol and glycerol and dispensed onto glass films coated with poly (tetrafluoroethylene). Raman analysis of these drug deposited films confirmed the presence of two polymorphs and it was concluded that the combination of thermal system with such kind of dispensing solution was the main reason for the formation of two polymorphs of prednisolone ²⁶⁰.

The feasibility of typical desktop thermal ink-jetting printer was characterised by dosing an aqueous drug solution onto a pharmaceutical substrate to develop oral films. For this purpose, a film of potato starch was used as a substrate on which salbutamol sulphate was printed to produce an oral film. It was reported that the viscosity of the drug solution affected the deposition of drug on the substrate. Deposition of the drug was minimised when the viscosity was more than $2 \text{ mm}^2\text{s}^{-1}$ and the optimal range of viscosity was found to be between 1.1 and $1.5 \text{ mm}^2\text{s}^{-1}$. Dissolution testing showed that the gelation time of films without drug was $10.4 \pm 1.0/\text{s}$ and for drug loaded films it was $9.6 \pm 0.5/\text{s}$ ²⁶¹.

Bioadhesive films containing anti-viral (cidofovir) and anti-cancer (paclitaxel) drugs were developed for the localised treatment of cervical cancer. Being a poorly soluble drug, a powder was prepared by incorporating paclitaxel into cyclodextrin inclusion complex. On the other hand, cidofovir was loaded into PCL nanoparticles using w/o/w emulsion technique. These ink formulations were then printed on HPC films and the dissolution profile of the printed films showed that 60% of paclitaxel was released within first 2 hours followed by complete release of drug within 8 hours for cidofovir, 50% was released in the first hour and complete release of cidofovir took 16 hours. *In vitro* cell culture studies showed that HPC films loaded with drugs were effective on human cervical adenocarcinoma cells ²⁶².

The potential of porous substrates to incorporate API was investigated using inkjet printing. Three different APIs solution (acetaminophen, theophylline and caffeine) were printed onto porous substrates (coated paper, uncoated paper and polyethylene terephthalate (PET) films). Square arrays of 10 x 10 mm² were printed by printing an array of 2 x 10 squares of each drug substance (paracetamol, caffeine, and theophylline) on the substrates. Light microscopy showed crystals of active substances when printed on PET substrate. The penetration of all drugs was seen on coated and uncoated paper substrates however, caffeine showed partial crystallisation on coated paper substrate. Scanning probe microscope (SPM) topographical images of substrates with inkjet printing of drugs are shown in Figure 2.47. The visual analysis of these films was confirmed with time-of-flight secondary ion mass spectroscopy reporting penetration of all drugs onto porous paper substrate. The content of theophylline was approximately 78 µg per printed area, whereas paracetamol content on paper substrate was 68 µg per printed area. The caffeine content on coated paper and PET was approximately 270 µg per printed area. Furthermore, no degradation of drugs was reported ²⁶³.

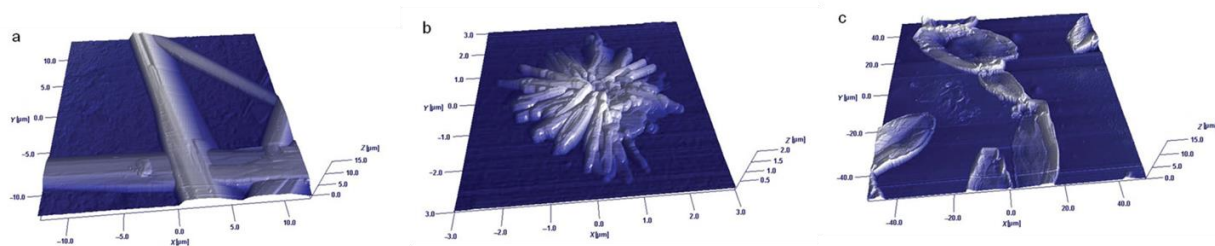


Figure 2.47: SPM topographical images of inkjet-printed substances (a) caffeine printed on coated paper, (b) theophylline printed on Mica, and (c) paracetamol printed on PET, reproduced with permission from ²⁶³.

Similarly, three different paper substrates were examined to tailor the drug release of two model drugs, propranolol hydrochloride and riboflavin sodium phosphate. These drugs were dispensed onto 1 cm x 1 cm areas of three substrates; substrate A: uncoated paper, substrate B: triple coated paper and substrate C: double coated paper. Ethyl cellulose was coated on the printed drugs with the help of flexographic printing and human cell line assay showed that substrates were non-toxic. Substrate B and C showed alike properties i.e. smoothest surface and less pores, whereas substrate A had totally different properties. The films with substrate B showed the slowest drug release rates followed by films with substrate C and the fastest drug release was observed with films of substrate A. Moreover, upon increasing the polymer content, the release rate decreased ²⁶⁴.

To minimise multiple and frequent administration of drugs, a novel drug dosage form, a microdot formulation, consisting of micron sized dried deposits from sprayed picoliter droplets containing a drug on a substrate was designed. The objective of this study was to print designed ratios of drugs and excipients as individual microdots onto a suitable substrate, each capable of the controlled release of the active from that deposit. Towards this objective, microdot formulations containing felodipine were developed to control the drug release rate. Felodipine and PVP were mixed in ethanol containing dimethyl sulfoxide to increase the boiling point of the solution and this mixture was then dispensed on hydrophobic substrate, glass cover slips through piezo inkjet printer in picoliter quantities. Raman microscopy confirmed the homogeneous distribution of drug in the dispensed drops. Dissolution studies revealed that drug release was dependent on drug loading and it was demonstrated that

excess loading of 33% drug by weight reduced the drug release, thus concluding that drug release could be altered by adjusting the drug loading ²⁶⁵.

To address the solubility issue of paclitaxel, PLGA micro particles loaded with paclitaxel were developed to improve drug release rate. Micro particles of different shapes, including honeycomb, grids, circles and rings, were fabricated and the printed micro particles were of homogeneous size and shape. The drug release profile showed burst release of drug in the beginning followed by slow release. It was concluded that the geometry affected the release rate and the descending release rate order was honeycomb > ring, grid > circle ²⁶⁶.

The drug-eluting stents reducing the incidence of restenosis from 20 to 30%. Inkjet printing has proven to be effective in coating the medical devices such as stent, in a reproducible and controlled manner. A stent was coated with a solution of phosphorylcholine-linked methacrylate tetra copolymer at first and then was coated with drugs via reagent jetting. These stents were then compared with conventional stents coated by spray atomisation. Total drug (rapamycin derivative, ABT-578) release from stents loaded with jetting technique was 90%, whereas from the stent with spray atomisation, total drug release was 100%. Moreover, drug stability was not compromised during the jetting process ²⁶⁷.

3D liver tissue model can provide great insight for high-throughput drug evaluations. For this purpose, hepatocytes and endothelial cells were integrated onto a chip. These cells account for more than 80% of the liver's mass. Layer-by-layer printing and single-cell printing of fibronectin-gelatin solutions were used for the fabrication of human tissue consisting of 440 microarrays containing multiple layers and cell types on one chip. To evaluate the drug metabolism activity, troglitazone, an anti-diabetic agent, was used. Cell death was observed which was dependent on dose, even at a low concentration there was extensive cell death. In conclusion, these 3D human micro-tissue chips could be successful in drug screenings ²⁶⁸.

2.3.1.4.2. Drop on demand printing and its applications

Drop on demand printing is like the ink jet printing. The difference is that in drop on demand printing there is piezoelectric actuator or nozzle controller to control the ink drops as shown in Figure 2.48 ²⁶⁹. This printing technique has been used for the development of personalised medicine as it allows accurate manufacturing of micro doses of potent drugs and dosage flexibility.

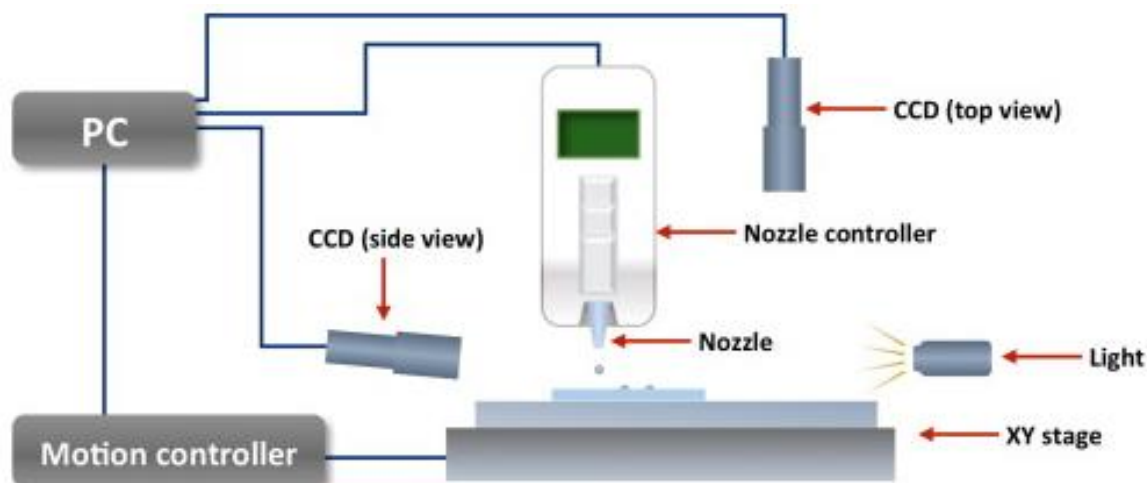


Figure 2.48: Schematic diagram illustrating working principle of drop on demand printing. Reproduced with permission from ²⁶⁹.

In a study by Rajada *et al.*, flexographic and drop on demand printing were successfully used for the development of printable dosage forms. Printable dosage forms of piroxicam, which is a drug with poor aqueous solubility and a slow dissolution rate, were printed onto edible paper substrates to study the dissolution behaviour. The dosage forms printed from both techniques resulted in 90% drug release in simulated gastric fluid in 5 minutes. The faster release was due to the fact that drug was in solution form which resulted in immediate release upon contact with dissolution media. Under ambient conditions, 20-25 °C and 30–40% relative humidity, the dosage forms were physically and chemically stable ²⁷⁰.

Dropwise additive manufacturing of pharmaceutical products (DAMPP) allows precise control of final product properties by manipulating the printing formulation including solid-state form of drug. Reproducible dosage forms were developed to evaluate the feasibility of DAMPP system. Two different formulations containing different ratio of drug and excipient were developed:

- i- Amorphous formulation, 30:70 (Naproxen: PVP) 0.3 g of naproxen and 0.7 g of PVP K90 dissolved in 10 mL of ethanol.
- ii- Semi-crystalline formulation, 70:30 (Naproxen: PVP), contained 0.7 g of naproxen and 0.3 g of PVP K90 dissolved in 10 mL of ethanol.

It was reported that change in drug polymer content and drop size can result in amorphous form of active pharmaceutical dosage form. For the amorphous forms, apparent crystallinity was always 0% because of the polymer inhibiting drug crystallization. For the semi crystalline formulations, it was found that the smallest drop size led to a dosage form that was approximately 33% crystalline, whereas the largest drop size led to a dosage form that was approximately 77% crystalline. Drug release equilibrium was achieved in 90 minutes during dissolution testing ²⁷¹.

Solid dispersions containing naproxen as a model drug were printed. These dispersions were coated with PEG of different molecular weights. It was reported that coating of PEG protected the solid dispersions from moisture-accelerated crystallisation. Moreover, the coating had the ability to prevent water permeation into the inner structure of the samples. It was observed that this ability of coating was increased with the use of high molecular weight PEG ²⁷².

The feasibility of drop on demand printing was also investigated for the coating of anticancer drugs 5-fluorouracil, cisplatin and curcumin on laser cut microneedle arrays for transdermal delivery. Different ratios of drug carriers, sodium fluorescein and Soluplus, were examined to optimise the drug release. MTT (micro culture tetrazolium) assay of drug coated microneedle arrays on human skin epidermoid carcinoma cells showed that increase in anti-proliferative activity was dependent on dose. Franz diffusion cell analysis was carried on porcine skin of two different thickness 750 μm and 900 μm to determine the drug release rates. Rapid release rates of sodium fluorescein of 65% and 45% for microneedles with 1:1 and 1:2 ratio of sodium fluorescein and Soluplus, respectively, were observed after one hour and 5-fluorouracil showed similar patterns as sodium fluorescein. Slower release rates of 5-fluorouracil were observed with skin of 900 μm thickness. Overall, both sodium fluorescein and 5-fluorouracil showed deep skin penetrations. All formulations containing different ratios of curcumin and Soluplus showed rapid release rates exhibiting 56% to 96% release within a period of one hour. Cisplatin also showed rapid dissolution rate, whereas increase in Soluplus resulted in slower release rates ²⁷³.

Printable inks of indomethacin were formulated to print the solution onto a paper substrate and on an impermeable transparent film to improve dissolution rate of indomethacin. 1x1

cm² squares of drug ink were printed on selected substrates and an increased dissolution rate was obtained for all formulations. Co-amorphous forms of indomethacin and arginine were observed when printed on transparent film ²⁷⁴.

Drug delivery of poorly soluble drugs has always been a serious issue. Nanoparticles have gained much importance to improve the delivery of drugs with poor solubility. Mesoporous silica nanoparticles suspensions functionalised with polyethyleneimine were developed for the delivery of furosemide and propylene glycol was added to increase the viscosity of the ink. These nanoparticles were loaded with 1%, 5% and 15% of furosemide and HPMC films were used as hydrophilic printing substrates. It was reported that all the ink formulations were electrostatically stable. Multiple light scattering showed that transmittance increased for nanoparticles suspension containing 1 mg/ml of furosemide, whereas transmittance decreased with 5 mg/ml nanoparticles suspension. Moreover, it was also noticed that net surface charge decreased with increased drug loading and no drug leakage was observed ²⁷⁵.

A self-emulsifying drug delivery system has been reported for the delivery of a poorly water-soluble drug, celecoxib. The dosage form contained 10% celecoxib and 90% glaucire. Raman analysis and XRD confirmed the absence of crystallinity of celecoxib in printed dosage forms. Drug release kinetics showed 70% dissolution of dosage forms within a period of 10 minutes and it was indicated that when the dosage form reached the limit of crystalline solubility of celecoxib, further increase in testing time had no effect on the release profile. It was concluded that self-emulsifying dosage forms are suitable for achieving rapid dissolution of poorly water-soluble drugs ²⁷⁶.

The use of drop on demand printing has also been reported to fabricate tablets to achieve personalised dosing of ropinirole HCL, a drug used in the treatment of Parkinson's disease. 0.5% Irgacure 2959 photo initiator was used with 2% wt. ropinirole HCL for ink formulation. UV curing was also applied to solidify the material. Dissolution testing revealed that 60% of the drug was released in first hour whereas 89% of drug was released with a period of 4 hours ²⁷⁷.

2.3.1.4.3. Material and binder jetting and its applications

Material jetting (Figure 2.49 ²²¹) involves pushing of binder liquid through tiny nozzles at high speed and deposit them onto a substrate in accordance with the CAD model. The jetting is controlled by piezoelectric or thermal jetting ²⁷⁸.

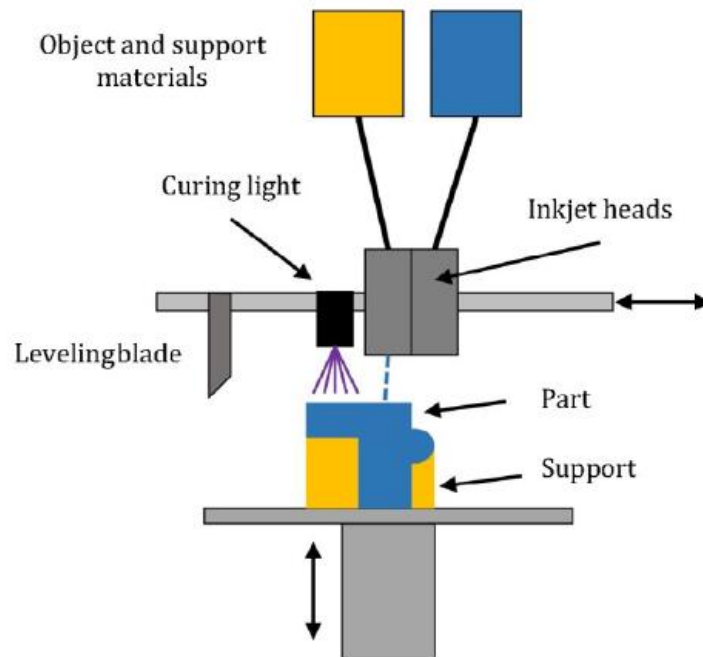


Figure 2.49: Schematic diagram illustrating working principle of material jetting, reproduced with permission from ²²¹.

Binder jetting (Figure 2.50 ²⁷⁹) involves jetting of binding liquid onto a bed of powder. It is also the only additive manufacturing technology that has been used in an FDA approved drug product, Spritam^{®278}.

3D printed fluidic device was developed to investigate the effect of drug on cells. The device contains 8 parallel channels, 3 mm wide by 1.5 mm deep, connected to a syringe pump through standard, threaded fittings. It was observed that 18-21% of drugs were able to migrate through porous membrane when levofloxacin and linezolid were introduced into the device to pump through the channels and it was dependent on drug concentration.

Endothelial cell line was cultured onto membrane inserts composed of porous polycarbonate and Hanks' Balanced Salt Solution (HBSS) or saponin (a detergent used to compromise cell membranes) was used to carry out the cell viability assay. Endothelial cells treated with saponin showed increase in fluorescence intensity as compared to cells treated with HBSS. It can be used for in vitro drug evaluations by using drug at desired concentrations ²⁸⁰.

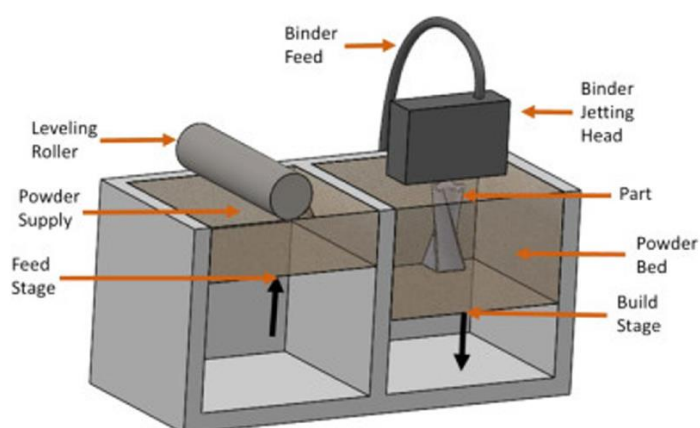


Figure 2.50: Schematic diagram illustrating working principle of binder jetting. Reproduced with permission from ²⁷⁹.

Sustained release tablets of theophylline and metoprolol tartrate were developed using HPMC and binding liquid composed of glycerine, ethanol, water and acetone. Dissolution test showed that for theophylline tablets, 97.63% of the drug was released in 24 hours ²⁸¹.

The effect of different liquid binders such as methyl cellulose, HPC, water HPMC, Kollidon VA64, PEG and HY122 (spectrum chemical) on the breaking force was measured. It was reported that the tablets produced with Kollidon VA64 were of higher breaking force as compared to others liquid binders. 5% indomethacin with 10% Kollidon VA64 was added to lactose monohydrate and along with water as binding agent to prepare tablets. The resulted tablets disintegrate within 5 seconds ²⁸².

The local delivery of antibiotic is important to achieve high doses, however, poly (methyl methacrylate) PMMA is not suitable for local delivery of rifampicin in treating chronic bone infections as it interferes with PMMA polymerisation. To overcome the problems associated with poly (methyl methacrylate), calcium phosphate scaffolds (CPS) loaded with vancomycin

and rifampicin were developed for the treatment of osteomyelitis. The antibiotics retained their efficacy after mixing with calcium phosphate powder and had no effect on the mechanical properties of the scaffolds. CPS constructs were more effective in reducing the bacterial growth in comparison to PMMA constructs ²⁸³.

Xi, *et al.* developed a nasal airway cast model to determine *in vitro* drug deposition using material jetting printing technique. This cast model was used to test commercially available nasal sprays and nebulisers including apotex, nasonex, miaoling and astelin. Deposition pattern and quantification of these sprays in the nose is shown in Figure 2.51 ²⁸⁴. It was reported that only a few droplets (< 4.6%) from the nasal spray deposited in the olfactory region while majority of the droplets resided in the anterior nose. On the other hand, unique deposition patterns were observed with nebulisers as most of the droplets deposited beyond the nasal valve. Moreover, administration via point release resulted in 9% deposition of drugs in the olfactory region, whereas use of Pari Sinus resulted in 15.7% administration of drug in the upper nose ²⁸⁴.

Lind, *et al.* used material jetting for developing a micro physiological cardiovascular device seeded with cardiomyocytes to imitate the structure of the heart, for the purposes of reading electronic signals continuously produced by contractile stress of multiple laminar cardiac micro tissues and to study drug responses using verapamil, isoproterenol. The device consisted of tissue-guiding layer, multilayer cantilevers and strain sensor. It was reported that the device was able to track temporary development in tissue mechanics enabling researchers get an insight into the phenomenon of pathogenesis and morphogenesis and provided a non-invasive read out of contractile stress signals. Moreover, the device showed positive chronotropic and negative inotropic response to isoproterenol and verapamil, respectively, during drug-response studies ²⁸⁵.

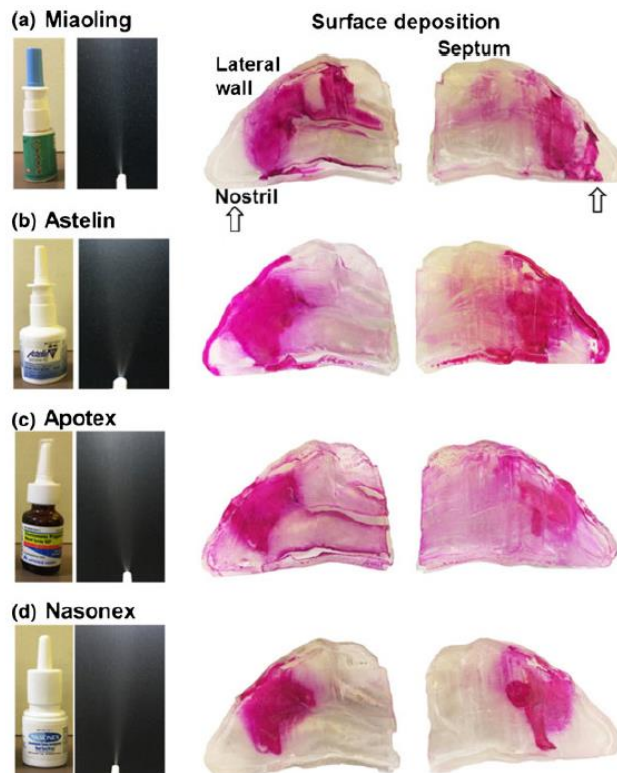


Figure 2.51: Deposition and quantification of four nasal sprays in the nose, reproduced with permission from ²⁸⁴.

2.3.1.4.4. E-jetting and its applications

In electro hydrodynamic printing technique, the ink is deposited onto the substrate via fluid flow created by using the electric fields ²⁸⁶. The main elements for E-jet printing are given in (Figure 2.52 ²⁸⁶). The applied voltage potential, offset height and the pressure applied to the nozzle are used to control the printing conditions and changes in these parameters affect the frequency and size of the droplets ²⁸⁷.

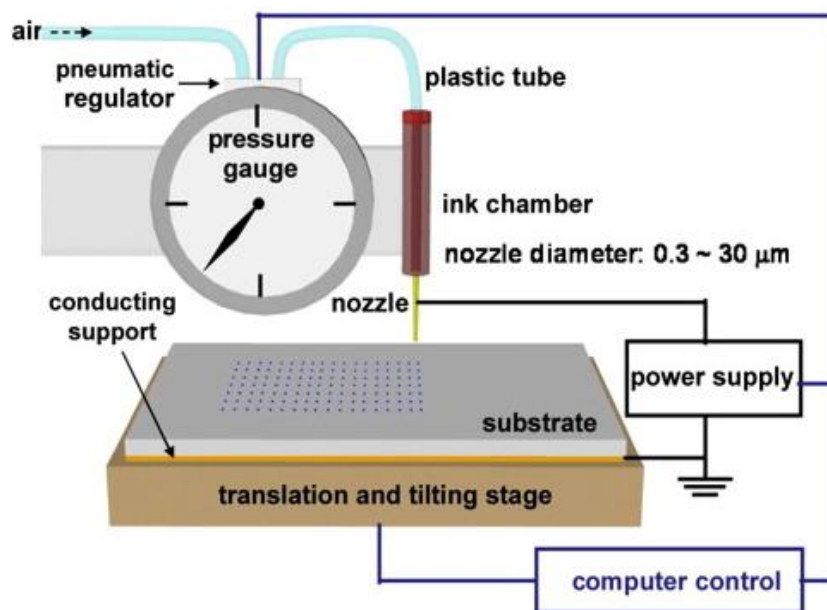


Figure 2.52: Schematic diagram illustrating working principle of E-jet printing technique. Reproduced with permission from ²⁸⁶.

Cancer is a major cause of death among humans. Among various treatments, magnetic hyperthermia therapy is an effective treatment due to its mild side effects. Nano-science has brought a revolution to this field with the advent of nanoparticles and magnetic nanoparticles which have been used effectively in cancer therapy. Towards this objective, magnetic heating mats with controllable shapes were printed using Fe_3O_4 starch nanoparticles using E-jet printing and these mats were capable of inducing hyperthermia. Under magnetic field, mats with 6 mmol/L, 0.07 g of Fe_3O_4 nanoparticles increased the temperature to 45°C within a period of 45 minutes. These mats were implanted in mice with tumours to carry out *in vivo* studies. These studies indicated that the mats were capable of inhibiting the growth of tumour and resulted in long term survival of mice bearing tumour after 4 weeks of treatment ²⁸⁸.

Benefited from the three-dimensionality, the 3D printing significantly improves the specific surface area of the membrane which can increase the contact area between the mats and the cancer cells and improves the effect of magnetic hyperthermia.

A range of multi-layered patches loaded with antibiotic were developed using E-jet printing. Patches of different polymer composition were prepared using PCL and PVP as carrier polymers and tetracycline hydrochloride as a model drug (Pure PCL, PCL-tetracycline-HCL, PCL/PVP and PCL-PVP-tetracycline-HCL). Drug release from the patches made with PCL, $12.5 \pm 2.8\%$ was released in 1 hour, was slow in comparison to PCL-PVP system, $25.3 \pm 1.8\%$ drug release ²⁸⁹.

E-jetting and electrospinning techniques were used to fabricate mechanically and biologically improved constructs for sustained drug delivery applications through a layer-by-layer materials approach. Multi-layered and well-aligned PCL fibres were used as the construct base (mechanically enforcing) and electro spun PVP membranes provided an overcoat layer. Classical burst release of Tetracycline-HCl was observed from constructs, which could be tailored through PCL foundation geometry. Furthermore, two-tier drug release was achieved based on PCL foundation (sustained) and PVP coating membrane (rapid). For the sustained release, auxiliary magnetic field trigger provided a route to increase antibiotic release. All constructs exhibited antibacterial activity and good cell biocompatibility. The findings indicated potential value for hybrid engineering and novel multi-stage therapies ²⁹⁰.

Figure 2.53 shows that the type of pharmaceutical dosage form mostly developed by jetting the techniques are tablets, films and implants. The summarised characteristics of research articles using jetting techniques are listed in Table 2.12. The table briefly describes the model drug, carrier polymer, plasticiser and results of the studies.

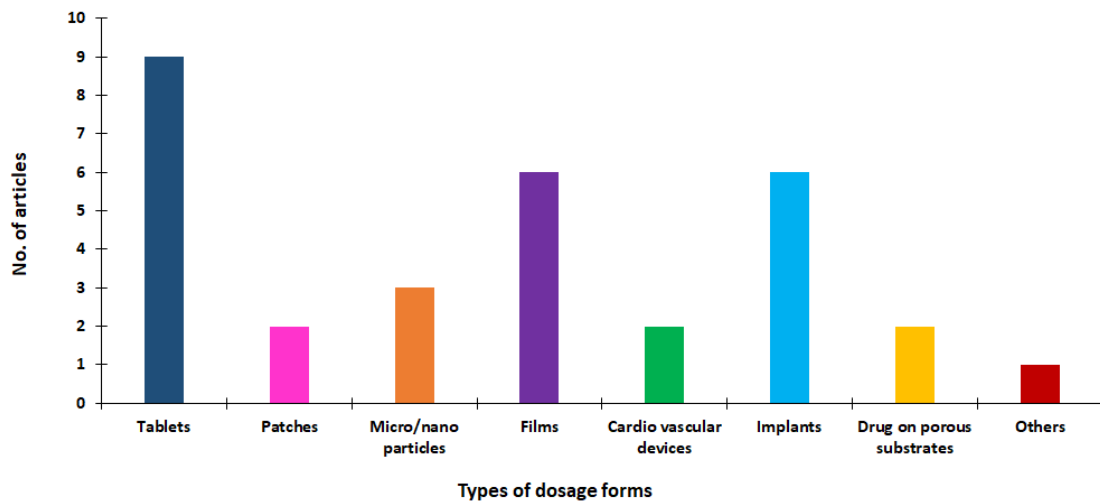


Figure 2.53: Bar chart representing the distribution of pharmaceutical dosage forms developed using Jetting techniques.

(Others include nose model, fluidic device, mats, fibre, hydrogel and bio printed cell laden model).

Table 2.12: Summarised characteristics of eligible studies used jetting printing techniques for developing medicines.

Active ingredient	Dosage forms	<i>In vitro/In vivo</i>	Carrier materials	Plasticiser	Printing technique	Study characteristics	References
Levofloxacin	Implants	<i>In vitro</i>	PLLA	..	Inkjet printing	Implants with different inner structures were printed. Implants containing two regions upper and lower showed pulse release of drug at 5 th day. Another pulse release was observed at day 50 th which ended at day 80 th .	252
Levofloxacin and Rifampicin	Implants	<i>In vivo</i>	PLLA	..	Inkjet printing	<i>In vivo</i> studies were carried out of implant containing rifampicin in the upper region and levofloxacin in lower region. In the beginning levofloxacin started to release and rifampicin started to release on 8 th day of study. Both drugs were released continuously for more than 6 weeks.	253
rhBMP-2, Heparin, Vancomycin	Implants	<i>In vitro</i>	HPMC, Chitosan hydrochloride, TCP	..	Inkjet printing	Bioceramic implants were fabricated by modifying the polymer. Modification of tricalcium phosphate with HPMC or chitosan hydrochloride resulted in reduction of diffusion of drug within the structure.	254

Rifampicin	Micro patterns for implants	<i>In vitro</i>	PLGA	..	Inkjet printing	Implants with micropatterns of antibiotics were introduced to prevent the formation of biofilm colonies. The micropatterns greatly affected the release properties of drug and were effective against <i>S.epidermidis</i> .	255
Sodium picosulphate	Orodispersible dosage forms	<i>In vitro</i>	PLGA	PEG 3000, 6000	Inkjet printing	Different solutions were prepared and dispensed onto hydrophilic and hydrophobic substrates. Smooth consistent surface texture was observed by printing on hydrophilic substrates whereas cap-shaped dots were observed with hydrophobic substrates.	256
Ropinirole HCL	Tablets	<i>In vitro</i>	HLA	PEGDT 1500, PEG 200	Inkjet printing	Drug loaded bioink was dispensed on directly compressed tablets. The dissolution test showed that the tablets exhibited immediate release profile.	257
Fenofibrate	Tablets	<i>In vitro</i>	White beeswax	..	Inkjet printing	Tablets with honeycomb structure were fabricated to modify the drug release and were compared with cylindrical tablets. Honeycomb tablets had higher drug release rates as compared to cylindrical tablets.	258

Carvedilol	Tablets	<i>In vitro</i>	Irgacure 2959, N-vinyl-2-pyrrolidone	PEGDA	Inkjet printing	Solid dispersion tablets of various geometries including mesh, ring, thin film and cylinders were printed. All the printed devices released 80% of the drug within 10 hours. Comparatively, fastest release was observed from thin film followed by ring, mesh and slowest release was observed from cylinders.	259
Prednisolone	Tablet	<i>In vitro</i>	HPMC, Pullulan, Poly(tetrafluoroethylene)	..	Inkjet printing	Polymorphic nature of prednisolone was studied using inkjet printing technique. The combination of dispensing solution and thermal system was responsible for the generation of two polymorphs.	260
Salbutamol sulphate	Films	<i>In vitro</i>	Glycerine	..	Inkjet printing	Oral films were developed for immediate use using potato starch as a substrate on which drug solution was deposited. There was no significant difference between gelation time of plain and drug loaded films showing that deposition of drug did not affect the mechanical properties of starch films.	261
Paclitaxel and Cidofovir	Bio adhesive films	<i>In vitro</i>	HPC	PEG-PCL	Inkjet printing	HPC films loaded with drugs were fabricated for the localised treatment of cervical cancer. The printed films were effective against human adenocarcinoma cells during in vitro cell culture studies.	262
Acetaminophen, caffeine, theophylline	Pharmaceutical dosage forms on porous substrates	<i>In vitro</i>	PG, PET	..	Inkjet printing	APIs were printed onto paper, coated paper and PET substrates. All drugs were penetrated onto porous paper substrates whereas crystals of APIs were observed on other substrates.	263

Propranolol hydrochloride and Riboflavin sodium phosphate	Films	<i>In vitro</i>	EC, PG, Glycerol	..	Combined inkjet printing with flexographic printing	Drugs were printed onto different substrates to tailor the drug release. Every substrate showed different release pattern.	264
Felodipine	Micro spots	<i>In vitro</i>	PVP K30	..	Inkjet printing	Microdot formulations on a hydrophobic substrate were developed to control the release of drug. Dissolution rate reduced with higher drug loadings thus drug release rate could be altered by adjusting the drug loading.	265
Paclitaxel	Intricate micro particles	<i>In vitro</i>	PLGA	..	Inkjet printing	Microparticles loaded with drug and of different shapes e.g. honeycomb, circle, grind and ring. Dissolution test showed that geometry of the particles affected the drug release rate.	266
Fenofibrate, Rapamycin derivative, ABT-578.	Stent	<i>In vitro</i>	Phosphorylcholin e-linked methacrylate tetra copolymer	..	Inkjet printing	Drug eluting stent was coated with drug solution using jetting technique. Total drug release from jetted stent was 90% and drug stability was not compromised.	267
Troglitazone	Bio printed cell laden model	<i>In vitro</i>	Fibronectin, Gelatine	..	Inkjet printing	Dose-dependent cell death was observed, and especially the three layered-multilayers clearly showed extensive cell death, even at a low concentration, as compared to the one and two layered.	268

Piroxicam	Printed dosage forms/films	<i>In vitro</i>	Edible paper substrate	PEG 400, PG	DoD printing	Printable dosage forms of piroxicam were printed onto edible paper substrates to study the dissolution behaviour. The printed dosage forms resulted in 90% drug release in simulated gastric fluid in 5 minutes.	270
Naproxen	Films	<i>In vitro</i>	HPMC, PVP	..	DoD printing	Formulations based on solvents were prepared using DoD printing. Drug release from printed dosage form reached equilibrium in 90 minutes.	271
Naproxen	Tablets	<i>In vitro</i>	..	PEG 3350, 2000, 3350, 6000, 8000	DoD printing	Solid dispersions with coating of PEG were prepared. The coating prevented the solid dispersions from moisture-accelerated crystallisation. Coating with high molecular weight PEG increased the capability of coating to prevent the permeation of water into inner structure of solid dispersions.	272
5-fluorouracil, Curcumin, Cis-platin,	Microneedles	<i>In vitro and ex vivo</i>	Soluplus®	..	DoD printing	Laser cut metal microneedles were coated with anticancer drugs for transdermal delivery. Different ratios of soluplus were examined. MTT assay showed that antiproliferative activity was dependent on dose.	273

Indomethacin	Transparent films	In vitro	PVP, Arginine	..	DoD printing	1x1 cm ² of drug ink were printed onto a paper substrate and an impermeable transparent film to improve dissolution rate. Increased dissolution rate was obtained for all formulations.	274
Furosemide	Films	<i>In vitro</i>	PG	..	DoD printing	Mesoporous silica nanoparticles suspensions were printed on HPMC films for the delivery of poorly soluble drug. All the formulations were electrostatically stable. The colloidal stability of suspension was decreased with increased drug loading.	275
Celecoxib	Tablets and films	<i>In vitro</i>	HPMC, Compritol 888ATO, Precirol ATO 5, Gelucire 44/14, Labrasol	..	DoD printing	Self-emulsifying dosage forms were developed for the delivery of poorly water-soluble drugs. The printed dosage form showed 70% of dissolution dosage form indicating that self-emulsifying dosage forms are suitable for rapid dissolution rate of poorly water-soluble drugs.	276
Ropinirole HCL	Tablets	<i>In vitro</i>	..	PEGDA 700	DoD printing	Tablets were fabricated to achieve personalised dosing of drug. In vitro test revealed that the 89% of drug was released within 4 hours.	277

Levofloxacin, Linezolid	Fluidic device	<i>In vitro</i>	Objet Vero White Plus Proprietary resin	..	MJ	3D printed fluidic device was developed to study the drug effect on cells. 18-21% of drug migrated through porous membrane when introduced to the device.	280
Theophylline, metoprolol tartrate	Tablets	<i>In vitro</i>	HPMC, PVP K30, HPC, Croscarmellose sodium, glycerine, ethanol, water, acetone	..	BJ	Sustained release tablets of theophylline and metoprolol tartrate were developed using HPMC and binding liquid composed of glycerine, ethanol, water and acetone. Dissolution test showed that for theophylline tablets, 97.63% of the drug was released in 24 hours.	281
Indomethacin	Tablets	<i>In vitro</i>	HPC, Kollidon VA64, HPMC, Lactose monohydrate, calcium sulphate hemihydrate	PEG 3350	BJ	The effect of different liquid binders on the breaking force was measured. It was reported that the tablets produced with Kollidon VA64 were of higher breaking force as compared to others liquid binders. 5% indomethacin with 10% Kollidon VA64 was added to lactose monohydrate and along with water as binding agent to prepare tablets. The resulted tablets disintegrate within 5 seconds.	282
Rifampicin and Vancomycin	Implants	<i>In vitro and in vivo</i>	PMMA, PLGA, TCP	..	BJ	Calcium phosphate scaffolds loaded with antibiotics were developed for the treatment of osteomyelitis. All the scaffolds reduced the bacterial infection during in vivo studies.	283

Nasal sprays: Apotex, Astelin, Miaoling, and Nasonex	Nose models	<i>In vitro</i>	PP	..	MJ	Nasal airway cast model was developed for in vitro evaluation of drug deposition. Different commercially available sprays were tested. 9% of drugs were administered to the olfactory region with point release administration.	284
Verapamil, Isoproterenol	Cardiovascular device	<i>In vitro</i>	Dextran, PDMS, PLA	PEGDA, PEG, PU, ABS	MJ	A cardiovascular device was developed to read out the electric signals produced by contractile stress of tissues and to study drug response. Device showed positive chronotropic response for isoproterenol and negative ionotropic response to verapamil.	285
Fe ₃ O ₄	Mats	<i>In vitro and in vivo</i>	Polycaprolactone, Starch	..	E-jetting	Magneto caloric mats containing nanoparticles of Fe ₃ O ₄ were developed for the treatment of cancer using thermal therapy. Mats increased the temperature to 45 ^o C within 45 minutes.	288
Tetracycline hydrochloride	Patch	<i>In vitro</i>	PVP, PCL	..	E-jetting	Patches prepared using PVP and TE-HCL displayed enhanced hydrophobicity. Release of antibiotic from PCL-PVP dosage forms was shown over 5 days and was slower compared to pure PCL or PVP. The printed patch void size also influenced antibiotic release behaviour.	289

Tetracycline hydrochloride	Constructs	<i>In vitro</i>	PVP, PCL	..	E-jetting	Classical burst release of TE-HCl was observed from constructs, which could be tailored through PCL foundation geometry. Furthermore, two-tier drug release was achieved based on PCL foundation (sustained) and PVP coating membrane (rapid). For the sustained release, AMF trigger provided a route to expedite antibiotic release.	290
----------------------------	------------	-----------------	----------	----	-----------	--	-----

2.4. Advantages and limitations of 3D printing technologies

Researchers have drawn great attention to the use of 3D printing technologies for the fabrication of drug delivery devices because of the advantages it provides. Digital control of the technologies has provided control over drug dose, size and shape and has made formation of complex geometries, deposition of drug on various substrates, fabrication of personalised dosage strength and on-demand fabrication of tablets or capsules much easier and simpler^{234, 291-293}. These advantages (Table 2.13) not only overcome the limitations imposed by conventional manufacturing systems but also has enabled 3D printing to excel exceedingly in the area of development of personalised drug delivery devices and to create awareness about “one size does not fit all” as only limited and predefined strength doses are available to such a diverse population. Moreover, the research has proven that for certain situations, customised or personalised treatment regimens are necessary for improved patient’s adherence. For instance, in cases where complicated treatment regimens comprising high frequency doses and polypharmacy are prescribed e.g. to the patients suffering from chronic illness disease, personalised drug dosage forms play an important and effective role that can be achieved via 3D printing. This is because it provides flexibility in formulation design, development of delivery devices with dual or multiple drugs exhibiting immediate, extended or multi-release drug kinetics that can be tailored as per patient’s requirements^{171, 236, 294-297}. It has been used to print personalised dosage forms of highly potent drugs like theophylline^{263, 298} and prednisolone³⁸. It has also overcome the issue of polypharmacy by printing a multi-drug dosage form ‘polypills’¹⁷⁰ thus increasing the patient compliance by removing multiple intake of medicines in a day. Drug delivery devices have been printed using drug-loaded inks intended for precise and accurate deposition of dosed units^{261, 263, 299}.

The feasibility of this technology for the printing of contemporaneous preparation of personalised drug delivery has also been investigated by producing oral films containing salbutamol sulphate for the paediatrics²⁶¹. It has also enabled printing of geometrical structures on supportive films²⁶⁶. Edible-substrates with fast-dispersion has been proposed by 3D printing to facilitate drug administration³⁰⁰. Digital control of 3D printing has simplified the tailoring of drug dose, release, dosage form design and overall manufacturing of drug delivery devices³⁰¹. Furthermore, it has also played an important role in improving the physical properties of the printed objects e.g. it has enabled printing of objects with negligible

friability making it suitable for handling and transportation. Printing of objects at higher resolution and at micro, nano, or picoliter scale has become achievable due to these advanced technologies. Higher loading of drug into devices is another important advantage provided by the 3D printing ^{302, 303}.

Though 3D printing has numerous advantages but there are general drawbacks (Table 2.10) associated with it that cannot be neglected. The major challenge that researchers are facing is the limited availability of appropriate materials suitable for the printing. ABS and PLA are the most used thermoplastic polymers for FDM technique and are commercially available ³⁸ however, drug-loaded or non-drug loaded filaments composed of pharmaceutical grade polymers are not commercially available ³⁰⁴. On the other-hand metal alloys, ceramics and powdered plastics are the commonly used materials for one-step technique, SLS ^{305, 306}, however, these materials are not suitable for drug delivery purposes. The use of the pharmaceutical grade polymers for SLS has low potential for energy absorption and there is a possibility of thermal degradation. In addition, the machines require regular maintenance otherwise nozzles get clogged or dried. Some techniques require post-processing including curing and drying which consumes time and require solvent evaporation at the end from the final product ³⁰³. Banding, warping, stringing, leaning, collapse and presence of residuals are the printing defects that can occur during or after printing and are usually because of the equipment drift. These defects can affect the operations afterwards through which 3D printed object might pass e.g. fluid bed coating and sterilisation ³⁰⁷. Some of the techniques are slow process like SLS with the printing speed of 1-5 cm/h and produce large amounts of powder waste ³⁰³.

Table 2.13: Summary of advantages and disadvantages of 3D printing techniques.

3D printing technology	Advantages	Limitations	References	
Fused deposition modelling (FDM)	<ul style="list-style-type: none"> • Easy to operate, widely and commonly used 3D printing technology • Solvent-free process, enables printing of objects with various geometrical configurations • Print objects with negligible friability and high uniformity of drug • Printing at high temperature may inhibit the risk of microbial growth 	<ul style="list-style-type: none"> • Requires already prepared filament prior to printing • The availability of suitable polymers as starting materials is limited • Breaking or distortion of the filament • Defects like shrinking and warping of the object can occur due to non-thermostated platform • Final printed products have surface imperfections 	39, 302, 308-314	
Extrusion based 3D printing	Pneumatic extrusion (PnE)	<ul style="list-style-type: none"> • Enables processing at room temperature • Maximum drug loading up to 90%. 	<ul style="list-style-type: none"> • Drying process is required post-printing • Printing speed is slow • Microbial contamination could be present in semisolid ink • Print objects with high friability 	278, 302, 310, 315
	Paste extrusion (PE)	<ul style="list-style-type: none"> • Room temperature operation • Enables higher drug loading 	<ul style="list-style-type: none"> • Limited resolution, drying process is required after printing, difficulty in controlling the flow of semi-solids via nozzle 	170, 171, 302, 316

Vat polymerisation base 3D printing	Stereolithography (SLA)	<ul style="list-style-type: none"> • Higher resolution and accuracy • Deci-micron and submicron size layer thickness • Preferable for the printing of micro delivery devices 	<ul style="list-style-type: none"> • Limited availability of biocompatible photopolymers • Curing is required after printing • Degradation of some APIs could happen due to the use of UV light • Limited drug loading • Slow process 	278, 302, 307, 315, 317
	Continuous liquid interface production (CLIP)	<ul style="list-style-type: none"> • Comparatively faster technique than DLP, does not involve intermediate recoating step • Fabrication of overhangs without any support • Utilize various substances as starting materials 	<ul style="list-style-type: none"> • Requires photopolymer resin 	14, 318, 319
	Two photon polymerisation (TPP)	<ul style="list-style-type: none"> • High resolution • Suitable for fabrication of products of complex geometries, transdermal delivery systems and direct loading of drug into the liquid 	<ul style="list-style-type: none"> • Limited number of starting materials available • Use only photo curable and photo-reactive starting materials • Risk of toxicity 	307, 320, 321
	Digital light processing (DLP)	<ul style="list-style-type: none"> • Shorter building time • Utilises a wide range of wavelength from UV to visible • Less affected by oxygen inhibition 	<ul style="list-style-type: none"> • Time consuming due to resin recoating step 	14

	Selective laser sintering (SLS)	<ul style="list-style-type: none"> • Solvent-free process • Provides highly controllable internal porosity and microstructure 	<ul style="list-style-type: none"> • Slow printing process • Increased powder waste • Possibility of degradation of APIs and excipients and limited availability of APIs and excipients suitable for laser energy • Finishing process required to remove extra powder from the printed object • Not cost-effective 	228, 302, 315
Powder bed fusion base 3D printing	Powder bed printing	<ul style="list-style-type: none"> • Operates at room temperature • Wide range of starting materials available 	<ul style="list-style-type: none"> • Drying process is required after printing • Print products with increased friability 	302
	Inkjet printing	<ul style="list-style-type: none"> • Provides accurate control of drug dose and drug release pattern • Suitable for drugs with low therapeutic doses 	<ul style="list-style-type: none"> • Requires drying process after printing • Significant amount of waste 	302, 322
	Selective laser melting (SLM)	<ul style="list-style-type: none"> • Provides selective melting of powder layers 	<ul style="list-style-type: none"> • Complex process 	214
Material jetting base 3D printing	Drop on demand (DoD) printing	<ul style="list-style-type: none"> • Precise dosing at nano-scale can be achieved • Suitable for drugs with poor solubility due to increase in bioavailability 	<ul style="list-style-type: none"> • Nozzles get clogged and dried more often • Use of supersaturated solutions also clog the nozzle due to nucleation 	276, 278, 323-326

	<ul style="list-style-type: none"> • Dosing at picoliter scale can be achieved with precision 	<ul style="list-style-type: none"> • Evaporation of solvent is too slow or too fast • Low drug loading • Use of liquid ink media may cause problem in the stability of API 	
Material Jetting	<ul style="list-style-type: none"> • Capable of utilizing combination of different materials • Fine layer printing 	<ul style="list-style-type: none"> • Requires curing via UV light after printing • Time consuming 	221
Binder Jetting	<ul style="list-style-type: none"> • Availability of wide range of suitable materials • Enables printing process at room temperature • Easy manufacturing of structures with increased porosity • High dose flexibility 	<ul style="list-style-type: none"> • Low resolution • Time consuming • Requires post-printing drying • Increased fragility • Powder wastage • Use of liquid ink media may cause problem in the stability of API 	303
E-jetting	<ul style="list-style-type: none"> • Enhanced printing speed • Printing of objects at micro and nano-scale range 	<ul style="list-style-type: none"> • Difficult to control droplet size and printing speed 	287

2.5. Regulatory challenges

3D printed medical devices has gained immense attention over the last few years, especially highly personalised medical devices such as implants, spine prosthesis and artificial knees for each patient. Such devices are marketed under current FDA regulatory guidelines by identifying the similarities with the medical devices already available in the market ³²⁷. In addition, regulatory guidelines for the manufacturing of implants and medical devices has been released by FDA in 2017. However, currently, no fixed guidelines are available by the FDA for the regulation of 3D printed pharmaceutical dosage forms ³²⁸.

SPRITAM[®] levetiracetam is an FDA approved 3D printed orodispersible medication for the treatment of epilepsy ³²⁹. It has been acknowledged as a major milestone for 3D printing technology however, a deep insight reveals that this approval was mostly related to the development of product using modern technology and was not entirely the case related to personalised pharmaceutical dosage forms. In addition to this, the technology, ZipDose[®], employed for the fabrication of SPRITAM[®] ³²⁹ is similar to conventional powder compaction method used for the bulk manufacturing of tablets as compared to other 3D printing technologies.

It is compulsory for the pharmaceutical dosage forms to meet the regulatory requirements employed by the FDA before getting commercialised. The usual regulatory criteria involves human clinical trials with 20 to 100 volunteers for different phases of clinical trials, conversely, in case of personalised treatment, each dosage form has only one related subject ³²¹ and large controlled trials which require time and funding could act as a barrier to the availability of 3D printed pharmaceutical dosage forms. Other regulatory barriers are the issues of data protection, intellectual rights and liability that need to be taken into consideration to protect the end-users and the manufacturers. Suitable storage conditions, safety of the digital design of medical device and dosage forms and the data related to the patient are also the important aspects and must be taken into account to prevent liability issues and to reduce the risk of manufacturing errors ³¹⁵. The 3D printers should be legally defined as compounding or manufacturing instrument to determine what laws they are subject to ²⁹⁵ and regulatory decisions should be made by equally considering both aspects i.e. science and technology ³³⁰.

Furthermore, it is possible to gain experience from the 3D printed devices approved by the FDA for pharmaceutical dosage forms developed via 3D printing. For instance, almost 85 3D printed medical devices such as implants and prosthetics have been approved by FDA under emergency use or 510 (k) pathway which demonstrates the 3D printed device as an equivalent product to a commercialised device. A regulatory approach, 510 (k) pathway, can also be used for 3D printed dosage forms, however, it is not possible to approve 3D printed dosage forms via emergency use pathway because drugs would be administering via intravenous rates instead of the tablet. Moreover, each personalised dosage form will be treated as a new entity or drug moiety and will then face additional regulatory requirements. Therefore, the present standard FDA approval routes should be clearly thought through and a new method or guideline especially designed to fulfil the requirements of regulatory approval of personalised 3D printed dosage forms should be design ¹⁵.

2.6. Future prospects and outlook

The fabrication of personalised 3D printed drug delivery devices is likely to exceed in the upcoming years and beyond. The development of 3D printed dosage forms and other medicinal devices will continue to increase at a steady pace and the system will eventually be evolved to provide improved therapies. Printers with quality control systems might be available in the market to be used at pharmacies and hospitals which in turns would not only allow the manufacturing of high-quality medicinal devices and dosage forms along with real-time monitoring but will also play an important role in achieving personalised medicine. Digital designs of the formulations would allow easy modification as per patient's requirement for on-demand printing and data transfer related to dosage form designs would also become easy ³³¹.

Moreover, the bioprinting of organs is highly anticipated application of 3D printing and the research work that has been done in this area is promising and encouraging ³³². As per estimation, research scientists are only twenty years away from printing a completely functioning heart ³³⁰ although there are challenges in printing network vessels and is therefore far from reality. The advancement of technology with time would also allow fabrication of complex tissues e.g. kidney and liver tissues. It might be a possibility to print out a patient's tissue as a strip that can be used in tests to determine what medication will be most effective ³³¹.

Another anticipated application of 3D printing is the *in-situ* printing in which living organs are printed in the human body during operations³³³. Biomaterial scaffolding, growth factors, and cells can be deposited with precise and accurate digital control to repair lesions of different thicknesses and types. This approach can be used for repairing partially malfunctioned, damaged or diseased internal organs and for this purpose a handheld portable 3D printer would be a great invention³³⁴. Advancements in robot-assisted surgery and robotic bio printers will further revolutionise this field³³³.

From the research and development point of view for drug delivery devices, it is essential to work towards the progress of versatility of materials suitable for printing technologies³³⁵ and the 3D printing operating process itself needs optimisation to enhance the efficiency and reduce wastage. Detailed examination of API and excipients including physical and chemical properties e.g. powder wettability, surface tension, rheology and viscosity can help in selecting the appropriate material for printing³¹⁴. From technological point of view, software for 3D printers should be designed in a way that not only meet the requirements of pharmaceutical manufacturing but are also easy to use.

2.7. Conclusions

The current systematic review has identified the applications of various 3D printing technologies which are clear evidence of the capabilities of 3D printing in developing novel personalised drug delivery devices. This review has reported greater number of applications of FDM followed by paste extrusion, pneumatic extrusion, inkjet printing, powder bed printing and stereolithography. The major advantage is the ability to develop personalised drug delivery devices and is common to all types. It can be concluded that the printed drug delivery devices have huge potential in implementing the personalised medication in practice required by patients. 3D printing with its unique functionalities have made possible the manufacturing of different drug delivery systems, such as sustained, zero order drug kinetics tablet or personalised microneedle patch and drug eluting implants which are difficult to achieve by traditional manufacturing methods and opens a wide range of possibilities in the pharma sector. Consequently, the advances in the dosage form design can increase patient compliance, adherence to get safe and effective treatment.

Nevertheless, additional research should be carried out before the concept of on demand 3D printed personalised dosage forms can become a reality in the clinical practice, for instance, the impact of printing parameters on the quality and how to improve the reproducibility. Optimistically, if the research carries on around 3D printing, owing to the number of advantages that 3D printing provides and the versatility of the 3D printed dosage forms, there is huge potential for these 3D printing technologies to step into the next phase, to become a mainstream manufacturing tool, from proof-of-concept phase.

Another important aspect or barrier that 3D printing technologies will go through before their innovative applications can be applied clinically, is that several regulatory affairs should be addressed, and the quality assurance of the printed dosage form is one of them and to expedite this process, FDA has provided guidelines for drug delivery devices developed via 3D printing. It is anticipated that the unique functionalities of 3D printing techniques have speed up the of personalised dosage forms, there is no doubt that 3D printing will become a mainstream manufacturing tool for the pharmaceutical applications in the future.

Since none of the studies addressed the effect of plasticiser induced gastric motility on the drug absorption thus it provided a strong rationale for our experimental work i.e., to extrude the plasticiser free filaments for the development of the personalised FDM printed hydrophilic matrices with extended drug release properties using glipizide as a model drug to target diabetes which is a chronic disease.

References

1. I. Seoane-Viaño, F. J. Otero-Espinar and Á. Goyanes, in *Additive Manufacturing*, eds. J. Pou, A. Riveiro and J. P. Davim, Elsevier, 2021, DOI: <https://doi.org/10.1016/B978-0-12-818411-0.00022-7>, pp. 569.
2. K. Liang, D. Brambilla and J. C. Leroux, *Advanced Materials*, 2019, **31**, 1805680.
3. I. Seoane-Viaño, S. J. Trenfield, A. W. Basit and A. Goyanes, *Advanced Drug Delivery Reviews*, 2021, **174**, 553.
4. B. J. Park, H. J. Choi, S. J. Moon, S. J. Kim, R. Bajracharya, J. Y. Min and H.-K. Han, *Journal of Pharmaceutical Investigation*, 2019, **49**, 575.
5. Z. Khizer, A. Sadia, R. Sharma, S. Farhaj, J. S. Nirwan, P.G. Kakadia, Y. Shahzad, B. R. Conway M. U. Ghori, *Pharmaceuticals*, 2021, **14(5)**, 409.
6. J. S. Nirwan, S. S. Hasan, B. R. Conway and M. U. Ghori, *Scientific reports*, 2020, **10**, 1.
7. J. S. Nirwan, S. S. Hasan, B. R. Conway and M. U. Ghori, *Turkish Journal of Gastroenterology*, 2019, **30**, S892.
8. S. S. Hasan, S. T. R. Zaidi, J. S. Nirwan, M. U. Ghori, F. Javid, K. Ahmadi and Z.-U.-D. Babar, *Journal of clinical medicine*, 2019, **8**, 1292.
9. L. Kmet, R. C. Lee, L. S. Cook, D. Lorenzetti, G. Godlovitch and E. Einsiedel, *Calgary: Alberta Heritage Foundation for Medical Research (AHFMR)*. [Google Scholar], 2004.
10. J. P. Higgins, J. Thomas, J. Chandler, M. Cumpston, T. Li, M. J. Page and V. A. Welch, *Cochrane handbook for systematic reviews of interventions*, John Wiley & Sons, 2019.
11. V. Portland, D. Kansagara, O. N. Maya Elin, K. Peterson, A. Low, S. Carson, L. M. Denneson, E. Haney and P. Shiroma, 2012.
12. D. Walsh and S. Downe, *Midwifery*, 2006, **22**, 108.
13. V. Korakakis, R. Whiteley, A. Tzavara and N. Malliaropoulos, *British journal of sports medicine*, 2018, **52**, 387.
14. S. C. Ligon, R. Liska, J. r. Stampfl, M. Gurr and R. Mülhaupt, *Chemical reviews*, 2017, **117**, 10212.
15. S. H. Lim, H. Kathuria, J. J. Y. Tan and L. Kang, *Advanced drug delivery reviews*, 2018.
16. S. Qi and D. Craig, *Advanced drug delivery reviews*, 2016, **100**, 67.
17. G. F. Acosta-Vélez and B. J. P. S. Wu, 2016, **2**, 11.
18. S. Masood, *Assembly automation*, 2007, **27**, 215.
19. A. Goyanes, A. B. Buanz, A. W. Basit and S. Gaisford, *International journal of pharmaceuticals*, 2014, **476**, 88.
20. A. Goyanes, A. B. Buanz, G. B. Hatton, S. Gaisford and A. W. Basit, *European Journal of Pharmaceutics and Biopharmaceutics*, 2015, **89**, 157.
21. X. Chai, H. Chai, X. Wang, J. Yang, J. Li, Y. Zhao, W. Cai, T. Tao and X. Xiang, *Scientific reports*, 2017, **7**, 2829.
22. S.-i. Kimura, T. Ishikawa, Y. Iwao, S. Itai and H. Kondo, *Chemical and Pharmaceutical Bulletin*, 2019, **67**, 992.
23. S. Lamichhane, J.-B. Park, D. H. Sohn and S. Lee, *Pharmaceutics*, 2019, **11**, 564.
24. Q. Li, X. Guan, M. Cui, Z. Zhu, K. Chen, H. Wen, D. Jia, J. Hou, W. Xu and X. Yang, *International journal of pharmaceuticals*, 2018, **535**, 325.
25. J. Boetker, J. J. Water, J. Aho, L. Arnfast, A. Bohr and J. Rantanen, *European Journal of Pharmaceutical Sciences*, 2016, **90**, 47.
26. Z. Khizer, M. R. Akram, R. M. Sarfraz, J. S. Nirwan, S. Farhaj, M. Yousaf, T. Hussain, S. Lou, P. Timmins and B. R. Conway, *Polymers*, 2019, **11**, 1095.
27. K. Shi, J. P. Salvage, M. Maniruzzaman and A. Nokhodchi, *International Journal of Pharmaceutics*, 2021, **597**, 120315.
28. C. Korte and J. Quodbach, *AAPS PharmSciTech*, 2018, 1.

29. H. Kadry, T. A. Al-Hilal, A. Keshavarz, F. Alam, C. Xu, A. Joy and F. Ahsan, *International journal of pharmaceutics*, 2018, **544**, 285.
30. C. I. Gioumouxouzis, O. L. Katsamenis, N. Bouropoulos and D. G. Fatouros, *Journal of Drug Delivery Science and Technology*, 2017, **40**, 164.
31. T. Tagami, K. Fukushige, E. Ogawa, N. Hayashi and T. Ozeki, *Biological and Pharmaceutical Bulletin*, 2017, **40**, 357.
32. A. Melocchi, F. Parietti, A. Maroni, A. Foppoli, A. Gazzaniga and L. Zema, *International Journal of Pharmaceutics*, 2016, **509**, 255.
33. H. Öblom, J. Zhang, M. Pimparade, I. Speer, M. Preis, M. Repka and N. Sandler, *Aaps Pharmscitech*, 2019, **20**, 1.
34. A. Isreb, K. Baj, M. Wojsz, M. Isreb, M. Peak and M. A. Alhnan, *International journal of pharmaceutics*, 2019, **564**, 98.
35. M. Saviano, R. P. Aquino, P. Del Gaudio, F. Sansone and P. Russo, *International journal of pharmaceutics*, 2019, **561**, 1.
36. Y. Yang, H. Wang, H. Li, Z. Ou and G. Yang, *European Journal of Pharmaceutical Sciences*, 2018, **115**, 11.
37. J. Zhang, W. Yang, A. Q. Vo, X. Feng, X. Ye, D. W. Kim and M. A. Repka, *Carbohydrate polymers*, 2017, **177**, 49.
38. J. Skowrya, K. Pietrzak and M. A. Alhnan, *European Journal of Pharmaceutical Sciences*, 2015, **68**, 11.
39. C. Korte, J. Quodbach and technology, 2018, 1.
40. J. R. Cerda, T. Arifi, S. Ayyoubi, P. Knief, M. P. Ballesteros, W. Keeble, E. Barbu, A. M. Healy, A. Lalatsa and D. R. Serrano, *Pharmaceutics*, 2020, **12**, 345.
41. S. Ayyoubi, J. R. Cerda, R. Fernández-García, P. Knief, A. Lalatsa, A. M. Healy and D. R. Serrano, *International Journal of Pharmaceutics*, 2021, **597**, 120336.
42. A. Goyanes, P. R. Martinez, A. Buanz, A. W. Basit and S. Gaisford, *International journal of pharmaceutics*, 2015, **494**, 657.
43. X. Xu, J. Zhao, M. Wang, L. Wang and J. Yang, *Scientific reports*, 2019, **9**, 1.
44. Y. J. N. Tan, W. P. Yong, J. S. Kochhar, J. Khanolkar, X. Yao, Y. Sun, C. K. Ao and S. Soh, *Journal of Controlled Release*, 2020, **322**, 42.
45. Q. Li, H. Wen, D. Jia, X. Guan, H. Pan, Y. Yang, S. Yu, Z. Zhu, R. Xiang and W. Pan, *International journal of pharmaceutics*, 2017, **525**, 5.
46. A. Goyanes, J. Wang, A. Buanz, R. Martínez-Pacheco, R. Telford, S. Gaisford and A. W. Basit, *Molecular pharmaceutics*, 2015, **12**, 4077.
47. M. Sadia, B. Arafat, W. Ahmed, R. T. Forbes and M. A. Alhnan, *Journal of Controlled Release*, 2018, **269**, 355.
48. D. M. Smith, Y. Kapoor, G. R. Klinzing and A. T. Procopio, *International journal of pharmaceutics*, 2018, **544**, 21.
49. B. Arafat, M. Wojsz, A. Isreb, R. T. Forbes, M. Isreb, W. Ahmed, T. Arafat and M. A. Alhnan, *European Journal of Pharmaceutical Sciences*, 2018, **118**, 191.
50. N. Genina, J. P. Boetker, S. Colombo, N. Harmankaya, J. Rantanen and A. Bohr, *Journal of Controlled Release*, 2017, **268**, 40.
51. D. Markl, J. A. Zeitler, C. Rasch, M. H. Michaelsen, A. Müllertz, J. Rantanen, T. Rades and J. Bøtker, *Pharmaceutical research*, 2017, **34**, 1037.
52. A. Goyanes, H. Chang, D. Sedough, G. B. Hatton, J. Wang, A. Buanz, S. Gaisford and A. W. Basit, *International journal of pharmaceutics*, 2015, **496**, 414.
53. T. C. Okwuosa, B. C. Pereira, B. Arafat, M. Cieszynska, A. Isreb and M. A. Alhnan, *Pharmaceutical research*, 2017, **34**, 427.
54. C. I. Gioumouxouzis, E. Tzimtzimis, O. L. Katsamenis, A. Dourou, C. Markopoulou, N. Bouropoulos, D. Tzetzis and D. G. Fatouros, *European Journal of Pharmaceutical Sciences*, 2020, **143**, 105176.

55. F. Fina, A. Goyanes, M. Rowland, S. Gaisford and A. W. Basit, *Polymers*, 2020, **12**, 1769.
56. C. I. Gioumouxouzis, A.-T. Chatzitaki, C. Karavasili, O. L. Katsamenis, D. Tzetzis, E. Mystiridou, N. Bouropoulos and D. G. Fatouros, 2018, **19**, 3362.
57. A. Goyanes, F. Fina, A. Martorana, D. Sedough, S. Gaisford and A. W. Basit, *International journal of pharmaceuticals*, 2017, **527**, 21.
58. A. Goyanes, M. Kobayashi, R. Martínez-Pacheco, S. Gaisford and A. W. Basit, *International Journal of Pharmaceutics*, 2016, **514**, 290.
59. B. C. Pereira, A. Isreb, R. T. Forbes, F. Dores, R. Habashy, J.-B. Petit, M. A. Alhnan and E. F. Oga, *European Journal of Pharmaceutics and Biopharmaceutics*, 2019, **135**, 94.
60. T. C. Okwuosa, D. Stefaniak, B. Arafat, A. Isreb, K.-W. Wan and M. A. Alhnan, *Pharmaceutical research*, 2016, **33**, 2704.
61. M. Sadia, A. Sośnicka, B. Arafat, A. Isreb, W. Ahmed, A. Kelarakis and M. A. Alhnan, *International journal of pharmaceuticals*, 2016, **513**, 659.
62. M. Sadia, A. Isreb, I. Abbadji, M. Isreb, D. Aziz, A. Selo, P. Timmins and M. A. Alhnan, *European Journal of Pharmaceutical Sciences*, 2018, DOI: <https://doi.org/10.1016/j.ejps.2018.07.045>.
63. C. I. Gioumouxouzis, A. Baklavaridis, O. L. Katsamenis, C. K. Markopoulou, N. Bouropoulos, D. Tzetzis and D. G. Fatouros, *European Journal of Pharmaceutical Sciences*, 2018, **120**, 40.
64. K. Pietrzak, A. Isreb and M. A. Alhnan, *European Journal of Pharmaceutics and Biopharmaceutics*, 2015, **96**, 380.
65. A. Goyanes, N. Allahham, S. J. Trenfield, E. Stoyanov, S. Gaisford and A. W. Basit, *International journal of pharmaceuticals*, 2019, **567**, 118471.
66. J. J. Ong, A. Awad, A. Martorana, S. Gaisford, E. Stoyanov, A. W. Basit and A. Goyanes, *International Journal of Pharmaceutics*, 2020, **579**, 119169.
67. N. G. Solanki, M. Tahsin, A. V. Shah and A. T. Serajuddin, *Journal of pharmaceutical sciences*, 2018, **107**, 390.
68. W. Kempin, V. Domsta, G. Grathoff, I. Brecht, B. Semmling, S. Tillmann, W. Weitschies and A. Seidlitz, *Pharmaceutical research*, 2018, **35**, 124.
69. G. Kollamaram, D. M. Croker, G. M. Walker, A. Goyanes, A. W. Basit and S. Gaisford, *International journal of pharmaceuticals*, 2018, **545**, 144.
70. R. Beck, P. Chaves, A. Goyanes, B. Vukosavljevic, A. Buanz, M. Windbergs, A. Basit and S. Gaisford, *International journal of pharmaceuticals*, 2017, **528**, 268.
71. A. Melocchi, F. Parietti, S. Maccagnan, M. A. Orteni, S. Antenucci, F. Briatico-Vangosa, A. Maroni, A. Gazzaniga and L. Zema, *AAPS PharmSciTech*, 2018, **1**.
72. G. Verstraete, A. Samaro, W. Grymonpré, V. Vanhoorne, B. Van Snick, M. Boone, T. Hellemans, L. Van Hoorebeke, J. P. Remon and C. Vervaet, *International journal of pharmaceuticals*, 2018, **536**, 318.
73. Y. Sun and S. Soh, *Advanced materials*, 2015, **27**, 7847.
74. A. Melocchi, F. Parietti, G. Loreti, A. Maroni, A. Gazzaniga and L. Zema, *Journal of Drug Delivery Science and Technology*, 2015, **30**, 360.
75. A. Maroni, A. Melocchi, F. Parietti, A. Foppoli, L. Zema and A. Gazzaniga, *Journal of Controlled Release*, 2017, **268**, 10.
76. A. Goyanes, U. Det-Amornrat, J. Wang, A. W. Basit and S. Gaisford, *Journal of Controlled Release*, 2016, **234**, 41.
77. J. Zhang, X. Feng, H. Patil, R. V. Tiwari and M. A. Repka, *International journal of pharmaceuticals*, 2017, **519**, 186.
78. T. C. Okwuosa, C. Soares, V. Gollwitzer, R. Habashy, P. Timmins and M. A. Alhnan, *European Journal of Pharmaceutical Sciences*, 2018, **118**, 134.
79. B. Arafat, N. Qinna, M. Cieszyńska, R. T. Forbes and M. A. Alhnan, *European Journal of Pharmaceutics and Biopharmaceutics*, 2018, **128**, 282.

80. W. Jamróz, M. Kurek, E. Łyszczarz, J. Szafraniec, J. Knapik-Kowalczyk, K. Syrek, M. Paluch and R. Jachowicz, *International journal of pharmaceutics*, 2017, **533**, 413.
81. T. Ehtezazi, M. Algellay, Y. Islam, M. Roberts, N. M. Dempster and S. D. Sarker, *Journal of pharmaceutical sciences*, 2018, **107**, 1076.
82. A. Hussain, F. Mahmood, M. S. Arshad, N. Abbas, N. Qamar, J. Mudassir, S. Farhaj, J. S. Nirwan and M. U. Ghori, *Polymers*, 2020, **12**, 3057.
83. M. Alhijaj, P. Belton and S. Qi, *European Journal of Pharmaceutics and Biopharmaceutics*, 2016, **108**, 111.
84. J. Jensen, J. H. D. Röfling, D. Q. Svend Le, A. A. Kristiansen, J. V. Nygaard, L. B. Hokland, M. Bendtsen, M. Kassem, H. Lysdahl and C. E. Bünger, *Journal of biomedical materials research Part A*, 2014, **102**, 2993.
85. J. A. Weisman, J. C. Nicholson, K. Tappa, U. Jammalamadaka, C. G. Wilson and D. K. Mills, *International journal of nanomedicine*, 2015, **10**, 357.
86. J. A. Weisman, D. H. Ballard, U. Jammalamadaka, K. Tappa, J. Sumerel, H. B. D'Agostino, D. K. Mills and P. K. Woodard, *Academic radiology*, 2018.
87. K. Tappa, U. Jammalamadaka, J. A. Weisman, D. H. Ballard, D. D. Wolford, C. Pascual-Garrido, L. M. Wolford, P. K. Woodard and D. K. Mills, *Journal of functional biomaterials*, 2019, **10**, 17.
88. P. F. Costa, A. M. Puga, L. Díaz-Gomez, A. Concheiro, D. H. Busch and C. Alvarez-Lorenzo, *International Journal of Pharmaceutics*, 2015, **496**, 541.
89. X. Farto-Vaamonde, G. Auriemma, R. P. Aquino, A. Concheiro and C. Alvarez-Lorenzo, *European Journal of Pharmaceutics and Biopharmaceutics*, 2019, **141**, 100.
90. Y.-C. Chou, W.-L. Yeh, C.-L. Chao, Y.-H. Hsu, Y.-H. Yu, J.-K. Chen and S.-J. Liu, *International journal of nanomedicine*, 2016, **11**, 4173.
91. S. H. Lim, S. M. Y. Chia, L. Kang and K. Y.-L. Yap, *Journal of pharmaceutical sciences*, 2016, **105**, 2155.
92. K.-C. Hung, C.-S. Tseng, L.-G. Dai and S.-h. Hsu, *Biomaterials*, 2016, **83**, 156.
93. Y.-C. Chou, D. Lee, T.-M. Chang, Y.-H. Hsu, Y.-H. Yu, E.-C. Chan and S.-J. Liu, *Journal of the mechanical behavior of biomedical materials*, 2017, **72**, 209.
94. C. Wang, Q. Zhao and M. Wang, *Biofabrication*, 2017, **9**, 025031.
95. S. Li, Y. Xu, J. Yu and M. L. Becker, *Biomaterials*, 2017, **141**, 176.
96. T. W. B. Kim, O. J. Lopez, J. P. Sharkey, K. R. Marden, M. R. Murshed and S. I. Ranganathan, *Medical hypotheses*, 2017, **102**, 65.
97. L. E. Visscher, H. P. Dang, M. A. Knackstedt, D. W. Hutmacher and P. A. Tran, *Materials Science and Engineering: C*, 2018, **87**, 78.
98. I. Rajzer, A. Kurowska, A. Jabłoński, S. Jatteau, M. Śliwka, M. Ziąbka and E. Menaszek, *Materials & Design*, 2018, **155**, 297.
99. M. Govender, S. Indermun, P. Kumar, Y. E. Choonara and V. Pillay, *Materials*, 2018, **11**, 1006.
100. J. Schmid, M. A. Wahl and R. Daniels, *Pharmaceutics*, 2021, **13**, 543.
101. X. Li, Y. Wang, Z. Wang, Y. Qi, L. Li, P. Zhang, X. Chen and Y. Huang, *Macromolecular bioscience*, 2018, **18**, 1800068.
102. M. Ø. Andersen, D. Q. S. Le, M. Chen, J. V. Nygaard, M. Kassem, C. Bünger and J. Kjems, *Advanced Functional Materials*, 2013, **23**, 5599.
103. N. Sandler, I. Salmela, A. Fallarero, A. Rosling, M. Khajeheian, R. Kolakovic, N. Genina, J. Nyman and P. Vuorela, *International journal of pharmaceutics*, 2014, **459**, 62.
104. J. J. Water, A. Bohr, J. Boetker, J. Aho, N. Sandler, H. M. Nielsen and J. Rantanen, *Journal of Pharmaceutical Sciences*, 2015, **104**, 1099.
105. D. H. Ballard, J. A. Weisman, U. Jammalamadaka, K. Tappa, J. S. Alexander and F. D. Griffen, *Surgery*, 2017, **161**, 1479.
106. D. J. Horst, S. M. Tebcherani, E. T. Kubaski and R. de Almeida Vieira, *Bioinorganic chemistry and applications*, 2017, **2017**.
107. K. Liang, S. Carmone, D. Brambilla and J.-C. Leroux, *Science advances*, 2018, **4**, eaat2544.

108. J. Holländer, N. Genina, H. Jukarainen, M. Khajeheian, A. Rosling, E. Mäkilä and N. Sandler, *Journal of pharmaceutical sciences*, 2016, **105**, 2665.
109. P. Arany, I. Papp, M. Zichar, M. Csontos, J. Elek, G. Regdon, I. Budai, M. Béres, R. Gesztelyi, P. Fehér, Z. Ujhelyi, G. Vasvári, Á. Haimhoffer, F. Fenyvesi, J. Váradi, V. Miklós and I. Bácskay, *Molecules*, 2020, **25**, 5889.
110. K. Shi, R. Aviles-Espinosa, E. Rendon-Morales, L. Woodbine, M. Maniruzzaman and A. Nokhodchi, *Colloids and Surfaces B: Biointerfaces*, 2020, **192**, 111068.
111. N. Genina, J. Holländer, H. Jukarainen, E. Mäkilä, J. Salonen and N. Sandler, *European Journal of Pharmaceutical Sciences*, 2016, **90**, 53.
112. K. Tappa, U. Jammalamadaka, D. H. Ballard, T. Bruno, M. R. Israel, H. Vemula, J. M. Meacham, D. K. Mills, P. K. Woodard and J. A. Weisman, *PLoS one*, 2017, **12**, e0182929.
113. J. Fu, X. Yu and Y. Jin, *International journal of pharmaceutics*, 2018, **539**, 75.
114. M. A. Luzuriaga, D. R. Berry, J. C. Reagan, R. A. Smaldone and J. J. Gassensmith, *Lab on a Chip*, 2018, **18**, 1223.
115. M. Pozzoli, H. X. Ong, L. Morgan, M. Sukkar, D. Traini, P. M. Young and F. Sonvico, *European Journal of Pharmaceutics and Biopharmaceutics*, 2016, **107**, 223.
116. Z. Muwaffak, A. Goyanes, V. Clark, A. W. Basit, S. T. Hilton and S. Gaisford, *International journal of pharmaceutics*, 2017, **527**, 161.
117. S. K. Misra, F. Ostadhosein, R. Babu, J. Kus, D. Tankasala, A. Sutrisno, K. A. Walsh, C. R. Bromfield and D. Pan, *Advanced healthcare materials*, 2017, **6**, 1700008.
118. S. Glatzel, M. Hezwani, P. J. Kitson, P. S. Gromski, S. Schürer and L. Cronin, *Chem*, 2016, **1**, 494.
119. S. A. Khaled, M. R. Alexander, D. J. Irvine, R. D. Wildman, M. J. Wallace, S. Sharpe, J. Yoo and C. J. Roberts, 2018, **1**.
120. T. J. Hinton, Q. Jallerat, R. N. Palchesko, J. H. Park, M. S. Grodzicki, H.-J. Shue, M. H. Ramadan, A. R. Hudson and A. W. Feinberg, *Science advances*, 2015, **1**, e1500758.
121. K. Hölzl, S. Lin, L. Tytgat, S. Van Vlierberghe, L. Gu and A. Ovsianikov, *Biofabrication*, 2016, **8**, 032002.
122. D. Yu, Q. Li, X. Mu, T. Chang and Z. Xiong, *International journal of oral and maxillofacial surgery*, 2008, **37**, 929.
123. M. Zhu, H. Wang, J. Liu, H. He, X. Hua, Q. He, L. Zhang, X. Ye and J. Shi, *Biomaterials*, 2011, **32**, 1986.
124. J.-H. Shim, S. E. Kim, J. Y. Park, J. Kundu, S. W. Kim, S. S. Kang and D.-W. Cho, *Tissue Engineering Part A*, 2014, **20**, 1980.
125. J. Zhang, S. Zhao, Y. Zhu, Y. Huang, M. Zhu, C. Tao and C. Zhang, *Acta biomaterialia*, 2014, **10**, 2269.
126. J.-H. Shim, M.-J. Kim, J. Y. Park, R. G. Pati, Y.-P. Yun, S. E. Kim, H.-R. Song and D.-W. Cho, *Tissue Engineering and Regenerative Medicine*, 2015, **12**, 283.
127. S. J. Lee, D. Lee, T. R. Yoon, H. K. Kim, H. H. Jo, J. S. Park, J. H. Lee, W. D. Kim, I. K. Kwon and S. A. Park, *Acta biomaterialia*, 2016, **40**, 182.
128. Y. Zhang, D. Zhai, M. Xu, Q. Yao, H. Zhu, J. Chang and C. Wu, *Biofabrication*, 2017, **9**, 025037.
129. H. Y. Lin, T. W. Chang and T. K. Peng, *Journal of Biomedical Materials Research Part A*, 2018, **106**, 1511.
130. T.-H. Song, J. Jang, Y.-J. Choi, J.-H. Shim and D.-W. Cho, *Cell transplantation*, 2015, **24**, 2513.
131. Q. Gao, Y. He, J.-z. Fu, A. Liu and L. Ma, *Biomaterials*, 2015, **61**, 203.
132. P. Rattanakit, S. E. Moulton, K. S. Santiago, S. Liawruangrath and G. G. Wallace, *International Journal of Pharmaceutics*, 2012, **422**, 254.
133. I. El Aita, J. Breitkreutz and J. Quodbach, *European Journal of Pharmaceutics and Biopharmaceutics*, 2019, **134**, 29.
134. T. Tagami, E. Ito, R. Kida, K. Hirose, T. Noda and T. Ozeki, *International Journal of Pharmaceutics*, 2021, **594**, 120118.

135. M. Siyawamwaya, L. C. du Toit, P. Kumar, Y. E. Choonara, P. P. Kondiah and V. Pillay, *European Journal of Pharmaceutics and Biopharmaceutics*, 2018.
136. M. K. Gupta, F. Meng, B. N. Johnson, Y. L. Kong, L. Tian, Y.-W. Yeh, N. Masters, S. Singamaneni and M. C. McAlpine, *Nano letters*, 2015, **15**, 5321.
137. A.-V. Do, A. Akkouch, B. Green, I. Ozbolat, A. Debabneh, S. Geary and A. K. Salem, *Annals of biomedical engineering*, 2017, **45**, 297.
138. J. Holländer, R. Hakala, J. Suominen, N. Moritz, J. Yliruusi and N. Sandler, *International Journal of Pharmaceutics*, 2018, **544**, 433.
139. T. Maver, D. Smrke, M. Kurečič, L. Gradišnik, U. Maver and K. S. Kleinschek, *Journal of Sol-Gel Science and Technology*, 2018, 1.
140. J. Sun, W. Zhou, L. Yan, D. Huang and L.-y. Lin, 2018, **220**, 1.
141. R. Chang, K. Emami, H. Wu and W. Sun, *Biofabrication*, 2010, **2**, 045004.
142. J. Snyder, Q. Hamid, C. Wang, R. Chang, K. Emami, H. Wu and W. Sun, *Biofabrication*, 2011, **3**, 034112.
143. S. M. King, V. Gorgen, S. C. Presnell, D. G. Nguyen, B. R. Shepherd and N. Ridge, *American Society of Biology, New Orleans, LA*, 2013.
144. Y. Zhao, R. Yao, L. Ouyang, H. Ding, T. Zhang, K. Zhang, S. Cheng and W. Sun, *Biofabrication*, 2014, **6**, 035001.
145. X. Dai, C. Ma, Q. Lan and T. Xu, *Biofabrication*, 2016, **8**, 045005.
146. S. Knowlton and S. Tasoglu, *Trends in biotechnology*, 2016, **34**, 681.
147. D. G. Nguyen, J. Funk, J. B. Robbins, C. Crogan-Grundy, S. C. Presnell, T. Singer and A. B. Roth, *PloS one*, 2016, **11**, e0158674.
148. K. A. Homan, D. B. Kolesky, M. A. Skylar-Scott, J. Herrmann, H. Obuobi, A. Moisan and J. A. Lewis, *Scientific reports*, 2016, **6**, 34845.
149. Q. Gu, E. Tomaskovic-Crook, R. Lozano, Y. Chen, R. M. Kapsa, Q. Zhou, G. G. Wallace and J. M. Crook, *Advanced healthcare materials*, 2016, **5**, 1429.
150. S. Tarafder, A. Koch, Y. Jun, C. Chou, M. R. Awadallah and C. H. Lee, *Biofabrication*, 2016, **8**, 025003.
151. T. Ahlfeld, A. R. Akkineni, Y. Förster, T. Köhler, S. Knaack, M. Gelinsky and A. Lode, *Annals of biomedical engineering*, 2017, **45**, 224.
152. C. Wu, Y. Luo, G. Cuniberti, Y. Xiao and M. Gelinsky, *Acta biomaterialia*, 2011, **7**, 2644.
153. J. Zhang, S. Zhao, M. Zhu, Y. Zhu, Y. Zhang, Z. Liu and C. Zhang, *Journal of Materials Chemistry B*, 2014, **2**, 7583.
154. M. Zhu, K. Li, Y. Zhu, J. Zhang and X. Ye, *Acta biomaterialia*, 2015, **16**, 145.
155. K. Li, M. Zhu, P. Xu, Y. Xi, Z. Cheng, Y. Zhu and X. Ye, *Journal of Materials Science: Materials in Medicine*, 2015, **26**, 102.
156. P. Pei, Z. Tian and Y. Zhu, *Microporous and Mesoporous Materials*, 2018, **272**, 24.
157. Z. Min, Z. Shichang, X. Chen, Z. Yufang and Z. Changqing, *Biomaterials science*, 2015, **3**, 1236.
158. Q. Wu, X. Zhang, B. Wu and W. Huang, *Ceramics International*, 2013, **39**, 2389.
159. H. Wang, G. Wu, J. Zhang, K. Zhou, B. Yin, X. Su, G. Qiu, G. Yang, X. Zhang and G. Zhou, *Colloids and Surfaces B: Biointerfaces*, 2016, **141**, 491.
160. Y. Wu, L. Woodbine, A. M. Carr, A. R. Pillai, A. Nokhodchi and M. Maniruzzaman, *Pharmaceutics*, 2020, **12**, 1077.
161. Y. S. Zhang, A. Arneri, S. Bersini, S.-R. Shin, K. Zhu, Z. Goli-Malekabadi, J. Aleman, C. Colosi, F. Busignani and V. Dell'Erba, *Biomaterials*, 2016, **110**, 45.
162. Y. Wang, Y. Miao, J. Zhang, J. P. Wu, T. B. Kirk, J. Xu, D. Ma and W. Xue, *Materials Science and Engineering: C*, 2018, **84**, 44.
163. I. Seoane-Viaño, N. Gómez-Lado, H. Lázare-Iglesias, X. García-Otero, J. R. Antúnez-López, Á. Ruibal, J. J. Varela-Correa, P. Aguiar, A. W. Basit, F. J. Otero-Espinar, M. González-Barcia, A. Goyanes, A. Luzardo-Álvarez and A. Fernández-Ferreiro, *Biomedicines*, 2020, **8**, 563.

164. A. Liaskoni, R. D. Wildman and C. J. Roberts, *International Journal of Pharmaceutics*, 2021, **597**, 120330.
165. S. A. Khaled, J. C. Burley, M. R. Alexander and C. J. Roberts, *International journal of pharmaceutics*, 2014, **461**, 105.
166. M. Cui, Y. Yang, D. Jia, P. Li, Q. Li, F. Chen, S. Wang, W. Pan and P. Ding, *Journal of Drug Delivery Science and Technology*, 2019, **49**, 14.
167. T. Tagami, M. Ando, N. Nagata, E. Goto, N. Yoshimura, T. Takeuchi, T. Noda and T. Ozeki, *Journal of pharmaceutical sciences*, 2019, **108**, 907.
168. Z. Wang, L. Liu, S. Xiang, C. Jiang, W. Wu, S. Ruan, Q. Du, T. Chen, Y. Xue, H. Chen, L. Weng, H. Zhu, Q. Shen and Q. Liu, *AAPS PharmSciTech*, 2020, **21**, 159.
169. H. Herrada-Manchón, D. Rodríguez-González, M. Alejandro Fernández, M. Suñé-Pou, P. Pérez-Lozano, E. García-Montoya and E. Aguilar, *International Journal of Pharmaceutics*, 2020, **587**, 119687.
170. S. A. Khaled, J. C. Burley, M. R. Alexander, J. Yang and C. J. Roberts, *Journal of controlled release*, 2015, **217**, 308.
171. S. A. Khaled, J. C. Burley, M. R. Alexander, J. Yang and C. J. Roberts, *International journal of pharmaceutics*, 2015, **494**, 643.
172. S. A. Khaled, M. R. Alexander, R. D. Wildman, M. J. Wallace, S. Sharpe, J. Yoo and C. J. Roberts, *International journal of pharmaceutics*, 2018, **538**, 223.
173. I. El Aita, J. Rahman, J. Breitreutz and J. Quodbach, *European Journal of Pharmaceutics and Biopharmaceutics*, 2020, **157**, 59.
174. Y. Yang, X. Wang, X. Lin, L. Xie, R. Ivone, J. Shen and G. Yang, *International Journal of Pharmaceutics*, 2020, **583**, 119360.
175. M. S. Algahtani, A. A. Mohammed, J. Ahmad and E. Saleh, *Polymers*, 2020, **12**, 1395.
176. I. E. Aita, J. Breitreutz and J. Quodbach, *European Journal of Pharmaceutical Sciences*, 2020, **146**, 105266.
177. Y. Cheng, H. Qin, N. C. Acevedo and X. Shi, *Journal of Biomedical Materials Research Part B: Applied Biomaterials*, 2021, **109**, 257.
178. D. Fang, Y. Yang, M. Cui, H. Pan, L. Wang, P. Li, W. Wu, S. Qiao and W. Pan, *AAPS PharmSciTech*, 2021, **22**, 37.
179. M. Kuźmińska, B. C. Pereira, R. Habashy, M. Peak, M. Isreb, T. D. Gough, A. Isreb and M. A. Alhnan, *International Journal of Pharmaceutics*, 2021, **598**, 120305.
180. J. Johannesson, J. Khan, M. Hubert, A. Teleki and C. A. S. Bergström, *International Journal of Pharmaceutics*, 2021, **597**, 120304.
181. M. Elbadawi, D. Nikjoo, T. Gustafsson, S. Gaisford and A. W. Basit, *Int J Pharm*, 2021, **595**, 120197.
182. H.-G. Yi, Y.-J. Choi, K. S. Kang, J. M. Hong, R. G. Pati, M. N. Park, I. K. Shim, C. M. Lee, S. C. Kim and D.-W. Cho, *Journal of Controlled Release*, 2016, **238**, 231.
183. D. Kokkinis, M. Schaffner and A. R. Studart, *Nature communications*, 2015, **6**, 8643.
184. G. R. Souza, H. Tseng, J. A. Gage, A. Mani, P. Desai, F. Leonard, A. Liao, M. Longo, J. S. Refuerzo and B. Godin, *International journal of molecular sciences*, 2017, **18**, 683.
185. S.-B. Kim, N.-H. Kim, J.-H. Kim and H.-S. Moon, 2018, **120**, 693.
186. J.-H. Lee, R. M. Pidaparti, G. M. Atkinson and R. S. Moorthy, *Journal of drug delivery*, 2012, **2012**.
187. A. Chi, S. Curi, K. Clayton, D. Luciano, K. Klauber, A. Alexander-Katz, S. D'hers and N. M. Elman, *Drug delivery and translational research*, 2014, **4**, 320.
188. A. El Merhie, L. Navarro, X. Delavenne, L. Leclerc and J. Pourchez, *Pharmaceutical research*, 2016, **33**, 1074.
189. J. Wang, A. Goyanes, S. Gaisford and A. W. Basit, *International journal of pharmaceutics*, 2016, **503**, 207.

190. A. V. Healy, E. Fuenmayor, P. Doran, L. M. Geever, C. L. Higginbotham and J. G. Lyons, *Pharmaceutics*, 2019, **11**, 645.
191. X. Xu, P. Robles-Martinez, C. M. Madla, F. Joubert, A. Goyanes, A. W. Basit and S. Gaisford, *Additive Manufacturing*, 2020, **33**, 101071.
192. P. R. Martinez, A. Goyanes, A. W. Basit and S. Gaisford, *International journal of pharmaceutics*, 2017, **532**, 313.
193. N. J. Castro, J. O'Brien and L. G. Zhang, *Nanoscale*, 2015, **7**, 14010.
194. W. Zhu, B. Holmes, R. I. Glazer and L. G. Zhang, *Nanomedicine: Nanotechnology, Biology and Medicine*, 2016, **12**, 69.
195. J. A. Parry, M. G. Olthof, K. L. Shogren, M. Dadsetan, A. Van Wijnen, M. Yaszemski and S. Kakar, *Tissue Engineering Part A*, 2017, **23**, 359.
196. S. D. Gittard, P. R. Miller, C. Jin, T. N. Martin, R. D. Boehm, B. J. Chisholm, S. J. Stafslie, J. W. Daniels, N. Cilz and N. A. Monteiro-Riviere, *Jom*, 2011, **63**, 59.
197. C. P. P. Pere, S. N. Economidou, G. Lall, C. Ziraud, J. S. Boateng, B. D. Alexander, D. A. Lamprou and D. Douroumis, *International Journal of Pharmaceutics*, 2018, **544**, 425.
198. A. R. Johnson, C. L. Caudill, J. R. Tumbleston, C. J. Bloomquist, K. A. Moga, A. Ermoshkin, D. Shirvanyants, S. J. Mecham, J. C. Luft and J. M. DeSimone, *PloS one*, 2016, **11**, e0162518.
199. J. R. Tumbleston, D. Shirvanyants, N. Ermoshkin, R. Januszewicz, A. R. Johnson, D. Kelly, K. Chen, R. Pinschmidt, J. P. Rolland and A. J. S. Ermoshkin, 2015, **347**, 1349.
200. C. L. Caudill, J. L. Perry, S. Tian, J. C. Luft and J. M. DeSimone, *Journal of Controlled Release*, 2018, **284**, 122.
201. C. J. Bloomquist, M. B. Mecham, M. D. Paradzinsky, R. Januszewicz, S. B. Warner, J. C. Luft, S. J. Mecham, A. Z. Wang and J. M. DeSimone, *Journal of Controlled Release*, 2018, **278**, 9.
202. S. Maruo and S. Kawata, 1997.
203. S. Pashneh-Tala, R. Owen, H. Bahmaee, S. Rekštyte, M. Malinauskas and F. Claeysens, 2018, **6**, 41.
204. A. Otuka, J. Almeida, V. Tribuzi, M. R. Cardoso, A. C. Hernandez, D. Correa and C. R. Mendonça, 2014, **17**, 352.
205. W.-E. Lu, X.-Z. Dong, W.-Q. Chen, Z.-S. Zhao and X.-M. Duan, 2011, **21**, 5650.
206. S. Juodkasis, V. Mizeikis, K. K. Seet, M. Miwa and H. Misawa, 2005, **16**, 846.
207. S.-H. Lee, J. J. Moon and J. L. West, 2008, **29**, 2962.
208. S. Basu, L. P. Cunningham, G. D. Pins, K. A. Bush, R. Taboada, A. R. Howell, J. Wang and P. J. Campagnola, 2005, **6**, 1465.
209. W. Haske, V. W. Chen, J. M. Hales, W. Dong, S. Barlow, S. R. Marder and J. W. Perry, 2007, **15**, 3426.
210. V. Mizeikis, K. K. Seet, S. Juodkasis and H. Misawa, 2004, **29**, 2061.
211. M. J. Ventura, C. Bullen and M. Gu, 2007, **15**, 1817.
212. S. D. Gittard, A. Ovsianikov, H. Akar, B. Chichkov, N. A. Monteiro-Riviere, S. Stafslie, B. Chisholm, C. C. Shin, C. M. Shih and S. J. Lin, *Advanced Engineering Materials*, 2010, **12**, B77.
213. T. Y. Huang, M. S. Sakar, A. Mao, A. J. Petruska, F. Qiu, X. B. Chen, S. Kennedy, D. Mooney and B. J. Nelson, *Advanced Materials*, 2015, **27**, 6644.
214. Q. Mu, L. Wang, C. K. Dunn, X. Kuang, F. Duan, Z. Zhang, H. J. Qi and T. Wang, 2017, **18**, 74.
215. P. Tesavibul, R. Felzmann, S. Gruber, R. Liska, I. Thompson, A. R. Boccaccini and J. Stampfl, 2012, **74**, 81.
216. X. Ma, X. Qu, W. Zhu, Y.-S. Li, S. Yuan, H. Zhang, J. Liu, P. Wang, C. S. E. Lai and F. Zanella, *Proceedings of the National Academy of Sciences*, 2016, **113**, 2206.
217. Y. Sun, X. Ruan, H. Li, H. Kathuria, G. Du and L. Kang, *International journal of pharmaceutics*, 2016, **513**, 717.
218. S. H. Lim, J. Y. Ng and L. Kang, *Biofabrication*, 2017, **9**, 015010.
219. G. Stanojević, D. Medarević, I. Adamov, N. Pešić, J. Kovačević and S. Ibrić, *Molecules*, 2021, **26**, 111.

220. I. Gibson, D. W. Rosen and B. Stucker, *Additive manufacturing technologies*, Springer, 2014.
221. S. Bose, D. Ke, H. Sahasrabudhe and A. Bandyopadhyay, *Progress in Material Science*, 2018, **93**, 45.
222. S. Chang, L. Li, L. Lu and J. Y. Fuh, *Materials*, 2017, **10**, 1313.
223. S. Kumar, *JOM*, 2003, **55**, 43.
224. F. Fina, A. Goyanes, C. M. Madla, A. Awad, S. J. Trenfield, J. M. Kuek, P. Patel, S. Gaisford and A. W. Basit, *International Journal of Pharmaceutics*, 2018, DOI: <https://doi.org/10.1016/j.ijpharm.2018.05.044>.
225. K. Low, K. Leong, C. Chua, Z. Du and C. Cheah, *Rapid Prototyping Journal*, 2001, **7**, 262.
226. C. M. Cheah, K. F. Leong, C. K. Chua, K. H. Low and H. S. Quek, *Proceedings of the Institution of Mechanical Engineers, Part H: Journal of Engineering in Medicine*, 2002, **216**, 369.
227. F. Fina, A. Goyanes, S. Gaisford and A. W. Basit, *International journal of pharmaceutics*, 2017, **529**, 285.
228. F. Fina, C. M. Madla, A. Goyanes, J. Zhang, S. Gaisford and A. W. Basit, *International Journal of Pharmaceutics*, 2018, **541**, 101.
229. A. Awad, F. Fina, S. J. Trenfield, P. Patel, A. Goyanes, S. Gaisford and A. W. Basit, *Pharmaceutics*, 2019, **11**, 148.
230. A. Awad, A. Yao, S. J. Trenfield, A. Goyanes, S. Gaisford and A. W. Basit, *Pharmaceutics*, 2020, **12**, 172.
231. T. T. Ngo, S. Blair, K. Kuwahara, D. Christensen, I. Barrera, M. Domingo and S. Singamneni, *The Journal of Supercritical Fluids*, 2018, **136**, 29.
232. B. M. Wu, S. W. Borland, R. A. Giordano, L. G. Cima, E. M. Sachs and M. J. Cima, *Journal of Controlled Release*, 1996, **40**, 77.
233. W. E. Katstra, R. D. Palazzolo, C. W. Rowe, B. Giritlioglu, P. Teung and M. J. Cima, *Journal of Controlled Release*, 2000, **66**, 1.
234. C. Rowe, W. Katstra, R. Palazzolo, B. Giritlioglu, P. Teung and M. Cima, *Journal of controlled release*, 2000, **66**, 11.
235. C.-C. Wang, M. R. Tejwani, W. J. Roach, J. L. Kay, J. Yoo, H. L. Surprenant, D. C. Monkhouse and T. J. Pryor, *Drug development and industrial pharmacy*, 2006, **32**, 367.
236. D. G. Yu, X. L. Yang, W. D. Huang, J. Liu, Y. G. Wang and H. Xu, *Journal of Pharmaceutical Sciences*, 2007, **96**, 2446.
237. D.-G. Yu, C. Branford-White, Y.-C. Yang, L.-M. Zhu, E. W. Welbeck and X.-L. Yang, *Drug Development and Industrial Pharmacy*, 2009, **35**, 1530.
238. D. G. Yu, X. X. Shen, C. Branford-White, L. M. Zhu, K. White and X. L. Yang, *Journal of Pharmacy and Pharmacology*, 2009, **61**, 323.
239. S. Infanger, A. Haemmerli, S. Iliev, A. Baier, E. Stoyanov and J. Quodbach, *International journal of pharmaceutics*, 2019, **555**, 198.
240. K. Shi, D. K. Tan, A. Nokhodchi and M. Maniruzzaman, *Pharmaceutics*, 2019, **11**, 150.
241. D.-G. Yu, C. Branford-White, Z.-H. Ma, L.-M. Zhu, X.-Y. Li and X.-L. Yang, *International Journal of Pharmaceutics*, 2009, **370**, 160.
242. G. Wu, W. Wu, Q. Zheng, J. Li, J. Zhou and Z. Hu, *Biomedical engineering online*, 2014, **13**, 97.
243. U. Gbureck, E. Vorndran, F. A. Müller and J. E. Barralet, *Journal of Controlled Release*, 2007, **122**, 173.
244. W. Wu, Q. Zheng, X. Guo, J. Sun and Y. Liu, *Biomedical Materials*, 2009, **4**, 065005.
245. W. Wu, C. Ye, Q. Zheng, G. Wu and Z. Cheng, *Journal of biomaterials applications*, 2016, **31**, 250.
246. S. Tarafder and S. Bose, *ACS applied materials & interfaces*, 2014, **6**, 9955.
247. F. Verhaeghe, T. Craeghs, J. Heulens and L. Pandelaers, *Acta Materialia*, 2009, **57**, 6006.
248. M. Brandt, *Laser Additive Manufacturing: Materials, Design, Technologies, and Application*, Woodhead Publishing, Duxford, 2016.

249. S. Maher, G. Kaur, L. Lima-Marques, A. Evdokiou and D. Losic, *ACS applied materials & interfaces*, 2017, **9**, 29562.
250. R. Allen, *HP Journal* 1985, 21.
251. L. Wang, S. T. Beyer, Q. C. Cronk and K. Walus, *Plant Methods*, 2011, **7**, 1.
252. W. Huang, Q. Zheng, W. Sun, H. Xu and X. Yang, *International journal of pharmaceuticals*, 2007, **339**, 33.
253. W. Wu, Q. Zheng, X. Guo and W. Huang, *Journal of Wuhan University of Technology-Mater. Sci. Ed.*, 2009, **24**, 977.
254. E. Vorndran, U. Klammert, A. Ewald, J. E. Barralet and U. Gbureck, *Advanced Functional Materials*, 2010, **20**, 1585.
255. Y. Gu, X. Chen, J.-H. Lee, D. A. Monteiro, H. Wang and W. Y. Lee, *Acta Biomaterialia*, 2012, **8**, 424.
256. C. Planchette, H. Pichler, M. Wimmer-Teubenbacher, M. Gruber, H. Gruber-Wölfler, S. Mohr, C. Tetyczka, W.-K. Hsiao, A. Paudel and E. Roblegg, *International journal of pharmaceuticals*, 2016, **509**, 518.
257. G. F. Acosta-Vélez, C. S. Linsley, M. C. Craig and B. M. Wu, *Bioengineering*, 2017, **4**, 11.
258. M. Kyobula, A. Adedeji, M. R. Alexander, E. Saleh, R. Wildman, I. Ashcroft, P. R. Gellert and C. J. Roberts, *Journal of Controlled Release*, 2017, **261**, 207.
259. E. A. Clark, M. R. Alexander, D. J. Irvine, C. J. Roberts, M. J. Wallace, J. Yoo and R. D. Wildman, *International Journal of Pharmaceuticals*, 2020, **578**, 118805.
260. P. A. Meléndez, K. M. Kane, C. S. Ashvar, M. Albrecht and P. A. Smith, *Journal of pharmaceutical sciences*, 2008, **97**, 2619.
261. A. B. M. Buanz, M. H. Saunders, A. W. Basit and S. Gaisford, *Pharmaceutical Research*, 2011, **28**, 2386.
262. C. Varan, H. Wickström, N. Sandler, Y. Aktaş and E. Bilensoy, *International Journal of Pharmaceuticals*, 2017, **531**, 701.
263. N. Sandler, A. Määttänen, P. Ihalainen, L. Kronberg, A. Meierjohann, T. Viitala and J. Peltonen, *Journal of Pharmaceutical Sciences*, 2011, **100**, 3386.
264. N. Genina, D. Fors, H. Vakili, P. Ihalainen, L. Pohjala, H. Ehlers, I. Kassamakov, E. Haeggström, P. Vuorela, J. Peltonen and N. Sandler, *European Journal of Pharmaceutical Sciences*, 2012, **47**, 615.
265. N. Scoutaris, M. R. Alexander, P. R. Gellert and C. J. Roberts, *Journal of Controlled Release*, 2011, **156**, 179.
266. B. K. Lee, Y. H. Yun, J. S. Choi, Y. C. Choi, J. D. Kim and Y. W. Cho, *International Journal of Pharmaceuticals*, 2012, **427**, 305.
267. P. J. Tarcha, D. Verlee, H. W. Hui, J. Setesak, B. Antohe, D. Radulescu and D. Wallace, *Annals of biomedical engineering*, 2007, **35**, 1791.
268. M. Matsusaki, K. Sakaue, K. Kadowaki and M. Akashi, *Advanced healthcare materials*, 2013, **2**, 534.
269. B. Han, G. Y. Yun, J. W. Boley, S. H. Kim, J. Y. Hwang, G. T.-C. Chiu, and K. Park and *International Journal of Heat Mass Transfer*, 2016, **97**, 15.
270. D. Raijada, N. Genina, D. Fors, E. Wisaeus, J. Peltonen, J. Rantanen and N. Sandler, *Journal of Pharmaceutical Sciences*, 2013, **102**, 3694.
271. L. Hirshfield, A. Giridhar, L. S. Taylor, M. T. Harris and G. V. Reklaitis, *Journal of pharmaceutical sciences*, 2014, **103**, 496.
272. H. Y. Hsu, M. T. Harris, S. Toth and G. J. Simpson, *AIChE Journal*, 2015, **61**, 4502.
273. M. J. Uddin, N. Scoutaris, P. Klepetsanis, B. Chowdhry, M. R. Prausnitz and D. Douroumis, *International journal of pharmaceuticals*, 2015, **494**, 593.
274. H. Wickström, M. Palo, K. Rijckaert, R. Kolakovic, J. O. Nyman, A. Määttänen, P. Ihalainen, J. Peltonen, N. Genina and T. de Beer, *European Journal of Pharmaceutical Sciences*, 2015, **75**, 91.

275. H. Wickström, E. Hilgert, J. O. Nyman, D. Desai, D. Şen Karaman, T. de Beer, N. Sandler and J. M. Rosenholm, *Molecules*, 2017, **22**, 2020.
276. E. İçten, H. S. Purohit, C. Wallace, A. Giridhar, L. S. Taylor, Z. K. Nagy and G. V. Reklaitis, *International journal of pharmaceuticals*, 2017, **524**, 424.
277. E. A. Clark, M. R. Alexander, D. J. Irvine, C. J. Roberts, M. J. Wallace, S. Sharpe, J. Yoo, R. J. Hague, C. J. Tuck and R. D. Wildman, *International journal of pharmaceuticals*, 2017, **529**, 523.
278. J. Goole and K. Amighi, *International journal of pharmaceuticals*, 2016, **499**, 376.
279. J. Gonzalez, J. Mireles, Y. Lin and R. B. Wicker, *Ceramics International*, 2016, **42**, 10559.
280. K. B. Anderson, S. Y. Lockwood, R. S. Martin and D. M. Spence, *Analytical chemistry*, 2013, **85**, 5622.
281. M. Cui, H. Pan, D. Fang, H. Sun, S. Qiao and W. Pan, *International Journal of Pharmaceuticals*, 2021, **596**, 120201.
282. S.-Y. Chang, S. W. Li, K. Kowsari, A. Shetty, L. Sorrells, K. Sen, K. Nagapudi, B. Chaudhuri and A. W. K. Ma, *Journal of Pharmaceutical Sciences*, 2020, **109**, 3054.
283. J. A. Inzana, R. P. Trombetta, E. M. Schwarz, S. L. Kates and H. A. Awad, *European cells & materials*, 2015, **30**, 232.
284. J. Xi, J. E. Yuan, Y. Zhang, D. Nevorski, Z. Wang and Y. Zhou, *Pharmaceutical research*, 2016, **33**, 1527.
285. J. U. Lind, T. A. Busbee, A. D. Valentine, F. S. Pasqualini, H. Yuan, M. Yadid, S.-J. Park, A. Kotikian, A. P. Nesmith and P. H. Campbell, *Nature materials*, 2017, **16**, 303.
286. K. Barton, S. Mishra, K. A. Shorter, A. Alleyne, P. Ferreira and J. Rogers, *Mechatronics*, 2010, **20**, 611.
287. S. Mishra, K. L. Barton, A. G. Alleyne, P. M. Ferreira, and J. Rogers, *Journal of Micromechanics and Microengineering*, 2010, **20**, 095026.
288. Y. Yang, C. Tong, J. Zhong, R. Huang, W. Tan and Z. Tan, *Journal of Biomedical Materials Research Part B: Applied Biomaterials*, 2017.
289. J.-C. Wang, H. Zheng, M.-W. Chang, Z. Ahmad and J.-S. Li, *Scientific Reports*, 2017, **7**, 43924.
290. B. Wang, Z. Ahmad, J. Huang, J.-S. Li and M.-W. Chang, *Chemical Engineering Journal*, 2018, **343**, 379.
291. S. E. Moulton and G. G. Wallace, *Journal of controlled release*, 2014, **193**, 27.
292. M. Alomari, F. H. Mohamed, A. W. Basit and S. Gaisford, *International Journal of Pharmaceuticals*, 2015, **494**, 568.
293. W. Katstra, R. Palazzolo, C. Rowe, B. Giritlioglu, P. Teung and M. Cima, *Journal of controlled release*, 2000, **66**, 1.
294. A. Jassim-Jaboori and M. Oyewumi, *Journal of Biomolecular Research & Therapeutics*, 2015, **4**, 1.
295. I. D. Ursan, L. Chiu and A. Pierce, *Journal of the American Pharmacists Association*, 2013, **53**, 136.
296. D. G. Yu, L.-M. Zhu, C. J. Branford-White and X. L. Yang, *Journal of pharmaceutical sciences*, 2008, **97**, 3666.
297. C. L. Ventola, *Pharmacy and Therapeutics*, 2014, **39**, 704.
298. H. Vakili, R. Kolakovic, N. Genina, M. Marmion, H. Salo, P. Ihalainen, J. Peltonen and N. Sandler, *International journal of pharmaceuticals*, 2015, **483**, 244.
299. R. Kolakovic, T. Viitala, P. Ihalainen, N. Genina, J. Peltonen and N. Sandler, *Expert opinion on drug delivery*, 2013, **10**, 1711.
300. N. Genina, E. M. Janßen, A. Breitenbach, J. Breitreutz and N. Sandler, *European Journal of Pharmaceuticals and Biopharmaceuticals*, 2013, **85**, 1075.
301. N. Sandler and M. Preis, *Trends in pharmacological sciences*, 2016, **37**, 1070.
302. M. A. Alhnan, T. C. Okwuosa, M. Sadia, K.-W. Wan, W. Ahmed and B. Arafat, *Pharmaceutical Research*, 2016, **33**, 1817.

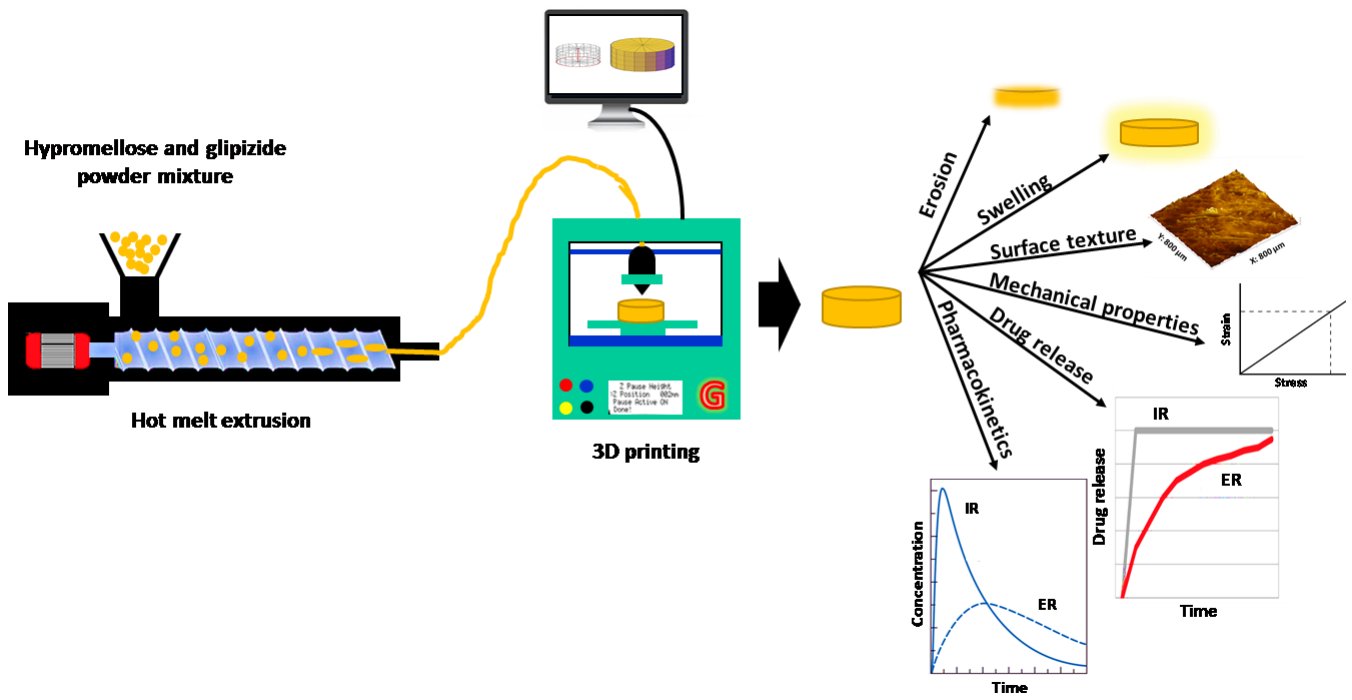
303. I.-B. Dumitrescu, D. Lupuliasa, C. M. Drăgoi, A. C. Nicolae, A. Pop, G. ŞARAMET and D. J. F. DRĂGĂNESCU, *Farmacia*, 2018, **66**, 365.
304. J. Zhang, A. Q. Vo, X. Feng, S. Bandari and M. A. Repka, *AAPS PharmSciTech*, 2018, **19**, 3388.
305. J.-P. Kruth, X. Wang, T. Laoui and L. J. Froyen, *Assembly Automation*, 2003, **23**, 357.
306. S. F. S. Shirazi, S. Gharekhani, M. Mehrali, H. Yarmand, H. S. C. Metselaar, N. A. Kadri, N. A. A. Osman, *Science and Technology of Advanced Materials*, 2015, **16**, 033502.
307. J. Norman, R. D. Madurawe, C. M. Moore, M. A. Khan and A. Khairuzzaman, *Advanced drug delivery reviews*, 2017, **108**, 39.
308. F. Fina, A. Goyanes, S. Gaisford and A. W. Basit, *International Journal of Pharmaceutics*, 2017, **529**, 285.
309. J. Long, H. Gholizadeh, J. Lu, C. Bunt and A. Seyfoddin, *Current Pharmaceutical Design*, 2017, **23**, 433.
310. L. Zema, A. Melocchi, A. Maroni and A. Gazzaniga, *Journal of Pharmaceutical Sciences*, 2017, **106**, 1697.
311. N. Economidou, D. A. Lamprou and D. J. Douroumis, *International Journal of Pharmaceutics*, 2018, **544**, 415.
312. N. G. Solanki, M. Tahsin, A. V. Shah and A. T. Serajuddin, *Journal of Pharmaceutical Sciences*, 2018, **107**, 390.
313. G. Verstraete, A. Samaro, W. Grymonpré, V. Vanhoorne, B. Van Snick, M. Boone, T. Hellemans, L. Van Hoorebeke, J. P. Remon and C. Vervaet, *International Journal of pharmaceutical Sciences*, 2018, **536**, 318.
314. W. Jamroz, M. Kurek, E. Łyszczarz, W. Brniak and R. Jachowicz, *Acta Poloniae Pharmaceutica. Drug Research*, 2017, 74.
315. M. Palo, J. Holländer, J. Suominen, J. Yliruusi and N. Sandler, *Expert review of medical devices*, 2017, **14**, 685.
316. S. A. Khaled, J. C. Burley, M. R. Alexander and C. J. Roberts, *International Journal of pharmaceutics*, 2014, **461**, 105.
317. K. Chockalingam, N. Jawahar and U. Chandrasekhar, *Rapid Prototyping Journal*, 2006.
318. J. M. DeSimone, E. T. Samulski, A. Ermoshkin and P. M. DeSimone, *Google patents*, 2016.
319. J. M. DeSimone, E. T. Samulski and J. P. Rolland, *US Google patents*, 2017.
320. A. Marino, J. Barsotti, G. de Vito, C. Filippeschi, B. Mazzolai, V. Piazza, M. Labardi, V. Mattoli, G. Ciofani, *ACS applied materials & interfaces*, 2015, **7**, 25574.
321. S. H. Lim, H. Kathuria, J. J. Y. Tan and L. Kang, *Advanced drug delivery reviews*, 2018, **132**, 139.
322. D. Rajjada, N. Genina, D. Fors, E. Wisaeus, J. Peltonen, J. Rantanen and N. Sandler, *Journal of Pharmaceutical Sciences*, 2013, **102**, 3694.
323. M. Scarpa, S. Stegemann, W.-K. Hsiao, H. Pichler, S. Gaisford, M. Bresciani, A. Paudel and M. Orlu, *International Journal of Pharmaceutics*, 2017, **523**, 327.
324. W. S. Cheow, T. Y. Kiew, and K. J. Hadinoto, *Biopharmaceutics*, 2015, **96**, 314.
325. M. Edinger, D. Bar-Shalom, N. Sandler, J. Rantanen and N. Genina, *International Journal of Pharmaceutics*, 2018, **536**, 138.
326. S. J. Trenfield, A. Awad, A. Goyanes, S. Gaisford and A. W. Basit, *Trends in pharmacological sciences*, 2018, **39**, 440.
327. M. Di Prima, J. Coburn, D. Hwang, J. Kelly, A. Khairuzzaman and L. Ricles, *3D printing in medicine*, 2016, **2**, 1.
328. M. R. Araújo, L. L. Sa-Barreto, T. Gratieri, G. M. Gelfuso and M. Cunha-Filho, *Pharmaceutics*, 2019, **11**, 128.
329. O. Bhusnure, V. Gholve, B. Sugave, R. Dongre, S. Gore and P. S. Giram, *International Journal of Bioassys*, 2016, **5**, 4723.
330. K. Wren, *Science*, 2013, **342**, 439.

331. C. Schubert, M. C. Van Langeveld and L. A. Donoso, *British Journal of Ophthalmology*, 2014, **98**, 159.
332. J. Banks, *IEEE pulse*, 2013, **4**, 22.
333. I. T. Ozbolat and Y. Yu, *IEEE Transactions on Biomedical Engineering*, 2013, **60**, 691.
334. X. Cui, T. Boland, D. DD'Lima and M. K Lotz, *Recent patents on drug delivery & formulation*, 2012, **6**, 149.
335. F. A. Maulvi, M. J. Shah, B. S. Solanki, A. S. Patel, T. G. Soni, D. O. Shah and Res, 2017, **9**, 44.

CHAPTER 3

**Plasticiser-free 3D printed hydrophilic matrices:
quantitative 3D surface texture, mechanical,
swelling, erosion, drug release and
pharmacokinetic studies.**

Graphical abstract



Notes for readers

- Hydroxypropyl methyl cellulose, HPMC, a hydrophilic polymer, is widely used for the development of extended-release hydrophilic matrices and it is also considered as a good contender for the fabrication of 3D printing of matrix tablets. It is often combined with plasticisers to enable the extrusion.
- The aim of the current project was to develop plasticizer-free 3D printed hydrophilic matrices using drug loaded filaments prepared via HME to achieve an *in vitro* (swelling, erosion and drug release) and *in vivo* (drug absorption) performance which is analogous to hydrophilic matrix tablets developed through conventional approaches.
- Additionally, the morphology of the printed tablets was studied using quantitative 3D surface texture studies and the porosity calculated. Filaments were produced successfully and used to produce matrix tablets with acceptable drug loading (95-105 %), mechanical and surface texture properties regardless of the employed HPMC grade.
- The viscosity of HPMC had a discernible impact on the swelling, erosion, HPMC dissolution, drug release and pharmacokinetic findings. The highest viscosity grade (K100M) results in higher degree of swelling, decreased HPMC dissolution, low matrix erosion, decreased drug release and extended drug absorption profile.
- Overall, this study demonstrated that the drug loaded (glipizide) filaments and matrix tablets of medium to high viscosity grades of HPMC, without the aid of plasticisers, can be successfully prepared. Furthermore, the *in vitro* and *in vivo* studies have revealed the successful fabrication of extended-release matrices.

3.1. Introduction

To understand the potential of the FDM printing process and how any variation or modification will affect the performance and the functionality of the products, additional work is required. Many research groups have attempted to develop filaments using individual or a combination of pharmaceutical polymers along with other excipients (plasticisers) by hot melt extrusion (HME) ¹⁻⁴. HME coupled with FDM has several advantages over conventional tablet manufacturing including an increased capacity for drug loading. A study carried out by Pietrzak et al., (2015) ⁵ combined FDM 3D printing with HME in an attempt to extend the range of polymers that can be used and achieve higher drug loading. They demonstrated the feasibility of printing immediate and extended theophylline caplets based on cellulosic or methacrylic polymeric filaments with 50% w/w drug loading. Moreover, numerous other studies have demonstrated the adaptability of various polymers with FDM including: acrylonitrile butadiene styrene ⁶, poly ϵ -caprolactone ², ethyl cellulose ¹, ethyl vinyl acetate ⁷, hydroxypropyl cellulose ^{5, 8}, hydroxypropyl methylcellulose acetate succinate ⁹, and hydroxypropyl methyl cellulose, (HPMC) ¹⁰⁻¹².

Among these polymers, HPMC is the most widely used for developing drug-loaded filaments and has previously been used to fabricate 3D printed tablets ¹⁰⁻¹². Polymers are often combined with plasticisers to facilitate their extrusion. The inclusion of plasticiser may impact the glass transition (T_g) temperature, as described by Bruce et al., (2005) ¹³ polyethylene glycol, triacetin and triethyl citrate are commonly used plasticisers ^{1, 3, 4} however, various studies have demonstrated that the presence of these aforementioned plasticisers either alone or in pharmaceutical formulations may have an impact on gastrointestinal motility, affecting gastric and intestinal transit times ¹⁴⁻¹⁶. Both gastric and intestinal transit play an important role during drug absorption. Thus, their presence especially in hydrophilic matrices could have an impact on their functional performance ¹⁷. Furthermore, these above findings, related to plasticiser induced gastric motility become more significant for individuals suffering from chronic diseases, for example diabetes and cardiac disorders, where patients have to be on life-long pharmacotherapy and excessive exposure to plasticisers might lead to drug absorption complications.

In order to be used in the FDM process, the drug-loaded filaments need to be mechanically robust as soft or brittle filaments will be damaged by the feeding gear. Mechanical studies

such as a three-point bending test can be used to characterize material properties. Additionally, using FDM for tablet production can lead to products with seam-line issues and unsatisfactory seam-line issues, affecting both appearance and possibly performance ¹⁸. Porosity is an important characteristic of hydrophilic matrices as higher overall porosity leads to rapid penetration of liquid molecules in comparison to lower overall porosity thus impacting the swelling behaviour ¹⁹. In order to address these challenges, we proposed to develop plasticizer-free 3D printed hydrophilic matrices using drug loaded filaments prepared via HME to achieve an in vitro (swelling, erosion and drug release) and in vivo (drug absorption) performance which is analogous to hydrophilic matrix tablets developed through conventional approaches. To address issues with tablet appearance, porosity and quantitative 3D surface texture studies) were carried out using mercury intrusion porosimetry and white light optical profilometry, respectively. Glipizide which is an anti-diabetic drug of the sulfonylurea class indicated to treat type 2 diabetes was used as a model drug. Glipizide is a weak acid (pKa = 5.9), practically insoluble in water and acid, and is highly permeable (biopharmaceutics classification system, BCS II). It appears to be an effective insulin secretagogue which reaches a peak plasma concentration within 1–3 h after a single oral dose with an elimination half-life of about 2–4 h ²⁰. Such rapidly absorbed drugs having fast elimination rates with short half-life make it suitable candidate to be considered for sustained delivery.

3.2. Material and methods

3.2.1. Materials

Glipizide was used as the model drug and purchased from TCI Europe (Zwijndrecht, Belgium). HPMC polymer of different grades with increasing molecular size/weight (Methocel® K4M, K15M and K100M) was kindly provided by Colorcon Ltd (UK). Specifications of different HPMC grades are listed in Table 3.1.

Table 3.1: Specifications of different HPMC grades used in this study.

Methocel®	Viscosity (cps)^a	Average molar mass g/mol^a
K4M	4351	~88000
K15M	17129	~125000
K100M	79279	~215000

3.2.2. Preparation of filaments

The glipizide loaded filaments of each HPMC grade (K4M, K15M and K100M) were developed from the premixed HPMC: glipizide (2.5% w/w) powder mixtures using a single screw extruder (Noztek® Pro pellet and powder extruder, Sussex, UK). The extrusion temperature and nozzle diameter were 155 °C and 1.75 mm, respectively. Once the filaments were extruded, they were stored in a desiccator at room temperature until further use.

3.2.3. Physicochemical characterisation of filaments

3.2.3.1. Determination of drug loading

A sample (0.2 g) of the glipizide-loaded filament of each polymer grade was placed in a 1 litre methanol: water (1:1) solvent mixture under magnetic stirring until complete dissolution. Liquid samples were then filtered, and the dissolved glipizide content was determined using UV spectroscopy, all the measurements were carried out in triplicate.

3.2.3.2. Differential scanning calorimetry (DSC)

Differential scanning calorimetry (Mettler Toledo SC 821, Mettler-Toledo Ltd., and Leicester, UK) was used to study all the powder samples (plain drug, polymers and their extruded filaments). Briefly, 5–10 mg of the samples were placed in standard aluminium pans and experiment was run under nitrogen environment (50 mL/min). To assess the physical form of the glipizide within the polymeric matrix a heat scan from 25-250 °C was applied to the samples at 10 °C/min.

3.2.3.3. Thermogravimetric analysis (TGA)

TGA was performed using Mettler Thermobalance TG50 (Mettler-Toledo Ltd., Leicester, UK). Open alumina crucibles were used to analyse all the plain powder samples and filaments (5-10 mg). Samples were heated from 25 - 250 °C at 10 °C/min heating rate and nitrogen was used as purge gas with a flow rate of 50 ml/min.

3.2.3.4. X-ray powder diffraction (XRPD)

Samples (plain drug and polymers) and filaments were characterised using a D2-Phase X-ray diffractometer (Bruker UK Ltd., Coventry, UK) equipped with a CuK α radiation source at 30 KV voltage and 10 mA current. Diffraction patterns were obtained in the 2 theta (θ) range of 5°–100° using 0.02 step sizes.

3.2.3.5. Scanning electron microscopy (SEM)

The morphology of all the drug loaded filaments was observed using scanning electron microscopy (SEM) ²¹. Briefly, samples were mounted onto stubs using double-sided adhesive tape and were sputter-coated with gold/palladium (80:20) for 60 seconds using a Quorum SC7620 Sputter Coater (Quorum Technologies, Laughton, UK) and were examined photometrically using Jeol JSM-6060CV, Jeol Inc. Peabody, MA, USA.

3.2.3.6. Mechanical testing

All the extruded HPMC: glipizide filaments were cut in to 10 cm pieces and were placed on a TA-95N 3-point bend probe set which was attached to a TA-XT2i texture analyser (Stable Micro Systems Ltd, Surrey, UK) for mechanical characterisation. The moving speed of the blade was 5 mm/s until it reached 15 mm under the sample. The mechanical data was collected and analysed using Exponent[®] software (Stable Micro Systems Ltd, Surrey, UK).

3.2.4. Fabrication of 3D printed glipizide matrix tablets

A cylindrical tablet was designed (5 mm in diameter with a 2.5 mm height) using SolidWorks[®] version 2015, then converted into stl. (stereolithographic) format. The drug loaded filaments were loaded into MakerBot replicator mini (MakerBot Inc., New York, NY, USA) using a

constant infill density (100 %) and pattern (linear). The 3D printing parameters used in the preparation of matrices are listed in Table 3.2.

Table 3.2: Parameters used for the 3D printing of HPMC/glipizide matrices.

Printing temperature °C	Number of shells	Layer height (mm)	Raft	Support	Infill density (%)	Speed while extrusion (mm/sec)	Speed while traveling (mm/sec)	Infill pattern
170	2	0.1	No	No	100	90	150	Linear

3.2.5. Characterisation of 3D printed matrices

3.2.5.1. Geometrical, porosity and morphological assessment of matrices

A digital calliper was used to determine the diameter and thickness of the tablets and the porosity of the 3D printed matrices was determined using mercury intrusion porosimetry (Auto Pore IV 9500, Micrometrics, USA) ²². The surface morphology of the printed matrices was assessed using Jeol JSM-6060CV, Jeol Inc. Peabody, MA, USA.

3.2.5.2. Determination of tablet strength

A general material testing machine (Testometric M500 – 50 CT, Testometric Company Ltd., United Kingdom) was used for hardness testing of the matrix tablets. The printed tablets were placed diametrically, and force was applied by the movement of upper punch at the rate of 10 mm/min until the tablet breaks. Ten tablets from each group of matrix tablets were tested.

3.2.5.3. Determination of tablet friability

10 tablets from each group were weighed and placed in the tablet friability testing instrument (PTF 20E, Pharmatest, Hainburg, Germany). The drum of the friability instrument was then rotated at 20 rpm for 5 min and tablets were re-weighed. The friability was calculated in terms of weight loss and expressed as a percentage of the original weight of the tablets.

3.2.5.4. 3D nanoscale surface texture analysis

Surface texture of 3D printed matrix tablets was examined using Talysurf CCI 3000 optical 3D surface profiler and the method was adopted as previously described by Diryak et al., 2018²³ and Khizer et al., 2019¹¹. Briefly, the tablet was fixed on a stainless steel wafer (3 × 3 cm) using double-sided transparent tape and a 800 × 800 μm region of each tablet was scanned and 3D quantitative surface texture parameters were calculated using MATLAB 2017 (The Math Works, Inc. Massachusetts, USA)¹¹.

3.2.5.5. Swelling studies

Swelling studies were carried out using USP apparatus I, SR II 6-flask (Hanson Research, USA) at 75 rpm at 37 °C. The pre-weighed 3D printed matrix tablets (W_i) were immersed in 900 mL swelling media for 2 h in simulated gastric fluid, SGF pH 1.2 and 22 h in simulated intestinal fluid, SIF pH 6.8. The previously weighed baskets, containing hydrated matrix tablets, were removed at different time points, lightly blotted with 125 mm filter paper (Whatman®, UK) to remove excess liquid, reweighed (W_s) and were rapidly replaced back into the swelling media in dissolution apparatus. The mean weight was determined for each formulation and degree of swelling (S) was calculated by using Equation 3.1²⁴⁻²⁶.

$$S = \frac{W_s - W_i}{W_i} \times 100 \quad Eq. 3.1$$

Where W_i and W_s are the initial dry and swollen weight of the matrix tablet, respectively, at immersion time (t) in the swelling media. The degree of swelling was determined from the mean of three replicates and presented as degree of swelling (S , %) against time (t).

3.2.5.6. In vitro glipizide dissolution studies

The in vitro glipizide dissolution studies were carried out using USP I basket apparatus where the basket rotation speed and temperature were maintained at 75 rpm and 37 °C, respectively. The pre-weighed 3D printed matrix tablets were immersed in 900 mL dissolution media for 2 h in simulated gastric fluid (pH 1.2) and then 22 h in simulated intestinal fluid (pH 6.8). At predetermined times, 5 mL aliquots were drawn from the dissolution apparatus and

replaced with 5 mL of fresh dissolution media. The released glipizide was quantified using UV-spectroscopy at λ max (225 nm) and glipizide mass was determined using a standard calibration curve, all the measurements were carried out in triplicate.

3.2.5.7. HPMC dissolution and overall erosion studies

To quantify dissolved HPMC, a previously described procedure was adapted to enable analysis of multiple samples²⁷⁻³⁰. In the modified method, 20 μ L of 5% v/v phenol was added to 20 μ L of liquid sample containing HPMC previously placed into a microplate followed by mixing (5 minutes) using shaking plate. Once these were mixed, 100 μ L of H₂SO₄ was added to each well and subjected to mixing again for 5 minutes. The solutions were then incubated for 15 min at room temperature (20-25 °C) before the UV absorbance was read at 488 nm using a microplate reader and dissolved HPMC was quantified using a standard calibration curve for each grade of HPMC. Moreover, overall matrix erosion was calculated by simply adding the quantities of drug and HPMC dissolved at a specified time point.

3.2.6. Pharmacokinetic studies

3.2.6.2. Animal housing and handling

White albino rabbits weighing 2.20 –2.50 kg were used in these experiments which were further divided into four groups, group I -IV (five rabbits per group). All rabbits were housed individually in cages under environmentally controlled conditions (25 \pm 2 °C; 50 \pm 5 % relative humidity). All the rabbits had free access to food and water except for during the final 24 h before the experiments. The study protocol was approved by the Pharmacy Research Ethics Committee (PREC) at the University of Sargodha, Pakistan (UOS/PERC/101).

3.2.6.3. In vivo experiments

A single-dose pharmacokinetic study was carried out and rabbits of group I were administered glipizide oral solution (2.5 mg in 20 mL of deionised water) and 3D printed glipizide matrix tablets of K4M, K15M and K100M (100 \pm 1.5 mg containing 2.5 % w/w glipizide) were administered to the rabbits of group II, III and IV, respectively. At different time intervals (0, 15, 30, 60, 90, 120, 150, 180, 240, 300, 360, 420, 480, 540, 600, 660, 720, 1080, 1440 minutes), 1 mL of blood samples were collected from the marginal ear vein into heparinised tubes. The

collected blood samples were then centrifuged for 15 min at an ambient temperature. After centrifugation the plasma layer was separated and was stored at -20 °C until analysed.

3.2.6.4. Quantification of glipizide in plasma

0.5 mL of the rabbit plasma was acidified with 150 µL 0.5 M HCl and vortex-mixed for 2 min. This acidified plasma was then further mixed with benzene for 3 min and centrifuged for 15 min at 4400 rpm. The organic layer was separated and dried at 35 °C under a nitrogen stream³¹. Once dried the residues were dissolved in 200 µL methanol and filtered. The filtrate (20 µL) was then injected into the HPLC consisting of reverse phase C-18 column (Phenomenex). The mobile phase used was acetonitrile: methanol: H₂O (40:10:50 % v/v) at a flow rate of 1mL/min and glipizide was detected using UV at a wavelength of 275 nm.

3.2.6.5. Determination of pharmacokinetic parameters

PKSolver program, an add-in macro for Microsoft Excel®, was employed for the calculation of the different pharmacokinetic parameters³².

3.3. Results and discussion

3.3.1. Development and characterisation of filaments

Glipizide loaded HPMC filaments were successfully extruded without the aid of plasticiser using HME (Figure 3.1a). The glipizide loading (2.5% w/w) in extruded filaments of each grade (K4M, K15M and K100M) was within the pharmacopoeial assay limit. Notably, in the present research higher glipizide loading was achieved in comparison to previously reported results³³ (Table 3.3).

Thermal analysis (DSC and TGA) and XRD were conducted on powdered drug sample and extruded filaments. Glipizide powder shows a sharp endothermic melting peak at 214.5 °C, demonstrating its crystalline nature (Figure 3.2a). The lack of a melting peak in the DSC thermograms of HPMC displayed in Figure 3.2b indicated that the polymer is amorphous. DSC thermograms were also acquired for HPMC: glipizide filaments for all grades of HPMC to investigate any drug-polymer interactions and they also confirmed there was no crystalline drug evident in the extruded filament (Figure 3.2c). The TGA results showed that onset of

degradation for both drug and filaments was above the operating temperature (170 °C) involved in the printing process (Figure 3.3). Furthermore, the crystalline structure of glipizide was confirmed by XRD of the drug which showed multiple high-intensity peaks (Figure 3.4a). XRD scans of different grades of HPMC filaments showed no peaks and scattering of x-rays was also not observed, highlighting the amorphous nature of the polymer (Figure 3.4b). Additionally, high intensity multiple peaks of glipizide were not seen in the XRD scan of drug loaded filaments which is likely due to the formation of a solid dispersion that might have masked the crystalline structure of glipizide (Figure 3.4c) ¹¹. Overall, XRD spectra of glipizide and drug loaded HPMC filaments were consistent with the DSC profiles, thus, both methods showed that glipizide has a crystalline structure, whereas HPMC and drug loaded filaments have amorphous nature. This may potentially enhance dissolution but could negatively impact stability. Additionally, SEM micrographs of HPMC filaments of different grades showed cylindrical shapes and smooth surfaces without any visible fine powder particles (Figure 3.5 a, e and i).

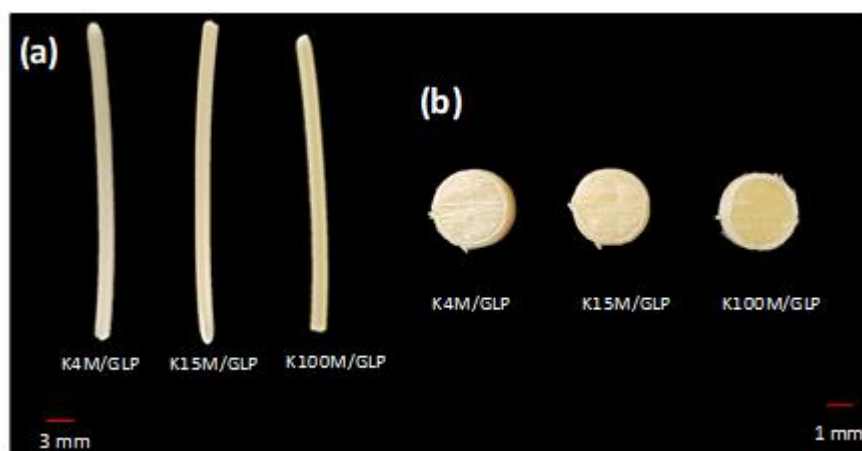


Figure 3.1: (a) Hot melt extruded filaments and (b) 3D printed hydrophilic matrices.

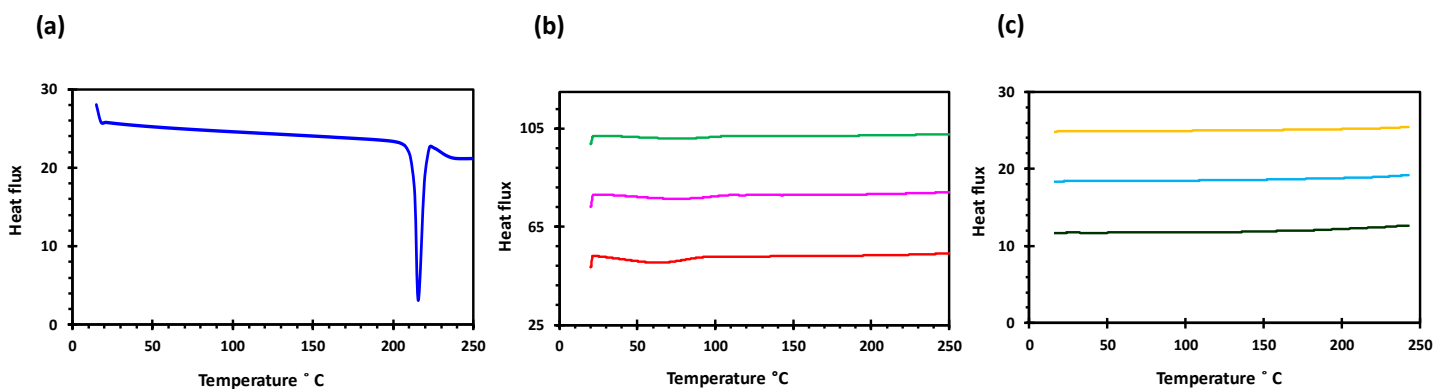


Figure 3.2: DSC profiles of (a) glipizide, (b) HPMC (K4M, K15M and K100M) and (c) K4M/GLP, K15M/GLP and K100M/GLP filaments.

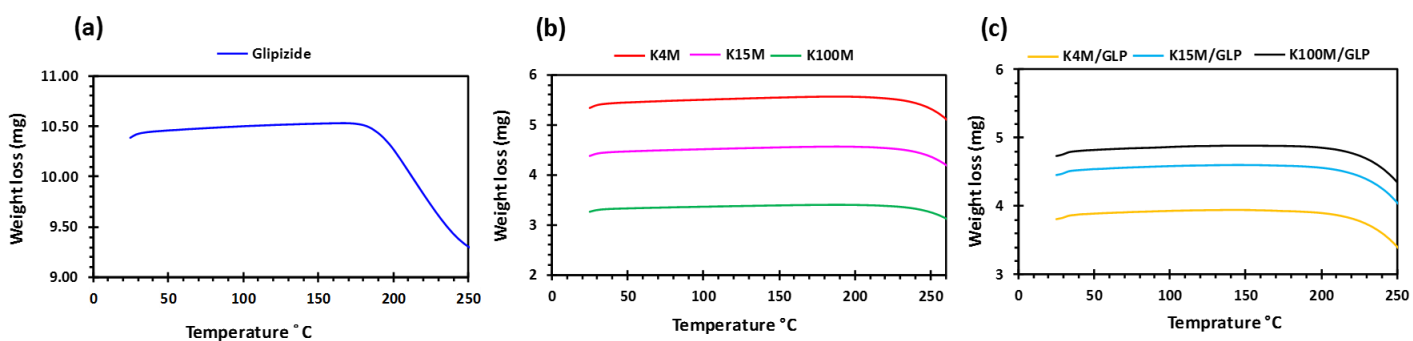


Figure 3.3: TGA profiles of (a) glipizide, (b) HPMC (K4M, K15M and K100M) and (c) K4M/GLP, K15M/GLP and K100M/GLP filaments.

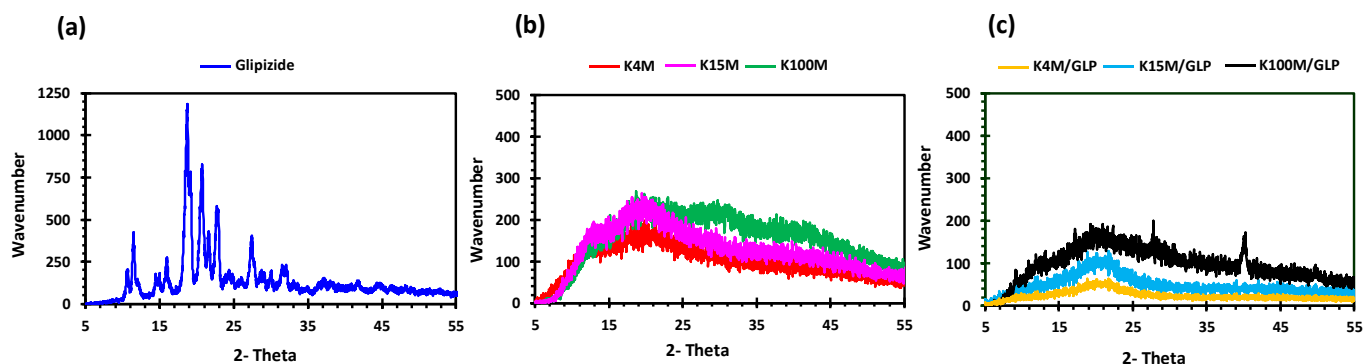


Figure 3.4: XRD profiles of (a) glipizide, (b) HPMC (K4M, K15M and K100M) and (c) K4M/GLP, K15M/GLP and K100M/GLP filaments.

For successful 3D printing, good mechanical properties are essential as brittle filaments tend to crumble whereas too soft filaments may be squeezed aside by the feeding gear leading to printing failure. Hence, in this study a three-point bending test was used to evaluate the mechanical properties of the extruded filaments^{34,35} (Table 3.3). The force required to break the filaments was lowest for K4M filaments (1.9 ± 0.2 N) followed by K15M (2.2 ± 0.6 N) and K100M (2.3 ± 0.3 N). This trend was also seen in the stress required to break the filaments with K4M requiring 12.3 ± 1.1 MPa, K15M requiring 14.2 ± 1.2 MPa and K100M requiring 16.9 ± 1.6 MPa. The breaking distance for all the filaments extruded in this study was in the range of 4.9 - 5.2 mm. Moreover, Young's modulus increased with polymer molar mass indicating increased polymer chain entanglement during the extrusion process. It has previously been reported that filaments with a breaking distance (toughness) of less than 1.5 mm were too brittle to be loaded into a 3D printer and were easily broken by the feeding gear³⁶. All the filaments in this study demonstrated good mechanical properties (Table 3.3) and were successfully employed for the manufacturing hydrophilic matrices with constant infill design (linear) and density (100%) (Figure 3.1b). Interestingly, the mechanical performance of the extruded filaments is comparable to those of filaments developed by different researchers using plasticisers¹⁰. This interesting behaviour might be linked to plasticisation of the polymer by the comparatively low molar mass glipizide which has not only reduced its Tg but also helped its extrusion. It could plasticise the polymer by reducing the secondary forces (hydrogen bonding and van der Waals forces) between the HPMC polymer chains by occupying intermolecular spaces. Therefore, the glipizide has changed the three-dimensional organisation of HPMC polymer chains which has reduced the overall energy required for molecular motion and the HME operating temperature well below the Tg of HPMC and has also improved the mechanical properties³⁷.

Table 3.3: Drug loading and three-point bending results of filaments (*n=10, standard deviations are in parenthesis).

Characteristics	K4M	K15M	K100M
Drug loading efficiency (%)	98.7 (2.2)	101.2 (1.1)	99.3 (1.6)
Force (N)	1.9 (0.2)	2.2(0.6)	2.3 (0.3)
Distance (mm)	4.9 (1.2)	5.1 (1.1)	5.2 (1.4)
Stress (MPa)	12.3 (1.1)	14.2 (1.2)	16.9 (1.6)
Strain	0.8 (0.2)	0.9 (0.2)	0.80 (0.1)
Young modulus, E (MPa)	14.7 (1.2)	17.1 (1.4)	21.1 (1.6)

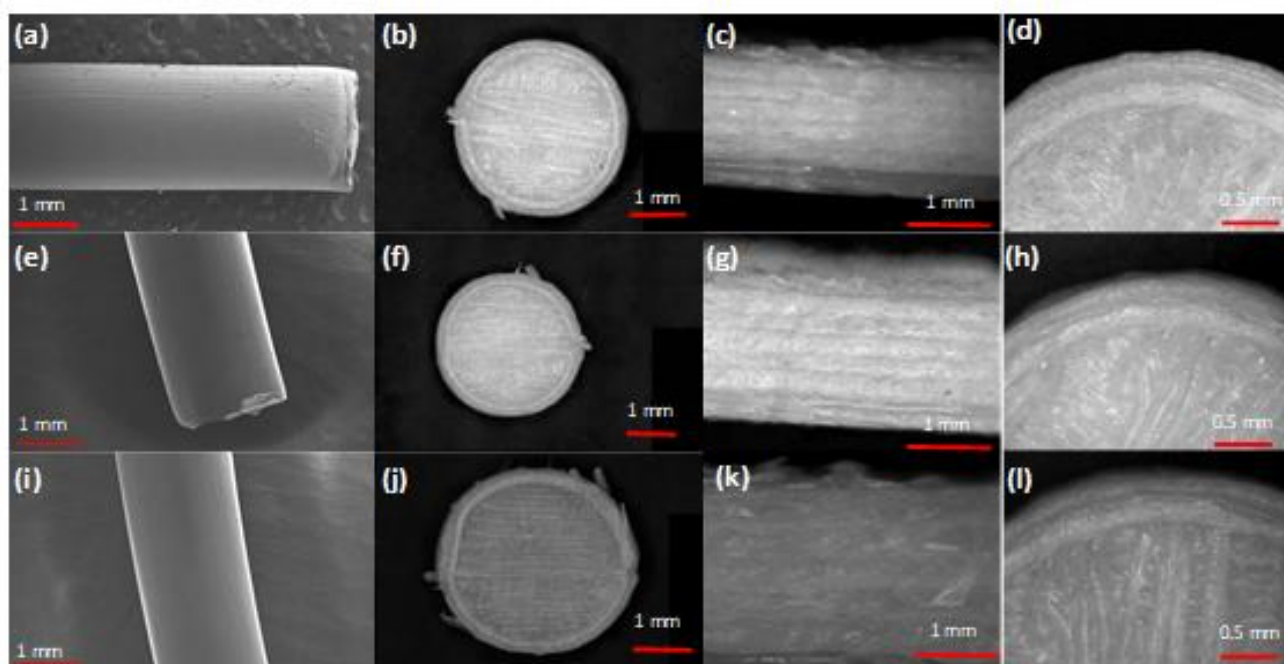


Figure 3.5: SEM micrographs of (a-d) K4M based filament and matrix tablet (a= filament, b= whole matrix tablet, c= side view of matrix tablet and d, surface view showing edges), (e-h) K15M based filament and matrix tablet (e= filament, f= whole matrix tablet, g= side view of

matrix tablet and h, surface view showing edges) and (i-l) K100M based filament and matrix tablet (i= filament, j= whole matrix tablet, k= side view of matrix tablet and l, surface view showing edges).

3.3.2. Development and characterisation of 3D printed matrix tablets

All the glipizide loaded filaments produced 3D printed hydrophilic matrices, characterised as detailed in Table 3.4. There were no statistically significant differences in thickness, diameter and weight. In accordance with drug loading in the filaments, the drug loading in the 3D printed matrices was within the pharmacopoeial assay limit (95-105 %) ³⁸. To evaluate the quality and investigate any structural defects of the printed matrices, porosimetry was carried out and matrices printed with K100M filaments had the lowest porosity ($0.8 \pm 0.1\%$) followed by K15M matrices ($1.5 \pm 0.2\%$) and K4M matrices ($2.2 \pm 0.2\%$), Table 3.4. The breaking strength of the tablets (N) was also determined. In comparison to traditional tableting press, the physical properties of tablets can be controlled by compression forces where 4 kg is the minimum breaking force value. Measured breaking force measurements for 3D printed hydrophilic matrices exceeded the accepted range [85.2-93.8 N (8.7-9.6 kg)] for solid tablets ³⁹. The 3D printing process does not involve compression forces, so it is obvious that this parameter does not exist to manipulate the hardness of 3D printed tablets. It is evident that these printed tablets are quite robust and can bear a reasonable amount of rough handling which is evident from the friability results, Table 3.4. SEM micrographs of 3D printed HPMC matrices shows that they are not smooth due to the printing pattern of FDM (Figure 3.5b, f, j). The layering pattern on the surfaces of the tablets is visible in the top-view SEM images of the tablets. Also, the layer-by-layer approach of the FDM technique can be seen in the side-view SEM images of the tablets (Figure 3.5c, g, k). Although the surface of the tablets is not smooth compared to compressed tablets, ²⁶ however, the images confirm successful extrusion of filaments during tablet printing (Figure 3.5 d, h, l).

Table 3.4: Geometrical and morphological characteristics of 3D printed hydrophilic matrices (n=5, standard deviations are in parenthesis).

Characteristics	K4M	K15M	K100M
Weight (mg)	100.1 (2.2)	99.6 (1.8)	99.3 (2.1)
Diameter	3.0 (0.1)	3.0 (0.1)	3.0 (0.1)
Thickness (mm)	1.5 (0.1)	1.5 (0.1)	1.5 (0.1)
Drug loading in tablets (%)	99.3 (2.6)	100.3 (2.9)	98.6 (1.4)
Porosity (%)	2.2 (0.2)	1.5 (0.2)	0.8 (0.1)
Breaking strength of tablets (N)	345.6 (10.3)	480.2 (14.6)	525.3 (9.3)
Friability (%)	0	0	0

Surface texture analysis of 3D printed tablets was conducted using a profilometer Figure 3.6 (a-c). Multiple surface texture parameters were calculated including amplitude, spacing, volume and hybrid parameters as presented in Table 3.5. Overall, these parameters displayed a spiked peak height distribution ($Sku > 3$) indicating the presence of inordinately high peaks and/or deep valleys and a predominance of valley structures ($Ssk < 0$) on the surface of the matrix tablets of all three grades of HPMC. Additionally, the surface roughness (Sa), density of peaks per unit area (Sds) and maximum height (sum of height of highest peak and height of deepest valley; Sz) were highest in K4M matrices followed by K100M and K15M, although the highest peak was present in the K100M matrix (Sp). The texture aspect ratio (Str) also followed the same trend with the highest in K4M followed by K100M and K15M matrices; however, all texture aspect ratios indicated strong isotropy ($Str > 0.5$). In addition, volume parameters, which represent the volume of space contained by the surface from a plane at a height corresponding to a chosen material ratio level to the lowest valley (vv and vvv), were highest in K4M matrix tablets followed by K100M and K15M, although the differences in vv were statistically insignificant. This trend was expected due to the deepest valley being found in K4M and the shallowest valley being found in K15M matrix tablets. On the other hand, material volume (vm), which represents the volume of space contained by the surface from a plane at a height corresponding to a chosen material ratio level to the highest peak, was greatest in K100M matrix tablets followed by K4M and K15M. This was anticipated due to the

highest peak being found in K100M matrices. Overall, it can be concluded that the 3D printed matrix tablets were considerably rougher than the conventional compressed tablets, and that roughness is not directly related to polymer viscosity or chain length.

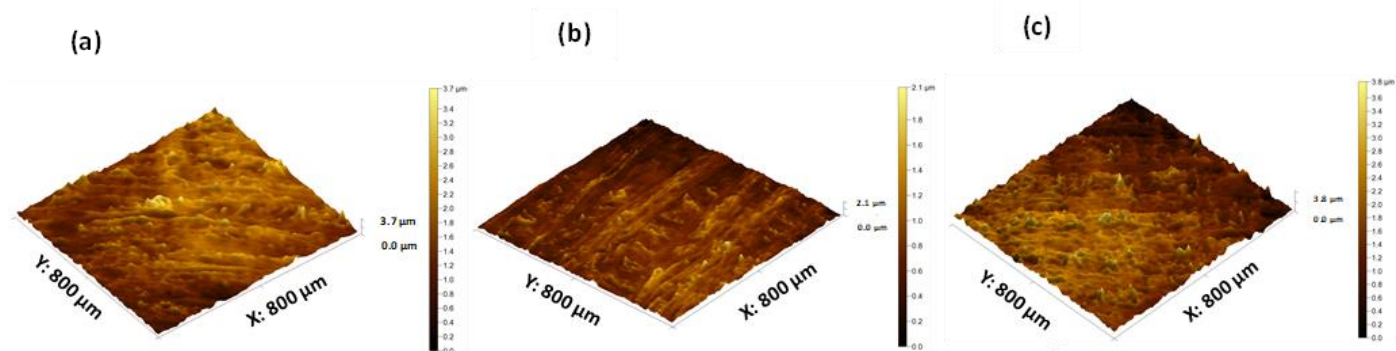


Figure 3.6: 3D surface texture images (a) K4M (b) K15M and (c) K100M based matrix tablet.

Table 3.5: 3D quantitative surface texture parameters of HPMC/glipizide hydrophilic matrices (n= 10, standard deviations are in parenthesis).

Parameter	K4M	K15M	K100M
Sa (μm)	22.6 (2.3)	14.6 (1.9)	16.4 (3.3)
Sq (μm)	26.5 (9.4)	20.3 (3.5)	23.7 (4.8)
Sz (μm)	75.0 (7.2)	60.0 (9.1)	70.0 (10.9)
Sp (μm)	33.7 (6.8)	30.7 (4.9)	36.3 (4.0)
Sv (μm)	41.3 (9.0)	29.4 (5.3)	33.7 (8.4)
Sku (μm)	5.3 (1.1)	4.9 (0.9)	5.1 (1.4)
Ssk (μm)	-0.6 (-0.1)	-0.4 (-0.2)	-0.7 (-0.2)
Sds ($1/\mu\text{m}^2$)	112.4 (11.4)	98.3 (5.6)	104.1 (9.7)
Sal (μm)	136.4 (20.4)	111.0 (11.0)	121.4 (9.0)
Str	0.9 (0.1)	0.9 (0.1)	0.8 (0.1)
Vm ($\mu\text{m}^3/\mu\text{m}^2$)	0.4 (0.1)	0.3 (0.09)	0.4 (0.1)
Vv ($\mu\text{m}^3/\mu\text{m}^2$)	6.9 (2.5)	5.2 (2.89)	6.4 (3.2)
Vvv ($\mu\text{m}^3/\mu\text{m}^2$)	0.6 (0.1)	0.4 (0.1)	0.3 (0.1)

3.3.3. Swelling and HPMC dissolution studies

Polymer swelling is an important property in controlling drug release from hydrophilic matrices ⁴⁰. Figure 3.7 displays the swelling profiles of all types of 3D printed HPMC based glipizide matrices with respect to time. It is apparent that there is a direct relationship between the amount of swelling and viscosity (molecular size) of the polymer. In acidic pH, the maximum swelling achieved by K4M, K15M and K100M matrices was nearly 180%, 200% and 230%, respectively. Within 720 min (12 h), the maximum swelling achieved by K4M matrices was more than 250%. K15M matrices swelled by 300% whereas the highest amount of swelling was observed in K100M matrices with more than 350%. After achieving maximum swelling, a slight decline in swelling was observed with K4M and K15M matrices which is attributed to matrix erosion. The relationship between the molecular size (viscosity) of HPMC and extent of swelling may be explained due to the fact that higher molecular size polymers exhibit increased liquid uptake resulting in rapid swelling of the polymer. This was also supported by the rate of swelling, K_w , obtained by fitting the data to a swelling kinetic model described by Vergnaud ⁴¹ as shown in Table 3.6. The R^2 values displayed in the table (0.97-0.99) indicate that the data was well described by the Vergnaud mathematical model and, as an n value <0.5 is indicative of a diffusion-controlled mechanism, it can be deduced that swelling by the 3D printed matrix tablets follows a diffusion-controlled mechanism. Figure 3.8 shows the percentage of HPMC dissolved over time. It can be seen that the HPMC dissolution increased over time but declines with an increase in viscosity of the polymer. This is because high viscosity HPMC matrices form a more resilient and thicker gel on the matrix surface. The highest percentage of HPMC dissolved was observed with K4M matrices and the lowest was observed with K100M matrices.

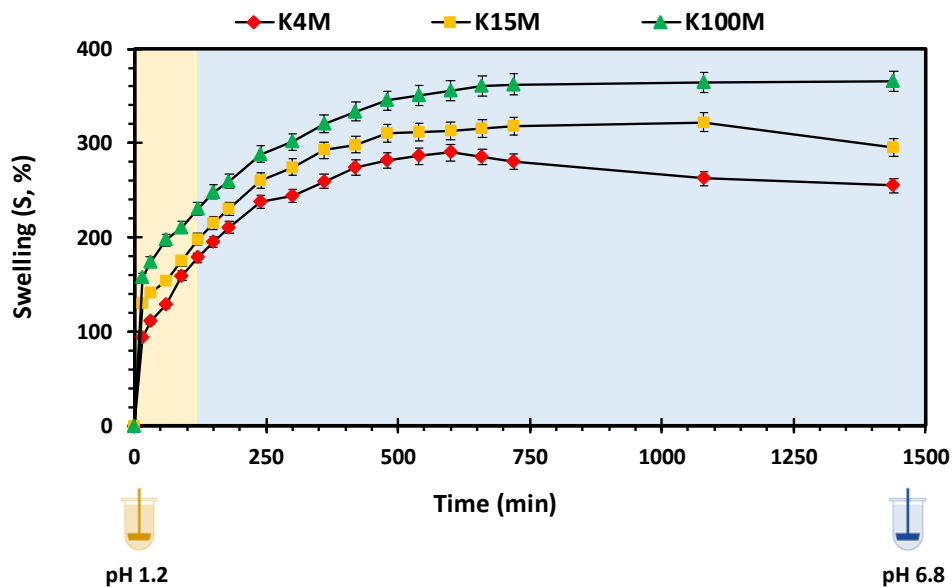


Figure 3.7: Swelling vs time profile of 3D printed HPMC matrix tablets.

Table 3.6: Swelling and erosion kinetics parameters of HPMC/glipizide hydrophilic matrices (n=5).

Type of matrix tablet	Swelling kinetic parameters			Erosion kinetic parameters	
	K_w^a	n	R^2	K_E^b	R^2
K4M	32.96	0.34	0.99	0.076	0.98
K15M	52.20	0.28	0.97	0.057	0.96
K100M	76.51	0.24	0.98	0.039	0.97

^a Swelling rate, K_w (% min⁻¹); ^b Erosion rate,

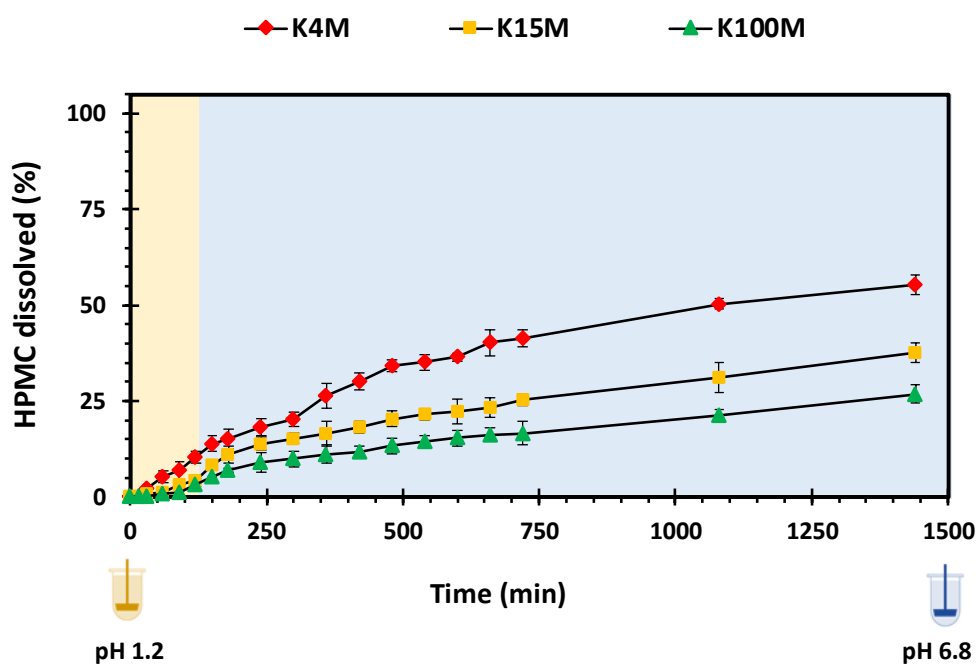


Figure 3.8: HPMC dissolution vs time profile of 3D printed HPMC matrix tablets.

3.3.4. Drug release studies

Initially, HPMC forms a gel on the surface of the matrix tablets after getting hydrated on contact with the dissolution medium. Progressive contact with the medium leads to subsequent bulk hydration of the matrix. With time, the hydration results in chain relaxation of HPMC, followed by erosion of the matrix. Matrix swelling, diffusion of drug through gel layer or matrix erosion are the factors that control the drug release rate and mechanism^{29, 40}. Figure 3.9 shows the drug release (%) from all three grades of HPMC matrices with respect to time. In the first 2 h in simulated gastric fluid (pH 1.2) the glipizide was released very slowly as expected from its limited solubility in acidic media⁴². However, as the medium was changed to simulated intestinal fluid (pH 6.8) glipizide release increased due to improved solubility⁴³. It is also apparent that the molecular size of HPMC played an essential role in regulating the glipizide release from hydrophilic matrices. Among these matrices, the highest drug release and lowest drug release was observed in K4M and K100M matrices, respectively. The drug release was inversely related to the swelling rate of matrices. Therefore, K100M matrices which presented the highest swelling rate (K_w), Table 3.6, showed slowest drug release and achieved nearly 75% drug release in 750 minutes. On the other hand, K4M

matrices, which displayed the lowest swelling rate (K_w), Table 3.6, achieved 100% drug release in 750 minutes. Moreover, K15M matrices attained more than 90% drug release at the same time. Overall, it is concluded that polymer with high viscosity leads to higher swelling rate which in turn results in slow and sustained release of the drug thus, the 3D printed tablets present similar drug release behaviour which is comparable to that of matrix tablets fabricated using conventional methods, hence, proving the applicability of 3D printing technologies in the development of hydrophilic matrices.

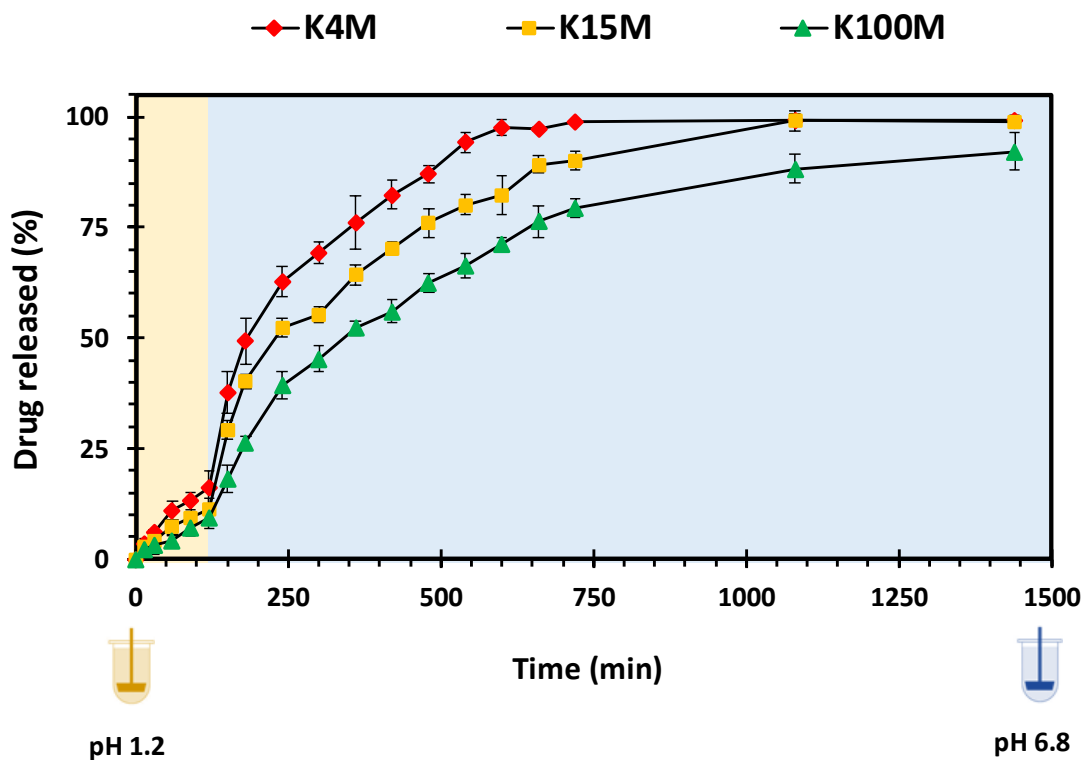


Figure 3.9: Drug (glipizide) release vs time profile of 3D printed HPMC matrix tablets.

3.3.5. Erosion studies

Matrix erosion reflects the collective amount of polymer and drug dissolved⁴⁴. The presence of polymeric carrier on the surface of hydrophilic matrices is principally responsible for the development of an outer viscous gel layer that will undergo erosion over time, and the outer gel layer controls the overall erosion rate. When the outer surface of the polymer is

completely hydrated, the polymeric chains start to dissolve leading to matrix erosion. The factors that influence the erosion and drug release rate are physicochemical properties of drugs especially solubility, viscosity, chemistry, ionic strength and particle size of drug and polymer ⁴⁰. The degree of matrix erosion is shown in Figure 3.10 and reported as % matrix erosion (E). In the present study, the degree of erosion from the matrices increased gradually over time. However, an increase in viscosity (molar mass) resulted in a decrease in matrix erosion (K4M > K15M > K100M). Additionally, Table 3.6 displays the erosion kinetic parameters in which K4M matrices showed the highest rate of erosion (KE) followed by K15M and K100M matrices. The R2 values in the table shows a linear profile for all types of matrices confirming that matrix erosion decreased with increased molecular size (viscosity) ^{28, 45}.

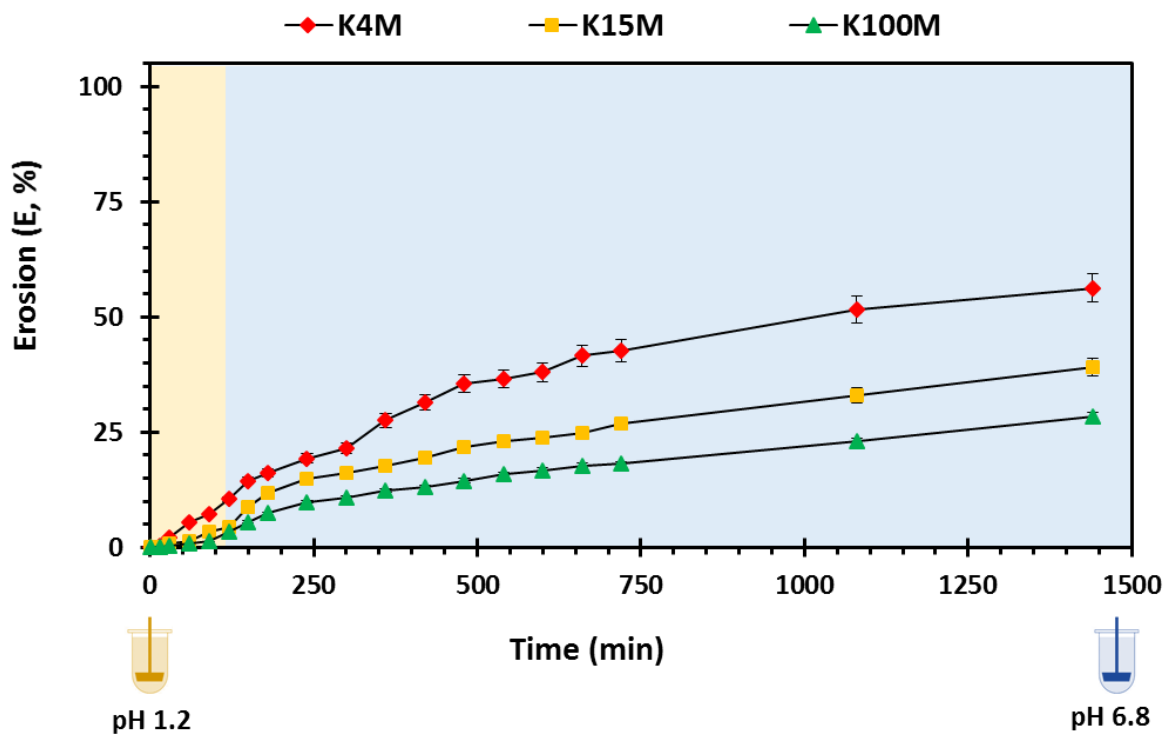


Figure 3.10: Overall matrix erosion vs time profile of 3D printed HPMC matrix tablets.

3.3.6. Pharmacokinetic studies of HPMC/glipizide hydrophilic matrices

For pharmacokinetic studies, rabbits were administered 3D printed hydrophilic matrices weighting 100 ± 1.5 mg containing 2.5% w/w glipizide. The mean plasma concentration-time curve of the printed samples and reference (oral solution) are shown in Figure 3.11, and the relevant pharmacokinetic parameters are given in Table 3.7.

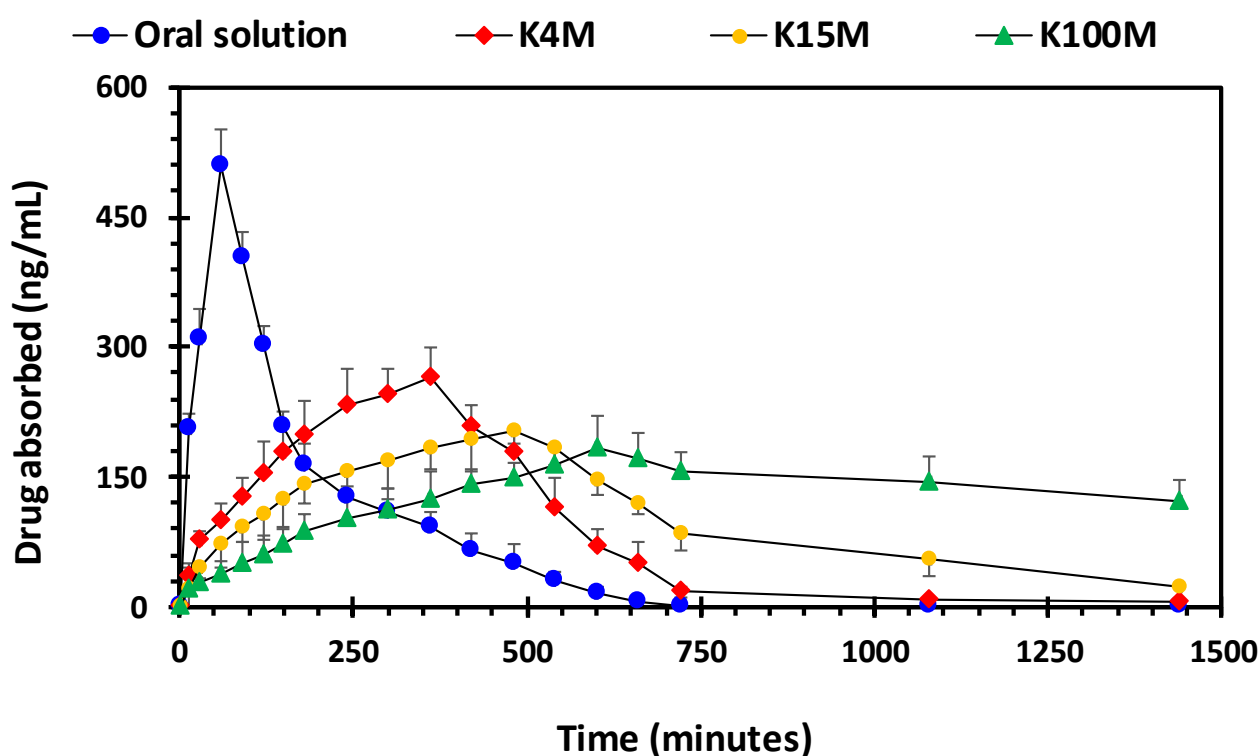


Figure 3.11: Drug (glipizide) absorption vs time profile of 3D printed HPMC matrix tablets.

Table 3.7: Pharmacokinetic parameters of hypromellose/glipizide hydrophilic matrices (n= 5, standard deviations are in parenthesis).

Parameters	K4M	K15M	K100M	Oral solution
T_{max} (h)	6 (0.00)	8 (0.00)	10 (0.00)	1 (0.00)
C_{max} (ng/ml)	264.88 (33.69)	202.85 (15.33)	182.66 (38.37)	509.17 (42.19)
AUC_{0-t} (ng/ml/h)	1959.46 (151.32)	2325.08 (269.40)	3082.36 (252.32)	1499.48 (164.65)

Out of all of the hydrophilic matrices, the area under the curve (AUC) of the plasma concentration (ng/ml) versus time (minutes) profile was highest for K100M matrices (3082.36 ± 251.32 ng/ml.h) followed by K15M matrices (2325.08 ± 269.40 ng/ml.h) and K4M matrices (1959.46 ± 151.32 ng/ml.h). It is evident from the findings that there is a marked difference in the AUC from different matrix tablets. Moreover, the AUC was significantly lower for the oral solution (1499.48 ± 164.65 ng/ml.h) compared with the HPMC: glipizide matrices. This is due to the decrease in drug absorption after reaching T_{max} (60 min). After approximately 400 min, drug absorption from the oral solution was significantly less than absorption from the HPMC: glipizide matrices (Figure 3.11). Furthermore, the highest maximum plasma concentration (C_{max}) was achieved by the oral solution (509.17 ± 42.19 ng/ml) followed by the K4M matrices (264.88 ± 33.69 ng/ml), K15M matrices (202.85 ± 15.33 ng/ml) and the lowest was attained by K100M matrices (182.66 ± 38.37 ng/ml). Although, the time taken to reach C_{max} (T_{max}) followed the opposite trend with the longest time being taken by K100M matrices (600 min) and the shortest time being taken by the oral solution (60 min). These pharmacokinetic parameters may be explained by the extended-release effect of HPMC which causes the drug to be absorbed into the bloodstream over a longer period compared with the oral solution, thus confirming the sustained release nature of the formulations. Additionally, the reduced drug release rate caused by the higher viscosity gel formed by, the higher molar mass HPMC grades further increases the T_{max} and reduces C_{max} .

3.4. Conclusions

The current study has successfully demonstrated the fabrication of HPMC: glipizide filaments and 3D printed matrix tablets without the addition of plasticiser. The XRD spectra of glipizide and drug-loaded HPMC filaments were consistent with the DSC profiles; thus, both methods showed that glipizide has a crystalline structure, whereas HPMC and glipizide loaded filaments are amorphous in nature. TGA confirmed the onset of degradation for both drug and filaments was above the operating temperature (170 °C) involved in the printing process. The mechanical properties of glipizide loaded filaments were robust and were successfully employed to 3D print matrix tablets. It can be concluded that the 3D printed matrix tablets were considerably rougher than the conventional compressed tablets and the current research findings have suggested that more attention is necessary to comprehend this research area. Furthermore, it can be concluded that the viscosity of HPMC has a noticeable impact of the swelling, erosion, HPMC dissolution, drug release and pharmacokinetic properties. The highest viscosity grade (K100M) tends to have a higher degree of swelling, decreased HPMC dissolution, low matrix erosion, decreased drug release and extended drug absorption profile. Overall, this study confirmed the successful fabrication of 3D printed matrix tablets which have functionalities analogous to matrix tablets fabricated using conventional technologies. Moreover, the current study has also demonstrated the usefulness of the FDM technique, providing a simple solution to develop personalised pharmaceutical formulations in a time and cost-effective manner addressing challenges confronted by conventional manufacturing processes.

References

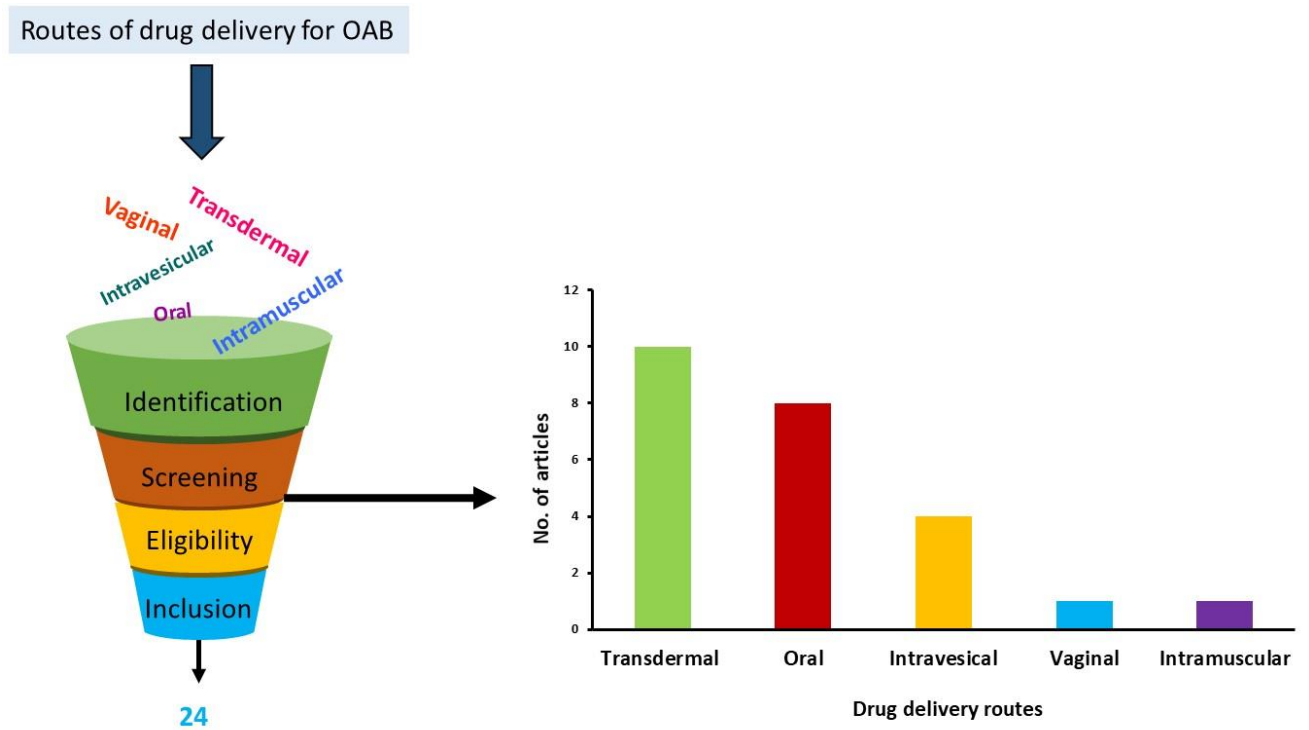
1. W. Kempin, C. Franz, L.-C. Koster, F. Schneider, M. Bogdahn, W. Weitschies and A. Seidlitz, *European Journal of Pharmaceutics and Biopharmaceutics*, 2017, **115**, 84.
2. J. Holländer, N. Genina, H. Jukarainen, M. Khajeheian, A. Rosling, E. Mäkilä and N. Sandler, *Journal of pharmaceutical sciences*, 2016, **105**, 2665.
3. R. Beck, P. Chaves, A. Goyanes, B. Vukosavljevic, A. Buanz, M. Windbergs, A. Basit and S. Gaisford, *International journal of pharmaceutics*, 2017, **528**, 268.
4. A. Goyanes, U. Det-Amornrat, J. Wang, A. W. Basit and S. Gaisford, *Journal of Controlled Release*, 2016, **234**, 41.
5. K. Pietrzak, A. Isreb and M. A. Alhnan, *European Journal of Pharmaceutics and Biopharmaceutics*, 2015, **96**, 380.
6. Z. Wang, J. Wang, M. Li, K. Sun and C.-j. Liu, *Scientific reports*, 2014, **4**, 5939.
7. N. Genina, J. Holländer, H. Jukarainen, E. Mäkilä, J. Salonen and N. Sandler, *European Journal of Pharmaceutical Sciences*, 2016, **90**, 53.
8. X. Chai, H. Chai, X. Wang, J. Yang, J. Li, Y. Zhao, W. Cai, T. Tao and X. Xiang, *Scientific reports*, 2017, **7**, 2829.
9. A. Goyanes, F. Fina, A. Martorana, D. Sedough, S. Gaisford and A. W. Basit, *International journal of pharmaceutics*, 2017, **527**, 21.
10. J. Zhang, X. Feng, H. Patil, R. V. Tiwari and M. A. Repka, *International journal of pharmaceutics*, 2017, **519**, 186.
11. Z. Khizer, B. Conway and M. Ghori, *British Journal of Pharmacy*, 2019.
12. H. Kadry, T. A. Al-Hilal, A. Keshavarz, F. Alam, C. Xu, A. Joy and F. Ahsan, *International journal of pharmaceutics*, 2018, **544**, 285.
13. L. D. Bruce, N. H. Shah, A. W. Malick, M. H. Infeld and J. W. McGinity, *European Journal of Pharmaceutics and Biopharmaceutics*, 2005, **59**, 85.
14. A. W. Basit, J. M. Newton, M. D. Short, W. A. Waddington, P. J. Ell and L. F. Lacey, *Pharmaceutical research*, 2001, **18**, 1146.
15. K. Oosaka, M. Tokuda and N. Furukawa, *World Journal of Gastroenterology: WJG*, 2014, **20**, 1054.
16. W. Johnson Jr, *International journal of toxicology*, 2002, **21**, 1.
17. S. Davis, J. Hardy and J. Fara, *Gut*, 1986, **27**, 886.
18. E. G. Gordeev, A. S. Galushko and V. P. Ananikov, *PloS one*, 2018, **13**, e0198370.
19. M. S. Asim, M. U. Ghori and B. R. Conway, *British Journal of Pharmacy*, 2017, **2**.
20. J. M. Sankalia, M. G. Sankalia and R. C. Mashru, *Journal of Controlled Release*, 2008, **129**, 49.
21. M. U. Ghori, E. Šupuk and B. R. Conway, *Materials*, 2015, **8**, 1482.
22. Y. Shahzad, S. Saeed, M. U. Ghori, T. Mahmood, A. M. Yousaf, M. Jamshaid, R. Sheikh and S. A. Rizvi, *International journal of biological macromolecules*, 2018, **109**, 963.
23. R. Diryak, V. Kontogiorgos, M. U. Ghori, P. Bills, A. Tawfik, G. A. Morris and A. M. Smith, *Macromolecular Chemistry and Physics*, 2018, **219**, 1700584.
24. M. U. Ghori, K. Alba, A. M. Smith, B. R. Conway and V. Kontogiorgos, *Food Hydrocolloids*, 2014, **42**, 342.
25. M. U. Ghori, M. A. Mohammad, S. R. S. Rudrangi, L. T. Fleming, H. A. Merchant, A. M. Smith and B. R. Conway, *Food Hydrocolloids*, 2017, **71**, 311.
26. E. Nep, K. Asare-Addo, M. U. Ghori, B. R. Conway and A. M. Smith, *International Journal of Pharmaceutics*, 2015, **496**, 689.
27. M. U. Ghori, University of Huddersfield, 2014.
28. M. U. Ghori, L. M. Grover, K. Asare-Addo, A. M. Smith and B. R. Conway, *Pharmaceutical development and technology*, 2018, **23**, 183.

29. M. U. Ghori, G. Ginting, A. M. Smith and B. R. Conway, *International Journal of Pharmaceutics*, 2014, **465**, 405.
30. J. S. Nirwan, B. R. Conway and M. U. Ghori, *RSC advances*, 2019, **9**, 16119.
31. O. Defang, N. Shufang, L. Wei, G. Hong, L. Hui and P. Weisan, *Drug development and industrial pharmacy*, 2005, **31**, 677.
32. Y. Zhang, M. Huo, J. Zhou and S. Xie, *Computer methods and programs in biomedicine*, 2010, **99**, 306.
33. Q. Li, H. Wen, D. Jia, X. Guan, H. Pan, Y. Yang, S. Yu, Z. Zhu, R. Xiang and W. Pan, *International journal of pharmaceutics*, 2017, **525**, 5.
34. C. Korte and J. Quodbach, *Pharmaceutical development and technology*, 2018, **23**, 1117.
35. H. Öblom, J. Zhang, M. Pimparade, I. Speer, M. Preis, M. Repka and N. Sandler, *Aaps Pharmscitech*, 2019, **20**, 1.
36. J. Edgar and S. Tint, *Johnson Matthey Technology Review*, 2015, **59**, 193.
37. M. Bocqué, C. Voirin, V. Lapinte, S. Caillol and J. J. Robin, *Journal of Polymer Science Part A: Polymer Chemistry*, 2016, **54**, 11.
38. British Pharmacopoeia <https://www.pharmacopoeia.com/reference-standards>, (accessed 27 June, 2019).
39. A. Goyanes, A. B. Buanz, A. W. Basit and S. Gaisford, *International journal of pharmaceutics*, 2014, **476**, 88.
40. M. U. Ghori and B. R. Conway, *American Journal of Pharmacological Sciences*, 2015, **3**, 103.
41. J. Vergnaud, *International journal of pharmaceutics*, 1993, **90**, 89.
42. H. Ammar, H. Salama, M. Ghorab, S. El-Nahas and H. Elmotasem, *Current drug delivery*, 2006, **3**, 333.
43. S. Jamzad and R. Fassihi, *Aaps Pharmscitech*, 2006, **7**, E17.
44. A. Goyanes, A. B. Buanz, G. B. Hatton, S. Gaisford and A. W. Basit, *European Journal of Pharmaceutics and Biopharmaceutics*, 2015, **89**, 157.
45. K. H. Khanvilkar, Y. Huang and A. D. Moore, *Drug development and industrial pharmacy*, 2002, **28**, 601.

CHAPTER 4

Drug Delivery Approaches for Managing Overactive Bladder (OAB): A Systematic Review

Graphical abstract



Notes for readers

- Overactive bladder syndrome (OAB) is characterised by urgency symptoms, with or without urgency incontinence, usually with frequency and nocturia and severely affects the quality of life.
- This systematic review evaluates the various drug delivery strategies used in practice to manage OAB.
- The present review was conducted according to the preferred reporting items for systematic reviews and meta-analyses guidelines.
- A total of 24 studies reporting the development of novel formulations for the treatment of OAB were considered eligible and were further categorised according to the route of drug administration.
- The review found that various drug delivery routes (transdermal, intravesicular, oral, vaginal, and intramuscular) are used for the administration of drugs for managing OAB, however, the outcomes illustrated the marked potential of transdermal drug delivery route.

4.1. Introduction

Overactive bladder (OAB) syndrome is characterised by “urinary urgency, usually accompanied by frequency and nocturia, with or without urgency urinary incontinence, in the absence of urinary tract infection (UTI) or other obvious pathology”¹. According to a population-based survey carried out in the United Kingdom, Canada, Sweden, Italy and Germany, the overall prevalence of OAB was estimated to be 11.8% for both men and women and was found to increase with age². However, this estimate may be an under-representation of the true prevalence of OAB as many patients may be reluctant and unwilling to discuss their condition with family members or healthcare providers, as observed in a population-based survey in which fewer than 50% of respondents with probable OAB had discussed their condition with their healthcare provider³. OAB can severely affect quality of life and can impact the social, sexual, occupational and psychological aspects of patient life². Consequently, OAB remains underreported, despite the availability of improved treatments and increased awareness^{4,5}.

The etiological factors of OAB can be neurogenic, myogenic and urotheliogenic^{6,7}. Abnormal afferent excitability and central sensory processing are the neurogenic causes, and it is prevalent in patients suffering from Parkinson’s disease, multiple sclerosis, and cerebrovascular disease⁷. Abnormal transmission of nonadrenergic noncholinergic neurotransmitter is another neurogenic factor that can also cause OAB⁸. The spontaneous contraction of the detrusor muscle (Figure 4.1) and hypersensitivity to incoming signals is a myogenic factor, whereas changes in ion channel, urothelial signalling and increased afferent activity are urotheliogenic factors⁹⁻¹¹. Changes or disturbances in any of these factors, including any combinations, can cause OAB. Additionally, metabolic derangement, bladder inflammation (interstitial cystitis), and bladder obstruction due to benign prostatic hyperplasia may also cause OAB. These factors typically increase the excitability of the nerve, the detrusor muscle and alter the barrier and sensory functions of the urothelium^{6,7}. A urodynamic study reported that 31-68% of OAB patients were diagnosed with bladder outlet obstruction¹². Yu et al., reported that, in Taiwanese women, hyperlipidaemia is linked with OAB¹³. Moreover, according to a survey conducted on 1359 patients suffering from diabetes mellitus, 22.5% of the patients had OAB syndrome¹⁴. Chuang et al., also reported that serum levels of CRP, a C-reactive protein which is secreted by the liver in response to inflammation

in the body, were higher in patients with OAB compared to those who were not suffering from OAB ¹⁵. However, the causes of OAB differ from one person to another and may involve one or more of the abovementioned factors.

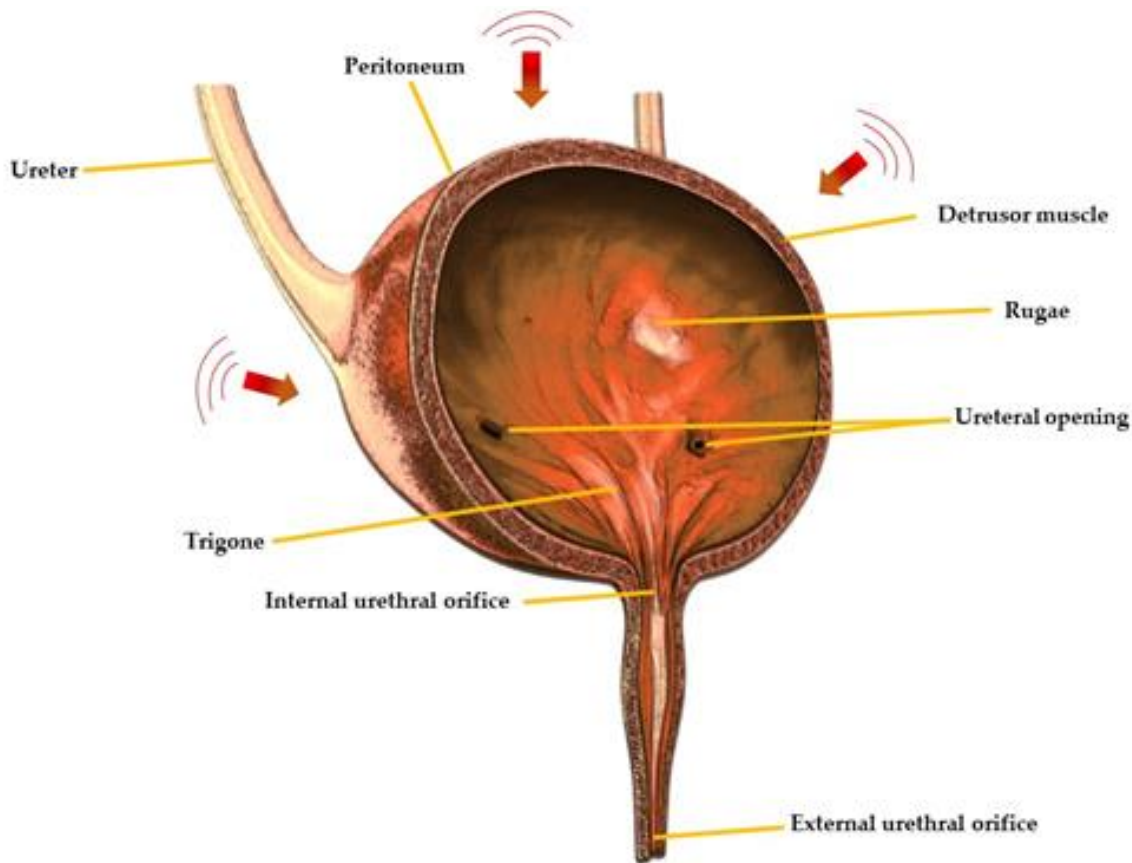


Figure 4.1: Cross-sectional view of urinary bladder showing different regions.

OAB management strategies include non-pharmacological and pharmacological approaches. Non-pharmacological interventions include behavioural and bladder training, whereas pharmacologic therapies include muscarinic receptor antagonists or anti-muscarinic drugs (tolterodine, solifenacin, darifenacin, propiverine, oxybutynin, trospium chloride), α -adrenoceptor antagonists (alfuzosin, doxazosin), β -adrenoceptor antagonists (terbutaline, salbutamol), vitamin D analogues (elocalcitol), a combination of drugs (anti-muscarinic + α -adrenoceptor antagonist), phosphodiesterase inhibitors (sildenafil, tadalafil), cyclooxygenase inhibitors (flurbiprofen, indomethacin), voltage-gated calcium channel inhibitor (gabapentin), capsicum plant derived drug, capsaicin (8-methyl-N-vanillyl-6-nonamide) and the μ -opioid receptor agonist ,tramadol ¹⁶⁻¹⁹. Various drug delivery routes including oral, transdermal,

intravesical and vaginal are used for the administration of drugs for the treatment of OAB with the oral route being the most common due to ease of ingestion, increased patient compliance and safety ²⁰. Currently, anti-muscarinic drugs are the mainstay of oral pharmacotherapy for the treatment of OAB, however, they may be associated with troublesome side effects including constipation and xerostomia ²¹⁻²⁴.

Delivery via the transdermal route is a painless way of systematic drug administration in which the formulation, usually in the form of a gel, cream or patch, is applied onto healthy, intact skin. This route also has many advantages including being suitable for unconscious patients, low incidence of side effects, improved bioavailability due to being able to avoid pre-systemic metabolism, and a large surface area which allows better transdermal absorption of the drug ²⁵⁻²⁸. However, it can cause skin irritation which can lead to potentially serious skin inflammatory problems.

Intravesical therapy involves direct instillation of a drug into the bladder after inserting a catheter into the urethra. Recently, this route has gained popularity in the management of overactive bladder syndrome and is used as an alternative to oral treatment or as a second line in clinical management. However, the urothelium membrane has low permeability which represents a challenge for intravesical drug delivery ²⁹. Hence, the vaginal route has several advantages such as high permeability to many drugs, avoidance of first-pass hepatic metabolism, and the suitability to accommodate relatively large doses ³⁰. A delivery system could be used to treat overactive bladder and vaginal dryness simultaneously, which are common issues faced by human females after menopause ³¹. However, it is obviously limited to females as well as being associated with local irritation and variability in the extent and rate of drug absorption ³².

Traditional drug delivery systems used in OAB are commonly associated with multiple side effects and low compliance. It is expected that this low compliance may lead to clinical challenges and even therapeutic failure. The aforementioned discussion and challenges warrant the need for a comprehensive review using a systematic search of literature reporting the development and characterisation of formulations for the management of OAB to identify any preferred routes and formulation approaches. (PRISMA) guidelines ³³ were adopted to review the various reported drug delivery strategies and their therapeutic potential.

4.2. Methodology

4.2.1. Search plot, information sources and screening process

The search plot, based on PRISMA ³³ guidelines which includes identification, screening, eligibility, and inclusion as its key determinants, is shown in Figure 4.2. A systematic search of published research studies from January 2004 to December 2019 was carried out. An inclusive search plot based on Google Scholar, PubMed, MEDLINE, EMBASE and Scopus databases was used. The authors conducted the search using the following search terms: *“overactive bladder syndrome” OR “development of OAB formulations” OR “drug delivery routes for OAB” OR “pharmacological treatment of OAB” OR “polymers used for OAB formulations”*. Titles and abstracts of the resultant studies were screened, and studies irrelevant to the scope of the current systematic review were removed. The full texts of the remaining studies were then screened to determine eligibility. Additional studies which were not aligned with the rationale were further removed.

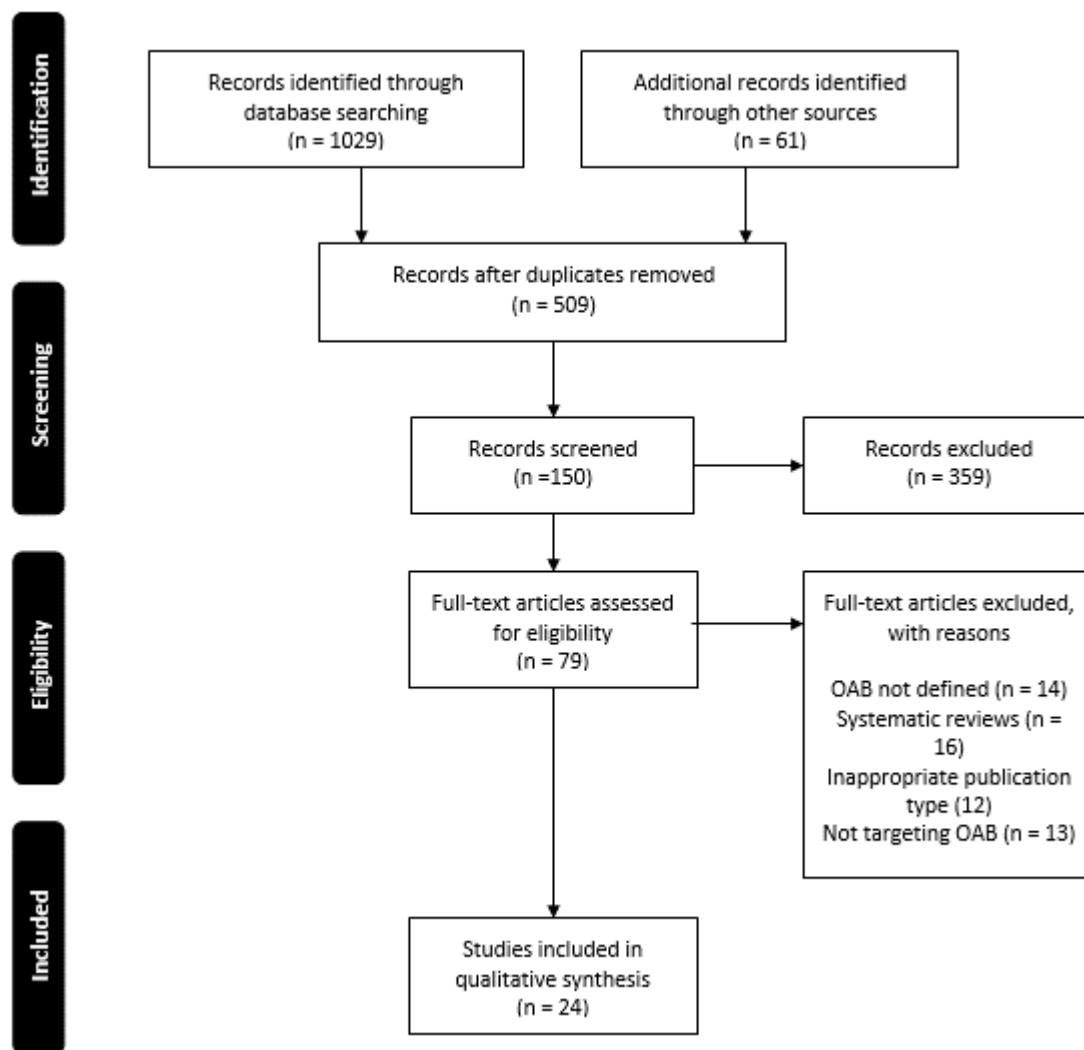


Figure 4.2: Systematic search and study selection process.

4.2.2. Study selection

The primary investigators independently evaluated the suitability of eligible studies. The full text was thoroughly screened against the rationale of the systematic review by two reviewers. Any disagreements and differences of opinion among reviewers over the eligibility of a particular study were resolved through a structured discussion. The study must include the development of the drug delivery system for the management of OAB, the administration route, the drug used and the relative drug release studies to be selected. Any study that fell outside this criterion was excluded.

4.2.3. Data extraction and collection

For data extraction and collection, the same procedure was adopted as described in the section 2.2.3 of the chapter 2. The extracted information includes active pharmaceutical ingredient used, drug delivery route, *in vitro/in vivo* studies, excipients, and study characteristics. Moreover, based on the retrieved list of active pharmaceutical ingredients in this systematic search exercise, a list of available commercial products was prepared using the British national formulary (BNF) ³⁴.

4.2.4. Risk of bias assessment

The criterion described in the section 2.2.4 chapter 2 to carry the risk of bias assessment was followed. The modified framework reported in the section 2.2.4 of the chapter 2 was thoroughly applied to investigate the risk of bias in each included study. It was assessed in the research rationale, methodology, results, discussion of results and conclusion domains of each study. The authors carried out the initial investigation individually; however, each study's final recommendation was assigned after the detailed structural panel discussion.

4.3. Results and discussion

The current systematic search plot yielded 1090 unique studies; however, after removal of duplicates, 509 studies were included. These studies were further screened by title and abstract, which resulted in the removal of 430 studies. Thus, 79 studies were subjected to full-text screening and finally 24 ^{31, 35-57} were selected and considered eligible to be included in the systematic review for further reporting and analysis (Figure 4.3). The main reasons for exclusion were a lack of focus on drug delivery and formulation development.

The included studies were then further categorised, and information was extracted according to the routes of drug delivery and the characteristics which were then tabulated in the Table 4.1 and discussed separately in the succeeding sections. Figure 4.3 depicts the distribution of the number of studies dedicated to each drug delivery approach. The distribution of risk of bias in the included studies is given in Figure 4.4. The studies generally had a low risk of bias with 3% unclear bias in the discussion sections, 0.5% in results and 1% in testing and methodology sections. Moreover, information regarding the commercial products of those drugs retrieved in this study was tabulated in Table 4.2 ³⁴.

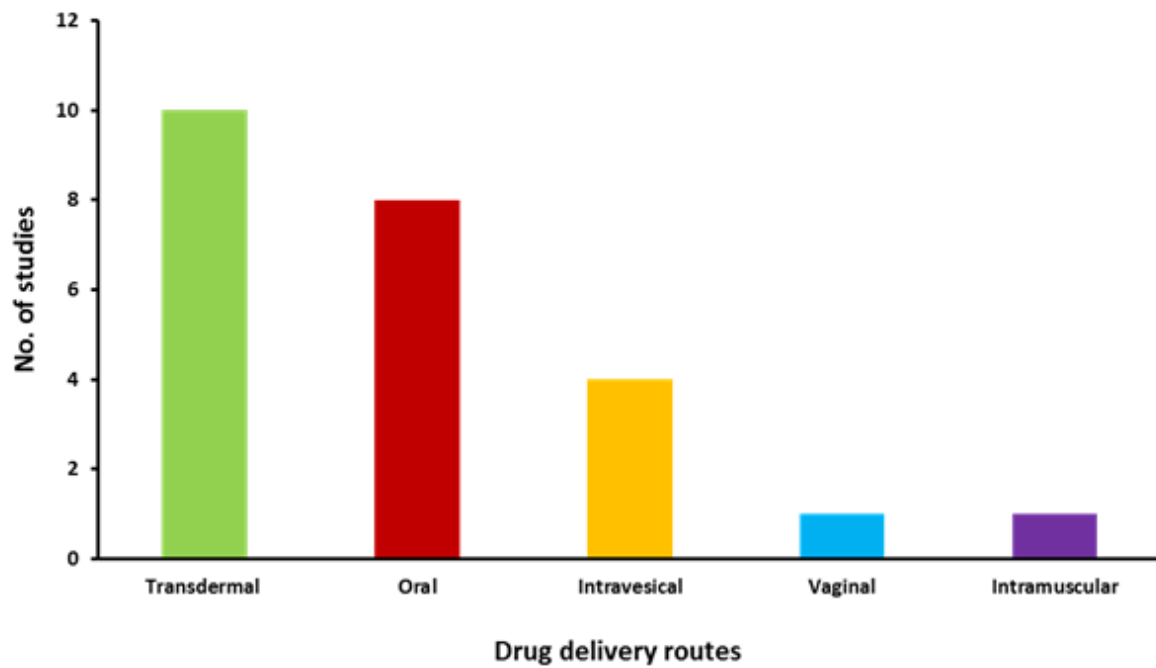


Figure 4.3: Distribution of eligible studies focused on different drug delivery routes.

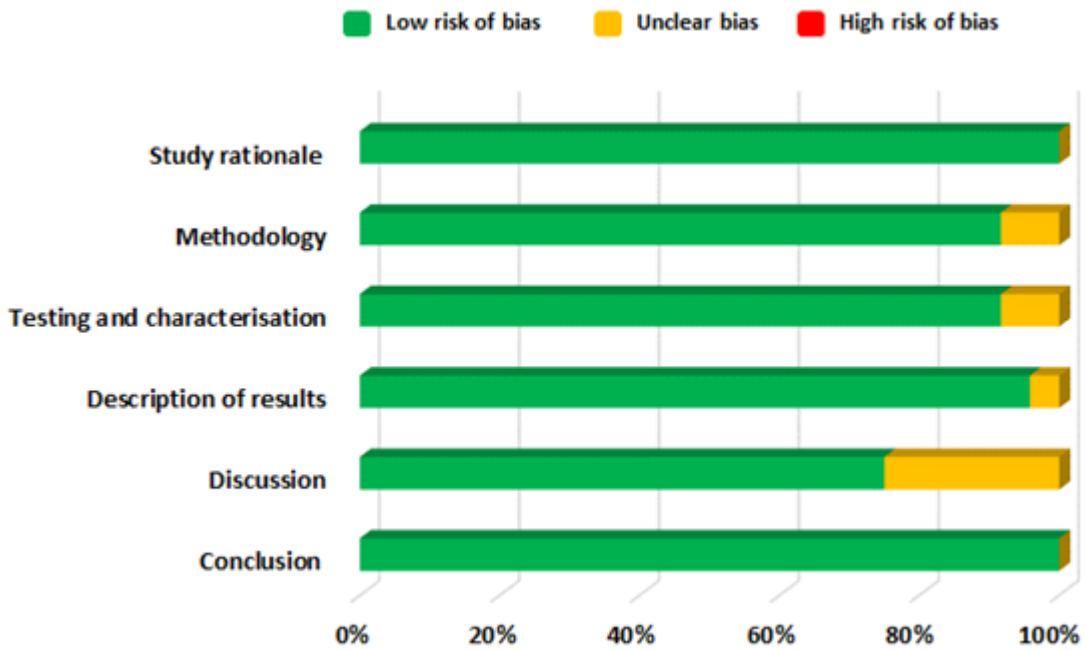


Figure 4.4: Risk of bias assessment of eligible articles.

Table 4.1: Summarised characteristics of eligible studies.

Study ID	Drug	Drug delivery route	Type of investigation	Excipients	Study characteristics	Reference
Nicoli et al., 2006	Oxybutynin	Transdermal	<i>In vitro</i>	PVA, sorbitol	The developed oxybutynin films showed good permeation characteristics across rabbit skin, oxybutynin permeation increased in a linear way for up to 7 hours and 50% of the drug permeation was achieved after 24 hours.	35
Banu et al., 2010	Oxybutynin	Transdermal	<i>In vitro</i>	Ethyl cellulose, Carbopol-934P and PG	Films containing 2% Carbopol-934P and 30% PG showed 87.28% drug release across rat abdominal skin whereas drug release from formulation containing 2% of ethyl cellulose: Carbopol-934P (1:3) and 30% PG was 88.32%.	36
Bakshi et al., 2008	Oxybutynin	Transdermal	<i>In vitro</i>	Lutrol F-127, Carbopol-940, myristyl lactate and glyceryl monooleate	The droplet size delivered from the formulations was within the range of 5-50 µm. The drug dose delivered per actuation of the pump was within the range of 101-106% by each formulation. Permeation studies were carried out on rabbit ear skin and showed that drug release was within the range of 45-50% during the period of 24 hours.	37
Rajabalaya et al., 2016	Oxybutynin chloride	Transdermal	<i>In vitro and in vivo (rat model)</i>	Span (S20, S40, and S60) and Tween (T20 and T80), cholesterol and glycerol distearate, isopropyl alcohol	All the formulations showed more than 87% entrapment efficiency which tended to increase with increase in surfactant. In vitro permeation studies determined that percent cumulative permeation after 8 hours was higher for gels containing Span than gels containing Tween.	38

Wang et al., 2018	Oxybutynin	Transdermal	<i>In vitro and in vivo (rat model)</i>	Acrylic adhesives, span 80	The patch with AACONH ₂ functional group acrylic adhesive had the highest (763.5 ± 58.8 µg/cm ²) oxybutynin cumulative levels during <i>in vitro</i> skin permeation study. The relative bioavailability of the developed patches was 97% in rats.	39
Pandit et al., 2009	Tolterodine tartrate	Transdermal	<i>In vitro</i>	Ethyl cellulose, Carbopol-934P, HPMC and PG	Different concentrations of polymers and PG were investigated. Combination of cabopol-934P: HPMC (1:3) with 30 % PG was effective in producing films of high endurance flexibility and with uniform drug content. Permeation study showed that there was 68.72% drug release across rat abdominal skin and 81.12% release across cellophane membrane for 12 hours.	40
Sun et al., 2013	Tolterodine	Transdermal	<i>In vitro and in vivo (rabbit model)</i>	Carbopol 980, N-methyl pyrrolidone	The formulation showed permeation rate of 770.19 µg cm ⁻² h ⁻¹ during <i>in vitro</i> percutaneous permeation experiment. The absolute bioavailability was 11.47% during pharmacokinetic studies.	41
W. Liu et al., 2017	5-hydroxymethyl tolterodine	Transdermal	<i>In vitro and in vivo (rat model)</i>	Carbopol 934, 940 and 980,	The formulation showed 20.7% absolute bioavailability during <i>in vivo</i> studies and no skin irritation was observed during skin irritation study.	42
X. Liu et al., 2014	Tolterodine	Transdermal	<i>In vitro and in vivo (rat model)</i>	Tween 80, HPMC, HPC, Carbopol 980	The formulation showed 86.02% cumulative drug release rate in 24 hours. The flux of tolterodine from the formulation was 81.82, 37.15, 18.55 and 15.83 µg cm ⁻² h ⁻¹ , across subcutaneous tissue, dermis, epidermis and full rat skin, respectively.	43

Rajabalaya et al., 2017	Tolterodine tartrate	Transdermal	<i>In vitro and in vivo (rat model)</i>	Eudragit (E 100, RSPO and RLPO), dibutyl sebacate (DBS), dibutyl phthalate (DBP) and triethyl citrate (TEC) and polyvinyl pyrrolidone (PVP)	Drug loaded formulations (i) E100, PVP, and DBS and (ii) RSPO, RLPO, PVP and DBS showed highest percent cumulative permeation and permeation rate during in vitro permeation studies	44
Tyagi et al., 2004	Capsaicin	Intravesical	-	Phosphatidylcholine, Cholesterol, PEG-PLGA-PEG, Saline solution with 30% ethanol	Three types of formulations, liposomes, hydrogel and 30% ethanolic solution, were developed. The results showed that the liposomes and 30% ethanolic solution completely blocked the micturition reflexes after intravesical administration. However, hydrogel of capsaicin was not successful in blocking the micturition reflexes completely but there was significant decrease in bladder contractions	45
Chuang et al., 2009	Botulinum toxin A	Intravesical	<i>In vivo (rat model)</i>	l- α -phosphatidylcholine and cholesterol	Intravesical delivery of lipotoxin (botulinum toxin A encapsulated in liposomes) was investigated to evaluate the effect of lipotoxin on bladder hyperactivity. The results showed that intercontraction interval was 21.1%.	46
Hopmann et al., 2015	Barium sulphate	Intravesical	<i>In vitro</i>	PLGA-PEG, polydimethylsiloxane	Samples were incubated in artificial urine for 27 days and CESP parameters including temperature, pressure and pressure release gradient were measured. The spheres and pills at constant temperature of 65 °C and pressure of 50 bar were totally dissolved in 27 days with pressure	47

					release gradient of 5 and 20 bar/min, respectively.	
Haupt et al., 2013	Trospium chloride	Intravesical	<i>In vitro</i>	Glyceryl tristearate, magnesium stearate	Extrudates and mini-tablets released drug for more than 5 days. The drug release from mini-moulds was very low or negligible and it was concluded that lipids provides good matrix for highly soluble drugs and with drug loading of only 30% the drug was released from several days up to weeks.	48
Tuçcu-Demiröz et al., 2013	Oxybutynin	Vaginal	<i>In vitro and in vivo (rabbit model)</i>	Chitosan, HPMC (K100M) and Poloxamer 407 (Pluronic F 127).	The hypromellose K100M formulation resulted in suitable permeation characteristics across the vaginal mucosa and also resulted in highest relative bioavailability and AUC during <i>in vivo</i> studies.	31
Sun et al., 2010	Tolterodine	Intramuscular	<i>In vivo (rat model)</i>	PLGA, palmitic acid, stearic acid	Drug entrapment efficiency was increased upon adding palmitic or stearic acid. The formulation was administered intramuscularly to beagle s. A sustained release following an initial burst was observed for 18 days.	49
Ploen et al., 2009	Propiverine hydrochloride	Oral	<i>In vitro</i>	Citric acid, Eudragit	At higher coating levels e drug release and citric acid release was reduced. The pellets extended the drug release for more than 16 hours.	50
Pradhan et al., 2014	Tolterodine-l-tartrate	Oral	<i>In vitro and in vivo (human volunteers)</i>	HPMC 2208 and HPMC 2910	The formulation showed sustained release profile up to 10 hours during <i>in vitro</i> dissolution testing. Similar results were obtained from <i>in vivo</i> results.	51

Patil et al., 2017	Tolterodine tartrate	Oral	<i>In vitro</i>	Mannitol, hypromellose	The <i>in vitro</i> dissolution profile of extended release capsule was similar to Detrol LA and resulted in more than 85% release during the period of 12 hours.	52
Naik et al., 2016	Oxybutynin chloride	Oral	<i>In vitro</i>	HPMC K4M, K100M, Carbopol, ethyl cellulose, PVP, sodium alginate	The formulation containing HPMC K4M along with ethyl cellulose was an optimised formulation that showed controlled drug release for period of 24 hour and resulted in cumulative release of 95.59% of drug release. The formulation followed first order kinetics.	53
Sudarsan et al., 2014	Darifenacin hydrobromide	Oral	<i>In vitro</i>	Ethyl cellulose, povidone, magnesium stearate	Formulation with highest level of ethyl cellulose coating was an optimised formulation as the results were satisfactory with regards to all parameters and drug release profile was similar to the marketed product.	54
SreeHarsha et al., 2019	Darifenacin	Oral	<i>In vitro</i>	Surfactant (Labrafil 1944 CS) and co-surfactant (polyethylene glycol 400) and peanut oil	SEDDS were developed using surfactant, co-surfactant and peanut oil. The average globule size of SEDDS was less than 200 nm and depicted negative zeta potential. The rate of dissolution of the developed formulations was also increased upon comparison with pure darifenacin.	55
Sonvico et al., 2017	Gabapentin and flurbiprofen	Oral	<i>In vitro and in vivo (human volunteers)</i>	HPMC K15M, PEO, PVP K30, Mannitol, sodium croscarmellose, sodium alginate, B-cyclodextrin	This was a tri-layered formulation and, during <i>in vitro</i> dissolution testing, layer B disintegrated in few minutes splitting the layer A and C eventually. Layer A started to float and layer B sank down in the bottom. Layer A floated for about 7 hours and for layer C there was no flurbiprofen release in the first 60 minutes. After	56

					transferring the layer C to pH 7.2 medium, accelerated dissolution was observed	
Abbas et al., 2019	Darifenacin hydrobromide	Buccal	<i>In vitro</i>	PVA, Tween 80, croscarmellose sodium, sodium starch glycolate, indion 414	The formulation containing 4% w/w indion 414, 30% w/w glycerol, 2% w/v PVA, 0.5% w/v tween 80 and 7.5 mg of darifenacin hydrobromide was an optimum formulation by showing shortest disintegration time of 31.28 seconds.	57

Table 4.2: List of commercial products of drugs used for managing OAB ³⁴.

Drug	Dose	Formulation type	Company name	Strength	Marketed name	Indicative NHS ^s price
Oxybutynin hydrochloride	Oral immediate-release: 5 mg 2-3 times a day	Tablet	Alliance Healthcare (Distribution) Ltd	2.5 mg	Oxybutynin 2mg tablets	56 tablet = £1.86 84 tablet = £2.79
				3 mg	Oxybutynin 3mg tablets	56 tablet = £17.91
				5 mg	Oxybutynin 5mg tablets	56 tablet = £2.00 84 tablet = £3.00
	Oral modified-release: 5 mg once daily to maximum of 20 mg once daily	Modified-release tablet	Janssen-Cilag Ltd	5 mg	Lyrinel XL	30 tablet = £13.77
				10 mg	Lyrinel XL	56 tablet = £27.54
				Oral solution	Brillpharma Ltd	500 µg/ml
	1 mg/ml	Oxybutynin 5mg/5ml oral solution sugar free	150 ml = £230.00			
	Transdermal patch: 1 patch twice weekly, 1 patch provides 3.9 mg of oxybutynin daily	Transdermal patch	Orion Pharma (UK) Ltd	3.9 mg/24 hour	Kentera 3.9mg/24hours patches	8 patch = £27.20
Tolterodine tartrate	Oral immediate-release: 2 mg twice daily	Tablet	Sandoz Ltd	1 mg	Tolterodine 1mg tablets	56 tablet = £1.46
				2 mg	Tolterodine 1mg tablets	56 tablet = £1.68
	Oral modified-release: 4 mg once daily	Modified-release capsule	Aspire Pharma Ltd	2 mg	Neditol XL	28 capsule = £11.60
				4 mg	Neditol XL	28 capsule = £12.89
Capsaicin	Apply 3-4 times a day	Cream	Teva UK Ltd	250 µg/g	Zacin 0.025% cream	45 gram = £17.71
				750 µg/g	Axsain 0.075% cream	45 gram = £14.58
		Cutaneous patch	Grunenthal Ltd	179 mg	Qutenza 179mg	1 patch = £210.00
Botulinum toxin type A	Information is specific to each individual preparation	Powder for solution for injection	Allergan Ltd	50 unit	Botox 50unit powder for solution for injection vials	1 vial = £77.50 (Hospital only)
				100 unit	Botox 100unit powder for solution for injection vials	1 vial = £138.20 (Hospital only)
				200 unit	Botox 200unit powder for solution for injection vials	1 vial = £276.40 (Hospital only)

			Galderma (UK) Ltd	125 unit	Azzalure 125unit powder for solution for injection vials	1 vial = £64.00
			Ipsen Ltd	300 unit	Dysport 300unit powder for solution for injection vials	1 vial = £92.40
				500 unit	Dysport 500unit powder for solution for injection vials	2 vial = £308.00
Trospium chloride	Oral immediate-release: 20 mg twice daily on empty stomach	Tablet	Galen Ltd	20 mg	Flotros 20mg tablets	60 tablet = £18.20
		Modified-release capsule	Contura Ltd	20 mg	Regurin XL 60mg capsules	28 capsule = £23.05
	Oral modified-release: 60 mg once daily					
Darifenacin hydrobromide	Initially 7.5 mg once daily to 15 mg after 2 weeks	Modified-release tablet	Norgine Pharmaceuticals Ltd	7.5 mg	Emselex 7.5mg modified-release tablets	28 tablet = £25.48
				15 mg	Emselex 15mg modified-release tablets	28 tablet = £25.48
Propiverine hydrochloride	Oral immediate-release: 15 mg 1-2 times a day	Tablet	Advanz Pharma	15 mg	Detrunorm 15mg tablets	56 tablet = £18.00
		Modified-release capsule	Advanz Pharma	30 mg	Detrunorm XL 30mg capsules	28 capsule = £24.45
				45 mg	Detrunorm XL 45mg capsules	28 capsule = £27.90
Gabapentin	Initial adult dose is 300 mg/day, 300 mg twice a day (2nd day of treatment), 300 mg three times a day (third day), with a maximum of 2.4 g a day.	Tablet	A A H Pharmaceuticals Ltd	600 mg	Gabapentin 600mg tablets	100 tablet = £9.78
				800 mg	Gabapentin 600mg tablets	100 tablet = £27.64
		Capsule	Accord Healthcare Ltd	100 mg	Gabapentin 100mg capsules	100 capsule = £3.50
				300 mg	Gabapentin 300mg capsules	100 capsule = £3.97
				400 mg	Gabapentin 400mg capsules	100 capsule = £6.50

		Oral solution	A A H Pharmaceuticals Ltd	50 mg/ml	Gabapentin 50mg/ml oral solution sugar free	150 ml = £66.36
			Imported (United States)	50 mg/ml	Neurontin 250mg/5ml oral solution	470 ml = no price available
Flurbiprofen	150 to 300 mg daily	Tablet	Mylan	50 mg	Flurbiprofen 50mg tablets	100 tablet = £21.30
				100 mg	Flurbiprofen 100mg tablets	100 tablet = £38.10
		Lozenge	Reckitt Benckiser Healthcare (UK) Ltd	8.75 mg	Strefen Honey and Lemon 8.75mg lozenges	16 lozenge = £3.42

[§] NHS: The National Health Services

4.3.1. Transdermal route

Transdermal drug delivery systems have proven to be an excellent for OAB patients owing to their painless approach, i.e., direct application of the drug formulation onto healthy and intact skin ^{25, 26}. These systems possess many advantages over other drug delivery routes including non-invasiveness for patients suffering from needle phobia and dysphagia, thus providing a suitable alternative to parenteral and oral routes, as well as minimising the need for multiple administration, hence improving patient compliance ²⁶. Moreover, in some cases, this route provides enhanced transdermal absorption and improved bioavailability as it avoids pre-systemic metabolism ²⁸.

Oxybutynin is an anti-muscarinic drug and is a selective M1 and M3 receptor antagonist ⁵⁸. The presence of both spasmolytic and anticholinergic properties makes it an effective therapeutic option for the treatment of OAB ⁵⁹. It is lipophilic and has a short half-life of 1-3 hours. Transdermal delivery of oxybutynin is preferred over oral administration for the treatment of OAB as oral administration leads to the production of N-desethyloxybutynin, which is an active metabolite of oxybutynin subject to hepatic first-pass metabolism in the liver and gut and causes severe dryness of the mouth ^{60, 61}. Conversely, transdermal delivery of oxybutynin decreases the onset of the active metabolite, hence reduce the drug induce xerostomia and increases the overall treatment adherence ⁶². Various clinical trials have reported that transdermal delivery of oxybutynin is associated with a low incidence of side effects which led researchers to develop transdermal formulations using different polymers and permeation enhancers ^{63, 64}. For example, oxybutynin bioadhesive films were prepared using polyvinyl alcohol (PVA) and sorbitol. The films showed good permeation characteristics across rabbit ear skin, oxybutynin permeation increased linearly for up to 7 hours, and 50% of drug permeation was achieved after 24 hours ³⁵. Banu et al., 2010 ³⁶ also developed oxybutynin films containing 2% carbopol-934P and 30% polyethylene glycol which showed 87% drug permeation across rat abdominal skin, whereas the permeation from the formulation containing 2% of ethyl cellulose: carbopol-934P (1:3) and 30% polyethylene glycol was 88%. The results showed that the films were suitable for the transdermal administration of oxybutynin for the treatment of OAB ³⁶.

Although the transdermal route provides many advantages, it is also associated with a few problems, one of which is skin irritation. For example, a topical gel of oxybutynin chloride was approved by the US Food and Drug Administration in 2009 and was intended for application on thighs, buttocks, or abdomen daily, but nearly 6% of patients suffered from skin irritation after applying this gel⁶⁵. To overcome this problem, a transdermal spray of oxybutynin was developed using Lutrol F-127 and carbopol-940 as polymers and myristyl lactate and glyceryl monooleate as permeation enhancers. Formulations took 65-70 seconds to dry and formed a thin film. Permeation studies showed 45-50% drug was permeated, and no erythema or oedema was observed, hence it was concluded to be safe to use in managing OAB³⁷. Proniosome gel formulations developed by Rajabalaya et al.,³⁸ were also successful in overcoming the skin irritation issue. These contained non-ionic surfactants (Spans (S20, S40, and S60) and Tweens (T20 and T80)), lecithin and cholesterol. Cholesterol provides high permeability and stability, and non-ionic surfactants form a layer that provides deeper penetration of the drug into the skin without causing side effects such as skin irritation. All the formulations had more than 87% entrapment efficiency, which tended to increase with an increase in surfactant concentration. Furthermore, in vitro permeation studies showed that the drug permeation was higher for gels containing Span than gels containing Tween. It was reported that transdermal application of these formulations resulted in decreased pilocarpine-induced salivation as it led to reduced production of N-desethyloxybutynin, N-DEO, (an oxybutynin metabolite) (Figure 4.5 a) and showed highly regenerative surfaces of transitional epithelium³⁸.

Moreover, commercially available oxybutynin patches may not possess good mechanical properties as pressure-sensitive adhesives are soft can lead to difficulties removing the patch from the primary packaging (Figure 4.5 b).

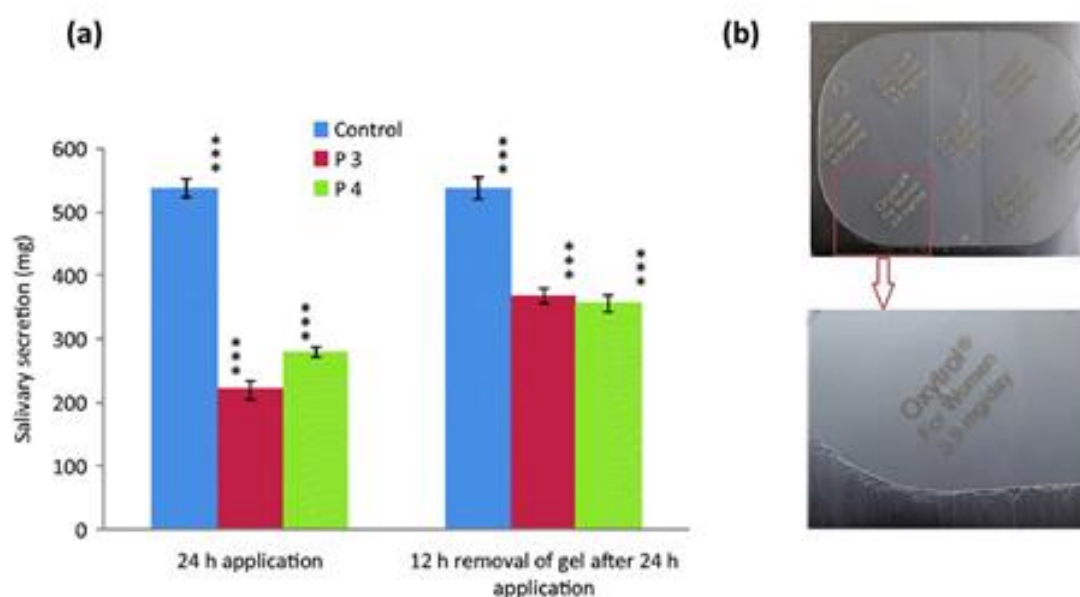


Figure 4.5: (a) Recovery of pilocarpine-induced salivation secretion in rats after transdermal administration of oxybutynin chloride (b) Appearance of commercial product in primary package, reproduced with permission from ^{38, 39}.

To overcome this problem, Wang et al., ³⁹ investigated acrylic adhesives with different functional groups and reported that adhesives with AACONH₂ functional group displayed good mechanical properties while also enabling the highest *in vitro* and *in vivo* (rat model) oxybutynin permeation. Tolterodine is another antimuscarinic drug that is widely prescribed for the treatment of OAB ⁶⁶. It is a non-selective muscarinic receptor antagonist, less lipophilic than oxybutynin and does not cross the blood-brain barrier (BBB) ⁵⁸. Like oxybutynin, oral administration of tolterodine also causes side effects which can lead to patient compliance issues; hence, transdermal delivery of tolterodine would be a suitable alternative ⁴⁴. For example, in a study conducted by Pandit et al., ⁴⁰ a combination of cabopol-934P: HPMC (1:3) with 30% propylene glycol was effective in producing tolterodine tartrate-based films with high endurance and flexibility and 69% of the drug was permeated through rat skin in in-vitro settings. In a separate study, a transdermal formulation was prepared using carbopol-940 as a gel matrix and N-methyl pyrrolidone as a permeation enhancer. The formulation had a permeation rate of 770 $\mu\text{g cm}^{-2} \text{ h}^{-1}$ with an absolute bioavailability of 11%. It was reported that the matrix formulation did not cause skin irritation ⁴¹. Liu et al., ⁶¹ also used Carbopol-940 and N-methyl pyrrolidone for the development of hydrogels containing 5-hydroxymethyl

tolterodine. The formulation resulted in 21% absolute bioavailability, and no skin irritation was observed.

In another study, Liu et al.,⁴³ reported the development of a tolterodine hydrogel formulation using Tween 80, HPMC, Carbopol-980 and hydroxypropyl cellulose (HPC). Morphological changes in the film-forming process of transparent hydrogels are shown in Figure 4.6. The formulation showed 86% cumulative drug permeation in 24 hours. The flux of tolterodine from the formulation was 81.82, 37.15, 18.55 and 15.83 $\mu\text{g cm}^{-2} \text{h}^{-1}$, across subcutaneous tissue, dermis, epidermis, and full rat skin, respectively. In vivo studies in rats also found that the hydrogel formulation exhibited sustained drug release and permeation over 24 hours and higher bioavailability (25%) than tolterodine tablets, with 15% bioavailability; hence, making this hydrogel a viable drug delivery system. The applicability of transdermal patches was also assessed where Rajabalaya et al.,⁴⁴ exploited different grades of Eudragit (E 100, RSPO and RLPO) with various plasticisers and polyvinyl pyrrolidone. These patches had a reduced impact on salivary secretions as compared to oral formulation, thereby proving their usefulness in reduction of common side-effects. The findings of these studies conclude that transdermal films, patches, and hydrogels proved to be effective and promising systems for delivery of tolterodine tartrate for the treatment of OAB.

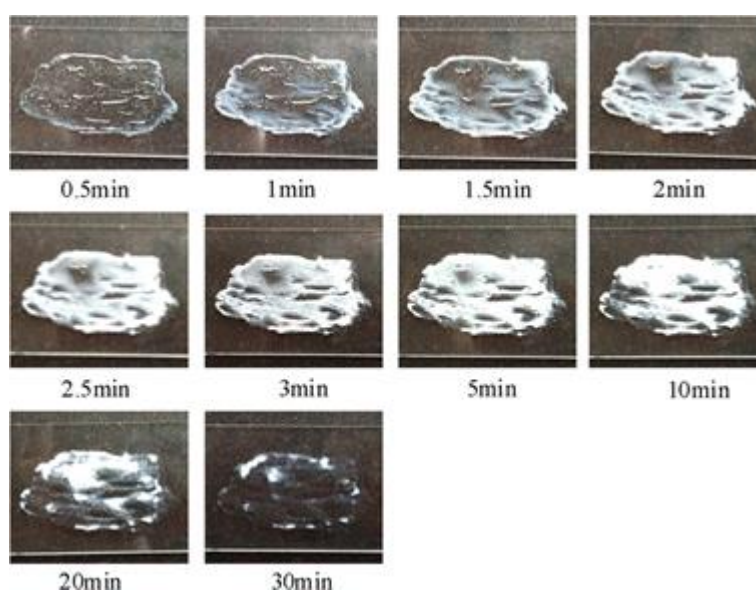


Figure 4.6: Real-time morphological changes during film-forming process of transparent hydrogels, reproduced with permission from⁴³.

Overall, the findings of these studies confirm that the transdermal delivery of anti-muscarinic drugs is useful and provides a suitable alternative to oral administration to avoid side effects.

4.3.2. Intravesical route

Intravesical therapies have been proposed to achieve inhibition of the overactive detrusor muscle and to avoid high systemic drug levels, thus providing a potentially effective therapeutic option in the management of OAB ⁶⁷. They involve the direct instillation of drug into the bladder followed by insertion of a catheter into the urethra ⁶⁸. This route of drug administration has gained significant attention in the clinical management of urinary tract disorders including overactive bladder and is considered as a second line treatment after oral pharmacotherapy ^{69, 70}. The urothelium, the lining of urinary bladder, is selective and impermeable due to blood-urine barrier (a high magnitude trans urothelial electrical resistance that reflect the net ion flux across the urothelium) ⁷¹ which offers many benefits and challenges. The relative impermeability of the urothelium restricts systemic distribution of drugs and may possibly minimises the risk of side effects ⁷².

Capsaicin, an insoluble vanilloid found in red pepper, is useful in treating overactive bladder and may be delivered via the intravesical route ⁷³. It is hydrophobic; therefore, capsaicin is prepared in normal saline solution with 30% ethanol for intravesical administration ⁷⁴ but this vehicle produces submucosal oedema and causes epithelium thinning ⁷⁵. To address this, Tyagi et al., ⁴⁵ encapsulated capsaicin in liposomes and polyethylene glycol-poly(lactic-co-glycolic acid) (PEG-PLGA) polymer was used as a vehicle, maintaining the formulation in a fluid state prior to instillation but transforming into a hydrogel in situ. Three types of capsaicin formulations, liposomes, hydrogel and 30% ethanolic solution, were administered intravesically to rats. The liposomes and ethanolic solution completely blocked micturition reflexes while the hydrogel, although it did not completely block micturition reflexes, led to a significant decrease in bladder contractions. Cystometry showed a significant decrease in calcitonin gene-related peptide (CGRP) staining of afferent nerves in the bladder wall for the liposome and alcoholic solutions, with significant histological changes for those treated with 30% ethanol alone. It was concluded those liposomes are superior vehicles for administration of capsaicin than 30% ethanolic solution. Similarly, liposomes were also employed by Chuang et al., 2009 ⁴⁶ for delivering botulinum toxin A. Rats treated with lipotoxin ((botulinum toxin A encapsulated in liposomes) exhibited decreased inflammatory reactions with a reduction

in SNAP-25 expression and an increase in calcitonin gene-related peptide (CGRP) compared to rats treated with unentrapped botulinum toxin A. Liposomes were found to be an effective vehicle for intravesical delivery of botulinum toxin A avoiding injections and effects on the detrusor muscle.

Although the intravesical drug route has shown promise for the management of OAB, frequent insertion of a catheter may lead to poor patient acceptability and compliance. Hopmann et al., in 2015⁴⁷ fabricated an implant comprising drug in poly (D, L-lactide-co-glycolide)-co-polyethylene glycol di-block copolymer microspheres embedded into a polydimethylsiloxane absorbable foam matrix. The device was shown to extend the release for up to four weeks in artificial urine and has the potential to extend the delivery of the highly soluble, tiroprium chloride. Entrapment in a lipid base may also control the release of this drug. Three systems comprising glyceryl tristearate, mini tablets made using compression, extrudates formed by solid-lipid extrusion and mini-moulds manufactured via a melting and casting technique. The preparation method impacted the drug release kinetics with extrudates and mini-tablets extending release of tiroprium chloride for more than 5 days; however, the drug release from the mini-mould was better. Overall, it was concluded that lipids may be a suitable matrix for controlling the release of highly soluble drugs and preparing delivery systems of a small size making insertion and excretion achievable, thus addressing some of the issues with this delivery route⁴⁸.

The above-mentioned studies show that intravesical route is an effective and suitable approach for the administration of drugs in the treatment of OAB with less incidence of side effects as compared to oral pharmacotherapy.

4.3.3. Vaginal route

The vaginal route is highly significant for drug delivery in women suffering from OAB. It has established merits compared with other routes enabling extended drug release and action. Also, avoidance of first pass metabolism may reduce dosing frequency which may improve patient compliance. The delivery of drugs via this route is considered favourable in managing overactive bladder and vaginal dryness simultaneously, which are common issues faced by human females after menopause⁷⁶⁻⁸².

Bioadhesive gels are the most used therapeutic delivery systems to pro-long the residence time in the vagina. Mucoadhesive gels of oxybutynin were developed using polymers such as Poloxamer 407, HPMC K100M and chitosan. The gel formulation containing HPMC K100M exhibited better mucoadhesion, adhesiveness, cohesiveness, and viscosity than chitosan and poloxamer gel formulations. Permeation studies across vaginal mucosa also confirmed better permeation of oxybutynin from HPMC K100M gel formulation. In vivo studies in rabbits showed that HPMC K100M gels resulted in the highest relative bioavailability (Figure 4.7). Conclusions were that oxybutynin mucoadhesive vaginal gels are innovative and a promising drug delivery system that can be used safely for vaginal dryness and overactive bladder after menopause ³¹.

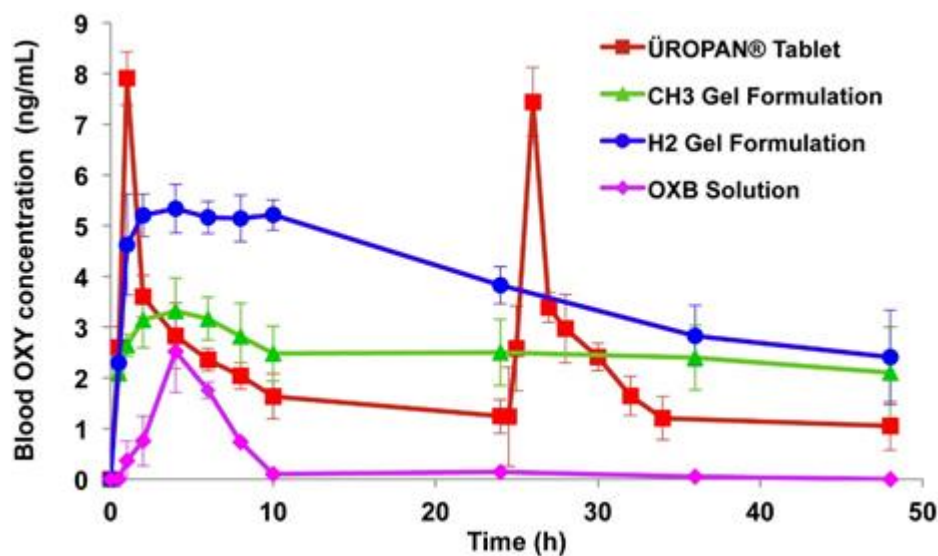


Figure 4.7: Blood oxybutynin concentration profiles of oral and vaginally administered formulations, CH3 (1% w/v glacial acetic acid and 3% w/v Chitosan H), H2 (2% w/v hypromellose K100M), reprinted with permission from ³¹.

4.3.4. Intramuscular route

Intramuscular route is another suitable alternative for the management of OAB. This route is suitable for unconscious patients or for drugs where pharmacokinetic findings recommend avoiding other routes of administration ⁸³. Microsphere based intramuscular formulations are designed to maintain drug release over a sustained period, reduce dose related adverse effects and improve therapeutic potential ⁸⁴⁻⁸⁶. Sun et al., 2010 ⁴⁹ developed intramuscular depot formulations of tolterodine using PLGA microspheres as a carrier. PLGA concentration affected the encapsulation efficiency and led to an increase from 63 to 79% when polymer

concentration was increased from 180 to 230 mg/ml. Drug entrapment efficiency also increased upon adding palmitic or stearic acid. The bioavailability of these formulations was studied in beagle dogs and a sustained drug release was observed for ~18 h; however, an initial burst release was also evident. The results concluded that these formulations resulted in continuous inhibition of muscarinic receptors in comparison to oral formulations that inhibit muscarinic receptor in a pulsatile fashion and can provide a more effective treatment for OAB patients.

4.3.5. Oral route

Oral pharmacotherapy is the mainstay of the treatment of OAB, especially for anti-muscarinic drugs⁶⁷. It is the most convenient and preferred route of drug administration due to ease of production, high patient compliance, cost-effectiveness, and flexibility in dosage form⁸⁷. However, the oral delivery of antimuscarinic drugs may lead to some side effects including constipation and xerostomia²¹⁻²⁴. Extended-release oral formulations are of enormous importance and provide great benefits. Propiverine is used for the treatment of OAB via the oral route and its solubility is pH dependent which presents problems in the development of extended-release formulations. Different coatings levels of Eudragit polymer and propiverine were applied to the citric acid crystals in a sequential manner to prepare extended-release pellets (Figure 4.8). Drug release profiles from the developed pellet formulations in the presence and absence of pH modifier and the free-base and hydrochloride salt were comparatively evaluated. The main objective of this formulation design was to create a favourable environment for drug dissolution within the pellet while extending the drug release. Upon contact with the dissolution medium, osmotic pressure built up inside the pellet core, which in turn caused drug release through the polymer coating. The results showed that, with higher level of coating, the drug release and citric acid release was reduced. In fact, citric acid release was slower than the drug release and stayed within the pellets for more than 16 h. However, if microcrystalline cellulose pellets are employed as a starting core, then the drug release is pH-dependant. Moreover, noticeable differences were noticed between the formulations containing the free drug base and those with the hydrochloride salt because of an altered microenvironmental pH. It was concluded that this approach is effective and feasible for extended-release formulations of propiverine for managing OAB⁵⁰.

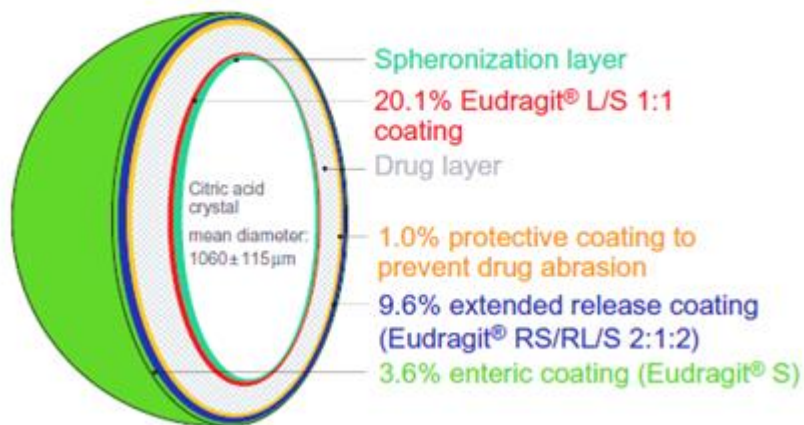


Figure 4.8: Illustration depicted the formulation principle of membrane-coated multiple units extended-release pellets, reproduced with permission from ⁵⁰.

Pradhan et al., 2014 ⁵¹ developed coated tablets of tolterodine tartrate using hypromellose 2208 and 2910 that extended release for 10 hours *in vitro* and was like a marketed product. Similar results were obtained from *in vivo* studies where the pharmacokinetic parameters of the developed formulation and commercial formulation were not significantly different from each other with formulations being bioequivalent. Therefore, the hypromellose based matrix tablet could be a suitable alternative to sustained release capsules. Patil et al., 2017 ⁵² also developed extended-release pellets of tolterodine tartrate using mannitol as an osmotic agent along with hypromellose. These pellets were then filled into capsules of suitable sizes and the *in-vitro* drug release compared with Detrol LA[®]; a generic version of the tolterodine tartrate. It was concluded that the extended-release capsule administered once a day can achieve similar results as that of Detrol LA[®]. Similarly, extended-release matrix tablets of oxybutynin chloride were prepared using combinations of polymers including hypromellose K4M, K100M, Carbopol, ethyl cellulose, PVP, and sodium alginate. A formulation containing hypromellose K4M along with ethyl cellulose demonstrated controlled drug release in buffer for 24 h ⁵³. This shows that extended-release formulations are suitable for the treatment of OAB as they are required to be administered only once in a day which reduces the need for multiple administration of doses as compared to immediate release formulations. Sudarsan et al., 2014 ⁵⁴ developed darifenacin hydrobromide reservoir tablets using ethyl cellulose as

a coating agent. These formulations were compared with the marketed product Enablex[®]. Tablets showed good friability and 90% drug release over 12 h in 0.1M HCl, similar to Enablex[®] tablets. SreeHarsha et al., 2019⁵⁵ developed a self-emulsifying drug delivery system (SEDDS) for the poorly soluble darifenacin using surfactant (Labrafil 1944 CS) and co-surfactant (polyethylene glycol 400) in a ratio of 2:1 with peanut oil. The dissolution rate of the developed formulations was greater than pure darifenacin in *in vitro* dissolution studies.

In 2008, a patent has been filed disclosing the synergistic effect gabapentin and flurbiprofen in relieving the OAB symptoms⁸⁸. Based on this patent's findings Sonvico et al., 2017⁵⁶ has developed an oblong shaped tri-layered tablet with multi drug release kinetic profiles containing gabapentin and flurbiprofen. Layer A (the top layer) and B (the middle layer) contained gabapentin for prolonged and immediate release, respectively. Layer C (the bottom layer) contained flurbiprofen for delayed but prolonged release. During *in vitro* dissolution testing, layer B disintegrated within a few minutes leading to the eventual splitting of layer A and C. Layer A started to float and layer C sank down in the bottom. Layer A floated for about 7 h and for layer C, there was no flurbiprofen release in the first 60 min. After transferring the layer C to pH 7.2 medium, accelerated dissolution was observed. The *in vitro* drug release assessment confirms the programmed drug delivery aspects of this tri-layer fixed dose formulation. Additionally, a higher bioavailability of gabapentin was noticed when delivered in fed condition (30 min after the meal) to human volunteers in comparison to dose administration 10 min before meal or in fasting condition, Figure 4.9. The researchers of this study have argued that these findings are supporting of the gastroretention potential of gabapentin prolonged release layer (layer A). The two drugs were delivered at different anatomical sites since the food presence prolonged the gastric absorption of gabapentin from the floating layer and delayed the flurbiprofen absorption. Moreover, the delayed or intestinal specific release of flurbiprofen was realised using a matrix-based polymer combination system negating the necessity of film coating. The results show that tri-layered tablet formulation provided modified release of drugs which may be a suitable option for managing OAB⁶⁶.

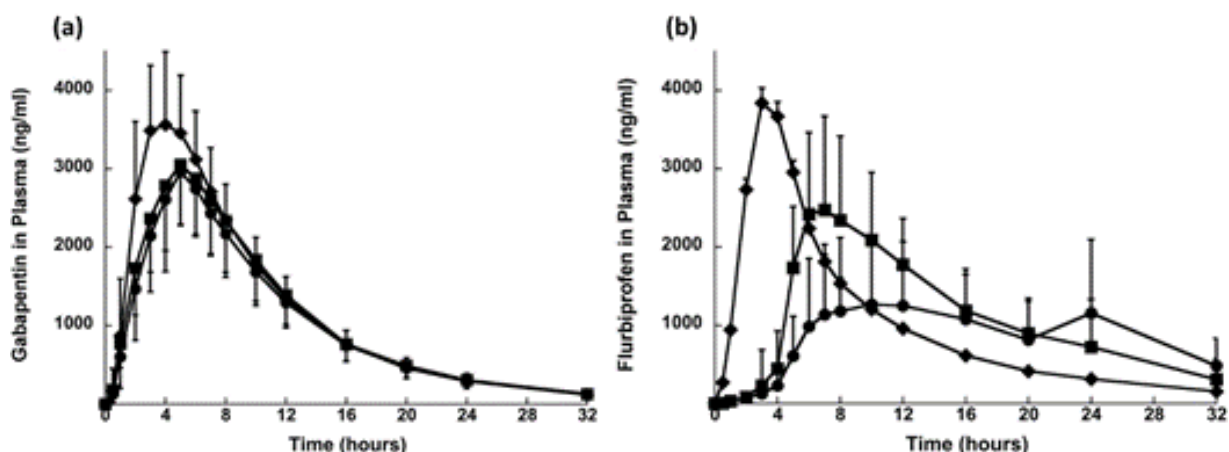


Figure 4.9: Plasma profiles of (a) gabapentin and (b) flurbiprofen after single dose administration in fed conditions of (●) TLT_HPMC Type I, (■) TLT_HPMC Type II and (◆) Immediate release dosage form (mean values \pm SD; n =24), reproduced with permission from 66.

Additionally, the fast-dissolving drug delivery systems have advantages for geriatric and paediatric patients due to rapid disintegration, ease of administration or self-administration, and non-requirement for chewing or water. Fast dissolving films of darifenacin hydrobromide were developed by Abbas et al., 2019⁵⁷ using PVA, Tween 80 and glycerol. Different types and concentrations of superdisintegrants including sodium starch glycolate, croscarmellose sodium and Indion 414 were investigated. The results revealed that the formulation containing 4% w/w indion 414, 30% w/w glycerol, 2% w/v PVA, 0.5% w/v tween 80 and 7.5 mg of darifenacin hydrobromide was an optimum formulation by showing the shortest disintegration time of 31 Sec. Such formulations provide faster therapeutic effects to patients suffering from OAB.

Overall, for oral drug delivery route various dosage form designs were identified which are easy to develop, such as reservoir drug delivery systems, tri-layered tablets, coated tablets and loading of microspheres in capsules.

4.4. Conclusions

The current systematic review has identified the various formulations strategies, marketed products, and has aided the comparison of diverse formulations approaches intended for different drug delivery routes where each route has its importance and challenges. The exploitation of different drug delivery routes can improve patient compliance and adherence, and advances in the formulation of dosage forms can help patients to get effective treatment with minimal side effects. This systematic review found evidence regarding the frequent use of the transdermal route which has led to commercial products; however, other routes such as oral, intravesical, vaginal and intramuscular were also identified. It can be concluded from the current systematic review that drug delivery routes other than oral are used to avoid the side effects caused by oral administration of drugs. For example, the oral delivery of antimuscarinic drugs can potentially cause bothersome side effects. Moreover, this review has identified the need for robust *in vitro* tests which should be aligned with *in vivo*/clinical testing. Generally, it is expected that the detailed discussion of various studies and enlisting of their marketed products will be a valuable resource for pharmaceutical scientists to better understand and comprehend the existing literature and challenges, which will be anticipated to provide a basis for designing and fabricating new effective formulations to manage OAB.

Although the systematic review resulted in greater number of studies reporting transdermal drug delivery system for the management of OAB, but it does not reduce the significance of oral drug delivery route which is the most preferred and convenient route. There are drugs other than antimuscarinics which can be given oral and are effective in relieving the symptoms of OAB and does not cause bothersome side effects. There are also cases where antimuscarinics failed to provide the therapeutic effect. These findings demand to investigate the drugs other than antimuscarinics for oral drug delivery to improve the patient compliance and adherence.

References

1. D. Robinson and L. Cardozo, *Climacteric*, 2019, **22**, 250.
2. D. E. Irwin, I. Milsom, S. Hunskaar, K. Reilly, Z. Kopp, S. Herschorn, K. Coyne, C. Kelleher, C. Hampel and W. Artibani, *European urology*, 2006, **50**, 1306.
3. J. S. Benner, R. Becker, K. Fanning, Z. Jumadilova, T. Bavendam, L. Brubaker and O. M. U. S. S. Committee, *The Journal of urology*, 2009, **181**, 2591.
4. P. Abrams, C. Kelleher, L. A. Kerr and R. G. Rogers, *Am J Manag Care*, 2000, **6**, S580.
5. F. A. Filipetto, K. G. Fulda, A. E. Holthusen, T. M. McKeithen and P. McFadden, *BMC family practice*, 2014, **15**, 96.
6. F. M. Chu and R. Dmochowski, *The American journal of medicine*, 2006, **119**, 3.
7. E. Meng, W. Y. Lin, W. C. Lee and Y. C. Chuang, *Low Urin Tract Symptoms*, 2012, **4 Suppl 1**, 48.
8. B. A. O'REILLY, A. H. Kosaka, G. F. Knight, T. K. Chang, A. P. Ford, J. M. Rymer, R. Popert, G. Burnstock and S. B. McMAHON, *The Journal of urology*, 2002, **167**, 157.
9. A. F. Brading, *Urology*, 1997, **50**, 57.
10. G. Sibley, *British journal of urology*, 1997, **80**, 54.
11. C. A. Maggi, P. Santicioli, M. Parlani, M. Astolfi, R. Patacchini and A. Meli, *Journal of pharmacy and pharmacology*, 1987, **39**, 653.
12. C. de NUNZIO, G. Franco, A. Rocchegiani, F. Iori, C. Leonardo and C. Laurenti, *The Journal of urology*, 2003, **169**, 535.
13. H.-J. Yu, C.-Y. Liu, K.-L. Lee, W.-C. Lee and T. H.-H. Chen, *Urologia internationalis*, 2006, **77**, 327.
14. R.-T. Liu, M.-S. Chung, W.-C. Lee, S.-W. Chang, S.-T. Huang, K. D. Yang, M. B. Chancellor and Y.-C. Chuang, *Urology*, 2011, **78**, 1040.
15. Y.-C. Chuang, V. Tyagi, R.-T. Liu, M. B. Chancellor and P. Tyagi, *Urological Science*, 2010, **21**, 132.
16. N. C. C. f. Women's and C. s. Health, 2006.
17. C. R. Chapple and E. A. GORMLEY, *BJU international*, 2006, **98**, 78.
18. H. Mostafaei, S. F. Shariat, H. Salehi-Pourmehr, F. Janisch, K. Mori, F. Quhal and S. Hajebrahimi, *Expert review of clinical pharmacology*, 2020, **13**, 707.
19. C. E. Painter and A. M. Suskind, *Current bladder dysfunction reports*, 2019, **14**, 377.
20. S. V. Sastry, J. R. Nyshadham and J. A. Fix, *Pharmaceutical Science & Technology Today*, 2000, **3**, 138.
21. J. S. Benner, M. B. Nichol, E. S. Rovner, Z. Jumadilova, J. Alvir, M. Hussein, K. Fanning, J. N. Trocio and L. Brubaker, *BJU international*, 2010, **105**, 1276.
22. C. R. Chapple, J. Nazir, Z. Hakimi, S. Bowditch, F. Fatoye, F. Guelfucci, A. Khemiri, E. Siddiqui and A. Wagg, *European urology*, 2017, **72**, 389.
23. C. Sexton, S. Notte, C. Maroulis, R. Dmochowski, L. Cardozo, D. Subramanian and K. Coyne, *International journal of clinical practice*, 2011, **65**, 567.
24. P. W. Veenboer and J. R. Bosch, *The Journal of urology*, 2014, **191**, 1003.
25. C. M. Schoellhammer, D. Blankschtein and R. Langer, *Expert opinion on drug delivery*, 2014, **11**, 393.
26. T. Han and D. B. Das, *European Journal of Pharmaceutics and Biopharmaceutics*, 2015, **89**, 312.
27. M. R. Prausnitz and R. Langer, *Nature biotechnology*, 2008, **26**, 1261.
28. K. Ita, *Journal of Drug Delivery Science and Technology*, 2014, **24**, 245.
29. P. Tyagi, M. Kashyap, H. Hensley and N. Yoshimura, *Expert opinion on drug delivery*, 2016, **13**, 71.
30. F. Acarturk, *Recent patents on drug delivery & formulation*, 2009, **3**, 193.

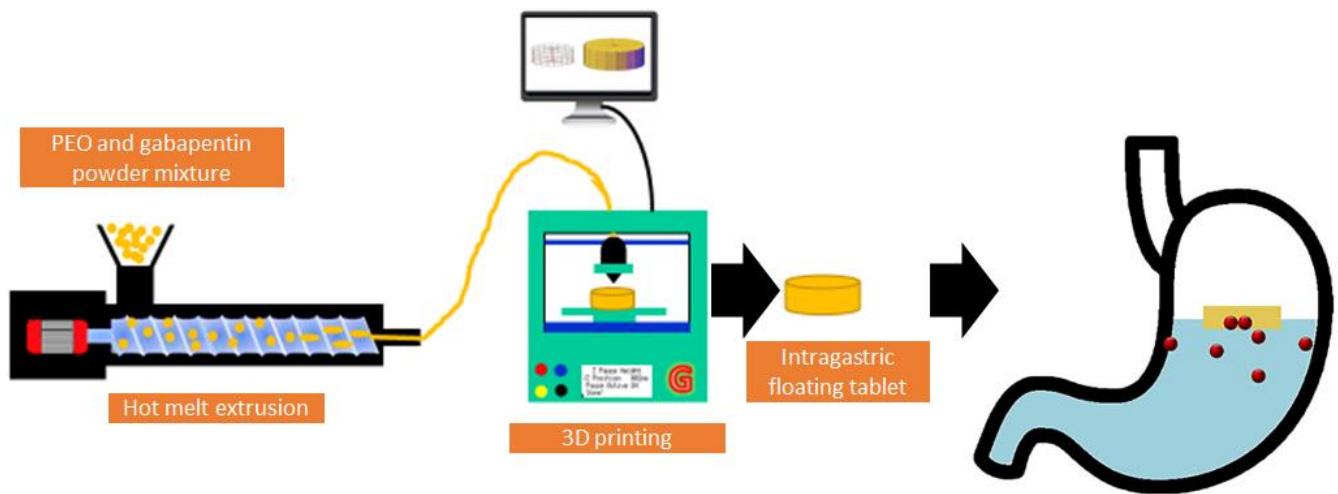
31. F. Tuğcu-Demiröz, F. Acartürk and D. Erdoğan, *International journal of pharmaceutics*, 2013, **457**, 25.
32. S. Srikrishna and L. Cardozo, *International urogynecology journal*, 2013, **24**, 537.
33. D. Moher, A. Liberati, J. Tetzlaff and D. G. Altman, *Annals of internal medicine*, 2009, **151**, 264.
34. British National Formulary (BNF), <https://www.bnf.org/products/bnf-online/>).
35. S. Nicoli, E. Penna, C. Padula, P. Colombo and P. Santi, *International journal of pharmaceutics*, 2006, **325**, 2.
36. T. S. Banu, S. Som and N. T. Havannavar, *Research Journal of Pharmaceutical, Biological and Chemical Sciences*, 2010, **1**, 412.
37. A. Bakshi, A. Bajaj, G. Malhotra, M. Madan and N. Amrutiya, *Indian journal of pharmaceutical sciences*, 2008, **70**, 733.
38. R. Rajabalaya, S. R. David, J. Chellian, G. Xin Yun and S. Chakravarthi, *Drug delivery*, 2016, **23**, 1578.
39. W. Wang, C. Liu, Z. Luo, X. Wan and L. Fang, *European Journal of Pharmaceutical Sciences*, 2018, **122**, 116.
40. V. Pandit, A. Khanum, S. Bhaskaran and V. Banu, *Int J Pharm Tech Res*, 2009, **1**, 799.
41. F. Sun, C. Sui, Y. Zhou, X. Liu, Y. Shi, Y. Wu and Y. Li, *International journal of pharmaceutics*, 2013, **454**, 532.
42. W. Liu, L. Teng, K. Yu, X. Sun, C. Fan, C. Long, N. Liu, S. Li, B. Wu and Q. Xu, *European Journal of Pharmaceutical Sciences*, 2017, **96**, 530.
43. X. Liu, L. Fu, W. Dai, W. Liu, J. Zhao, Y. Wu, L. Teng, F. Sun and Y. Li, *International journal of pharmaceutics*, 2014, **471**, 322.
44. R. Rajabalaya, C. Y. Mun, J. Chellian, S. Chakravarthi and S. R. David, *Acta Pharmaceutica*, 2017, **67**, 325.
45. P. Tyagi, M. B. Chancellor, Z. Li, W. C. de GROAT, N. Yoshimura, M. O. Fraser and L. Huang, *The Journal of urology*, 2004, **171**, 483.
46. Y.-C. Chuang, P. Tyagi, C.-C. Huang, N. Yoshimura, M. Wu, J. Kaufman and M. B. Chancellor, *The Journal of urology*, 2009, **182**, 786.
47. C. Hopmann, D. Kaltbeitzel, T. Kauth, B. Dittrich, J. Grosse, N. Huppertz, U. Schwantes, C. Neumeister, M. von Walter and A. Hemoteq, *Plastics Engineering*, 2015, **71**, 60.
48. M. Haupt, M. Thommes, A. Heidenreich and J. Breitreutz, *Journal of controlled release*, 2013, **170**, 161.
49. F. Sun, C. Sui, L. Teng, X. Liu, L. Teng, Q. Meng and Y. Li, *International journal of pharmaceutics*, 2010, **397**, 44.
50. J. Ploen, J. Andersch, M. Heschel and C. S. Leopold, *Drug development and industrial pharmacy*, 2009, **35**, 1210.
51. R. Pradhan, Y.-I. Kim, S. W. Chang and J. O. Kim, *International journal of pharmaceutics*, 2014, **460**, 205.
52. V. Patil and D. Belsare, *Int J App Pharm*, 2017, **9**, 29.
53. S. Naik, K. Venkateswarlu and K. Chandrasekhar, *Indo Am J Pharm Res*, 2016, **6**, 4179.
54. G. V. Sudarsan and T. V. B. Reddy, 2014.
55. N. SreeHarsha, A. Shariff, Y. A. Shendkar, B. E. Al-Dhubiab and G. Meravanige, *INDIAN JOURNAL OF PHARMACEUTICAL EDUCATION AND RESEARCH*, 2019, **53**, S204.
56. F. Sonvico, C. Conti, G. Colombo, F. Buttini, P. Colombo, R. Bettini, M. Barchielli, B. Leoni, L. Loprete and A. Rossi, *Journal of Controlled Release*, 2017, **262**, 296.
57. I. K. Abbas, N. A. Rajab and A. A. Hussein, *Iraqi Journal of Pharmaceutical Sciences*, 2019, **28**, 83.
58. D. G. Waller and A. P. Sampson, in *Medical Pharmacology and Therapeutics (Fifth Edition)*, eds. D. G. Waller and A. P. Sampson, Elsevier, 2018, DOI: <https://doi.org/10.1016/B978-0-7020-7167-6.00015-4>, pp. 231.

59. Y. E. Yarker, K. L. Goa and A. Fitton, *Drugs Aging*, 1995, **6**, 243.
60. G. W. Davila, J. S. Starkman and R. R. Dmochowski, *Urologic Clinics*, 2006, **33**, 455.
61. K. Andersson and C. Chapple, *World journal of urology*, 2001, **19**, 319.
62. J. Salinas-Casado, M. Esteban-Fuertes, O. Serrano and J. Galván, *Actas Urológicas Españolas (English Edition)*, 2015, **39**, 599.
63. R. Dmochowski, *Drug safety*, 2005, **28**, 583.
64. R. R. Dmochowski, P. K. Sand, N. R. Zinner, M. C. Gittelman, G. W. Davila, S. W. Sanders and T. O. S. Group, *Urology*, 2003, **62**, 237.
65. M. J. Kennelly, *Reviews in urology*, 2010, **12**, 12.
66. A. Athanasopoulos and K. Giannitsas, *Advances in urology*, 2011, **2011**.
67. C. B. Slotoroff, D. Shupp-Byrne and P. J. Shenot, in *Female Urology*, Springer, 2007, pp. 201.
68. H. Zargar, J. Aning, J. Ischia, A. So and P. Black, *Nature Reviews Urology*, 2014, **11**, 220.
69. H.-C. Kuo, H.-T. Liu, Y.-C. Chuang, L. A. Birder and M. B. Chancellor, *European urology*, 2014, **65**, 1117.
70. J. Parkin, C. Shea and G. R. Sant, *Urology*, 1997, **49**, 105.
71. J. Eldrup, J. Thorup, S. Nielsen, T. Hald and B. Hainau, *British journal of urology*, 1983, **55**, 488.
72. J. Kaufman, H. Hensley, J. Jacobs, M. Anthony, V. Tyagi, P. Tyagi and M. Chancellor, *The Journal of Urology*, 2010, **183**, e628.
73. M. B. Chancellor and W. C. de GROAT, *The Journal of urology*, 1999, **162**, 3.
74. A. Giannantoni, S. M. Di Stasi, R. L. Stephen, P. Navarra, G. Scivoletto, E. Mearini and M. Porena, *The Journal of urology*, 2002, **167**, 1710.
75. D. S. BYRNE, A. DAS, J. SEDOR, B. HUANG, D. A. RIVAS, H. J. FLOOD, W. DEGROAT, M. L. JORDAN, M. B. CHANCELLOR and P. MCCUE, *The Journal of urology*, 1998, **159**, 1074.
76. R. M. Levin, C. Whitbeck, A. Borow, O. Burden and R. E. Leggett, *Urology*, 2003, **61**, 1273.
77. K. Malcolm, D. Woolfson, J. Russell, P. Tallon, L. McAuley and D. Craig, *Journal of Controlled Release*, 2003, **90**, 217.
78. A. Schröder, R. M. Levin, B. A. Kogan, A. K. Das, F. Kay and A. Mahashabde, *Urology*, 2000, **56**, 1063.
79. A. Woolfson, R. Malcolm and R. Gallagher, *Journal of controlled release*, 2003, **91**, 465.
80. N. J. Alexander, E. Baker, M. Kaptein, U. Karck, L. Miller and E. Zampaglione, *Fertility and sterility*, 2004, **82**, 1.
81. K. Vermani and S. Garg, *Pharmaceutical science & technology today*, 2000, **3**, 359.
82. C. E. Kast, C. Valenta, M. Leopold and A. Bernkop-Schnürch, *Journal of Controlled Release*, 2002, **81**, 347.
83. D. Greenbatt, *N. Eng. J. Med.*, 1976, **295**, 542.
84. U. Edlund and A.-C. Albertsson, in *Degradable aliphatic polyesters*, Springer, 2002, pp. 67.
85. B. S. Zolnik and D. J. Burgess, *Journal of controlled release*, 2008, **127**, 137.
86. T. Morita, Y. Sakamura, Y. Horikiri, T. Suzuki and H. Yoshino, *Journal of controlled release*, 2001, **73**, 213.
87. P. Viswanathan, Y. Muralidaran and G. Ragavan, in *Nanostructures for Oral Medicine*, eds. E. Andronescu and A. M. Grumezescu, Elsevier, 2017, DOI: <https://doi.org/10.1016/B978-0-323-47720-8.00008-0>, pp. 173.
88. A. Leonardi, L. Guarneri and P. Angelico, *Journal*, 2008.

CHAPTER 5

Personalised 3D printed mucoadhesive gastroretentive matrices for managing overactive bladder (OAB)

Graphical abstract



Notes for readers

- Overactive bladder (OAB) is a symptom complex condition characterised by frequent urinary urgency, nocturia, and urinary incontinence with or without urgency. Gabapentin is an effective treatment for OAB, but the drug has drawbacks such as narrow absorption window as it is preferentially absorbed from upper small intestine which in turn results in poor bioavailability.
- Our aim was to develop extended release intragastric floating system to overcome the drawbacks of gabapentin. For this purpose, plasticiser free filaments of PEO and the drug were developed using hot melt extrusion. PEO is a hydrophilic, linear and uncross linked polymer and has wide applications in extended-release hydrophilic matrices.
- The filaments were extruded successfully with 98% drug loading, possessed good mechanical properties and were successful in printing the tablets using FDM. Tablets were printed with varying shell number and infill density to investigate the floating capacity. Among seven different tablet formulations F2 (2 shells, 0% infill) showed highest floating time i.e., more than 10 hours.
- Drug release studies showed the extended release of the drug in a 12-hour study. It was observed that the drug release was decreased with increase in infill density and shell number. However, among all the formulation F2 was the optimum formulation with longer floating time and sustained release of the drug and was chosen for *in vivo* studies.
- The extended-release effect of PEO was also seen during the pharmacokinetic studies that made the drug to be absorbed into bloodstream over longer period. Overall, *in vitro*, and *in vivo* studies showed successful fabrication of the tablets.

5.1. Introduction

Overactive bladder (OAB) is a symptom complex condition characterised by frequent urinary urgency, nocturia, and urinary incontinence with or without urgency ^{1,2}. It can affect people of any age and is the most common voiding dysfunction in the children ³. The global prevalence of OAB in children is 15-20%, 10.8% for men and 12.8% for women that increases with age and severely affects the patients' quality of life ^{4,5}. As per European and American studies, more than 10% of the population show symptoms and people older than 65 years are more likely to be affected ⁶. Patients suffering from neurogenic diseases (multiple sclerosis, cerebral palsy, brain tumours, Parkinson's diseases, cerebrovascular pathology, and spinal cord injuries) can develop symptoms of overactive bladder known as neurogenic detrusor overactivity or neurogenic OAB ^{7,8}. The neurogenic diseases affect the central nervous system responsible for controlling the functions and thus can cause neurogenic detrusor overactivity ⁹. Contrarily, detrusor overactivity in non-neurogenic OAB can result from non-neurological diseases like urinary tract infection, muscle disease, bladder stones or can be idiopathic ² or can be induced by drugs e.g. benzodiazepines and antidepressants ¹⁰⁻¹².

The treatments available for OAB comprise oral pharmacotherapy medication, bladder training programs, modification in diet, surgery and electrical stimulation ^{10, 13}. Anti-muscarinic drugs including oxybutynin, trospium chloride, solifenacin, darifenacin and tolterodine are 65-75% effective in reducing the OAB symptoms and are therefore, the first-line treatment for OAB ¹⁴⁻¹⁶. Oral anti-muscarinic therapy for detrusor overactivity is usually prescribed for long period; nevertheless, the incidence of side effects associated with this therapy is relatively high. The most common side effects are due to blocking of muscarinic receptors in colon, salivary gland and ciliary smooth muscle induced constipation, dry mouth, and blurred vision, respectively. It also causes drowsiness and heart related side effects such as palpitations and arrhythmia that are difficult to tolerate for some patients, particularly the patients of older age who are likely to present cardiovascular comorbidities and the paediatrics ¹⁷⁻¹⁹ leading to poor patient compliance and adherence. For instance, as per discontinuation rate of anti-muscarinic drugs reported by Gopal et al., 42% of OAB patients discontinued the prescribed antimuscarinic medication after four months and the rate increased to 77% after 1 year ²⁰. In the UK clinical practice, repeat prescription data analysis reported a low adherence rate i.e. the average duration of using antimuscarinic drugs was

only 3 months²¹. Furthermore, 30-40% of children suffering from OAB does not respond to anti-muscarinic treatment. In some neurogenic OAB cases, these drugs even fail to relieve the symptoms and lead to refractory neurogenic detrusor overactivity²².

For many years, the researchers have targeted the detrusor muscle to depress the contractility *via* antimuscarinic drugs for the treatment of OAB²³. However, the poor adherence, tolerability and patient compliance due to the bothersome side effects did not grant any success and hence the focus has shifted towards new interventions e.g. other mechanisms or structures of the bladder such as urothelial signalling and afferent nerves^{11, 24} which makes way for the centrally acting drugs in the treatment of OAB²⁵.

Gabapentin, a centrally acting anticonvulsant drug has not only used for the treatment of epilepsy but has also proven effective in psychiatric and neurologic disorders²⁶. The mechanism of action of gabapentin is controversial and does not involve interaction with GABA (γ -aminobutyric acid) receptors²⁷. It can cross the blood-brain barrier and is also used for sleep and anxiety disorders due to lack of toxicity. Gabapentin was used for the treatment of refractory interstitial cystitis, in the field of urology, for the first time^{28, 29}. The possible pathogenesis of interstitial cystitis in this regard was proposed as up-regulation of afferent C-fibre sensory neurons. The study reported reduced pain in 10 of 21 patients suffering from interstitial cystitis. The hypothesis was proposed that few cases of OAB show the same pathophysiology of up-regulation of afferent C-fibre sensory neurons which further promoted the use of gabapentin for the treatment of OAB²⁹. Carbone et al., 2006 reported the effect of gabapentin on neurogenic overactive bladder. Gabapentin was effective in improving the urodynamic parameters and relieving the symptoms, in addition, no significant adverse effects were reported and none of the patient discontinued the treatment⁷. Similarly, Kim et al., 2004 investigated the effects of oral gabapentin in OAB patients who did not respond to the antimuscarinic therapy. It was reported that the drug was well-tolerated and symptoms were improved in 14 of 31 patients with refractory OAB³⁰.

However, when given orally, along with some favourable characteristics like absence of enzyme induction and hepatic metabolism and low protein binding^{31, 32} gabapentin has two major drawbacks i.e. short half-life (5-7 h)³³ and narrow absorption window as it is preferentially absorbed from upper small intestine³⁴⁻³⁶ which in turn results in poor bioavailability³⁷ due to a saturable L-amino acid transport system. Owing to this, immediate

release gabapentin requires frequent and multiple administration to achieve optimal efficacy. The multiple administration reduces the patient compliance, adherence and is unable to tolerate by some patients as gabapentin cause somnolence and dizziness as side effects ^{38, 39}. Drugs with such drawbacks need a sophisticated and practical delivery system e.g., an extended release gastroretentive floating system. Floating systems are basically dynamically controlled systems with density lower than the gastric fluid (must be $< 1.004 \text{ g/cm}^3$) that have enough buoyancy to float in the stomach for longer periods without affecting the gastric emptying rate and with desired drug release rate. The floating gastroretentive delivery system is suitable for drugs with narrow absorption window, short half-life, and low solubility at alkaline pH ⁴⁰⁻⁴². The rationale behind selecting this drug delivery system is to overcome the absorption related and multiple administration, drawbacks of gabapentin, allowing the dosage form to stay in the stomach for several hours along with the sustained release thereby increasing the absorption extent. Development of gastroretentive floating drug delivery system where dose can be easily modified and controlled is possible with the help of additive manufacturing technology ⁴³⁻⁴⁵ i.e. fused deposition modelling (FDM) technique, one of the most commonly and widely used additive manufacturing technology ⁴⁶. Infill pattern and the number of shells are the basic parameters of FDM technique in defining the internal structure and outlining the outer shape of the object to be print. The minimum number of shells required to print an object is one, however, the number of shells can be increased to enhance the strength and weight of the object as per requirement but will take more time to print and more material will be consumed. It can produce fully solid filled structure and hollow objects by adjusting the infill density that ranges from 0% to 100%.

In the present study we envisage to cater the personalised delivery and narrow absorption window issue of gabapentin using hot-melt extrusion (HME) coupled with FDM without the aid of any plasticiser. The manufacturing of personalised drug delivery devices is a challenging process as it requires manufacturing of small batches particularly tailored to patient's requirements which can be non-economical and time consuming. Nonetheless, the recent emergence of 3D printing technologies and its pharmaceutical applications exploited by the researcher have provided on demand manufacturing, an easy path to the development of personalised drug delivery devices. In addition to personalised aspect, the technology also provides an easy and efficient way of developing gastroretentive floating drug delivery system

to overcome the drawbacks of gabapentin. This research project is, therefore, aimed at overcoming the absorption related issues of gabapentin by developing gastroretentive floating drug delivery system via FDM. In summary, drug loaded filaments were extruded using FDM. Filaments were then employed to develop a total of seven formulations with varying printing parameters i.e., infill density and shell number. The printed tablets were thoroughly characterised by performing geometric, mucoadhesion, surface texture analysis using ETL-based imaging system, *in vitro* floating and drug release study. Pharmacokinetic studies were also carried out on rabbits using optimum formulation F2 (2hsells, 0% infill, floating time > 10 hours) and oral solution of gabapentin.

5.2. Materials and methods

5.2.1. Materials

Model drugs, gabapentin was purchased from TCI Europe (Zwijndrecht, Belgium). Polyethylene oxide (PEO), a carrier polymer, having average viscosity molecular weight (Mw) 200,000 was purchased from Sigma-Aldrich, UK. All other chemical reagents used were of analytical grade and used as supplied.

5.2.2. Preparation of filaments

A single screw extruder (Noztek® Pro pellet and powder extruder, Sussex, UK) was employed for the extrusion of gabapentin loaded filaments using powder blend of PEO: gabapentin. The HME parameters used during extrusion of filaments are given in the Table 5.1. The nozzle diameter and extrusion temperature were 1.75 mm and 155 °C, respectively. Once successfully extruded, filaments were stored in a desiccator at room temperature until further investigation.

Table 5.1: HME parameters for developing filaments.

Formulation (weight ratio)	Extrusion temperature (°C)	Screw speed (rpm)	Torque (N/cm)
PEO: Gabapentin (80:20)	155	30	18

5.2.3. Physicochemical characterisation of filaments

5.2.3.1. Determination of drug loading

0.2 g sample of gabapentin loaded filament was placed in a 1 L water: methanol (1:1) solvent mixture separately, under magnetic stirring until complete dissolution. Jenway 6405 UV spectrophotometer, Staffordshire, UK, was then used to analyse the filtered liquid samples to determine the gabapentin content. All the measurements were carried out in triplicate.

5.2.3.2. Differential Scanning Calorimetry (DSC)

DSC of all the powder samples and extruded filaments were carried out using Mettler Toledo SC 821, Mettler-Toledo Ltd., Leicester, UK. Concisely, standard aluminium pans were used to place 5-10 mg of samples to run the analysis under nitrogen flow of 50 mL/min and temperature program of 10 °C/min from 25-300 °C.

5.2.3.3. Thermogravimetric Analysis (TGA)

TGA was performed using Mettler Thermobalance TG50 (Mettler-Toledo Ltd., Leicester, UK). All the powder samples, plain and blend, and drug loaded filaments were placed in open alumina crucibles for analysis. Samples were heated under temperature range of 25-300 °C at heating rate of 10 °C/min. Nitrogen gas was used as a purge gas with a flow rate of 50 mL/min.

5.2.3.4. X-ray diffraction studies (XRD)

D2-Phase X-ray diffractometer (Bruker UK Ltd., Coventry) equipped with a CuK α radiation source at 30 KV voltage and 10 mA current, was used for XRD study of all the powder samples (polymer, drug, powder blend). 2 theta (θ) range of 5°–100° using 0.02 step size settings were used to obtain the diffraction patterns.

5.2.3.5. Scanning Electron Microscopy (SEM)

SEM was used to examine the morphology of drug loaded filaments. Briefly, double-sided adhesive tape is used to mount the samples onto stubs. A Quorum SC7620 Sputter Coater

(Quorum Technologies, Laughton, UK) is then used for sputter-coating of samples with palladium/gold (20:80) for 60 seconds and were photo metrically examined Jeol JSM-6060CV, Jeol Inc., Peabody, MA, USA ⁴⁷.

5.2.3.6. Mechanical testing of filaments

TA-XT2i texture analyser (Stable Micro Systems Ltd, Surrey, UK) was used to carry out mechanical testing. All the extruded filaments were cut into 10 cm pieces and were placed onto TA-95N 3-point bend probe set which was attached to the analyser, keeping the moving speed of blade at 5 mm/s until it reached 15 mm under the sample. Exponent[®] software (Stable Micro Systems Ltd, Surrey, UK) was then used to analyse the collected data.

5.2.4. Fabrication of 3D printed tablets

A cylindrical tablet of 5 mm diameter and 2.5 mm height was designed using SolidWorks[®] version 2015, the file was then converted into *stl*. (Stereolithographic) format for further use. Gabapentin loaded filament was loaded into MakerBot replicator mini (MakerBot Inc., New York, NY, USA) separately to print the tablets. Keeping the dimensions and infill pattern (linear) constant, gabapentin tablets were printed with different shell numbers (1, 2, 3, and 4) infill density (10%, 20% and 30%), respectively. Other 3D printing parameters were kept constant and includes printing temperature (215-220 ° C), height layer (0.1 mm), extrusion speed (90 mm/sec) and travelling speed (150 mm/sec).

5.2.5. Characterisation of 3D Printed Matrices

5.2.5.1. Geometrical and morphological assessment of matrices

To determine the thickness and diameter of the tablets, a digital Vernier calliper was used. The volume, mass and density of the tablets were also calculated ⁴⁸. The surface morphology of the printed tablets was observed using SEM.

5.2.5.2. 3D surface texture analysis

A 3D surface texture analysis was carried out using electrically tunable lens-based imaging system (Figure 5.1) described and used by ⁴⁹. The sample was prepared by using method described by ^{50, 51}. The tablet was placed on a stainless-steel wafer (3 x 3 cm) using double-sided adhesive tape and a whole tablet was scanned instead of a specified region. Afterwards,

3D surfaces texture parameter, root mean square roughness (S_q) was calculated using software MATLAB[®] 2017 software (The MathWorks, Inc., Natick, MA, USA).

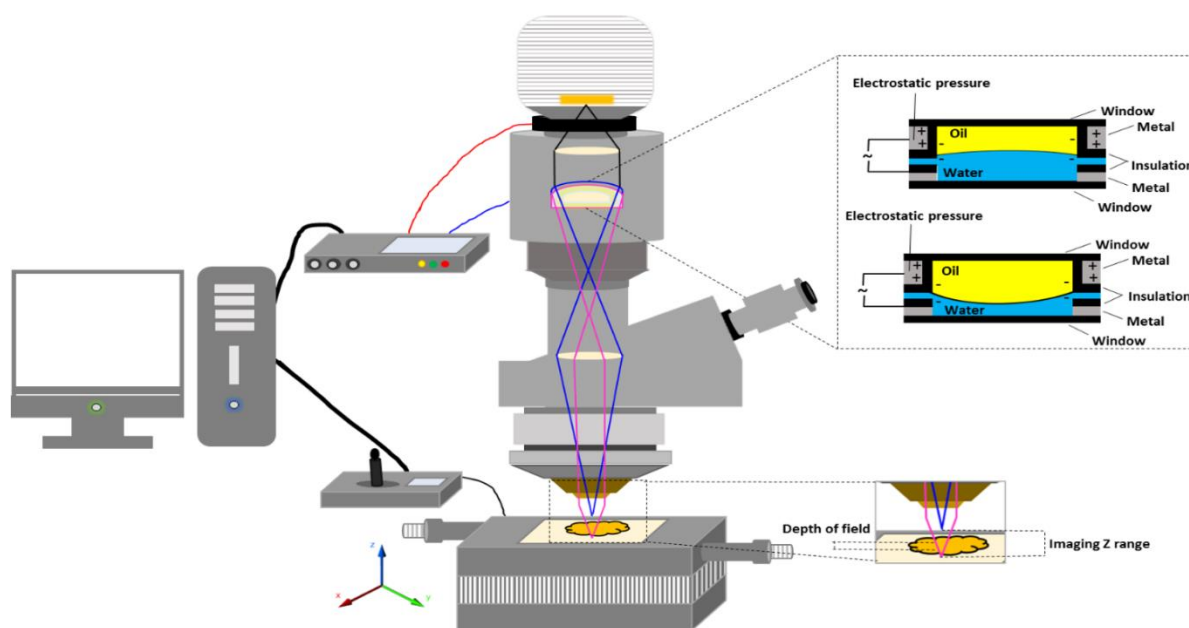


Figure 5.1: Schematic illustration of electrically tunable lens (ETL)-based variable focus imaging system used for the surface texture analysis of the 3D printed tablets, (1) computer; (2) ETL driver; (3) camera; (4) ETL; (5) automatic motorized vertical translation stage ; and (6) stage controlling system ⁴⁹.

5.2.5.3. Determination of tablet strength

To measure the tablet strength, Testometric M500–50 CT, Testometric Company Ltd., Rochdale, United Kingdom, machine was used. Ten tablets from each formulation were selected randomly and were tested. The tablets were placed diametrically, and force was applied at the rate of 10 mm/min by moving the upper punch until the tablet was broken.

5.2.5.4. Determination of tablet friability

10 tablets were randomly selected for friability testing. Tablets were weighed and placed in the firabilator (PTF 20E, Pharmatest, Hainburg, Germany), the drum was rotated at speed of 20 rpm for 5 minutes. After that, tablets were weighed again to calculate the friability in terms of weight loss and expressed as a percentage of original weight of the tablet.

5.2.5.5. Mucoadhesive test using texture analyser

A texture analyser equipped with mucoadhesive holder was used to study the mucoadhesive property of the polymer⁵². The 3D printed tablet was attached to the cylindrical probe having 10 mm diameter using double-sided tape. The porcine gastrointestinal mucosa (20 x 20 mm) was equilibrated at $37 \pm 0.5^\circ\text{C}$ for 15 minutes before placing on the stage of mucoadhesive holder and afterwards the temperature of 37°C was maintained in 150 ml of 0.1 N HCL. Figure 5.2 demonstrates the schematic illustration of mucoadhesive testing of 3D printed tablets using texture analyser with specialised mucoadhesive holder (a) probe attached with 3D printed tablet was moved downward, (b) 3D printed tablet was attached with gastrointestinal mucosa with specified force and time and (c) probe was moved upward at a specified rate. The specified force applied was 0.5 N and the contact time between the tablet and the gastrointestinal mucosa was 200 seconds. The probe was withdrawn at a speed of 0.2 mm/s. A software was used to measure the maximum detachment force F_{max} , required to separate the probe from the gastrointestinal mucosa. Work of adhesion (Wad) which is the total force involved in the probe separation during withdrawal phase was also calculated from the area under the curve (AUC) of the force vs distance profile (Figure 5.3).

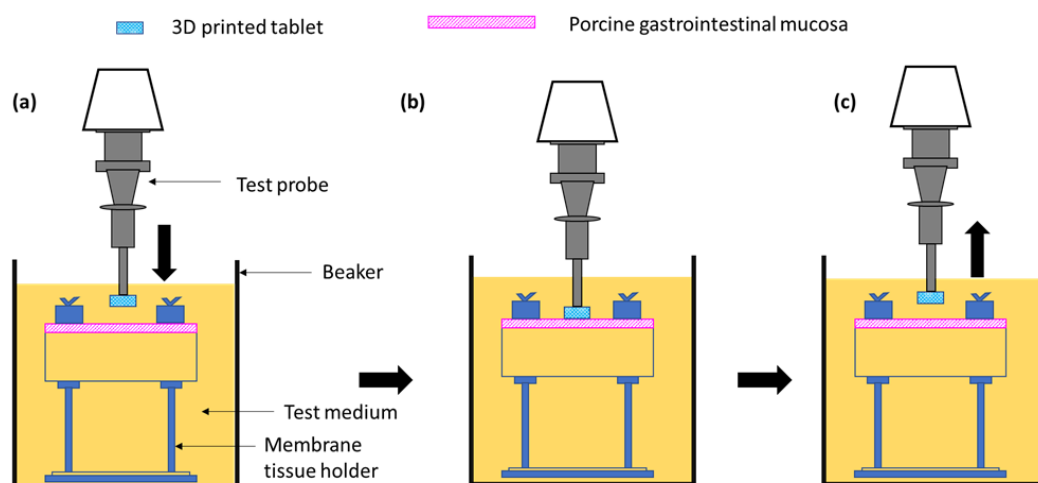


Figure 5.2: Schematic illustration of mucoadhesive testing of 3D printed tablets using texture analyser with specialised mucoadhesive holder (a) probe attached with 3D printed tablet was moved downward, (b) 3D printed tablet was attached with gastrointestinal mucosa with specified force and time and (c) probe was moved upward at a specified rate.

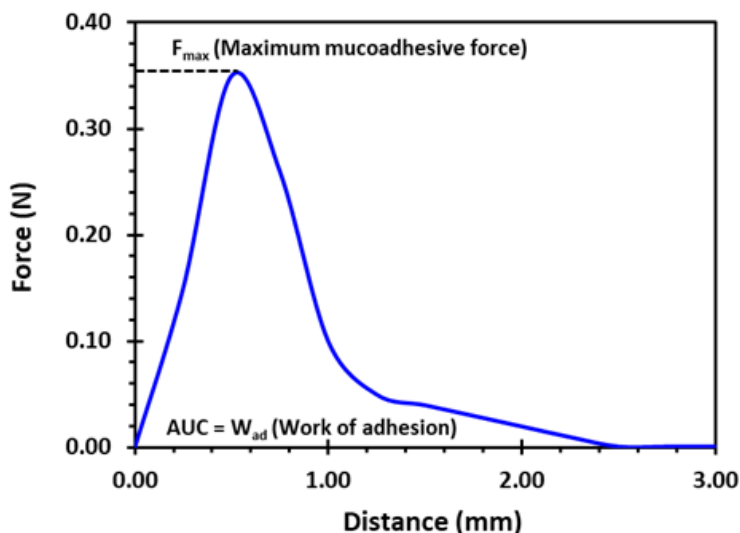


Figure 5.3: A typical Force vs Distance profile for 3D printed tablet (F2, (2 shell with 0 % infill)) from the mucoadhesion test performed in 0.1N HCl (150 mL) at 37 °C using texture analyser. F_{max} is the highest force required to separate the probe from the gastric tissue which is determined from the maximum peak height of the profile. However, W_{ad} is the total force involved in the probe separation during withdrawal phase which is calculated from the area under the curve (AUC) of the force vs distance profile.

5.2.6. *In vitro* dissolution testing

The dissolution study was performed using USP II paddle apparatus where the temperature and paddle rotation speed were maintained at 37 °C and 50 rpm, respectively. Tablets were placed in 900 ml simulated gastric fluid media (pH 1.2). The total time of dissolution study was 12 hours. 5 ml aliquots were drawn from each vessel at predetermined interval times and replenished with 5 ml of dissolution media to maintain the sink condition. HPLC system was utilised to analyse the dissolution samples with an injection volume of 20 μ l. Acetonitrile: ammonium carbonate (5: 95) at pH 8.0 was used as mobile phase for gabapentin at the flow rate of 1 ml/min and gabapentin was detected at a wavelength of 340 nm via UV-detector. All the measurements were carried out in triplicate.

5.2.7. Floating test

Floating test was also carried out along with the dissolution test. The gastroretentive gabapentin tablets were taken out from the dissolution vessels to 15 ml glass vials containing the dissolution media at different time intervals (2h, 4h, 6h, 8h, 10h and 12h) and the photos

were then taken immediately. The tablets were put back to the dissolution vessel after taking the photos.

5.2.8. Pharmacokinetic studies

The *in vivo* study was carried out on white albino rabbits weighing 2.8-3.5 Kg. The rabbits were further categorised into two groups each containing 6 rabbits per group. All rabbits were housed individually in cages and environmentally controlled conditions were applied (25 ± 1 °C; $44 \pm 3\%$ relative humidity). Rabbits were given free access to water and food until the last 24 hours before the experiment was started after this the rabbits have free access to water but not the food. The study protocol was approved by the Pharmacy Research Ethics Committee (PREC) at the University of Sargodha, Sargodha, Pakistan (UOS/PERC/102).

A single-dose pharmacokinetic study was carried out in which rabbits of group 1 were administered oral solution of gabapentin (25 mg in 0.5% methylcellulose based oral solution) and 3D printed gabapentin tablets (F2, containing 25 mg gabapentin) were administered to the group 2. At different time intervals (0, 30, 60, 120, 240, 300, 360, 420, 480, 600 and 720 minutes), 1 mL of blood samples were collected from the marginal ear vein into heparinised tubes. The collected blood samples were then centrifuged for 10 min at an ambient temperature. After centrifugation the plasma layer was separated and was stored at -20 °C until analysed.

50 μ L of rabbit plasma was added to amlodipine besylate solution and 100 μ L of acetonitrile was also added for protein precipitation and was centrifuged for 10 minutes. The supernatant layer was separated in a clean tube and 1 ml of acetonitrile, 30 μ L of 1-fluoro-2,4-dinitrobenzene (FDNB, derivatisation agent) and 200 μ L of 0.25 M borate buffer were added. The tube was then inverted and kept at 65 °C for 10 minutes to allow derivatisation reaction. After derivatisation, samples were brought to room temperature and 25 μ L of 1 M HCl solution was added, were inverted and dried. Once dried, residues were mixed with 200 μ L of mobile phase and 20 μ L were injected into HPLC containing reverse phase C-18 column (Phenomenex). The mobile phase used was 50 mM sodium phosphate buffer (pH 3.9): methanol (27:73, v/v), at flow rate of 1.2 mL/min and UV wavelength of 360 nm was used to detect the gabapentin⁵³. PKSolver program, an add-in macro for Microsoft Excel®, was employed for the calculation of the different pharmacokinetic parameters.

5.3. Results and discussion

5.3.1. Development and characterisation of filaments

PEO filaments loaded with gabapentin were successfully extruded using HME without using any plasticiser. (Figure 5.4 a). The drug loading of 98% was achieved in the extruded filaments and was within the pharmacopoeial assay limit (Table 5.2). Thermal analyses (DSC and TGA) were conducted on the powdered samples and the extruded filaments. DSC thermogram of pure gabapentin powder showed that it has a crystalline structure as a sharp endothermic melting peak around 170 °C was observed (Figure 5.5 a). The two anomalies of pure PEO were observed during DSC analysis i.e., one, a sharp endothermic melting peak around 65 °C which shows its crystalline nature and second an exothermic peak around 160 °C which depicts the polymer decomposition⁵⁴ (Figure 5.5 b). DSC thermogram of the extruded filament was also carried out, no drug crystallinity and drug-polymer interaction were observed in the extruded filament (Figure 5.5 c). The TGA profiles showed that the onset of degradation for drug, polymer and the extruded filament was above the operating temperature (170 °C) used in the printing process (Figure 5.6). In addition to DSC, XRD analysis was also carried out that confirmed the crystalline nature of gabapentin and PEO as sharp high intensity peaks were observed (Figure 5.7 a, b). Moreover, no high intensity peaks of gabapentin and PEO were observed in the extruded filaments which indicates successful dispersion of the drug and the polymer (Figure 5.7 c). In summary, it was concluded that the DSC and XRD results coincided with each other, both analyses confirmed the crystalline nature of gabapentin and PEO whereas, the extruded drug loaded filaments were of amorphous nature.

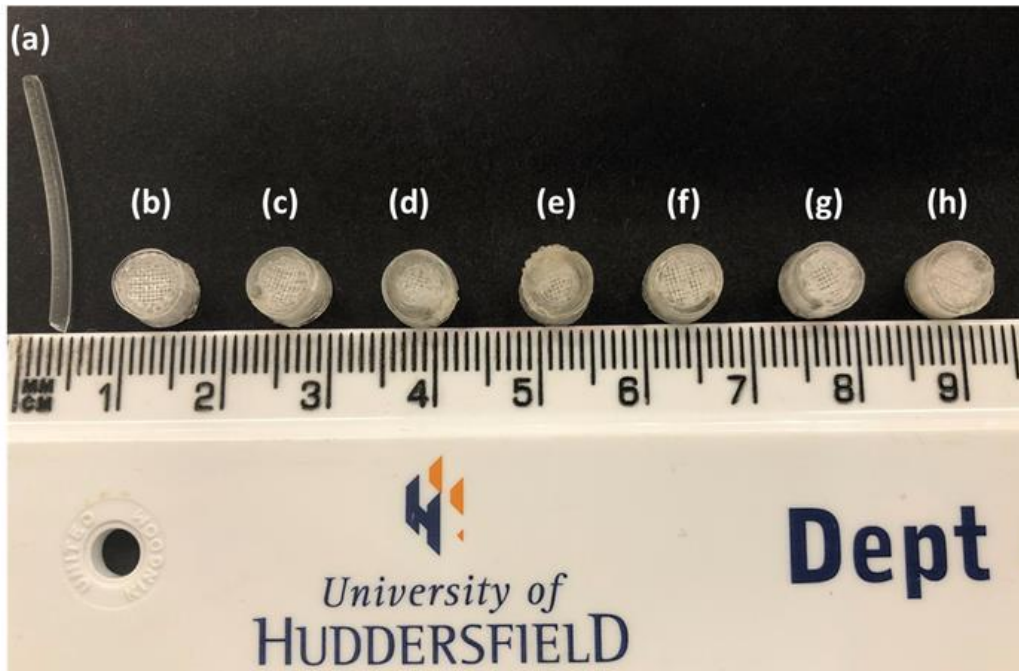


Figure 5.4: (a) hot-melt extruded filament of gabapentin/polyethylene oxide (PEO)/polyethylene glycol (PEG), (b) F1 (1 shell with 0 % infill), (c) F2 (2 shell with 0 % infill), (d) F3 (3 shell with 0 % infill), (e) F4 (4 shell with 0 % infill), (f) F5 (2 shell with 10 % infill), (g) F6 (2 shell with 20 % infill) and (h) F7 (2 shell with 30% infill).

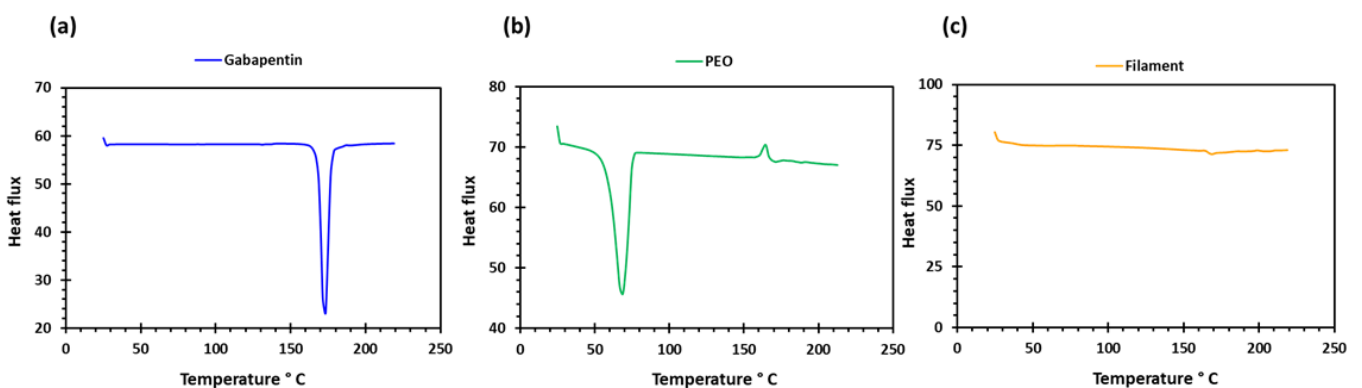


Figure 5.5: DSC profiles of (a) gabapentin (b) polyethylene oxide (PEO) (c) GBP/PEO filament.

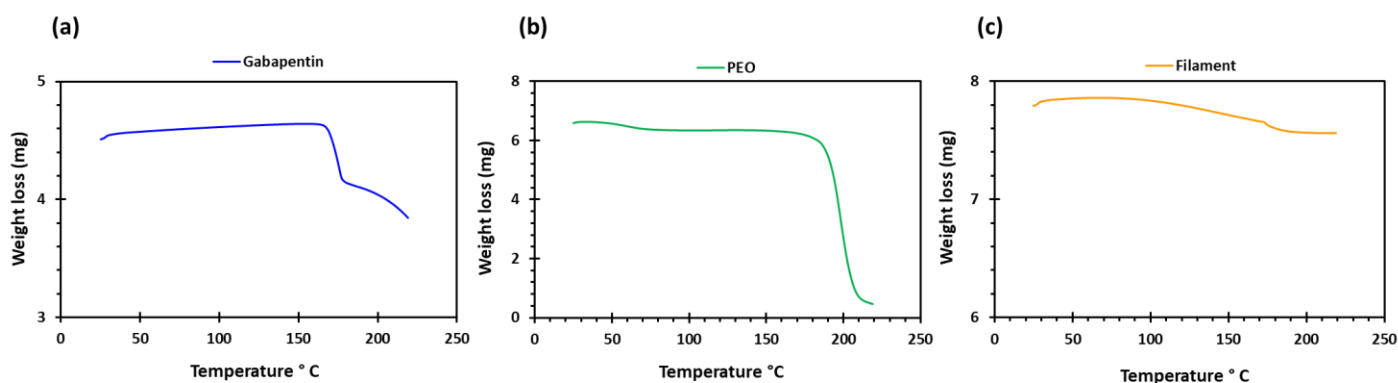


Figure 5.6: TGA profiles of (a) gabapentin (b) polyethylene oxide (PEO) (c) GBP/PEO filament.

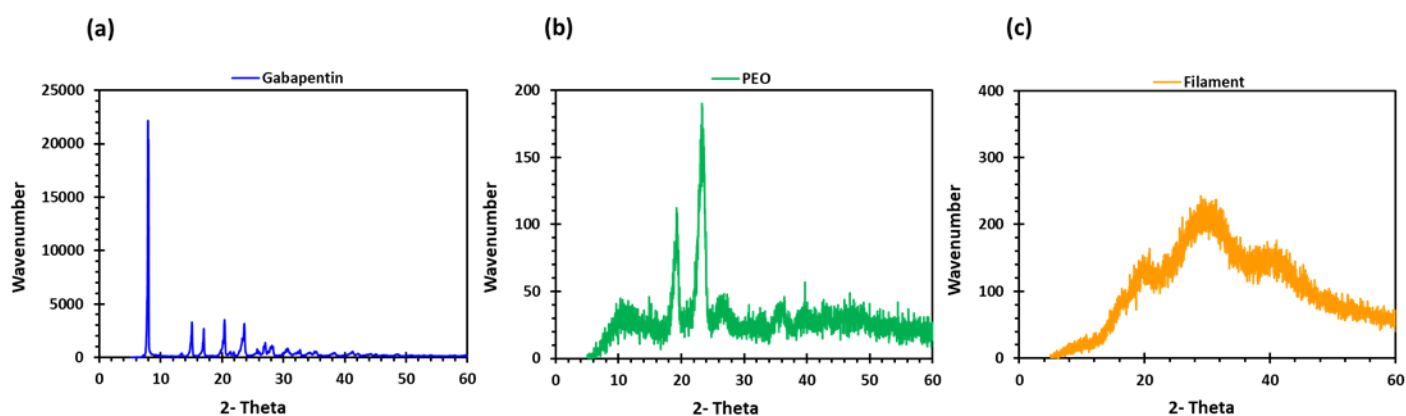


Figure 5.7: XRD profiles of (a) gabapentin (b) polyethylene oxide (PEO) (c) GBP/PEO filament.

Filament should possess good mechanical properties to be used for 3D printing. If the filament is too brittle, it would break while feeding through the gears of the FDM printer and if the filament is too soft it would start collecting inside instead of extruding through the nozzle⁵⁵,⁵⁶. Three-point bending test was, therefore, performed to investigate the mechanical properties of the filament. The force and the stress required to break the filament was found to be 2.4 N and 17.22 MPa, respectively. The breaking distance for the filament was 5.9 mm whereas young's modulus was found to be 18.12 (Table 5.2). The breaking distance which shows toughness of the filament should not be less than 1.5 mm⁴⁶. Moreover, the successful extrusion of PEO filaments without any plasticiser can be attributed to the basic structural unit of the PEO polymer which is the ethylene glycol skeleton [HO-(CH₂ - CH₂ -O) n -H]. It is

basically the molecular weight of the polymer that defines the grades of PEO. Below the molecular weight of 25, 000 Da, PEOs are known as polyethylene glycols (PEGs) and PEGs are efficient plasticisers due to their non-toxicity and biodegradability^{57,58}. Because the structural unit in PEO and PEG is the same, it was possible to extrude the PEO filaments without any plasticiser. Literature has also reported the extrusion of PEO at temperatures higher than its melting point and without any plasticisers⁵⁹. Overall, the filaments possessed good mechanical properties and after characterisation, the filaments were successfully used to print the tablets with varying shell number and infill density via FDM (Figure 5.4 b-h).

Table 5.2: Drug loading and three-point bending results of filaments (*n=10, standard deviations are in parenthesis).

Drug loading (%)	Force (N)	Distance (mm)	Stress (MPa)	Strain	Young modulus (E)
98.5 (1.05)	2.4 (0.22)	5.9 (1.15)	17.22 (1.35)	0.95 (0.21)	18.12 (1.19)

5.3.2. Development and characterisation of 3D printed tablets

The extruded filaments were successful in printing the tablets. Seven different types of tablet formulations having same formulation composition (PEO: gabapentin-80:20 %) and dimensions (7 x 4 mm) but varying shell numbers (1, 2, 3, and 4) and infill density (10%, 20% and 30%) were printed (Table 5.3).

Table 5.3: Formulation composition, dimension, and printing parameters of tablets.

Formulation code	Formulation composition (Weight ratio %)	Dimensions (D x H mm)	Shell number	Infill percentage (%)
F1	PEO: Gabapentin (80:20)	7 x 4	1	0
F2	PEO: Gabapentin (80:20)	7 x 4	2	0
F3	PEO: Gabapentin (80:20)	7 x 4	3	0
F4	PEO: Gabapentin (80:20)	7 x 4	4	0
F5	PEO: Gabapentin (80:20)	7 x 4	2	10
F6	PEO: Gabapentin (80:20)	7 x 4	2	20
F7	PEO: Gabapentin (80:20)	7 x 4	2	30

Table 5.4 shows that the drug loading in the 3D printed tablets increased with increase in the shell number and infill density. However, the highest drug loading was observed in the tablet F3 and lowest was seen in F5. This is because the infill density is basically the amount of material used inside the printing object and therefore with increase in infill density, the material inside the printing object increased which resulted in increased drug loading. The breaking strength of the tablets were also measured, and the values were in the range of 398.66 – 421.55 N. These values show that the printed tablets were robust enough to manage rough handling and the friability of all the printed tablets was also 0%.

Table 5.4: Drug loading and mechanical properties of 3D printed tablets (n=5).

Formulation code	Drug loading (%)	Breaking strength of tablets (N)	Friability (%)
F1	97.51 (0.75)	411.65 (5.59)	0
F2	98.33 (1.10)	404.32 (6.20)	0
F3	100.05 (2.53)	399.21 (11.39)	0
F4	99.1 (2.65)	421.55 (10.35)	0
F5	97.33 (0.61)	398.66 (12.35)	0
F6	98.21 (1.10)	414.99 (15.36)	0
F7	98.87 (0.56)	410.36 (6.55)	0

SEM image analysis of the printed tablets given in the Figure 5.8 shows the layer-by-layer manner of the printing technique. Although the surface of the tablet (Figure 5.8 a) is not smooth but the layering pattern which is visible on the side view (Figure 5.8 b, c) confirms the successful extrusion of filaments with good mechanical properties.

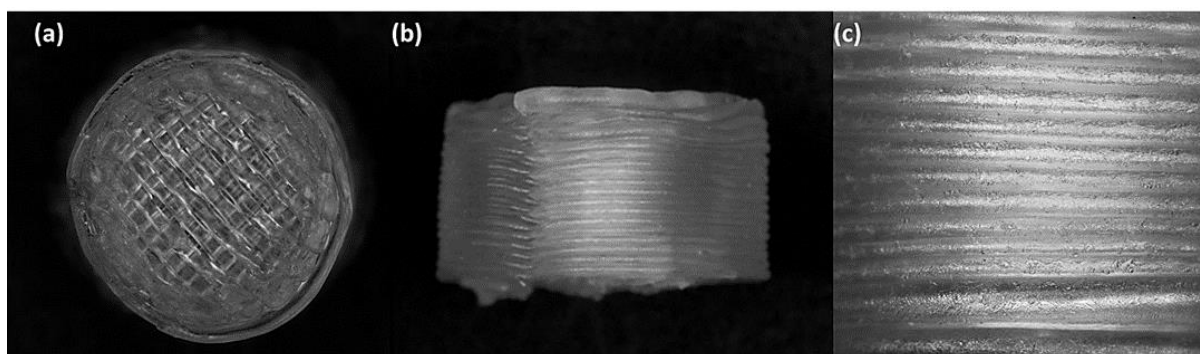


Figure 5.8: SEM micrographs of 3D printed tablet, F2 (2 shell with 0 % infill), (a) whole matrix tablet, (b) side view of matrix tablet and (c) side surface view.

2D and 3D surface texture analyses were performed using ETL-based imaging system Figure 5.9 and 5.10, respectively. The layering pattern of the tablets was also evident by the 2D images (Figure 5.9) and showed almost identical surface texture of all the tablets. In addition, the varying shell numbers in the formulations F1 to F4 are also evident in the Figure 5.9 (a-d). 3D images, on the other hand, showed the presence of the inordinate peaks and the valleys on the surface of the printed tablets (Figure 5.10). To further explore the surface texture analysis, surface texture parameter, root mean square roughness (Sq), was also studied. Figure 5.11 shows the Sq values of all the 3D printed tablets. It is evident from the Figure 5.11 that there was no significant difference in the Sq values of the 3D printed tablets. This is because the varying parameters i.e., shell number and infill density, during the printing make changes on the inside of the tablet and not on the surface⁶⁰. Therefore, the Sq values of all the formulations lie close to each other and are not statistically different.

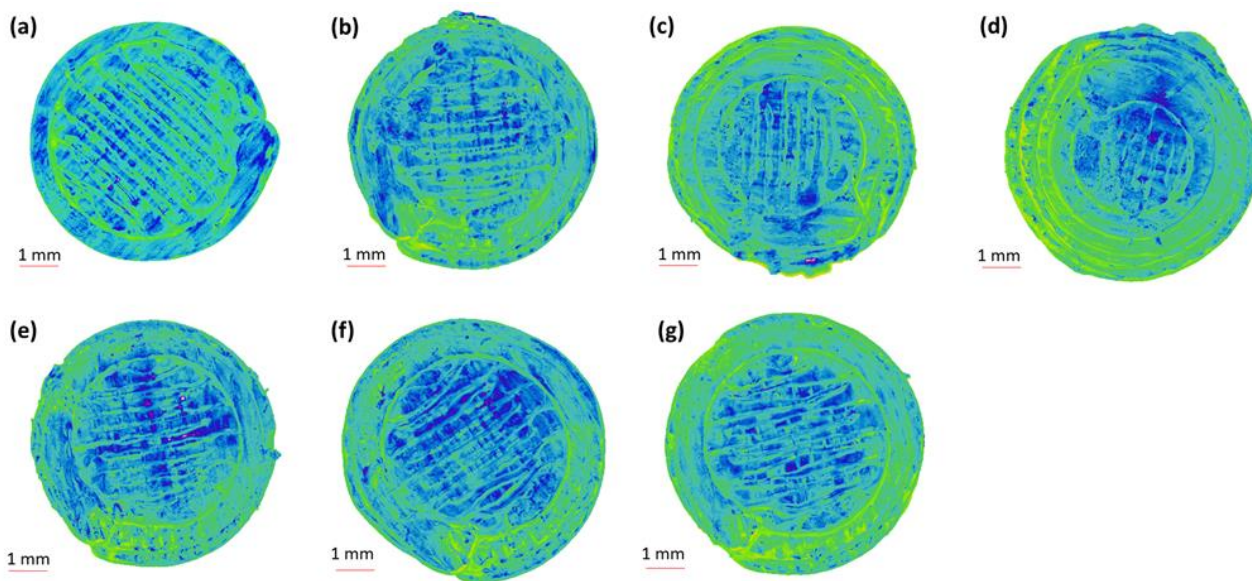


Figure 5.9: 2D surface texture images of 3D printed tablet, (a) F1 (1 shell with 0 % infill) , (b) F2 (2 shell with 0 % infill), (c) F3 (3 shell with 0 % infill), (d) F4 (4 shell with 0 % infill), (e) F5 (2 shell with 10 % infill), (f) F6 (2 shell with 20 % infill) and (g) F7 (2 shell with 30% infill).

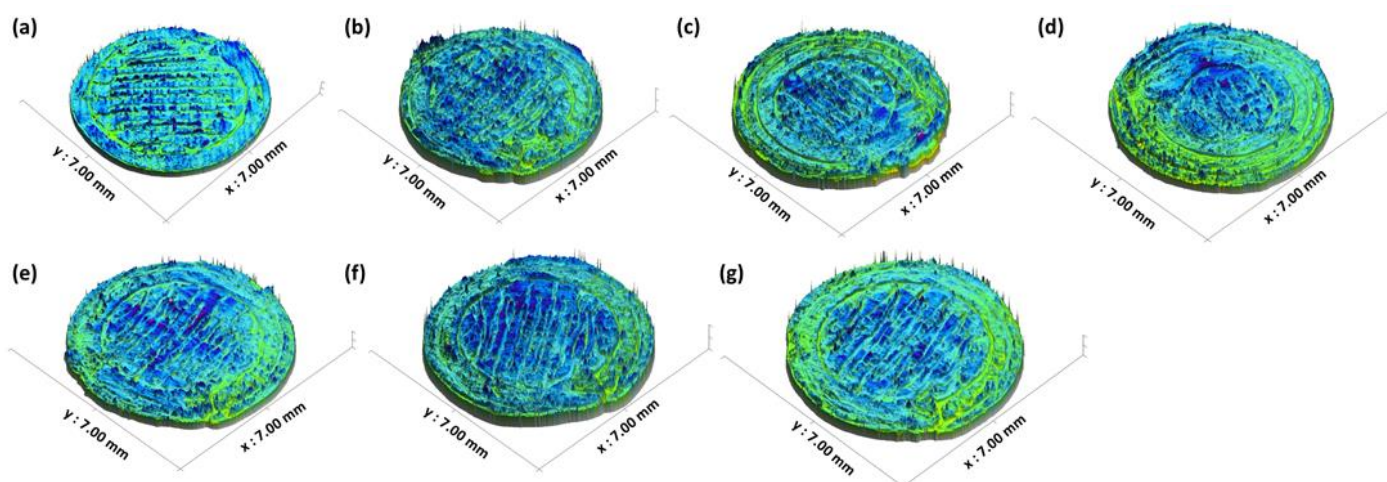


Figure 5.10: 3D surface texture images of 3D printed tablet, (a) F1 (1 shell with 0 % infill) , (b) F2 (2 shell with 0 % infill), (c) F3 (3 shell with 0 % infill), (d) F4 (4 shell with 0 % infill), (e) F5 (2 shell with 10 % infill), (f) F6 (2 shell with 20 % infill) and (g) F7 (2 shell with 30% infill).

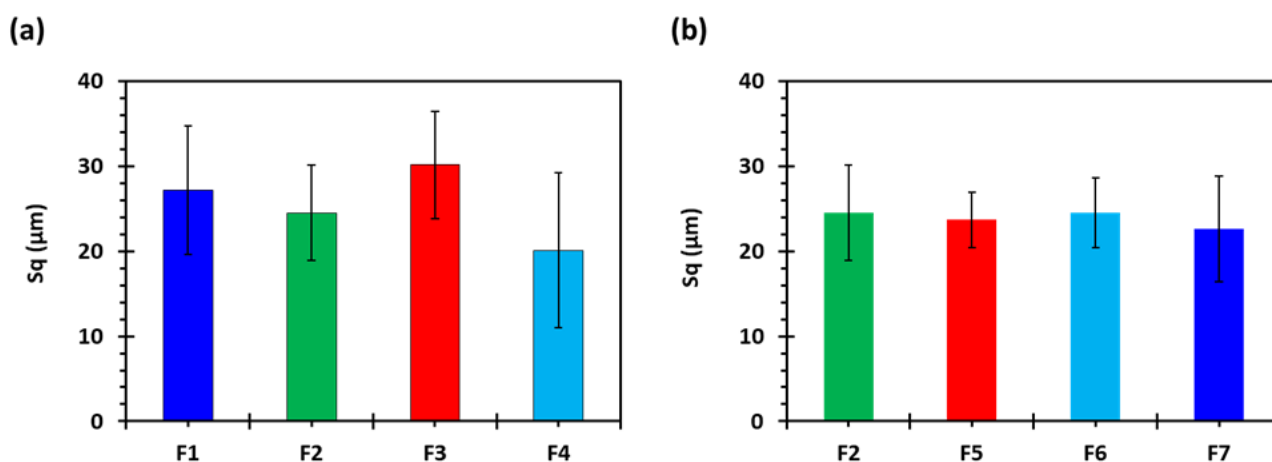


Figure 5.11: Surface roughness properties of 3D printed tablets, showing the effect of (a) shell number and (b) infill percentage (n= 5). F1 (1 shell with 0 % infill), F2 (2 shell with 0 % infill), F3 (3 shell with 0 % infill), F4 (4 shell with 0 % infill), F5 (2 shell with 10 % infill), F6 (2 shell with 20 % infill) and F7 (2 shell with 30% infill).

5.3.3. Mucoadhesion analysis

The texture analyzer method is a convenient method of measuring mucoadhesive property of the polymers. Mucoadhesion is the interaction between pharmaceutical dosage form and mucus membrane. This property allows better contact between formulations and membranes and prolongs the residence time⁶¹. The process involves wetting and hydration of the polymer that is known as the contact stage and is essential in developing the mucoadhesive interaction. The next stage consists of interpenetration between mucosal membrane and polymeric chains forming a chemical bond due to hydrogen bonding, van der Waals, or electrostatic interaction⁶². These surface forces result in adhering the substance to the mucosal membrane. PEO consists of long and linear chains of ethylene oxide. At low molecular weight, PEO possesses very weak mucoadhesive properties. i.e., forms weaker gels with mucus, which may be due to less availability of sites for hydrogen bonding or conformation for interpenetration between polymeric chains and mucosal membrane is not favourable. Therefore, high concentrations of low molecular weight PEO are required to detect any mucoadhesion. However, on the other hand, PEO with high molecular weight possess excellent mucoadhesive properties and does not require high concentrations⁶³.

Figure 5.12 (a and b) shows maximum mucoadhesion detachment force and (c and d) work of adhesion, against porcine stomach mucosa in 0.1N HCl solution at 37 ± 0.5 °C. It is evident from the Figure 5.12 (a and b) that the maximum detachment force was high for all the formulations. The values lied close to each other and were not statistically different. However, the F2 formulation showed the highest detachment force and F4 showed the lowest. The work of adhesion values (Figure 5.12 (c and d)) also lied close to each other and there was no significant difference. The reason for not markedly different values is that the mucoadhesion phenomenon involves contact between the surfaces whereas all the tablet formulations with varying shell number and infill density are different from the inside and there is no change on the surface ⁶⁰. Therefore, the detachment force and work of adhesion values were not markedly different for each tablet formulation and there was no significant difference.

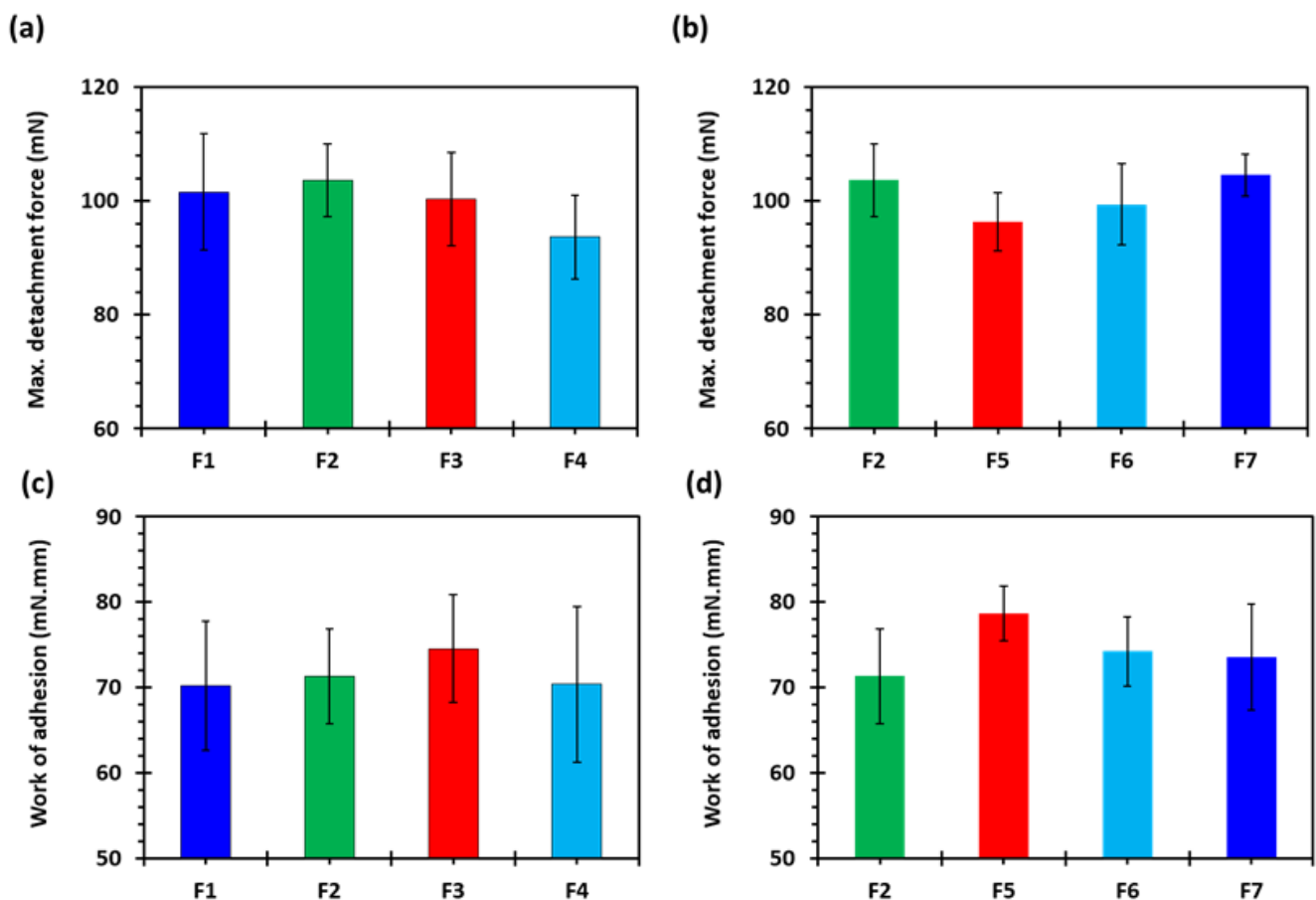


Figure 5.12: (a and b) maximum mucoadhesion detachment force and (c and d) work of adhesion, against porcine stomach mucosa in 0.1N HCl solution at 37 ± 0.5 °C (n= 3). F1 (1 shell

with 0 % infill), F2 (2 shell with 0 % infill), F3 (3 shell with 0 % infill), F4 (4 shell with 0 % infill), F5 (2 shell with 10 % infill), F6 (2 shell with 20 % infill) and F7 (2 shell with 30% infill).

5.3.4. *In vitro* floating and drug release

The major reason for printing the tablets with varying shell number and infill density was to investigate the floating capacity so that the tablet can stay in the stomach for longer period and provide extended drug release profile. Figure 5.13 shows the images of floating F2 tablets at different time intervals. During dissolution testing, the F2 formulation having density of 0.77 mg/mm^3 (2 shells, 0% infill) showed the highest floating time i.e., floated for more than 10 hours followed by F1 (1 shell, 0% infill) with density of 0.73 mg/mm^3 and floating time of less than 8 hours. The F4 (4 shells, 0% infill) tablets showed the highest density 0.93 mg/mm^3 followed by F7 (2 shells, 30% infill) with density of 0.89 mg/mm^3 , both the formulations showed the lowest floating time of less than 2 hours and tended to sink to the bottom of the vessel (Table 5.5). Overall, it was concluded that the tablet density increased with increase in the shell number and the infill density, however, the floating time did not follow the trend and decreased with increase in tablet density. Tablets with density above 0.84 mg/mm^3 did not float for longer period and sink to the bottom in less than 2 hours (Table 5.5).

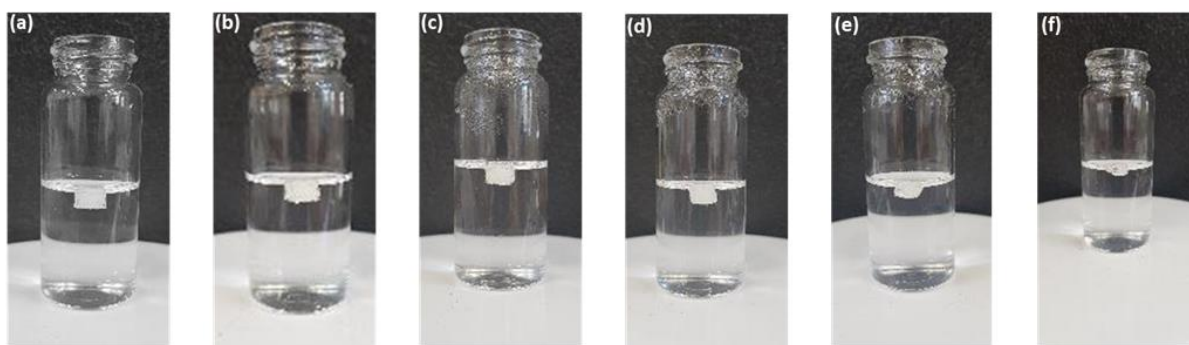


Figure 5.13: Images of 3D printed tablet, F2 (2 shell with 0 % infill) floating in dissolution medium (0.1N HCl solution) at $37 \pm 0.5 \text{ }^\circ\text{C}$ (a) $t = 2\text{h}$, (b) $t = 4\text{h}$, (c) $t = 6\text{h}$, (d) $t=8\text{h}$, (e) $t = 10\text{h}$ and (f) $t = 12\text{h}$.

Table 5.5: Physical parameters and floating time of 3D printed tablets (n=5).

Formulation code	Measured volume (mm ³)	Measured mass (mg)	Tablet density (mg/mm ³)	Floating time (h)
F1	150.69	110.15	0.73	>8
F2	154.32	120.15	0.77	>10
F3	157.16	130.82	0.83	>6
F4	154.12	144.28	0.93	<2
F5	149.49	124.3	0.83	>6
F6	160.50	135.62	0.84	>6
F7	158.63	141.21	0.89	<2

PEO is a linear, uncross-linked and a hydrophilic polymer, once in contact with dissolution media PEO hydrates and disentanglement of polymeric chain starts. The persistent penetration of dissolution media and interaction between polymeric chains and penetrating media results in accommodating water molecules, which leads to the formation of a layer of hydrogel around the matrix tablet. Hydrogel, a semi-dilute or concentrated solution of the polymer, outside the dry core, is basically formed as PEO reaches its glass transition temperature (T_g), the temperature at which glass-to-rubbery phase transition occurs. The T_g of a polymer is an important characteristic to know with respect to sustained release drug delivery system as the polymeric chains are not mobile below the T_g. In comparison, the polymeric chains are highly mobile above the T_g. Drug release rate is controlled by hydration and dissolution of the polymer, which depends on the viscosity, and concentration of the polymer^{64, 65}. In this study, we have kept the viscosity and concentration of the polymer constant. Figure 5.14 shows the drug release from all the printed formulations. All the formulation showed sustained release of the drug. Figure 5.14 (a) shows the effect of varying shell number by keeping the infill density constant on the drug release from the printed tablets. It can be seen from the Figure 5.14 (a) that F1 showed the faster drug release followed by F2. The drug release from F3 and F4 was the slowest and almost similar. It was observed that the drug release was decreased with increase in the shell number. The same trend was seen with respect to the increase in the infill density i.e., drug release was decreased with

increase in the infill density. Figure 5.14 (b) shows the gradual release of the drug from the tablets, nonetheless, the F2 tablets showed the faster drug release and F7 showed the slowest drug release. This is because by increasing the shell number and infill density, we are increasing the amount of filament (drug and polymer) in the tablet⁶⁰. In addition, at low infill density there is less deposition of the material which results in the formation of more porous tablet leading to faster release of the drug. On the contrary, increase in infill density will increase deposition of the material which will result in less porous tablet with slow release of the drug⁶⁶. Among all the formulations, the F2 formulation was chosen for *in vivo* studies as it showed the highest floating capacity with sustained release of the drug.

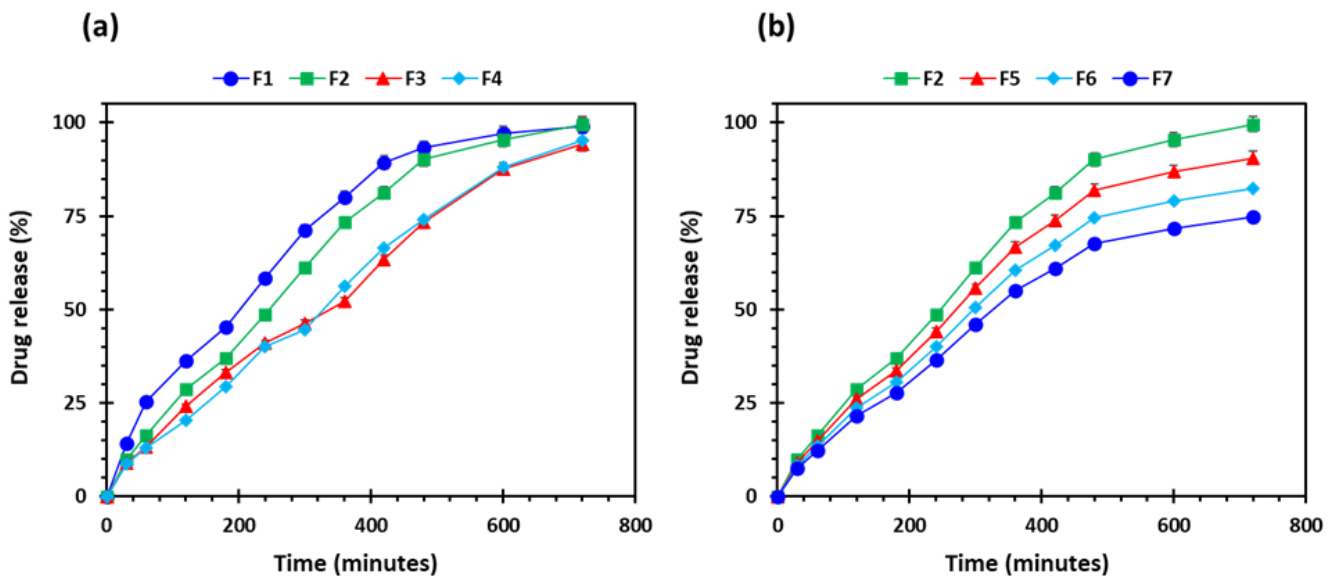


Figure 5.14: Drug release profile 3D printed tablets (n=5), (a) effect of number of shells and (b) influence of percentage infill. F1 (1 shell with 0 % infill) , F2 (2 shell with 0 % infill), F3 (3 shell with 0 % infill), F4 (4 shell with 0 % infill), F5 (2 shell with 10 % infill), F6 (2 shell with 20 % infill) and F7 (2 shell with 30% infill).

5.3.5. Pharmacokinetic parameters

In vivo studies were carried out in the rabbits. Figure 5.15 shows the drug absorption versus time profile of oral solution and 3D printed tablet. It is evident from the findings that

pharmacokinetic parameters of the oral solution and F2 tablet were markedly different from each other (Table 5.6). In addition, AUC of the F2 printed tablets was significantly higher than the oral solution. The maximum plasma concentration (C_{max}) was higher for oral solution and lower for the printed tablet. However, the time required to achieve C_{max} known as T_{max} was longer for F2 tablet as compared to the oral solution. This is because the 3D printed tablets comprise PEO and extended-release effect of PEO enabled the drug to be absorbed into bloodstream for longer period as compared to oral solution.

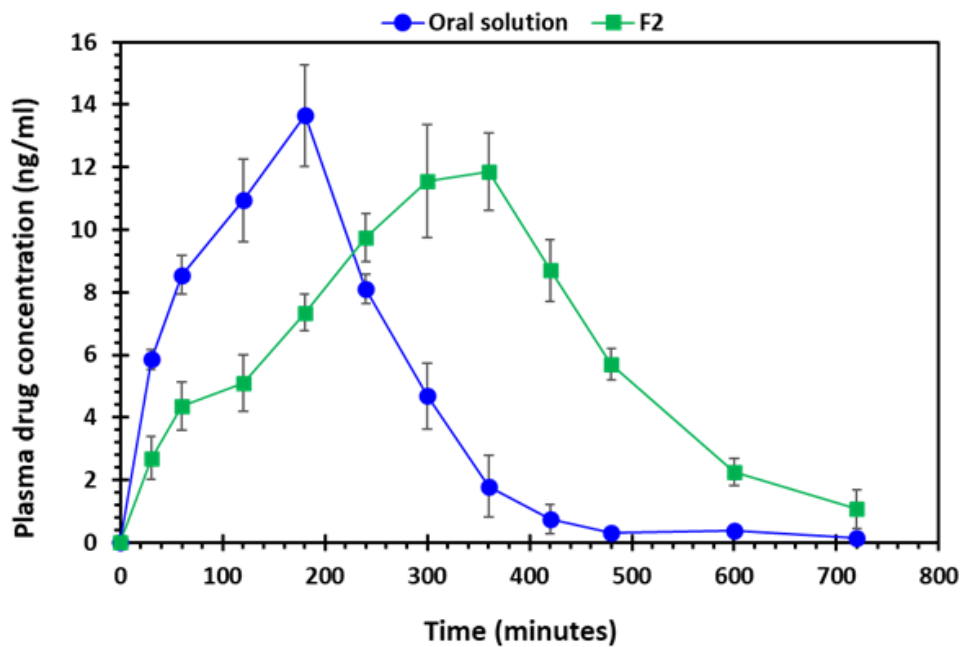


Figure 5.15: Plasma drug (gabapentin) absorption vs time profile of oral solution and 3D printed tablet, F2 (2 shell with 0 % infill), n=6.

Table 5.6: Pharmacokinetic parameters of gabapentin solution and 3D printed tablet (F2, 2 shell with 0 % infill) after oral administration, n=6.

Parameters	Oral solution	F2
$T_{1/2}$ (min)	79.99 (11.59)	97.96 (8.87)
T_{max} (min)	180 (0.00)	360 (0.00)
C_{max} (ng/ml)	13.65 (3.21)	11.85 (2.29)
AUC_{0-t} (ng/ml/h)	3037.05 (174.81)	4381.65 (251.37)

5.4. Conclusions

The present study has successfully addressed the absorption related issues of gabapentin along with the personalisation aspect by developing 3D printed gastroretentive floating drug delivery system. The present study reports the successful extrusion of PEO filaments loaded with gabapentin and without using any plasticiser and were successfully employed in developing the printed tablets with varying shell number and infill density. The tablets showed different floating capacity and it was concluded that increase in infill density and shell number does not increase the floating time. All the tablets showed extended drug release, however, drug release was also decreased with increase in the shell number and infill density. It was concluded that by varying the printing parameters, floating time and drug release can be modified. These *in vitro* drug release results were also observed in the pharmacokinetic parameters. It was also concluded that 3D printing technology was easy to use and beneficial in developing gastroretentive floating drug delivery system as compared to conventional processes.

References

1. B. T. Haylen, D. De Ridder, R. M. Freeman, S. E. Swift, B. Berghmans, J. Lee, A. Monga, E. Petri, D. E. Rizk and P. K. Sand, *Neurourology and Urodynamics: Official Journal of the International Continence Society*, 2010, **29**, 4.
2. J. Arnold, N. McLeod, R. Thani-Gasalam and P. Rashid, *Australian family physician*, 2012, **41**, 878.
3. I. Franco, *The Journal of urology*, 2007, **178**, 761.
4. D. E. Irwin, I. Milsom, S. Hunskaar, K. Reilly, Z. Kopp, S. Herschorn, K. Coyne, C. Kelleher, C. Hampel and W. Artibani, *European urology*, 2006, **50**, 1306.
5. R. Botlero, S. R. Davis, D. M. Urquhart and R. J. Bell, *The Journal of urology*, 2011, **185**, 1331.
6. G. F. Wolff, G. A. Kuchel and P. P. Smith, *Research and reports in urology*, 2014, **6**, 131.
7. A. Carbone, G. Palleschi, A. Conte, G. Bova, E. Iacovelli, R. M. Bettolo, A. Pastore and M. Inghilleri, *Clinical neuropharmacology*, 2006, **29**, 206.
8. M. S. Ansari, A. Bharti, R. Kumar, P. Ranjan, A. Srivastava and R. Kapoor, *Journal of Pediatric Urology*, 2013, **9**, 17.
9. R. Kurpad and M. J. Kennelly, *Current Urology Reports*, 2014, **15**, 444.
10. A. J. Wein and R. R. Rackley, *The Journal of urology*, 2006, **175**, S5.
11. K.-E. Andersson, *Urology*, 2002, **59**, 43.
12. P. Tsakiris, M. Oelke and M. C. Michel, *Drugs & Aging*, 2008, **25**, 541.
13. K.-E. Andersson, *Urology*, 2002, **59**, 18.
14. N. Zinner, J. Susset, M. Gittelman, M. Arguinzoniz, L. Rebeda and F. Haab, *International journal of clinical practice*, 2006, **60**, 119.
15. S. A. MacDiarmid, *BJU international*, 2007, **99**, 8.
16. P. Madhuvrata, J. D. Cody, G. Ellis, G. P. Herbison and E. J. C. Hay-Smith, *Cochrane Database of Systematic Reviews*, 2012.
17. A. C. Wang, S.-Y. Chih and M.-C. Chen, *Urology*, 2006, **68**, 999.
18. C. Verpoorten and G. M. Buyse, *Pediatric nephrology*, 2008, **23**, 717.
19. G. M. Rosa, M. Bauckneht, C. Scala, E. Tafi, U. Leone Roberti Maggiore, S. Ferrero and C. Brunelli, *Expert Opin Drug Saf*, 2013, **12**, 815.
20. M. Gopal, K. Haynes, S. L. Bellamy and L. A. Arya, *Obstetrics & Gynecology*, 2008, **112**, 1311.
21. R. K. Basra, A. Wagg, C. Chapple, L. Cardozo, D. Castro-Diaz, M. E. Pons, M. Kirby, I. Milsom, M. Vierhout and P. Van Kerrebroeck, *BJU international*, 2008, **102**, 774.
22. F. Cruz and C. Silva, *International Journal of Clinical Practice*, 2006, **60**, 22.
23. K.-E. Andersson, *Therapeutic advances in urology*, 2009, **1**, 71.
24. L. A. Birder and W. C. De Groat, *Nature clinical practice Urology*, 2007, **4**, 46.
25. A. J. Wein, *The Journal of Urology*, 2004, **172**, 2502.
26. P. Striano and S. Striano, *Drugs Today (Barc)*, 2008, **44**, 353.
27. Y. Maneuf, M. Gonzalez, K. Sutton, F.-Z. Chung, R. Pinnock and K. Lee, *Cellular and Molecular Life Sciences CMLS*, 2003, **60**, 742.
28. N. Yoshimura and M. B. Chancellor, *The Journal of urology*, 2002, **168**, 1897.
29. H. C. Hansen, *Southern medical journal*, 2000, **93**, 238.
30. Y. T. Kim, D. D. Kwon, J. Kim, D. K. Kim, J. Y. Lee and M. B. Chancellor, *International braz j urol*, 2004, **30**, 275.
31. C. Y. Chang, C. K. Challa, J. Shah and J. D. Eloy, *BioMed research international*, 2014, **2014**.
32. A. Beydoun, B. M. Uthman and J. C. Sackellares, *Clinical neuropharmacology*, 1995, **18**, 469.
33. Clarke's Analysis of Drugs and Poisons, <https://www.medicinescomplete.com/#/content/clarke/CLK0777>.
34. B. H. Stewart, A. R. Kugler, P. R. Thompson and H. N. Bockbrader, *Pharmaceutical research*, 1993, **10**, 276.

35. H. Uchino, Y. Kanai, D. K. Kim, M. F. Wempe, A. Chairoungdua, E. Morimoto, M. Anders and H. Endou, *Molecular pharmacology*, 2002, **61**, 729.
36. L. Kagan and A. Hoffman, *Journal of Drug Delivery Science and Technology*, 2009, **19**, 233.
37. C. Murphy, V. Pillay, Y. E. Choonara, L. C. du Toit, V. M. Ndesendo, N. Chirwa and P. Kumar, *AAPS PharmSciTech*, 2012, **13**, 1.
38. A. J. Claxton, J. Cramer and C. Pierce, *Clinical therapeutics*, 2001, **23**, 1296.
39. A. Rice, S. Maton and P. N. S. Group1UK, *Pain*, 2001, **94**, 215.
40. C. M. Lopes, C. Bettencourt, A. Rossi, F. Buttini and P. Barata, *International journal of pharmaceutics*, 2016, **510**, 144.
41. S. Arora, J. Ali, A. Ahuja, R. K. Khar and S. Baboota, *Aaps PharmSciTech*, 2005, **6**, E372.
42. U. Kotreka and M. C. Adeyeye, *Critical Reviews™ in Therapeutic Drug Carrier Systems*, 2011, **28**.
43. A. Goyanes, A. B. Buanz, A. W. Basit and S. Gaisford, *International journal of pharmaceutics*, 2014, **476**, 88.
44. A. Goyanes, A. B. Buanz, G. B. Hatton, S. Gaisford and A. W. Basit, *European Journal of Pharmaceutics and Biopharmaceutics*, 2015, **89**, 157.
45. K. Pietrzak, A. Isreb and M. A. Alhnan, *European Journal of Pharmaceutics and Biopharmaceutics*, 2015, **96**, 380.
46. J. Edgar and S. Tint, *Johnson Matthey Technology Review*, 2015, **59**, 193.
47. M. Ghori, E. Šupuk and B. Conway, 2015, **8**, 1482.
48. Y. Shahzad, S. Saeed, M. U. Ghori, T. Mahmood, A. M. Yousaf, M. Jamshaid, R. Sheikh and S. A. Rizvi, *International journal of biological macromolecules*, 2018, **109**, 963.
49. J. S. Nirwan, S. Lou, S. Hussain, M. Nauman, T. Hussain, B. R. Conway and M. U. Ghori, *Micromachines*, 2022, **13**, 17.
50. Z. Khizer, M. R. Akram, R. M. Sarfraz, J. S. Nirwan, S. Farhaj, M. Yousaf, T. Hussain, S. Lou, P. Timmins and B. R. Conway, *Polymers*, 2019, **11**, 1095.
51. R. Diryak, V. Kontogiorgos, M. U. Ghori, P. Bills, A. Tawfik, G. A. Morris and A. M. Smith, *Macromolecular Chemistry and Physics*, 2018, **219**, 1700584.
52. N. Thirawong, J. Nunthanid, S. Puttipipatkachorn and P. Sriamornsak, *European journal of Pharmaceutics and Biopharmaceutics*, 2007, **67**, 132.
53. P. A. Yamamoto, J. R. de Lima Benzi and N. V. de Moraes, *Revista de Ciências Farmacêuticas Básica e Aplicada*, 2021, **42**, 1.
54. M. I. Delgado Rosero, N. M. Jurado Meneses and R. Uribe Kaffure, *Materials*, 2019, **12**, 1464.
55. C. Korte and J. Quodbach, *Pharmaceutical development and technology*, 2018, **23**, 1117.
56. H. Öblom, J. Zhang, M. Pimparade, I. Speer, M. Preis, M. Repka and N. Sandler, *Aaps Pharmscitech*, 2019, **20**, 1.
57. M. R. Mucalo and M. J. Rathbone, 2012.
58. D. Li, Y. Jiang, S. Lv, X. Liu, J. Gu, Q. Chen and Y. Zhang, *PLoS One*, 2018, **13**, e0193520.
59. K. Coppens, M. Hall, P. Larsen, S. Mitchell, P. Nguyen, M. Read, U. Shrestha and P. Walia, 2004.
60. D. Syrlybayev, B. Zharylkassyn, A. Seisekulova, M. Akhmetov, A. Perveen and D. Talamona, *Polymers*, 2021, **13**, 1587.
61. R. Harris, N. Acosta and A. Heras, in *Inhaler devices*, Elsevier, 2013, pp. 77.
62. G. Sandri, M. Ruggeri, S. Rossi, M. C. Bonferoni, B. Vigani and F. Ferrari, *Nanotechnology for Oral Drug Delivery*, 2020, 225.
63. F. Madsen, K. Eberth and J. D. Smart, *Journal of controlled release*, 1998, **50**, 167.
64. L. Ma, L. Deng and J. Chen, *Drug development and industrial pharmacy*, 2014, **40**, 845.
65. M. U. Ghori, G. Ginting, A. M. Smith and B. R. Conway, *International Journal of Pharmaceutics*, 2014, **465**, 405.
66. J. Pyterał, W. Jamróz, M. Kurek, J. Szafraniec-Szczęsny, D. Kramarczyk, K. Jurkiewicz, J. Knapik-Kowalczyk, J. Tarasiuk, S. Wroński and M. Paluch, *Molecules*, 2021, **26**, 3106.

CHAPTER 6

Conclusions

6.1. Conclusions

The main goal of this thesis was to contribute to the field of personalised drug delivery using 3D printing technology. For this purpose, two systematic reviews were conducted along with the research work. Plasticiser free filaments of HPMC with glipizide and PEO with gabapentin were successfully extruded and 3D printed tablets were produced. The objectives mentioned in 1.2 section of chapter 1 were successfully achieved with the conclusions summarised in the sections given below.

3D printed patient centric medicines: a systematic review

A systematic review was conducted to investigate the pharmaceutical applications of 3D printing technologies. It was concluded that the 3D printing technologies can develop novel personalised drug delivery devices. Its digital design and control can develop devices with unique functionalities which are difficult to produce via conventional processes. This review has reported greater number of applications of FDM. Along with personalisation aspect, 3D printing technologies also offer opportunities to develop such a dosage form design that can address issues of patient compliance, adherence, and tolerance. It was concluded that increased ongoing research in investigating its potential will bring this technology from proof-of-concept phase to mainstream manufacturing tool, however, there are regulatory affairs that should also be addressed. Moreover, it did not only provide information on the various materials used by the researchers but also provided strong basis for our experimental work (chapter 3) by confirming that none of the studies mentioned the drug absorption related challenges caused by using plasticiser induced gastric motility.

Plasticiser-Free 3D Printed Hydrophilic Matrices: Quantitative 3D Surface Texture, Mechanical, Swelling, Erosion, Drug Release and Pharmacokinetic Studies

Chapter 3 represented the successful extrusion of HPMC, an extended-release polymer, filaments without the aid of plasticiser followed by printing of the hydrophilic matrices using glipizide as a model drug. It was concluded that HPMC had the potential to retain its properties during the process of HME and FDM printing and the viscosity of the HPMC had a pronounced effect on the drug release behaviour. The highest viscosity grade of HPMC resulted in increased swelling, decreased HPMC dissolution, low matrix erosion and decreased drug release. *In vivo* results also showed an extended drug absorption profile.

Overall, it can be concluded that HPMC is not only a suitable polymer for conventional manufacturing processes of hydrophilic matrices but has also shown promising feasibility for digital manufacturing technology which is not only cost-effective but also provides great opportunity for personalisation and on demand manufacturing to achieve personalised therapeutic needs of individuals.

Drug Delivery Approaches for Managing Overactive Bladder (OAB): A Systematic Review

This systematic review analysed and compared the different drugs and their routes of administration for managing OAB. Overactive bladder syndrome (OAB) is characterised by urgency symptoms, with or without urgency incontinence, usually with frequency and nocturia and severely affects the quality of life. It was concluded that the availability of different drug delivery routes makes management of the disease easier and increase patient compliance and adherence. According to this systematic review, transdermal drug delivery route is preferable over other routes to avoid the side effects of the drugs. Overall, it can be concluded that, such systematic reviews are of great importance among researchers for providing them enough justification for further research and enabling them to keep their selves up to date with their respective field. It also provides a fundamental approach for developing novel drug delivery system for the management of OAB. The review was helpful in selecting the drug delivery route and a drug for the experimental work (chapter 5).

Personalised 3D printed mucoadhesive gastroretentive matrices for manging overactive bladder (OAB)

Chapter 5 discussed the absorption related issues of gabapentin, an effective drug for the treatment and management of OAB and has successfully represented the gastroretentive floating system to overcome those issues. It can be concluded that combining the use of PEO along with gastroretentive system was successful in achieving the goal i.e., to retain the tablet in the stomach for longer period with extended release of drug. The PEO filaments were successfully developed without using plasticiser followed by printing using different shell numbers and infill density. It was concluded that the digital control of the FDM technique was not only easy to use but was also efficient and successful in developing gastroretentive floating drug delivery system. The change in shell number and infill density greatly affects the floating capability of the tablets and the drug release behaviour and *in vivo* results were also

in consistent with *in vitro* results. In summary, it was concluded from the results that gastroretentive floating drug delivery system was a suitable approach for gabapentin with narrow absorption window. The optimum formulation floated for more than 10 hours showing extended drug release thereby increasing absorption extent.

CHAPTER 7

Future work

7.1. Future work

FDM requires suitable printing materials for pharmaceutical applications. In our thesis, we have utilised polymers of synthetic and semi-synthetic origin for the development of filaments followed by printing. In future, the feasibility of natural polymers for 3D printing may be investigated.

The study has shown the extrusion of plasticiser-free HPMC filaments in the presence of an oral hypoglycaemic drug, glipizide. In this study, the effect of three different viscosity grades on drug release was investigated, however, polymer concentration and their chemical confirmation may also influence the functional characteristics of 3D printed hydrophilic matrices. Therefore, the present study can be further expanded in this direction. Moreover, in developing 3D printed matrices higher amount of polymeric content has been employed to ease the extrusion process, this may be a future area of research where the amount of polymer in 3D printed tablets can be rationalised to avoid polymer accumulation in the body and reduced the risk of any unwanted adverse effects.

The effect of viscosity of PEO on drug release behaviour in gastroretentive floating system should be investigated. This can be further expanded to investigate the other gastroretentive systems e.g., high density and magnetic systems, mucoadhesive system, expandible, unfold able and super porous system. The feasibility of 3D printing technology in developing these should be explored.

With respect to the 3D printing technology, we have explored the effect of varying shell numbers and infill density on the drug release, whereas there are other printing parameters that should also be investigated. In our research projects, we have utilised single screw extruder for the extrusion of filaments. The twin screw extruder is also available and should be explored in terms of material feeding, dispersing, and kneading capacity.

Appendix I

Appendix I

1. **Plasticiser-free 3D printed hydrophilic matrices: quantitative 3D surface texture, mechanical, swelling, erosion, drug release and pharmacokinetic studies.**





Zara Khizer ,Muhammad R. Akram ,Rai M. Sarfraz ,Jorabar Singh Nirwan ,Samia Farhaj, Maria Yousaf ,Tariq Hussain ,Shan Lou, Peter Timmins, Barbara R. Conway, and Muhammad Usman Ghori. **Polymers** 2019, 11(7), 1095.

2. **Drug Delivery Approaches for Managing Overactive Bladder (OAB): A Systematic Review.**

Zara Khizer, Amina Sadia, Raman Sharma, Samia Farhaj, Jorabar Singh Nirwan, Pratibha G. Kakadia, ,Talib Hussain, Abid Mehmood Yousaf, ,Yasser Shahzad, Barbara R. Conway, and Muhammad Usman Ghori. **Pharmaceuticals** 2021, 14(5), 409.

Article

Plasticiser-Free 3D Printed Hydrophilic Matrices: Quantitative 3D Surface Texture, Mechanical, Swelling, Erosion, Drug Release and Pharmacokinetic Studies

Zara Khizer ¹, Muhammad R. Akram ², Rai M. Sarfraz ², Jorabar Singh Nirwan ¹, Samia Farhaj ¹, Maria Yousaf ¹, Tariq Hussain ^{3,4}, Shan Lou ⁵ , Peter Timmins ¹ , Barbara R. Conway ¹  and Muhammad Usman Ghori ^{1,*} 

¹ Department of Pharmacy, School of Applied Sciences, University of Huddersfield, Huddersfield HD1 3DH, UK

² College of Pharmacy, University of Sargodha, Sargodha 40100, Pakistan

³ System Engineering Department, Military Technological College, Muscat 111, Oman

⁴ The Wolfson Centre for Bulk Solid Handling Technology, University of Greenwich, London SE10 9LS, UK

⁵ School of Computing and Engineering, University of Huddersfield, Huddersfield HD1 3DH, UK

* Correspondence: m.ghori@hud.ac.uk; Tel.: +44-0-1484-47-3295; Fax: +44-0-1484-47-2182

Received: 2 May 2019; Accepted: 25 June 2019; Published: 28 June 2019



Abstract: Hydroxypropyl methyl cellulose, HPMC, a hydrophilic polymer, is widely used for the development of extended release hydrophilic matrices and it is also considered as a good contender for the fabrication of 3D printing of matrix tablets. It is often combined with plasticisers to enable extrusion. The aim of the current project was to develop plasticizer-free 3D printed hydrophilic matrices using drug loaded filaments prepared via HME to achieve an *in vitro* (swelling, erosion and drug release) and *in vivo* (drug absorption) performance which is analogous to hydrophilic matrix tablets developed through conventional approaches. Additionally, the morphology of the printed tablets was studied using quantitative 3D surface texture studies and the porosity calculated. Filaments were produced successfully and used to produce matrix tablets with acceptable drug loading (95–105%), mechanical and surface texture properties regardless of the employed HPMC grade. The viscosity of HPMC had a discernible impact on the swelling, erosion, HPMC dissolution, drug release and pharmacokinetic findings. The highest viscosity grade (K100M) results in higher degree of swelling, decreased HPMC dissolution, low matrix erosion, decreased drug release and extended drug absorption profile. Overall, this study demonstrated that the drug loaded (glipizide) filaments and matrix tablets of medium to high viscosity grades of HPMC, without the aid of plasticisers, can be successfully prepared. Furthermore, the *in vitro* and *in vivo* studies have revealed the successful fabrication of extended release matrices.

Keywords: 3D printing; hot melt extrusion; hydroxypropyl methyl cellulose (HPMC); swelling; erosion; drug release; pharmacokinetics; Young's modulus; 3D surface texture

1. Introduction

Presently, pharmaceutical industries utilise well established methods for the fabrication of tablets with predetermined dose, size and shape [1]. Although the current methods are common and cost-effective, they offer little opportunity for personalisation and on-demand manufacturing as the change in size, shape and dose of a tablet require alterations at each manufacturing step and retooling of tableting machines [2–4]. Consequently, a technology capable of producing dosage



Review

Drug Delivery Approaches for Managing Overactive Bladder (OAB): A Systematic Review

Zara Khizer¹, Amina Sadia², Raman Sharma³ , Samia Farhaj¹, Jorabar Singh Nirwan¹, Pratibha G. Kakadia⁴ , Talib Hussain⁵, Abid Mehmood Yousaf⁵ , Yasser Shahzad⁵, Barbara R. Conway¹ and Muhammad Usman Ghori^{1,*}

- ¹ Department of Pharmacy, School of Applied Sciences, University of Huddersfield, Huddersfield HD1 3DH, UK; zara.khizer@hud.ac.uk (Z.K.); samia.farhaj@hud.ac.uk (S.F.); jorabar.nirwan@hud.ac.uk (J.S.N.); b.r.conway@hud.ac.uk (B.R.C.)
² District Headquarter Hospital, Sahiwal 57000, Pakistan; draminasadia@yahoo.com
³ Parkside Medical Practice, Horton Park Health Centre, Bradford BD7 3EG, UK; raman.sharma7@nhs.net
⁴ Behavioral & Social Science, Integrated Behavioral Health Research Institute, San Gabriel, CA 91775, USA; pratibhakakadia@gmail.com
⁵ Department of Pharmacy, COMSATS University Islamabad, Lahore Campus, Lahore 45550, Pakistan; t.h.kayani@live.com (T.H.); abid.ucp@hotmail.com (A.M.Y.); y.shahzad@live.com (Y.S.)
* Correspondence: M.Ghori@hud.ac.uk or Muhammad.Ghori@outlook.com; Tel.: +44-1484-47-3295



Citation: Khizer, Z.; Sadia, A.; Sharma, R.; Farhaj, S.; Nirwan, J.S.; Kakadia, P.G.; Hussain, T.; Yousaf, A.M.; Shahzad, Y.; Conway, B.R.; et al. Drug Delivery Approaches for Managing Overactive Bladder (OAB): A Systematic Review. *Pharmaceuticals* 2021, 14, 409. <https://doi.org/10.3390/ph14050409>

Academic Editors:
Yoshihiro Tokudome
and Serge Mordon

Received: 15 February 2021
Accepted: 1 April 2021
Published: 26 April 2021

Publisher's Note: MDPI stays neutral with regard to jurisdictional claims in published maps and institutional affiliations.



Copyright © 2021 by the authors. Licensee MDPI, Basel, Switzerland. This article is an open access article distributed under the terms and conditions of the Creative Commons Attribution (CC BY) license (<https://creativecommons.org/licenses/by/4.0/>).

Abstract: Overactive bladder syndrome (OAB) is characterised by urgency symptoms, with or without urgency incontinence, usually with frequency and nocturia and severely affects the quality of life. This systematic review evaluates the various drug delivery strategies used in practice to manage OAB. Advanced drug delivery strategies alongside traditional strategies were comprehensively analysed and comparatively evaluated. The present review was conducted according to the preferred reporting items for systematic reviews and meta-analyses guidelines. A total of 24 studies reporting the development of novel formulations for the treatment of OAB were considered eligible and were further categorised according to the route of drug administration. The review found that various drug delivery routes (transdermal, intravesicular, oral, vaginal and intramuscular) are used for the administration of drugs for managing OAB, however, the outcomes illustrated the marked potential of transdermal drug delivery route. The findings of the current review are expected to be helpful for pharmaceutical scientists to better comprehend the existing literature and challenges and is anticipated to provide a basis for designing and fabricating novel drug delivery systems to manage OAB.

Keywords: overactive bladder; drug delivery; transdermal drug delivery; pharmacotherapy; oral drug delivery; systematic review

1. Introduction

Overactive bladder (OAB) syndrome is characterised by “urinary urgency, usually accompanied by frequency and nocturia, with or without urgency urinary incontinence, in the absence of urinary tract infection (UTI) or other obvious pathology” [1]. According to a population-based survey carried out in the United Kingdom, Canada, Sweden, Italy and Germany, the overall prevalence of OAB was estimated to be 11.8% for both men and women and was found to increase with age [2]. However, this estimate may be an under-representation of the true prevalence of OAB as many patients may be reluctant and unwilling to discuss their condition with family members or healthcare providers, as observed in a population-based survey in which fewer than 50% of respondents with probable OAB had discussed their condition with their healthcare provider [3]. OAB can severely affect the quality of life and can impact the social, sexual, occupational and psychological aspects of patient life [2]. Consequently, OAB remains underreported, despite the availability of improved treatments and increased awareness [4,5].